NASA CONTRACTOR

NASA CR-2646

THE THEORY AND APPLICATIONS OF OCEAN WAVE MEASURING SYSTEMS AT AND BELOW THE SEA SURFACE, ON THE LAND, FROM AIRCRAFT, AND FROM SPACECRAFT

Willard J. Pierson

Prepared by
CITY UNIVERSITY OF NEW YORK
New York, N. Y.
for Goddard Space Flight Center

NATIONAL AERONAUTICS AND SPACE ADMINISTRATION • WASHINGTON, D. C. • JANUARY 1976

1. Report No.	2. Government Accession No.	3. Recipient's Catalog No.
NASA CR-2646		

4. Title and Subtitle	5. Report Date
The Theory and Applications of Ocean Wave Measuring Systems at and Below the Sea Surface on the Land, from Aircraft and from Spacecraft	January 1976
	6. Performing Organization Code
7. Author(s)	8. Performing Organization Report No.
Willard J. Pierson	
9. Performing Organization Name and Address	10. Work Unit No.
University Institute of Oceanography of the City University of New York New York, N. Y.	11. Contract or Grant No. NAS 5-20041
	13. Type of Report and Period Covered
12. Sponsoring Agency Name and Address	Contractor Report
National Aeronautics and Space Administration Washington, D. C. 20546	14. Sponsoring Agency Code

15. Supplementary Notes

16. Abstract

A subtitle of this report could be "The Study of Ocean Waves: From Spark Plugs and Ferris Wheels to Spacecraft". Nearly all of the known methods for measuring and analysing ocean waves are described, including those presently in use on spacecraft and planned for SEASAT-A. Potential difficulties with synthetic aperture systems for a spacecraft are described and an alternate design is suggested. The different methods can yield different kinds of spectra and other kinds of imagery. Ways to compare different kinds of data are given. The scientific and practical applications of data from spacecraft are given.

17. Key Words (Selected by Author(s))	18. Distribution Statement
Ocean waves Wave systems Wave data applications	Unclassified-Unlimited Cat. 48

19. Security Classif. (of this report)	20. Security Classif. (of this page)	21. No. of Pages	22. Price*
Unclassified	Unclassified	400	$10.25

For sale by the National Technical Information Service, Springfield, Virginia 22161

A B S T R A C T

A subtitle of this report could be "The Study of Ocean Waves: From Spark Plugs and Ferris Wheels to Spacecraft". Nearly all of the known methods for measuring and analysing ocean waves are described, including those presently in use on spacecraft and planned for SEASAT-A. Potential difficulties with synthetic aperture systems for a spacecraft are described and an alternate design is suggested. The different methods can yield different kinds of spectra and other kinds of imagery. Ways to compare different kinds of data are given. The scientific and practical applications of data from spacecraft are given.

A C K N O W L E D G E M E N T S

A policy of NASA for Contractor's Reports is that the efforts of those who contribute to a report as a part of their official duties are not to be acknowledged. These acknowledgements thus omit the names of several dozens of scientists who aided in the formulation of the concepts expressed herein by means of spirited discussions of problems in wave measurement and remote sensing. They know who they are, and this should suffice.

There are others, however, who contributed to this work by providing material and information as requested by correspondence and personal communication. Their help can be more formally acknowledged.

Aerial photographs of waves as shown in Figures 4.3, 4.4, 4.5, 4.10, 4.11, and 4.12 were provided by scientists from the Coastal Engineering Research Center. I am particularly indebted to Dr. D. Lee Harris for this material and numerous references.

Original glossy prints of the photographs in Figures 3.8 to 3.13 were provided to us by Mr. J. R. H. Noble, the director of the Meteorological Services of Canada so that the high quality of the originals could be maintained in reproduction. The photographs used are only a part of the full publication which contains many additional magnificent illustrations.

Mr. Duncan Ross provided the material for Figure 4.2 in advance of his own publication of it. He also gave me the imagery shown in Figure 4.20, as described in the text.

TABLE OF CONTENTS

CHAPTER 1 INTRODUCTION

PURPOSES OF PAPER

The purposes of this paper are (1) to summarize the presently available wave measuring systems from both the surface truth verification viewpoint and from the remote sensing viewpoint, (2) to comment on the range of frequencies that these systems can cover, on their calibration and on their accuracy as they are used in the oceans, bays, and lakes (but not in the laboratory, except as an aside), and (3) to summarize briefly the available theory for waves and comment on the applications of aspects of this theory to the understanding and application of the measurements of the waves carried out by the various systems.

Two Broad Categories

For the many different kinds of wave systems to be described, there are often two broad categories into which they fall. One category consists of systems that are used routinely on an operational basis so as to obtain wave data on a preassigned schedule, or during a predetermined sequence of events. Examples from this category are the shipborne wave recorders on European and Canadian weather ships, which obtain wave records every three hours whenever a ship with such an instrument is on station, and the array of wave recording wave poles mounted on oil drilling structures in the Gulf of Mexico, which were turned on to record waves whenever a hurricane came close enough to the platform to made the recordings of value. Another example is the system of wave recorders along the United States coastline operated by the Coastal Engineering Research Center.

For the other category, there are numerous wave recording systems that are not used operationally and that are used for scientific purposes only. Examples are the arrays used in Japan by Dr. H. Mitsuyasu in various studies, the systems employed by scientists of the Soviet Union for numerous studies, and the array of recording instruments used in the JONSWAP experiment. Also under this category may be found the laser altimeters used to obtain surface truth wave measurements for various remote sensing programs of NASA. In general, the instruments that are used for scientific purposes do not have the ruggedness and the on-line reliability to make it possible to use them every day on a predetermined schedule.

The Importance of Good Measurements and the Need to Discard or Discount Poor Ones

All wave recording systems have some kind of calibration and interpretation problem associated with them. Even the simplest system imaginable, which consists of a wave wire or a wave pole sticking through the water surface that senses the rise or fall of the water along its length has a problem of interpretation because of the variations in the frequency response of the recording system used to record the rise and the fall of the water and the different properties of the wires used. Many of these systems have a high frequency roll off that can distort the interpretation of the data. Any wave recording system that is employed on a moving platform introduces problems. The airborne laser altimeter for example, when on a moving aircraft, does not record the instantaneous position of the sea surface along a line, nor does it record the rise or fall of the sea surface at a point. Imaging radar systems on aircraft also introduce problems. Therefore, it is always important to be able to determine how the recorded wavelengths and wave periods, or equally well the recorded wave numbers and wave

frequencies, are distorted and perhaps mapped to false wave numbers and frequencies so that the data can be interpreted properly. Once the system is understood these effects can be corrected.

The spectrum of a wind roughened sea surface covers at least four orders of magnitude in frequency and many orders of magnitude in spectral values. Most wave recording systems cannot cover this extreme range of frequency and spectral amplitudes. It is, therefore, important to delineate the range that is covered and to describe the nature of whatever band pass filter has been applied to the data by the recording system.

A lot of wave data has been obtained during the past 20 years, or so. Much of it has been published in various forms in the scientific literature. As will be pointed out below, some it has been transformed by means of dimensionless variables to a form where it is virtually impossible to recover the original numbers that were obtained from the analysis of the data. If the ideas that went into the data reduction are ever proved to be faulty, then data published in this form have very little practical use. It becomes necessary to return to the original sources in order to recover and use the data. Also in many cases, doubts can now be raised concerning the recording accuracy of the original systems. When data yield results that scatter over large ranges in the various plots that are used, it becomes necessary to ask whether or not some of the data are to be preferred over other data because of the nature of the recording system that was used.

These comments are particularly appropriate when the problem of extreme waves arises. The data for waves on the open ocean with significant wave heights in excess of 8 or 9 meters are not very abundant. The major source for these data, for example, is the Tucker shipborne wave recorder. Without it and the data it has provided, it is doubtful that techniques for numerical wave prediction,

based on spectral concepts, could have been developed at all. Attempts to develop improved spectral wave forecasting methods, have also involved wave recording systems on offshore oil towers in the Gulf of Mexico. These are the only extensive data sets for waves of great height in large bodies of water. There may be a danger in attempting to extrapolate data obtained for more limited bodies of water such as bays, and such as in the North Sea for the JONSWAP experiment, where the waves rarely exceed 3 meters in significant wave height, to these open ocean conditions, especially when the data are made to conform to various nondimensional concepts concerning the shape of the wave spectra. It may indeed be necessary to discard some of the data obtained in the past for carefully thought out reasons in order to obtain consistent data for the development of a better understanding of wind generated waves and swell.

THE NEED FOR MORE AND BETTER WAVE DATA AS A CLIMATOLOGICAL BASE

Wave data have been collected for many years. The most extensive data consists of reports of ships of visually observed wave conditions. The quantities reported are the "average height of a train of well defined waves" and the "period" of these waves. Such reports leave much to be desired; however, since they are all that are available for vast areas of the ocean, there is little that can be done at the present time except to interpret them carefully and use them with caution. As this report develops, it will be seen that the availability of more and better wave data to form an adequate global oceanic data base may soon become a reality. Theories and models for wave forecasting are important of themselves, but there are many engineering and scientific applications where the best way to proceed is quite simply to measure the waves on a routine basis and to store the data in archive form so that an adequate

climatological data base can be built up over the course of the years. If the data are correctly recorded, and correctly located, there is no substitute for actual measurements of the waves on a routine basis.

Scientific Applications

There are many scientific applications of such data. They would provide a better understanding of air sea interaction effects. One important effect is that breaking waves have the property that the small air bubbles below the surface on breaking through the surface, eject a drop of water into the atmosphere. When these drops evaporate before falling back to the surface, a nucleus of salt is left behind in the air. These salt nuclei play an important role in the hydrological cycle by providing the condensation points for rain, both over the oceans and over the land. Examples of studies of the salt nuclei in the air are those of Toba (1961). The problem, however, with these studies is that the wind water tunnel analysis of salt nuclei generation does not scale up to the open ocean because of the larger size and greater area of the white caps and foam involved. The research of D. Ross (Ross and Cardone (1974), for example) is directed toward this problem, in part.

The waves on the surface of the ocean are an important sink for the mommentum of the atmosphere. There are reasons to believe that much of the atmosphere's mommentum is transformed to wave motion before it is transformed to ocean currents. This momentum is finally dissipated by turbulence and whitecaps and at the shore line by breaking waves on beaches. Here it is responsible for the erosion of beaches and the transport of sand in suspension along the coast, resulting in the various problem of shore protection and beach erosion.

The wavy sea surface has a greater area than a calm sea surface, and thus the fluxes of heat and water vapor across the air sea interface can be enhanced in the presences of waves. A true climatological description of the waves over the world ocean can aid in the understanding of this problem.

Although wave data have been made available for selected parts of the world ocean by means of shipborne wave recorders, there are far to few measurements to describe other important areas of the world ocean. There are many reasons to believe that the wave properties will be quite different in other parts of the world ocean. As one example, the centers of the subtropical highs, which are semipermanent features of the atmospheric circulation, could be controlled almost entirely by swell waves that have been generated by the more poleward transient cyclonic centers with high winds. These areas should be understood from a scientific point of view.

As another example, the trade winds should contain locally generated waves of substantially the same spectral properties for many months on end. The spectra will grow and shrink only slightly as the winds vary by perhaps ± 10 or 20 percent about their climatological averages. In addition to the local wind seas of the trades, for the extreme winter season in either hemisphere, there will be a succession of swell waves traveling through the trades at an angle to the trade winds, as produced by the extratropical cyclones of the more polar regions. The climatology of these transient swells is not well understood, and so these waves need to be studied further. Examples where knowledge of these swells would be important are the coasts of Mexico as it borders the Pacific, Southern California, and North Africa, near Casablanca.

Finally, the Southern Hemisphere oceans are reputed to have much more intense storms, the roaring forties and fighting fifties, and much higher waves than the Northern Hemisphere. The fetches can be much longer and the oceanic areas involved are one-third larger than for the Northern Hemisphere.

Applications to Ship Design and Marine Systems

As the economy of the world changes, there will be an increasing need for new types of ships and for more ships throughout the world. The new types of ships will be hydrofoils and surface effects ships. A climatological wave data base will prove to be very important for the design of both these new kinds of ships and of larger conventional ships. Material on this subject can be found in Seakeeping 1953-1973, a recent publication of the Society of Naval Architects and Marine Engineers. There will also be the need for improved designs for floating movable oil drilling rigs that can be towed from one part of the world to the other safely, for oil drilling platforms in waters of increasing depth for locations where the wave environment may be even more severe then that caused by hurricanes in the Gulf of Mexico, for other types of offshore structures such as the Chesapeake Bay Light Station and atomic energy plants protected by breakwaters, and for new and improved coastal defense structures such as seawalls and breakwaters.

Applications of Improved Wave Forecasts

A knowledge of the day to day variations in waves can be used to improve a wave forecasting method by providing an adequate verification of the method and by demonstrating where it can be improved with minimum cost and effort. Longer range and more accurate forecasts will make it possible to operate ships more safely and more efficiently on the international trade routes of the world.

For these particular applications, it is not necessary to know in great detail the higher frequency, shorter wavelength, part of the spectrum. In fact for waves much shorter then about one-fourth of the length of the ships involved, there is very little effect on the ship and her motions. The shorter waves can, however, contribute to bow submergence and the amount of water on deck for a heaving and pitching ship.

DIRECT AND REMOTE SENSING SYSTEMS FOR WAVES

To outline briefly the wave recording and measuring system that are presently available, or that may be become available, the instruments that are possible have been placed into four different categories. They are direct ocean wave measuring systems, coastal and shallow water direct systems, aircraft remote sensing systems, and spacecraft remote sensing systems. The instrumentation for each of these categories is described briefly below.

The direct wave measuring systems for the deep ocean are characterized by the fact that they operate at or near the sea surface. The most extensively used system is the Tucker shipborne wave recorder, which will be described in detail later. Also used are accelerometer - pitch, roll buoys that can obtain information from which certain properties of the wave number spectra, or the directional wave spectra, can be inferred. Inverted sonars have also been used on submarines hovering below the wavy surface to measure waves. Finally certain kinds of Spar buoys that float up ended in the water and that move up and down in the waves only slightly have been used to record waves in deep water. Photographs of waves taken from ships are not strictly measurements. Yet they can provide certain kinds of valuable information.

For the continental shelves where the water is not too deep, various kinds of platforms are available upon which sensors can be mounted. Most of these sensors are essentially wave wires or wave poles mounted either singly or in patterns on these platforms. A pattern of wave wires in which a number of signals are recorded simultaneously can be used to obtain some information on the direction of travel of the waves. One of the earliest type of wave recorder is the pressure transducer placed on the bottom in shallow water that records the changes in pressure at the sea bottom caused by the waves passing overhead. Such pressure transducers yielded the first data for the spectral analysis of waves, and they could play an important role in defining the wave environment over the continental shelf using modern technology because they are relatively insensitive to damage and to loss.

Aircraft have been used to measure waves in a number of different ways. Although usually not quantitative there is a wealth of data available from aerial photographs that define some of the complexities of wave refraction patterns. Single aerial photographs under proper lighting conditions can be used to obtain wave spectra. An early study of waves used a pair of stereo photographs obtained simultaneously from two aircraft with a substantial base line between them to determine the topography of the sea surface and compute the vector wave number spectrum from the data. A very short pulse narrow beam radar is under development that will be able to privide almost the equivalent of a stereo-photogrammetric sea surface. A very recent addition, historically speaking, is the laser altimeter which can measure the distance between the aircraft and the ocean surface as the aircraft flys rapidly over the ocean at a fairly low altitude. Many important scientific contributions to the study of waves have been made by such laser altimeter data. Presently in the experimental stage as used on aircraft are real aperture radars and

synthetic aperture radars. There is a great deal of new information on this method for studying ocean waves and swell, which will be reviewed in this paper.

Finally, there is the opportunity to measure the waves from spacecraft. Under active consideration and, in fact, in use on Skylab, is the radar altimeter whose prime objective is geodetic. However, the shape of the return pulse is a function of the significant wave height. After verification from the Skylab experiments, the routine analysis of the Geos-3 altimeter data should provide global climatological data on wave height. Proposed for Seasat-A is a synthetic aperture radar. This radar could be used to obtain wave number spectra for the open ocean, and to study quantitatively the effects of shallow water over the continental shelves in refracting waves.

Other systems have also been proposed. One is a short pulse narrow beam system that in principle could provide a profile of the derivative of the wavy surface along a line as a function of horizontal distance from the spacecraft. Another proposes to beat two radio frequencies together in such a way that the different frequency can be used to carry out a wave number spectrum analysis for the projection of the wave on the line of sight of the radar beam.

Also, although it has not been proposed, should some of these methods not yield the desired information about the waves over the ocean, it is possible to conceive of a downward looking telescope that could obtain either stereo photographs or ordinary photographs of waves through clear skies that could be used to obtain wave information and in particular wave spectra, over the open ocean. There are areas of high winds in certain sectors of cyclones where there are few clouds and where such a system could peer down to the sea surface and obtain useful wave data.

The advantage of radar systems is, of course, that stratiform clouds have little or no effect and that waves can be measured routinely with them whereas systems based on photography, or television-type images, require clear skies.

Two remote sensing systems that are not used on either aircraft or spacecraft have recently been tested. Both are based on land and use radio waves to obtain information on ocean waves. One system is capable of providing information on the direction of wave travel for a particular frequency on a scientific basis. The other is capable of providing some information on the wave spectrum for an extensive area. These systems will be described in Chapter 3.

CHAPTER 2 REVIEW OF WAVE THEORY

SIMPLE HARMONIC PROGRESSIVE WAVES AS THE ELEMENTS OF THE IRREGULAR SEA SURFACE

Preliminary Remarks

The general theory of gravity waves and capillary waves is treated in Neumann and Pierson (1966), Kinsman (1965), and Phillips (1966). Certain parts of the material in Phillips will be discussed in later sections. Some of the assumptions therein do not appear to have been correct. This brief review is meant to contain simply the essentials of the material in the above three references.

The most elementary treatment of wave theory begins with the hydrodynamical equations and makes a great many simplifications so as to obtain a tractable problem. These simplifications yield the concept of a simple harmonic progressive wave for water of infinite depth on a plane ocean. Such effects as the density of the water, the nonlinear terms in the equations of motion, breaking waves, and vorticity in the wave field are all neglected in this approach. Nevertheless, it does yield a useful representation of actual waves. There has been a great deal of material published in journals such as the Journal of Geophysical Research and the Journal of Fluid Mechanics in which the various assumptions made concerning this linear model are investigated, and if possible removed, so as to obtain more useful representations for waves on the ocean surface. The linear superposition of simple harmonic progressive waves as defined by a variance spectrum yields the simplest possible representation of a realistic sea surface. It remains a fact, however, that even for this simple representation, not enough data are available to characterize the full variation from place to place as a function of time of the waves on the ocean surface. Some of the areas that may need more careful in-

vestigation in the future are concerned with such assumptions as the one involving the tangent plane approximation to the roughly spherical sea surface.

Simple Harmonic Waves and Their Superposition

With the above preliminary remarks in mind, the equation for a simple harmonic progressive wave is given by equation (2.1).

$$\eta(x,y,t) = a\cos(\ell\, x + m\, y - \omega\, t + \epsilon) \qquad (2.1)$$

The properties of wave motion are such that ℓ, m, and ω are not independent. They are interrelated in deep water in terms of the magnitude of the vector wavenumber ℓ, m, given by k and the equation connecting the frequency of the wave, ω, to the wavenumber as shown by equation (2.2).

$$k = (\ell^2 + m^2)^{\frac{1}{2}} \qquad \omega = (gk)^{\frac{1}{2}} \qquad (2.2)$$

Such a wave can travel in any direction and have any amplitude (within reason) and phase at the coordinate system origin. An alternate representation for equation (2.1) places emphasis on the frequency of the wave, ω, and the direction toward which the wave is traveling, X. Equations (2.3) define the two components of the vector wavenumber in terms of ω and X. It then follows that a second way to describe a simple harmonic progressive wave is given by equation (2.4).

$$\ell = \frac{\omega^2}{g}\cos X \quad , \qquad m = \frac{\omega^2}{g}\sin X \qquad (2.3)$$

$$\eta(x,y,t) = a\cos\left(\frac{\omega^2}{g}(x\cos X + y\sin X) - \omega t + \epsilon\right) \qquad (2.4)$$

The surface of the ocean for a region many tens of kilometers on a side and for times of the order of twenty minutes up to an hour or so,

depending on location, can be considered to be a summation of many elementary waves of the form of equation (2.1) or equation (2.4). The rules for carrying out the summation depend upon the spectrum of the waves. If the spectrum is defined in wavenumber space as $S(\ell,m)$, then equation (2.5) defines a set of amplitudes, a_{pq}, for a sum of waves of the form given by equation (2.1)

$$a_{pq} = \sqrt{2\, S(\ell_p, m_q)\, \Delta\ell\, \Delta m} \tag{2.5}$$

This summation is indicated by equation (2.6)

$$\eta\,(x,y,t) = \sum_q \sum_p a_{pq} \cos \Psi_{pq} \tag{2.6}$$

as $\Delta\ell$ and Δ m approach zero.

where

$$\Psi_{pq} = \ell_p x + m_p y - \omega_{pq} t + \epsilon_{pq} \tag{2.7}$$

If a large number of waves of this form, say several hundred, are added up, where the amplitudes are calculated from equation (2.5) and where ϵ is chosen for each term in the sum to be distributed between 0 and 2π with equal probability, the result will be a function of x,y, and t that will look remarkably like the sea surface.

If, on the other hand, the spectrum is defined in terms of frequency and direction as $S(\omega,\chi)$, then the terms in the sum that give the amplitudes are defined by equation (2.8), the summation is indicated by (2.9) where Ψ_{rs} is defined by equation (2.10).

$$a_{rs} = \sqrt{2\, S(\omega_r, \chi_s)\, \Delta\omega\, \Delta\chi} \tag{2.8}$$

$$\eta(x,y,t) = \sum_r \sum_s a_{rs} \cos \Psi_{rs}, \tag{2.9}$$

as $\Delta\ \omega$ and $\Delta\ \chi$ approach zero,

where

$$\Psi_{rs} = \frac{\omega_r^2}{g}\left(x \cos \chi_s + y \sin \chi_s\right) - \omega_r t + \epsilon_{rs} \tag{2.10}$$

Again, except for the nature of the rules defining the procedure to obtain the sum, and in this case ϵ is also uniformly distributed at random between 0 and 2π, the result will be another sea surface that looks remarkably like the ones observed.

There will be some difference, however. For one thing the surfaces represented by these equations could be turned over, that is multiplied by a minus sign, and it would not be possible to tell, without knowing that it has been done, that this operation had been performed. Actual gravity waves, and the superimposed capillary waves have been neglected so far, would be different in that the peaks would be sharper and the troughs would be broader and shallower than this model indicates. Up to the present time, the writer knows of no way to analyze a nonlinear sea surface with these added effects of nonlinearity, assuming they were correctly observed. The problems of analyzing both wave records, that is any of these surfaces observed as a function of time for x and y fixed, and wave images still reduces to the problem of recovering either $S(\ell,m)$ or $S(\omega,\chi)$, or perhaps $S(\omega)$ where the effects of direction have been integrated out.

Recovering the Spectrum

A wave wire, or wave pole, that records the rise and fall of the sea surface at a fixed point simply yields a function of time. Given such a record, the expected value of this time history times the expected value of the time history delayed τ seconds can be computed (or estimated

from a finite sample) and represented by $Q(\tau)$, from equation (2.9), and the appropriately defined terms in it. The result is the last expression in equation (2.11).

$$Q(\tau) = E\left(\eta(t),\ \eta\ (t + \tau)\right) = \int_0^{\infty}\left[\int_{-\pi}^{\pi} S(\omega,\chi)d\chi\right] \cos\ \omega\tau\ d\ \omega \tag{2.11}$$

The even Fourier transform of $Q(\tau)$ then yields the frequency spectrum of the waves as given by equation (2.12).

$$S(\omega) = \frac{2}{\pi}\int_0^{\infty} Q(\tau)\ \cos\ \omega\tau\ d\ \tau \tag{2.12}$$

The integral of equation (2.12) over all frequencies is the variance averaged over time of the wave record and is generally designated by m_o as in equation (2.13)

$$m_o = \int_0^{\infty} S(\omega)\ d\ \omega \tag{2.13}$$

If, on the other hand, it were possible to observe an instantaneously frozen portion of the sea surface given by $\eta(x,y)$, then the expected value of this surface times itself displaced a distance given by x* and y* yields a function $Q(x^*, y^*)$ defined by equation (2.14).

$$Q(x^*,y^*) = E\left(\eta(x,y),\eta(x + x^*,\ y + y^*)\right) = \int_{-\infty}^{\infty}\int_{-\infty}^{\infty} S(\ell m)\ \cos\ (\ell x^*+my^*)d\ell dm \tag{2.14}$$

Equation (2.14) has a very interesting property. The quantity $Q(x^*,y^*)$ equals $Q(-x^*,-y^*)$. This means that a spectrum of the form $S(\ell,m)$ cannot be distinguished from a spectrum of the form $S(-\ell,-m)$. The Fourier transform in two dimensions of this covariance surface therefore yields both the true wave number spectrum and its "alias" where ℓ can transform into $-\ell$

and m into -m as in equation (2.15). An instantaneous area measurement of the sea surface will always contain this ambiguity. It is important to separate out by means of supplementary information such as the wind direction and other factors, what part of this transform should be considered to be the true spectrum and what part should be considered to be the false spectrum. The integral over whatever turns out to be the true spectrum for the full range of ℓ and m should again yield the total variance of the wavy surface, m_o, and m_o as defined by equations (2.16), should equal the m_o of (2.13) if the wave pole record and the instantaneously obtained sea surface were observed in the same area of the ocean.

$$S(\ell,m)+S(-\ell,-m) = \frac{4}{\pi^2}\int_{-\infty}^{\infty}\int_{-\infty}^{\infty} Q(x^*,y^*)\cos(\ell x^*+my^*)\,dx^*dy^* \qquad (2.15)$$

$$m_o = \int_{-\infty}^{\infty}\int_{-\infty}^{\infty} S(\ell\, m)\,d\ell\,d\,m \qquad (2.16)$$

Complications

The complications involved in recovering either the frequency spectrum or the vector wavenumber spectrum, as defined above, are many. They are involved with the fidelity of the various recording systems, the fact that some of the recording systems are in motion, the fact that the recording systems do not respond with unit gain and zero phase shift to every simple harmonic wave that passes them, and the fact that some recording systems actually record the derivatives, or some other related quantity, of the sea surface. There is no such thing as a perfect wave recording system. They all have some kind of filter, or transfer function, interposed between what was desired to be measured and what is actually measured. Some smooth over a part of the wavy surface and filter out short waves. Some respond differently to one frequency than to another. Some have noise sources and extraneous signals of one kind

or another mixed in with the desired signal. If the recording system is in motion, it will distort the effects of frequency and wavenumber. One of the purposes of this paper is to indicate to the best of what is known at the present time how to correct each of the different kinds of recording systems so as to recover the best possible estimate of the spectra defined above.

Although not mentioned yet, it is possible to transform these two different kinds of spectra into other kinds of spectra using the relationships between frequency and wavenumber, as even extended to include the effects of surface tension, and obtain many other kinds of spectra, each with a special kind of interpretation. It will often be possible to take wave data several different ways and process each data set in such a way that all of the data will yield the same function to be compared. If these functions agree, then it can be said that the different wave recording systems check internally and yield results that provide a consistent description of the sea surface, within the constraints of a linear theory. Perhaps, under these constraints, it may be possible to recognize that the discrepancies that exist are due to non-linear features in which case it can be claimed that the different methods of wave recording are at least internally consistent.

Wave Recording from a Moving Platform

Many different kinds of wave recording systems are mounted on a moving platform. One such system would be a Tucker shipborne wave recorder on a moving ship. In general the Tucker shipborne wave recorder is not used in this way, but for certain applications to naval architecture, it might be. The airborne laser altimeter is another example of a wave recording obtained from a moving platform. Here the speed of the aircraft is large compared to the speeds of most gravity waves and

the usual solution to the problem is to treat the wave record as if it had been obtained instantaneously along the flight line, thus mapping it into a distorted wavenumber space. Most of the published material in this area has gotten away with this approximation within the level of accuracy of the measurements. However, it is possible to do something more refined. Airborne imaging systems with either real aperture side scanning radars, or with synthetic aperture radars, pose a host of different problems in the interpretation of the images that would be obtained. They will be discussed in greater detail in the appropriate part of this paper.

Without loss of generality, the moving recording system can be considered to be moving along the positive x direction with the velocity v t. Any position normal to the direction of motion will preserve its location in the y coordinate system. This situation is indicated by equation (2.17).

$$x = v\,t\ ,\ y \tag{2.17}$$

If the value for x given by v t, where v is the velocity of the platform, is substituted into equation (2.1) the result is equation (2.18).

$$\begin{aligned} \eta\,(y,t) &= a\cos(\ell\, v\, t + m\, y - \omega\, t + \epsilon) \\ &= a\cos\,(m\, y - (\omega - \ell\, v)\, t + \epsilon) \end{aligned} \tag{2.18}$$

The result can be considered to be a function of time and the position normal to $x = 0$, given by y. From the alternate definition of a simple harmonic progressive wave given by equation (2.4), the frequency in (2.18) that would be observed along the line $y = 0$ is given by equation (2.19).

$$\omega_e = \omega - \frac{\omega^2 v}{g}\cos X \tag{2.19}$$

This equation is a very famous equation in naval architecture. If a ship were to travel along the line $x = 0$ at the velocity v t in the positive x direction in a simple harmonic progressive wave, also traveling in the positive x direction, the frequency with which it would encounter the waves is given by ω_e. With $\chi = 0$, it is clear that there is a velocity, v, such that the frequency of encounter would be zero. For example, a wave with a period of five seconds has a speed of approximately 15 knots, and if it is traveling in the positive x direction, a ship with a speed of 15 knots would stay in the same position relative to the wave crests, just as if both were not moving.

One of the interesting implications of this equation has to do with the rolling motions of a ship. Certain waves approaching a ship from astern, but at an angle to the course of the ship, with quite short periods can cause the ships to roll at its natural period of roll, which may be three or four times greater than the period of the wave.

The implications of this particular equation as a function of the heading of the wave relative to the course of the ship were worked out in detail in the paper by St. Denis and Pierson (1953). There are numerous aspects of this study in naval architecture that have yet to be fully exploited because many applications do not treat the total effect of a directional wave spectrum of the form, $S(\omega, \chi)$. It should be noted in passing that the direction convention adopted by St. Denis and Pierson (1953) is opposite to those of equation (2.19). The ship was assumed to be traveling in the positive x direction but the waves traveling towards the ship, that is towards negative x, were treated as head seas.

For an aircraft flying in the positive x direction, it is probably more realistic to treat the function of x and y that might be observed by a side scanning radar as if time had been removed from the equation

of a simple harmonic progressive wave in contrast to removing one space variable. If (2.17) is solved for t in terms of x, and if this value of t, given by x/v, is substituted into equation (2.1) the result is equation (2.20).

$$\eta(x,y) = a \cos\left(\ell x + m y - \frac{\omega x}{v} + \epsilon\right)$$
$$= a \cos\left(\left(\ell - \frac{\omega}{v}\right) x + m y + \epsilon\right) \tag{2.20}$$

The wavenumber of encounter ℓ_e and the one orthogonal to it m_e are then given by equation (2.21) and (2.22).

$$\ell_e = \ell - \frac{\omega}{v} = \ell - \frac{g^{\frac{1}{2}}}{v}\left(\ell^2 + m^2\right)^{\frac{1}{4}} \tag{2.21}$$

$$m_e = m \tag{2.22}$$

The ℓ component of the wavenumber of encounter involves the y component of the true wavenumber, and these two equations are really quite complicated to interpret. They have a very important application to the understanding of synthetic aperture radar images and of real aperture images as obtained by aircraft and to a side scanning short pulse altimeter type radar presently under development.

Both synthetic aperture and real aperture radars appear to yield signals along the line scan that are related to the slope of the sea surface in the direction of the scan. Equation (2.1) can be differentiated with respect to y, the rest of the steps are similar, and the function of x and y that would be seen for the slope of a simple harmonic progressive wave on the sea surface is given by equation (2.23).

$$\frac{\partial \eta(x, y)}{\partial y} = -a m \sin\left(\left(\ell - \frac{\omega}{v}\right) x + m y + \epsilon\right) \tag{2.23}$$

Finally it is useful to consider what a spacecraft might record under the same set of constraints. In equations (2.20) and (2.23), the velocity of the moving platform appears in the denominator of the fraction, ω/v. In general, the speed of a spacecraft is so high that, for most practical purposes, the slight distortions in the x components of the vector wavenumber can probably be omitted. However, to verify some of these concepts from aircraft, instead of spacecraft, will require great care. The effect of the term ω/v can easily be 10 to 20 percent of the wavenumbers involved for typical aircraft speeds, and thus the images are distorted with reference to the apparent direction of the wave travel and the apparent wavelengths. The spectra that can be recovered from these images are not those for the true wavenumbers, ℓ and m.

WAVE FORECASTING

General Review

A wave forecast by definition must tell something about the waves as they will be at some future time. The rules for forecasting in general are that the forecaster or the forecast system (if it is a computer based system) is given all available information to prepare the forecast up to a certain cut-off time, say, twelve o'clock Greenwich mean time on a certain day. The forecast problem is then to make a definite statement, of some kind or another, about what the wave will be like twelve hours, twenty-four hours, two days, or what have you, in the future.

There are a variety of methods available, as used by wave forecasters and based upon computer techniques, for forecasting waves. In principle, they must all start with the best available forecast of what the winds will be like over the ocean. The hand graphical techniques are often referred to as the Sverdrup - Munk - Bretschnieder method*, the Pierson, Neumann and

*See, for example, a review of this method in Silvester (1974).

James (1955) method, and their variations. Recently Silvester (1974) has incorporated the Pierson-Moskowitz spectrum into the Pierson-Neumann-James method and produced a new hand graphical procedure for forecasting, and/or specifying, waves given the winds over the ocean. These techniques are called hand-graphical because they involve a set of graphs that describe the waves as a function of wind speed, duration and fetch for the generation of the waves, the swell that travels out of a generating area is described by additional graphs. Various European weather offices also prepare charts that show wave forecasts for the North Atlantic.

There are a number of computer based techniques available for forecasting waves. Examples are the ones described by Ewing (1971), Gelchi et al. (1956, 1957), one that uses the Sverdrup-Munk-Bretschnieder graphs in a computerized way as presently used by the National Weather Service, and the one recently described by Salfi (1974). This last method was described by Pierson, Tick and Baer (1966). Computer programs have been prepared for use on the computers at the Fleet Numerical Weather Facility and for a Univac 1108. It is now operational at the Fleet Numerical Weather Facility, and Lazanoff and Stevenson (1974) have given reports on this method at two recent scientific meetings. Another slightly different model is in operation for forecasts in the Mediterranean Sea as described by Lazanoff et al. (1973).

Finally there is a special effort consisting of the work of Cardone et al. (1974) that specified wave condition in some hurricanes that were recorded in the Gulf of Mexico. This numerical forecasting model had a twenty mile triangular resolution and described the waves by means of 312 numbers at each point. It can be used to forecast the waves in hurricanes, if the motion and the winds in a hurricane can be correctly forecasted.

Wave forecasting models and techniques can also be used in those parts of the world where waves are not observed to compute what the waves would have been like given the winds observed over the oceans. Different scientists use different terms to describe this procedure. Some call it wave hindcasting, and others call it wave specification; either way, in principle it is possible to take a series of surface weather charts, either in computer or in manuscript form, and compute from them what the waves were like every three, six, or twelve hours for as long as desired. This has been done a number times for a number of different places in connection with various programs concerned with beach erosion problems and the design of various structures.

These various wave forecasting techniques, or hindcasting techniques, attempt to do different things. Some of them only attempt to give the height of the waves, the direction towards which they are traveling, and some sort of an average time interval between the waves, often called the significant wave period. The spectral wave forecasting methods attempt to find the spectrum of the waves to an adequate resolution for a set of grid points on the deep ocean. These ideas will be discussed in detail for the method recently published by Salfi (1974), but all spectral wave forecasting techniques should be roughly similar to this method.

The Fully Developed Wind Sea

Before proceeding with a description of a numerical wave forecasting procedure, it is necessary to discuss briefly the work of Moskowitz (1964), Pierson and Moskowitz (1964), and Pierson (1964). To carry out these studies, several hundred wave records from the Tucker shipborne wave recorder obtained by weather ships on station at stations Item and Jig were obtained from the National Institute of Oceanography of Great Britian.

These records were chosen for several purposes. One series was chosen for conditions such that the winds had blown with a nominally constant speed, in a nominally constant direction for a long time. From these many hundreds of records, as described in the work of Moskowitz, Pierson, and Mehr (1962, 1963) a subset could be chosen that represented spectra for winds near 20, 25, 30, 35, and 40 knots. Moskowitz (1964) was able to show that the spectra obtained by averaging somewhere between 8 and 10 different spectra obtained for these nominal wind speeds did indeed have the property that for a wide range of frequencies, not necessarily all, they came from the same population in a statistical sense. The constraints used to choose this subset of spectra were very rigid. The wind had to increase to the nominal value from below and not exceed this value prior to the time of the observation. The direction of the wind was not allowed to shift by more than a certain number of degrees prior to the time of the observation. Moskowitz also selected a similar subset of spectra obtained when the winds were near these five different values, but for which the other two very strict criteria were eliminated. It was possible to show that these subsets of spectra did not come from the same population.

The subsets that were shown to come from the same population were called fully developed spectra for the five different wind speeds. It was possible to show that the frequency where the maximum occurred in this subset of spectra shifted toward lower frequency with increasing wind, that the area under the spectra grew as the fourth power of the wind speed, and that the significant wave height, which is defined to be the average of the heights of the one-third highest waves to pass a fixed point on the sea surface, grew as the square of the wind speed.

Kitaigorodskii (1961) had proposed certain non-dimensional properties that wave spectra should have. A special case for fully developed seas, as proposed by Kitaigorodskii, was tested on the data obtained by Moskowitz (1964) by Pierson and Moskowitz (1964). Kitaigorodskii proposed that a non-dimensional spectrum $\bar{S}$ (f) would be a universal function F_1 of a non-dimensional frequency, $\bar{f}$, as defined by equation (2.24).

$$\bar{S}\ (f) = F_1\ (\bar{f}) \tag{2.24}$$

The spectrum would be non-dimensionalized by taking the spectrum as a function of frequency, multiplying by g^3 and dividing by U^5 as defined by equation (2.25).

$$\bar{S}\ (f) = \frac{S(f)g^3}{U^5} \tag{2.25}$$

The non-dimensional frequency, $\bar{f}$, is given by equation (2.26).

$$\bar{f} = fU/g \tag{2.26}$$

When this was carried out, the non-dimensional functions $F_1(\bar{f})$ did not all fall on a universal form. It was realized that the shape of this function was controlled by variations that depended on the fifth power of the wind speed and that the winds over the ocean were not measured with anywhere near that accuracy. By changing the nominal wind speeds mentioned above to 19.5, 25.82, 31.7, 33.6, and 40 knots, the non-dimensional function $F_1(\bar{f})$ was made to agree at its peak. The five different functions then fell fairly close to each other on a linear plot of $F(\bar{f})$ and $\bar{f}$.

Several different functional forms for this function were tried, and, of those that were tried, the one that seemed to give the best

overall agreement, was then transformed back to frequency space. The result was equation (2.27) where $\omega_o = g/U$ and $\omega = 2\pi f$.

$$S(\omega) = \frac{2g^2}{\omega^5} \; e^{-\beta(\omega_o/\omega)^4} \tag{2.27}$$

The wind speed in this equation and the three that follow was measured at a height of 19.5 meters above the sea surface by the weather ships that obtained the wave data.

This spectral form for a fully developed sea has many interesting properties. Three of them are given here. The first is that the frequency at which the spectral maximum, ω_{max} occurs, times the wind speed, is a constant as indicated by equation (2.28). The second is that the significant wave height is given by equation (2.29) where the wind speed is in meters per second and the height is in meters. The third is that the area under the spectrum, m_o, as defined previously, is proportional to the fourth power of the wind speed.

$$\omega_{max} \, U = \text{const} \tag{2.28}$$

$$H_{\frac{1}{3}} = 2.12 \times 10^{-2} \, U^2 \tag{2.29}$$

$$m_o \sim U^4 \tag{2.30}$$

Numerous efforts to verify this equation using other data have been made. There are a number of scientists who do not believe it is right, and there are also a number of scientists who seem to find that this function represents the spectrum of a fully developed wind sea whenever the same requirements are applied that Moskowitz applied originally to the analysis of the data.

It should be pointed out that spectra computed from data from wave recorders that record the rise and fall of the sea surface as a function of time will usually not agree with equation (2.27). Too many things are happening over most parts of the oceans that do not correspond to the conditions imposed in its determination. In general, the wind usually has not blown in the same direction with nearly a constant speed for a long enough time over a large enough area, and other waves have traveled to the area from other parts of the ocean to complicate the wave record and change the spectrum.

The Wind in the Planetary Boundary Layer

When the first two phases of this study were completed, there were four different formulas, similar to equation (2.29), for the height of a fully developed wind sea. One had been proposed by Neumann (1953) and it predicted that the significant wave height grew as $U^{2.5}$. One had been given by Sverdrup and Munk (1947) and it proposed that the significant wave height grew as the square of the wind speed, but with a different constant, and still another one had recently been proposed by Darbyshire (1963). They all gave wildly different results for the significant wave height for different wind speeds. Pierson (1964) recognized the fact, after reading a paper by Charnock (1958), that, first of all, Darbyshire had a calibration error which he had recently corrected and which brought his data into closer agreement with equation (2.29), that Neumann had recorded the winds used in his equation at 7.5 meters above the sea surface, and that Sverdrup and Munk's equation applied to a wind measured approximately 10 meters above the sea surface. The then available equations that represented the logarithmic variation of wind speed with height above the sea surface, and that depended upon a wide variety of different equations for the drag coefficient, were then reviewed. One of the formulations for the drag

coefficient was selected, namely the one given by Sheppard (1958), and all of the formulas were referred to the wind measured at the same anemometer height. The result was quite remarkable. The different equations then agreed fairly well, but not exactly. It is interesting to read the comments of Silvester (1974) on the importance of this particular step in the hand graphical wave forecasting procedures that he has recently developed.

One thing that became clear from this series of studies was that it was extremely important to get the wind speed correct in any numerical computer based procedure for forecasting or hindcasting waves. A twenty percent error in forecasting the wind speed, or for that matter in measuring it at an anemometer height of 19.5 meters, or 55 feet, will produce, if the waves are fully developed, a 20% error in the location of the spectral peak in the opposite sense according to equation (2.28), a 44% error in the significant wave height according to equation (2.29), and a 107% error in the total area under the spectrum.

The solution to this problem of defining the winds more accurately was obtained in the study by Cardone (1969). Given the then available data, which consisted of all of the ships on the ocean reporting the wind speed and direction, the atmospheric pressure at the surface of the ocean, and the air-sea temperature difference, Cardone developed a way to define the quantity, U, for these equations and to give its direction. The procedures are quite sophisticated because the quantity, U, no longer refers to the wind as measured at this elevation, but to the wind that would have been measured has the air-sea temperature difference been zero. If the drag coefficient, which was deduced from the very important study of DeLeonibus (1971)* is defined for a neutral atmosphere, then the wind at 19.5 meters becomes a unique function of the friction velocity, u_*. For stable atmospheric conditions in which the air is warmer than the water, the wind profile will not be logarthmic and for the same u_*, the wind will be higher at this anemometer height.

*Provided to Cardone long before publication of the results.

For unstable atmospheric conditions, and for the same u_*, the wind will be lower at this anemometer height. Or stated another way, for an anemometer height of 20 meters, a wind of twenty meters per second in unstable air can raise higher waves than wind of twenty meters per second in stable air.

Moreover, the angle that the average wind in the planetary boundary layer, that is the wind for the first fifty or a hundred meters above the sea surface, can make with the sea surface isobars can be a complicated function of the gradient wind, the atmospheric stability, and the thermal structure of the air over the water between the surface and the gradient wind level. The analysis techniques developed by Cardone (1969), treat all of these aspects of the problem and not only predict the wind structure in the planetary boundary layer, but also its direction and the vector stress of the wind on the sea surface, as well as the wind at the gradient wind level. It is almost axiomatic that any wave forecasting model that attempts to compete with the model described by Salfi (1974), and does not include at least as sophisticated a wind analysis procedure, as well as a high quality technique for forecasting the winds, will not succeed simply because of the kind of errors that can occur as described immediately above. These procedures developed by Cardone have been incorporated in the numerical forecasting models for forecasting waves for the Northern Hemisphere and in hurricanes. They are a standard part of the analysis of the Skylab data in another program, and they are also a standard part of the proposed procedure for the analysis of the winds in the Seasat-A system presently under development.

Angular Spreading

The research described above used time histories of the rise and fall of the sea surface at a fixed point. There remains the problem of describing which way the waves are going. Given the frequency spectrum $S(\omega)$ and that the wind is blowing steadily in one direction, the question arises as to how the frequency spectrum is spread out over direction, as in the expression $S(\omega, \chi)$. All kinds of techniques have been attempted in order to find out about the angular spreading of an ocean wave spectrum. One attempt was that of the so-called Stereo Wave Observation Project, to be described later as an airborn remote sensing system, and another was the attempt by the scientists at the, then called, National Institute of Oceanography of Great Britian to measure certain properties of $S(\omega, \chi)$ with floating buoys. These buoys measured not only the vertical accelerations caused by the waves but certain properties of the sea surface that caused them to pitch and roll and, in even more sophisticated designs, to respond to the curvature of the sea surface.

It suffices to say here that knowledge of the angular spreading of the wave spectrum is meager indeed and that numerical wave forecasting procedures are built upon a very limited data base for this particular part of their theoretical foundation. What has been done will be described in later sections of this paper.

Several approaches have been attempted. One is defined by equation (2.31).

$$S(\omega,\chi) = \frac{S(\omega)}{\pi}\left[1 + \sum_{n=1}^{\infty} a_n(\omega,u) \cos 2 n \chi\right]$$

$$\text{for } -\frac{\pi}{2} < \chi < \frac{\pi}{2} \text{ and zero otherwise} \qquad (2.31).$$

This equation has the property that it expands the angular variation as an even cosine function of the even harmonics for each frequency ω of importance. Equation (2.31) has the property that the function is defined only between $-\frac{\pi}{2}$ and $\frac{\pi}{2}$ and is zero otherwise. As indicated by the coefficients, which are shown to be functions of the frequency and the wind speed, the shape of the spectra as a function of angle can vary with both wind speed and frequency.

An alternate representation to equation (2.31) is equation (2.32) if the series is truncated at $n = 2$.

$$S(\omega, \chi) = \frac{S(\omega)}{\pi}\left[k_1(\omega, \chi) + k_2(\omega, u)\ \cos^2 \chi + k_3(\omega, u)\ \cos^4 \chi\right] \tag{2.32}$$

In this form, the even harmonics, cos 2χ and cos 4χ, have been expanded in such a way that they can be represented by $\cos^2 \chi$ and $\cos^4 \chi$ with wind speed dependent coefficients. Again the spectrum is defined to be zero outside of the interval from $-\frac{\pi}{2}$ to $\frac{\pi}{2}$. This second representation is a way to show that the spectral resolution of the variance of a quantity cannot yield negative numbers. It has the advantage of showing that the term in the square brackets is everywhere positive.

Another useful way to describe the angular variation of the frequency spectrum is given by equation (2.33).

$$S(\omega, \Psi) = k(P)\ S(\omega)\ (\cos\ \Psi/2))^{P(\omega, u)} \tag{2.33}$$

In this equation, to distinguish it from the previous equations the angular variable is a Ψ instead of a χ. As Ψ varies from $-\pi$ to $+\pi$, the cosine of $\Psi/2$ will range from zero to +1 and back down to zero.

Therefore, this function does not by definition go negative and can be defined over the full angular range. In this representation, the cosine can be raised to any power of P as shown which may even contain a decimal part. This power, or exponent, is still dependent upon both frequency and wind speed. The coefficient K(P) is a normalizing factor such that the integral defined by equation (2.34) yields $S(\omega)$.

In all cases, the integral over the range of definition should yield the frequency spectrum observed by a wave pole recording the passing waves at a fixed point as a function of time as shown by equation (2.34).

$$\int_{-\frac{\pi}{2}}^{\frac{\pi}{2}} S(\omega, \chi)\, d\chi = \int_{-\pi}^{\pi} S(\omega, \Psi)\, d\Psi = S(\omega) \qquad (2.34)$$

One of the theoretical results of the work by Phillips (1957), which succeeded for the first time in showing how winds generate waves, was that the spectrum as a function of angle could be bimodal for the higher frequencies. There was some evidence in the SWOP spectrum that this did indeed occur and that the estimated spectra had two peaks roughly in the direction predicted by the theories of Phillips. However, other work in particular the application of equation (2.31), and a Fourier analysis fit to circles around the SWOP spectrum indicated that these peaks were not very strong and could have been the result of sampling variability. The numerical wave forecasting and hindcasting model described by Salfi (1974) does not include this particular feature of Phillips' theory. When more and better ways to determine the directional properties of ocean wave spectra become available so that spectra of the form of $S(\ell,m)$, or $S(\omega,\chi)$, can be studied, an important problem will be

to find out whether or not these bimodal peaks in the angular spread occur for those cases where the wind is fairly uniform in direction and has blown over a sufficiently large area.

Waves Generated by Wind

Prior to 1957, there was no adequate theory that explained how the wind blowing over the ocean could generate waves. There was an assortment of unsatisfactory theories. One was the sheltering theory; others involved in one way or another the stress of the wind on the sea surface. A stress acting on the sea surface should in principle produce a vorticity field in the water, and it was known that waves were very nearly irrotational as in the assumption made in the derivation of the theory of the waves. Ursell (1956) reviewed all of the available theories of wave generation and concluded that none of them was satisfactory.

The first major breakthrough was by O.M. Phillips, who succeeded in explaining how the turbulent motions in the atmosphere generated waves by means of a resonance mechanism. This was an important concept to bring to bear on the problem because preceeding work had assumed a constant mean wind at each elevation above the surface, and, with this assumption, it is not possible to explain how the initial waves can start from a flat calm ocean. Phillips (1957) recognized the fact that the turbulent eddy structure in the mean air flow had certain components in space and time that could resonate with an induced disturbance in the water and that these turbulent eddies could travel at just the right speed over the surface to produce the pressure fluctuations on the ocean surface that would, in turn, cause the waves to grow. The theory due to Phillips is the resonance theory of wave generation. It predicts certain regions in wave number space where the waves will grow more rapidly than in other regions.

This theory requires knowledge of the turbulent eddy structure in the air over the water. This knowledge has been very difficult to obtain, and, in fact, most of the theories that implement the Phillips mechanism to start the growth of waves over a flat calm use data on turbulent fluctuations obtained over a grassy plot of land obtained by Priestly (1965). Attempts to verify this theory have been partially successful, and it is known that if a given spectral component is followed at group velocity as a function of distance in an offshore wind it will grow for relatively short distances away from the coast according to the values obtained from this resonance theory. The work on this subject was done by Snyder and Cox (1966).

The theory predicts that the spectral component at a given frequency will grow linearly as a function of time. It would require many days for the spectral components in a fully developed wind sea, or for the spectral components in any sea that is observed over the ocean of a height of the order of five to ten meters, to grow to these heights if this were the only mechanism available.

The next part of the problem was solved by J.W. Miles (1957, 1959) in a series of papers on the generation of waves by wind that began with the assumption that a sinusoidal wave was already present on the ocean surface. With a wind profile assumed to be logarithmic according to the then available knowledge of wind profiles over the ocean, it was possible to show that a sinusoidal wave traveling in the wind direction would extract energy from the mean flow in this profile and grow at a rate proportional to how high it was already. These ideas were easily extended to spectra and at the same time the resonance mechanism of Phillips were added as another way that the waves could grow. The result was a differential equation that incorporates the resonance

mechanism and the ability of the wave, once it was generated, to extract energy from the mean wind profile. The constant that determines the growth rate for this part of the theory showed that the energy that was used to make the waves grow came from that height in the profile for which the wind speed equalled the wave speed and depended upon the curvature of the profile at that height. The theory was also extended to describe the properties of the wind near the sea surface and quite interesting flow diagrams as a perturbation of the mean logarithmic profile were obtained.

Theoretical calculations showed that this particular mechanism was most effective for the shorter waves in the wave spectrum and that it was still quite difficult to explain the growth of the longer waves. The last contribution to this problem, in this particular context, was again made by Phillips (1966) who incorporated certain concepts of the eddy structure of turbulence to show how additional energy could be extracted from the mean wind profile and cause stronger growth rates in this expotential mode. The theory of wave generation by wind might be therefore most properly be called the Phillips-Miles-Phillips theory, designating a succession of works that taken as an entity provide an explanation for the growth of waves by wind.

There have been a number of field studies and wind water tunnel studies to try to measure the quantities in the air that these theories predict should occur as the waves grow and to correlate them with the observed growth of the waves. The measurements in the JONSWAP program are directed toward this objective. The research by Shemdin (1969), Shemdin and Hsu (1967) and Shemdin et al. (1972) is an example of experiments in this problem area. The observations do not yield exact agreement with the theories, although some of the research indicates fairly close agreement.

The differential equation that describes these two combined effects is given in a highly simplified form by equation (2.35) where $f = \omega/2\pi$.

$$\frac{dS(f)}{dt} = A(u_*, f) + B(u_*, f)\, S(f) \tag{2.35}$$

Strictly speaking the terms should also be a function of the direction of wave travel relative to the mean wind direction. However, it was necessary in the development of at least the spectral wave model described by Salfi (1974) to treat the growth of the waves in terms of an integration over direction.

The integration of this equation for an initial time, t_o, and an initial spectral value S_o, to a final time t, and a final spectral value S, is indicated by equation (2.36).

$$\int_{S_o}^{S} \frac{dS}{A+BS} = \int_{t_o}^{t} dt \tag{2.36}$$

The solution is given by equation (2.37).

$$S(t) = \frac{A}{B}\left(e^{B(t-t_o)} - 1\right) + S_o\, e^{B(t-t_o)} \tag{2.37}$$

For very small values of $t-t_o$, this equation has a linear growth rate with time given by $A(t-t_o)$, if the initial value of the spectrum is zero. For any reasonable initial value for the spectrum, the right hand side dominates.

At the time that these results were available, not too much was known about the behavior of the quantity, B, but the functional form for A could be estimated from measurements over grass. Inoue (1967)

---

*See Priestly (1959).

studied the variation of the quantity, B, using the same set of data that was published by Moskowitz, Pierson and Mehr (1962, 1963, 1965). These results were then modified to a slightly different equation than (2.35) to describe the growth of a band of frequencies in a wind generated sea given any initial value of the spectrum, S_o, at a particular frequency. This modification simply caused the equation to level off at the value given by the spectrum defined by equation (2.27). In the actual numerical model, if a spectral component has reached 95% of saturation, during the next time step it is filled to saturation instead of approaching this saturated value asymptotically from below as the modified differential equation would require.

To compute the growth of a given spectral component in a finite difference model that attempts to describe the behavior of a wind generated sea, all components traveling within the ± 90° direction are summed. This yields the initial value S_o for that particular frequency. The time t_o is calculated that would be required to reach S_o starting from zero, and then an additional growth due to the time step involved, which is three hours, is computed and added to the spectrum. Certain rules are assumed that spread the growth over direction as governed by the present wind direction.

The wind field over the oceans can be fairly adequately represented on a triangular grid of points spaced approximately 160 nautical miles apart, to define the spatial resolution, by assuming that the values observed and analysed every six hours, last for six hours starting three hours before the observation and ending three hours after the observation. The wind speeds and directions would appear to have a histogrammic, i.e. step and stairs, appearance if

graphed, with both speed and direction changing at, for example, 03, 09, 15, and 21 GMT and being treated constant from 03 to 09, 09 to 15, 15 to 21, and 21 to 03 GMT of the next day.

Since the computation of the wind field is a small part of the total computational effort and since the wave model had a three hour time step, a relatively inexpensive improvement may be possible by specifying the winds every three hours for the initial value update and using forecast winds every three hours for the wave forecasts.

The hurricane wave specification model described by Cardone et al. (1974) and by Cardone, Pierson and Ward (1975) could not use a three hour time step and this simple growth algorithm because of the rapidly changing wind speeds and directions in a hurricane as it moves past a fixed point. One hour time steps were needed on a much denser grid. The rules for partitioning the spectral growth were based on the angular spread of the spectrum on each frequency band and not on the total contribution within $\pm \frac{\pi}{2}$ to the wind direction.

Dissipation

One of the problems of the hand-graphical procedures for hindcasting and forecasting waves is that the concepts of fetch and duration are difficult to apply. The winds over the ocean rarely remain constant in velocity and direction over a large area. More typically, they increase in speed and then decrease again at a given point and change direction from hour to hour. Also, over an area, the winds change direction as one proceeds upwind in order to describe the circulation around a cyclone or an anticyclone. One of the advantages of the computer based numerical models is that they treat each point only as a function of what the wind is at that point so that variations in the wind field from point to point are properly taken care of in the large.

Another very difficult problem for most of the hand graphical techniques has been that of treating the waves that were traveling against the wind. Much of the earlier literature attempted to find out what happened to trains of swell waves that propagated out of a generating area, called a fetch, and across an oceanic area with lighter winds. It was very difficult to detect any changes in the height of the swell, upon arriving at a coastline or a point of measurement, that depended upon whether the swell was traveling against the wind, or with the wind, or through a crosswind as it traversed a given region. Also, in the open ocean the wind changes direction during the passage of an extratropical cyclone and can end up blowing in exactly the opposite direction a day or so later. It is therefore important to be able to treat the effects of waves traveling against the wind. If this were not done, the spectrum of the waves could end up being very nearly isotropic after a computer based model has run for several days.

The computations that model the effect of an opposing wind on a traveling group of waves in the procedures described by Salfi (1974) and Cardone et al. (1974) are based on equation (2.38).

$$\frac{S_{\Delta}(f,\chi)}{S_{o}(f,\chi)} = \left[e^{-690/\sqrt{S_w}\, f^4} \right]^N \qquad (2.38)$$

In this equation the right hand side in the square brackets contains a term, $\sqrt{S_w}$. This represents the square root of the sum of the spectral values in the wave spectrum at that point that are traveling

within ± 90° of the local wind. In turn, this represents the height of the local wind sea and therefore varies roughly in proportion to the square of the wind speed. The expotential damping term then contains a factor times this quantity times the frequency to the fourth power. This states that the higher frequencies in the wave spectrum traveling against this local wind sea are strongly attenuated. A wave with a frequency of 0.1 hertz will be attenuated sixteen times more strongly than a wave with a frequency 0.05 hertz. The term on the left represents the ratio of the spectral component after dissipation to the spectral component at the time of the start of the computation for a three hour time step. The value, N/3, would be used in a one hour time step. The power N on the right hand side varies as a function of whether the spectral component on the left hand side is traveling directly against the local wind direction or at 15, 30, 45, 60, 75 or 90° to the wind direction. The value of N is 7 if the spectral component directly opposes the local wind and decreases to small values at cross wind. This term assures that high frequency waves will not travel very far through a local wind sea if they are traveling against the wind. However, low frequency waves, corresponding to long periods, can travel through a local wind sea. For those portions of the world ocean where the local wind sea is weak, such as in the subtropical highs, the spectral components can travel through this region with negligible attenuation.

A dramatic effect of this particular dissipation algorithm occurs when the warm front sector of a traveling extratropical cyclone is replaced by a cold front sector. In the warm front sector, the winds from the south, for the Northern Hemisphere, generate spectral

components traveling toward the north. They can be fairly high although, in general, the air in the warm air sector is stable and a given measured wind speed at anemometer height will not generate as high waves as the same wind speed in the cold air sector. When the cold front passes, the winds can rapidly shift to the northwest. The waves in the cold front sector advance with the cold front sector because they frequently have a group velocity comparable to the speed of the cold front. Two opposing wave trains centered around directions traveling toward the north and centered around directions traveling towards the southeast then coexist and produce a confused sea, often described in the literature. The mechanism described by equation (2.38) very rapidly attenuates the waves traveling toward the north in such a pattern because the waves behind the cold front are high.

The physical basis for equation (2.38) is quite simple. An equation is found in the literature on waves that describes the dissipation due to molecular viscosity of a sinusoidal wave as a function of its frequency. This equation has simply been broad banded for practical purposes to the concept of the spectral band width and the molecular viscosity has been replaced by an austauch viscosity that depends upon the height of the local wind generated sea.

There have been numerous other mechanisms proposed for the dissipation of spectral wave components traveling against the wind. The generation mechanisms described previously can almost be run backwards to provide a type of dissipation. Another possibility is to quantify the concept of breakers and whitecaps that in turn would produce turbulent motions at the sea surface due to the influx of energy from the atmosphere to the waves once the spectral bands involved become saturated. This breaking mechanism produces the

turbulence that in turn generates the gross-austauch that causes the dissipation of waves traveling against the wind. The work of Ross and Cardone (1974) is a start toward a better way to model this effect of dissipation.

Propagation

For the problem of spectral wave analysis both as a function of frequency and as a function of vector wave number (or frequency and direction) and for the problem of computing the growth and dissipation of waves, the spectral resolution of the computation is not an important consideration. It is not difficult to resolve a spectrum into 50 bands as a function of frequency or into 400, or more bands, as a function of vector wave number in two dimensions. It is not difficult to compute how the spectrum grows or changes at any frequency. However, in computer based numerical models, the number of spectral bands becomes an overriding factor in the problem. The spectral resolution is controlled by the size of the available memory and the grid point spacing, and there is one difficult step in a numerical model that involves treating each component of the spectrum for the entire ocean and propagating it at group velocity. Obtaining an adequate resolution for this propagation step is most difficult. For the models discussed here, and for any other model for that matter, a choice must eventually be made.

The choice that was made is summarized by equation (2.39)

$$S(f_i,\chi_j) = \int_{f_i-\Delta f}^{f_i+\Delta f} \left[\int_{\chi_j-\Delta\chi}^{\chi_i+\Delta\chi} S(f,\chi)d\chi \right] d\, f \qquad (2.39)$$

This equation shows that the spectrum, treated in terms of f instead of ω, is represented by a set of numbers, $S(f_i,\chi_j)$, where the f_i and χ_j represent the center values for each of the bands. For the models described by Cardone et al. (1974), Cardone, Pierson and Ward (1975) and Salfi (1974) there are 312 numbers in the hurricane model and, for practical purposes, 180 numbers in the second model to describe the wave spectrum. A 360 component version for this second model with the spatial grid halved exists but it is prohibitedly expensive to run for an ocean wide scale at the present time on computers comparable to the Univac 1108. For scientific purposes, if absolutely essential, it can be run. Table 2.1 summarizes the frequency bands and the direction bands for the two different models, with the only difference between them being the band width in the angular direction.

The frequency bands are not all of the same width. For purposes of describing the spectrum the frequencies are ordered from 1 to 15 in the order of decreasing frequency. The lowest frequency, numbered 15, is centered on the value, f = 7/180 and has a band width of $\Delta f = 1/180$. The bands from 15 to 7 in this table are given by f = N/180 where N increases from seven to fifteen. Each one has a total band width of f = 1/180, with ½ of this above and ½ below the center frequency as given in the band width table. The next two bands are centered on values of N given by 16.5 and 18.5. They have a band width of $\Delta f = 2/180$. The next two bands numbered 4 and 3 in the table are centered on N = 21 and N = 24. They have a band width of $\Delta f = 3/180$. The band width given for i = 2 is centered on N = 27.5. It has a band width of $\Delta f = 4/180$. The shape of the spectrum is

Table 2.1 Center frequencies, frequency bands and center directions for $S(f_i,\chi_j)$(Full model). $\Delta\chi_j$ is ± 7.5° as tabulated.

	Frequency			Direction			
i	Center frequency	Frequency range	Band width	j	χ_i	j	χ_i
1	none	0.164 to ∞	∞	1	0	13	180°
2	27.5/180	0.142 to 0.164	4/180	2	15°	14	195°
3	24/180	0.125 to 0.142	3/180	3	30°	15	210°
4	21/180	0.108 to 0.125	3/180	4	45°	16	225°
5	18.5/180	0.097 to 0.108	2/180	5	60°	17	240°
6	16.5/180	0.086 to 0.097	2/180	6	75°	18	255°
7	15/180	0.080 to 0.086	1/180	7	90°	19	270°
8	14/180	0.075 to 0.080	1/180	8	105°	20	285°
9	13/180	0.069 to 0.075	1/180	9	120°	21	300°
10	12/180	0.064 to 0.069	1/180	10	135°	22	315°
11	11/180	0.058 to 0.064	1/180	11	150°	23	330°
12	10/180	0.053 to 0.058	1/180	12	165°	24	345°
13	9/180	0.047 to 0.053	1/180				
14	8/180	0.042 to 0.047	1/180				
15	7/180	0.036 to 0.042	1/180				

For the half resolution model j runs from 1 to 12, with values of 0, 30°, 60°, and so on, and $\Delta\chi_j$ ± 15°. For the hurricane model bands for i = 14 and 15 are not needed.

such that larger band widths can be tolerated for the high frequencies. They correspond to quite narrow period ranges.

Because of the rapid response of the very short waves to the local wind, the entire effect of the local wind is contained in the first bandwidth. It is treated to be infinitely wide. It starts at a frequency given by f = 29.5/180 and extends to f equals infinity.

As more has been learned about the response of the short waves to the local wind, this part of the original model has been changed. It can be updated easily to include any new effects of short waves. In particular, the present model corrects the high frequency part of the spectrum according to the Kitaigorodskii form where the spectrum is proportional to a constant times the friction velocity divided by the frequency to the fourth power. Other changes in this area are also easy to apply. For examples, the capillary spectrum that is the high frequency part of the spectrum from f = 5 to f = 30 hertz can be added on according to some of the concepts given by Pierson and Stacy (1973) or as updated in terms of the high frequency information obtained by Mitsuyasu and Honda (1974) as will be done in Chapter 6. In the numerical model, this highest frequency band is instantaneously updated according to the information provided by the wind speed and direction at that particular time step. It is never propogated or dissipated because of this update.

After the above steps have been carried out for the generation of the waves and the dissipation of the waves for a three hour time interval, or a one hour time interval for the hurricane model, the result is a set of tables containing either 180, 312, or 360 numbers. Each number in one of these tables corresponds to a particular fre-

quency band and a particular direction band. If every single number for the same frequency and direction in all of the tables is considered, and thought of as being of graphed or plotted over the ocean, the result is a so-called frequency direction field. For the higher frequencies nearly every point of these fields will have non zero values in directions near the wind direction over the oceanic area involved. For some of the lower frequencies only those portions of the ocean with high winds and regions downwind from those portions with high wind will have numerical values assoicated with a particular frequency direction field. At the end of the growth and dissipation part of the program, the next step is to propagate each of these frequency-direction fields in the direction given for that field at a group velocity given by the center frequency of the frequency band involved.

There are a great many ways to accomplish this particular objective. In an early numerical model developed by Baer (1962) a jump technique was used on a rectangular grid for the North Atlantic Ocean. This rectangular grid has the property that direction is not fully preserved so that upon traveling across the North Atlantic Ocean some of the spectral values will be a grid point away from where they should have ended up on a spherical earth. This early version did fairly well however for an ocean of the size of the North Atlantic Ocean. The model described by Salfi (1974), as based upon the work described by Pierson, Tick and Baer (1966), involves a complicated scheme for propagating these frequency-direction fields. It is based on the work of Baer (1962) and on several reports prepared for this program [Baer et al. (1965) and Baer et al. (1966)].

The basic unit is a triangle on an icosahedron that represents the figure of the earth. Each triangle on the icosahedron is a gnomonic projection centered at the center of the triangle. Within each triangle, therefore, any straight line is a great circle. Waves that are propagated along any straight line therefore travel on a great circle. The problem with this projection is the distortion in the scale, but the propagation algorthms correct for this distorted scale and for the changes of direction for each spectral component with reference to true north as it moves along a great circle.

Problems also arise when the f-D field is moved from one triangle to an adjacent triangle, the direction of spectral component in the second triangular undergoes a substantial change depending upon which way it approaches the line boardering the two triangles. It is necessary to augment each of the triangles by an outer edge of points and to do a substantial amount of interpolation in this outer edge of points in order to propagate the waves correctly across the internal boundaries of the model.

With these added points in mind, and depending upon whether a 24 direction or a 12 direction model is involved, the general description of the program that accomplishes this is that its goal is to cause these different f-D fields to move across the ocean preserving variations in the spectral amplitudes over great distances and causing them to arrive at the various points in the field as if they had travelled at group velocity. For an early study in the propagation of waves at group velocity, Kinsman (1965) has reviewed an analysis carried out by Pierson many years ago concerning what

would happen if a sinusoidal wave with many thousands of cycles were cut off sharply at the front and back and set equal to zero outside of this interval and were then set in motion on a plane ocean. Roughly, the same ideas should hold if the amplitude of such a sinusoidal wave were to vary slowly within the domain in which it was found. For rapid variations, however, more sophisticated analysis might indicate some appropriate changes.

These propagation routines automatically take the effect of fetch into account, since the effect of duration is properly incorporated in the generation part of the computation. As a spectral component moves away from the land a zero moves in from the land and occupies the appropriate offshore grid point at a speed governed by the group velocity of the frequency involved. If the wind continues to blow, the spectral component at this point will be regenerated during the next time step. The combined effect of a sequence of growth, dissipation, propagate repetitions at three hour time steps is that the high frequencies are quickly regenerated near shore and approximate the values given by partially developed fetch limited seas, whereas, the low frequencies which have high group velocities never get to be generated at all except for very low values caused by the A term in the previous equations.

Features of the Model

There are many fascinating features of the numerical wave specification and forecasting models that have just been described. First of all there is no way to observe the 180, 312 or 360, numbers that describe the spectrum at the end of a particular time step at

all of the grid points of the model. Therefore, there is no way to initialize the computation by means of a set of observations of the wave spectra on an appropriate grid. The model is, therefore, not analogous to some numerical weather forecasting models that have enough meteorologically observed parameters for it to be possible to start them up at a certain time based on observed quantities.

This particular model is started up by assuming that the oceans are flat calm everywhere and that all spectral values at a certain time are zero. This is not true. However, after about a week with the winds applied as they happen the spectra at the various points in the model begin to look quite realistic, and, from then on, the spectra computed by the model can be considered to be a fairly adequate representation of the spectra that would have been present at each grid point. If all of the computations are based on an analysis of data containing observed winds and surface pressure fields, then, from this time on, the waves could have been considered to have been specified by the model. The problem of verifying the wave specification aspect of the model then depends upon obtaining enough information about wave spectra at enough points over the ocean to see how well the spectra that are estimated from measurements of waves correspond to the spectra that are generated by the model.

Once the model has settled down at some particular time, say, midnight GMT, the spectra that are specified at this time can then be used as the initial value specification for a wave forecast. The forecasted wind field at six hourly intervals for the next day or so can then be put into the model and used to produce forecast wave spectra for as far as possible into the future. If the forecast procedure is

repeated daily, the wave specified at the end of a certain time interval with observed winds should be stored. Observed winds for the next 24 hour period should be used to update the specification, and then the forecast should be continued from the newly updated values for the next forecast cycle. After many months of operation there will exist fields of forecasted wave spectra and fields of specified spectra for each six hour interval for as many points and times as it is desired to save them. The calculations of the hindcasted waves can serve many useful purposes as a climatological file of the best estimate of what the waves were like over the particular ocean involved, given the best possible analysis of the winds that occurred over the oceans up to and at this particular time.

From the description of these models, it is clear that there are many ways that they can be improved. Just as in the historical development of numerical weather prediction models, these models will be replaced by new models as time goes on. A better explanation of the physics of wave generation may be obtained. The technique for dissipating the waves can be improved. Smaller angular increments and smaller frequency bands may become possible when computers with larger memories and faster input-output times become available. There may be more sophisticated techniques developed to handle narrow bands in frequency and direction then those that have been developed up to the present. For small scale very intense extra tropical cyclones, the area covered by a particular f-D field can be small. The next field for a low resolution model will be traveling at an angle of 30° to the first one, and the next one will be 30° away from that. If these f-D fields propagate a great distance across the ocean they will separate and

there will be gaps between them. For real waves this would not have happened because the spectrum is a continuum in both frequency and direction. An intense storm in the Southern Hemisphere near New Zealand may well produce such widely dispersed packets in these f-D fields by the time they have travelled to the Northern Hemisphere and reached the coast of Alaska that the discritization will completely invalidate the usefulness of the forecast. The routine operation of this model at the Fleet Numerical Weather Facility with attempts to verify it at a variety of points in both the North Pacific and the North Atlantic, along with the studies to be made of data obtained during the Skylab program should provide new information on the value of this low resolution model.

Once a computer based numerical scheme for specifying and forecasting wave spectra over the oceans exists, such a computer model takes on life of its own. The reduced simple version uses for the North Atlantic alone, 94,000 words of main memory and 2,000,000 words of mass storage to accomplish the computations. The output for the North Atlantic for thirty days, giving the spectra every six hours only, takes up one roll of magnetic tape. Within present data capability, it is possible to verify this output at only a selected subset of grid points and for only a selected sequence of times. Since the vector wave number spectra, or directional spectra of the form, $S(f,\chi)$ are rarely if ever observed, the verification of the full information content of the output of the model is not possible. About all that can be verified is the integrals over direction of the spectra which can then be compared with frequency spectra estimated from wave records obtained as a function of time at a fixed point. A particu-

larly valuable data source are those wave records obtained with the Tucker shipborne wave recorder in the deep ocean. The spectra boardering the coastlines of the United States are being saved routinely, and then can be compared, with care because of wave refraction, with spectra from wave records obtained at coastal sites.

WAVE REFRACTION THEORY

Snell's Law and Its Extension

When the water depth is less than one-half the length of the waves, the speed of the waves is changed. Since the frequency of the waves is constant for each spectral component and the speed is decreased, the wave length must shorten. Thus, as waves travel in toward the coast from the deeper water, they slow down in the shallow water, and the lengths of the waves become shorter. The shallower the water, the smaller the speed of the waves.

The speed of a wave in water of constant depth, h, is given by equation (2.40)

$$C = \left(\frac{g}{k} \tanh k\, h\right)^{\frac{1}{2}} \tag{2.40}$$

For very shallow water, the hyperbolic tangent can be represented by the first term in its series expansion, and the speed of a water wave that is in very shallow water compared to its depth is given by equation (2.41).

$$C^2 = gh \tag{2.41}$$

It is interesting to comment that the waves of the tidal motions of the earth and tsunamis are both so long that the ocean is shallow everywhere for these waves, and this equation applies.

For wind generated gravity waves, the depth of the ocean is so great that all of the equations given above in Chapter 2, which were for deep water, apply over nearly all the ocean except near the coast and over the continental shelves of the world's ocean. This complication is particularly important for the North Sea, which is shallow compared to the length of some of the waves that occur and for a band off the east coast of the United States including Georges Bank that extends several hundred miles out to sea. For these areas, the water is shallow compared to the length of the longer waves that can be generated by the winds in intense extratropical cyclones and in tropical cyclones that move northward over the Atlantic Ocean. Since many of mankinds activities take place on the continental shelf, it is important to be able to describe the waves in these regions of shallow water.*

The simplest example of wave refraction is to treat a train of waves traveling from water of one depth across a discontinuous line such that on the other side of this line the depth is shallower. The change in direction of waves then follows the well known laws of optics as described originally by Snell's Law. When these concepts are applied to a continuously varying depth field, the result is that rules and formulas quite similar to those obtained in geometrical optics can be derived.

One of the most important extensions of these ideas were carried out recently by Chao (1972) who showed that it was necessary to treat the effects of a curved earth in wave refraction problems. The width of the continental shelf is large enough so that the waves should be refracted along great circle paths instead of along a

*See Collins (1972) for many aspects of this problem.

straight line on some map projection of the earth. The equations that govern the refraction of waves along great circle paths will not be reviewed here. They can be obtained in the reference cited immediately above . Chao (1971) also solved the problem of the caustic, and Pierson and Chao (1972) tested aspects of this theory for both transient wave groups and monochromatic waves.

In the modern computer based technique for studying wave refraction, the concept of an orthogonal arises. The wave orthogonal is comparable to a light ray and is everywhere perpendicular to the family of wave crests that would represent a simple harmonic progressive wave in deep water. As a family of orthogonals originating in deep water is constructed and caused to travel in towards the coastline, each orthogonal will turn always towards shallower water and in principle will end up perpendicular to the coast at the zero depth contour. In the appropriate part of this paper, the use of photographs and radar images to study wave refraction will be described.

NON-LINEAR ASPECTS OF WAVE THEORY

General Comments

The equations that have to be solved to describe the waves on the sea surface, and under the sea surface, are not linear. To say that a system of equations is not linear, as opposed to saying that another system is linear, is the equivalent of saying that a particular piece of fruit is not a banana. The statement does not tell very much about the extreme complexity of the problem of imposing the boundary conditions at an unknown surface and satisfying the equations that must be satisfied for not linear wave motions. These equations are not linear because they contain squares of unknown functions and products of two different unknown functions that occur in equations

that have to be satisfied at an unknown boundary. The general technique for making headway with such an intractible set of equations is outlined briefly in Neumann and Pierson (1966). Kinsman (1965) treated this problem in great detail and reviewed various aspects of non-linear wave theory. Much more has been done since then. In this report, some of the aspects of nonlinear wave theory are highlighted with particular emphasis on problems that have to do with wave forecasting and with observing waves by means of remote sensing techniques.

The essential point is that the linear superposition of simple harmonic progressive waves, which permits the sea surface to be random, still yields the most realistic pattern for actual waves on the ocean surface. It is possible to add corrections to such a model that bring it into closer reality to the non-linear equations but the ability to do this is somewhat limited at the present time.

Long Crested Periodic Waves

One problem that has received a great deal of attention is the problem of solving the appropriate set of hydrodynamic equations for which the irrotational assumption has been made and for infinite depth under the assumption that the disturbance is a periodic function of space and time, in the strict mathematical definition of the term, periodic. With this strict mathematical definition, perturbation expansions have been carried out to very high order. The results then define a wave profile with sharper crests and shallower troughs than a sinusoid and modify the speed of the wave by increasing it as a function of how high the wave is. Within a linear theory, the speed

of a wave is independent of its height. The assumptions that have to be made to push the perturbation analysis to such a high order are so restricted from the point of view of trying to describe real waves on the real ocean that these solutions, although facinating from the point view of mathematical ingenuity, have little to do with actual waves. The actual waves on the ocean have a continuum of frequencies and directions even for the most narrow band swell.

This problem, however, intrigues the theoreticians, and it is well worth pursuing from the point of view of gaining insight into the nature of the hydrodynamic equations. A most recent example of the kind of thing that can be done is given in a paper by Longuet-Higgins (1973). This particular study maps the domain in which the equations are to be solved into a very interesting polygon, approximates the boundary conditions on the edges of this polygon and determines an approximate solution to the wave profile that is extremely close to reality.

Third Order Non-Linear Interactions

If the linear model consisting of three simple harmonic progressive waves each with a different vector wave number, and therefore an assigned frequency which is a function of that wave number, is considered to exist on a plane ocean, the perturbation expansion of the initial linear model can be carried out in a formalized procedure. At second order, the vector sums and differences of each of the vector wave numbers in pairs becomes involved, combined with the sums and differences of the three different frequencies. The mathematics of the problem yields a term in the denominator of the second order corrections to the linear theory that involves these sum and difference combina-

tions. Phillips (1960, 1961) showed that all of these possible sums and differences could not yield a term in the denominator of the second order perturbation that was zero, and therefore the second order terms were corrections to the first order solutions. However, on continuing the same kind of analysis to third order so that the second order terms again interact with the first order terms, the result is a number of terms with a factor in the denominator described by equation (2.42)

$$F\left(\vec{k}_1,\vec{k}_2,\vec{k}_3,\omega_1\ \omega_2\ \omega_3\right) = g\left|\vec{k}_1\pm\vec{k}_2\pm\vec{k}_3\right| - \left(\omega_1\pm\omega_2\pm\omega_3\right)^2 \qquad (2.42)$$

For certain specific combinations of three vector wave numbers added together as the sums and differences arising from products of trigonometric terms there exists frequencies, again as sums and differences of the three frequencies involved, such that this term is identically zero.

One of the items of faith of those who carry out perturbation schemes is that the higher order terms should turn out to be smaller than the lower order terms. Here, at third order, in a most disconcerting way, one of the many terms at third order, and there are a large number, becomes infinite. This discovery was siezed upon by hydrodynamic theoreticians, and resulted in many dozens of theoretical papers on the general subject of third order nonlinear interactions. The references at the end of this report contain a selected bibliography of results that have been achieved. There have been a few mild dissenters who believe that this singularity can be removed by less drastic assumptions than those that have been made in most of these papers, including the present writer, but they are distinctly a minority, and perhaps even a minority of one. The discussion in

Ocean Wave Spectra between the writer and Phillips summarizes some of these questions.

The phenomenon of third order nonlinear interaction has been used to derive many interesting features of waves. It provides a mechanism for one part of the vector wave number spectrum to interact with another part. This interaction can result in the redistribution of the spectral variance in a spectrum of the form, $S(\ell,m)$ in such a way that one part of the spectrum may grow and another part of the spectrum may shrink. These third order nonlinear interactions suggest for example that a very low spectral value at a low frequency can interact with a high spectral value at a somewhat higher frequency and cause the low component to grow in amplitude by transferring the kinetic and potential energy of the higher frequency component to the lower frequency component. If the concepts of third order nonlinear interactions are applied to a spectrum of the form of equation (2.31) as given above, and allowed to operate for a sufficiently long time, the effect of these nonlinear interactions is to decrease the spectrum in the middle range of wave numbers, or frequencies, increase it for the lowest wave numbers and increase it for the highest wave numbers. Since the highest wave numbers are already, in some sense perhaps, saturated this part of the nonlinear transfer may cause additional breaking for the high wave numbers. The nonlinear transfer will cause the low wave numbers to grow and since these correspond to the longer wave they can be much higher for a given length without breaking.

The problem from a practical point of view with this concept is that the computations are very lengthy and very intricate for the

calculation of how the spectrum changes with time. J.A. Ewing has simplified and parameterized the extensive computation so as to describe the changes in the spectrum that would occur after a certain amount of time has elapsed.*

Changes in a Random Sea

If these concepts are correct, they should be modelled in numerical wave forecasting procedures under the assumption that they have not been implicity modelled by some other aspect of the computational procedure. The difficulty in this context with the models described by Salfi (1974) and Cardone et al. (1974) is that the growth formulation, as based on the work of Inoue (1967), may already have incorporated some of this effect in the growth of the lower frequencies. It would be incorrect to put it in twice. Therefore, any computation of nonlinear interactions will require that they be treated simultaneously with the Phillips-Miles-Phillips mechanism when the waves are growing and that ways to determine each effect separately be developed.

Overshoot and Undershoot

Still another phenomenon attributed by many scientists to these nonlinear interactions is the phenomenon of overshoot and undershoot associated with a wave spectrum that grows as a function of fetch with the winds blowing offshore. Many scientists who have analyzed a series of spectra obtained at increasing distances from a coastline find that the lowest frequencies in the fetch limited spectrum tend to be high compared either to a spectrum given by equation (2.27) or to a spectrum bounded by $\alpha g^2/\omega^5$, and that for frequencies slightly higher than the lowest frequencies, the spectral values tend to be lower than this same nominal function. This often observed feature has been termed

*Personal Communication

overshoot and undershoot and there are numerous papers that attempt to describe it and to explain why it occurs. It might be added here that one of the problems in the interpretation of spectra is the problem of sampling variability and of taking adequate care that such results are not a statistical artifact of the spectral analysis and sampling procedures.

Problems Connected with Extreme Waves

When waves are recorded as a function of time at a fixed point, it is possible to go through the recorded waves and pick out the crest and trough height of successive portions above and below the average of the record. If a minimum between two maxima where the record is positive for the entire length of time involved, and if maxima between minima where the record is negative for the entire length of record involved are ignored, and if the highest of the two maxima for the positive part of the record and the lowest of the two minima for the negative part of the record are added, the results is a wave height. These wave heights will be found to be very nearly distributed according to a Rayleigh distribution.

One of the earliest studies in the probablistic structure of wave records was that of Longuet-Higgins (1952) who derived a theory for the expected value of the highest of N waves to pass a given point as a function of time. The essential result of this theory was that after scaling in terms of the total area under the spectrum, that is, m_o, as defined previously, the expected value of the highest wave out of N waves varied as the logarithm of N. As an example, if the waves were truly stationary in a statistical sense so that the spectrum was invariant and m_o was truly a constant then the highest wave in 1,000

waves would only be expected to be 50% higher than the highest wave in 100 waves. This particular theory has been tested on randomly generated waves in wave tanks and found to hold only up to values of N of about 100 as shown by Loukakis (1970). The highest wave in 1,000 was considerably less than the theory predicted for random waves in a wave tank. (See also Abkowitz (1974)).

In actual fact, as Longuet Higgins showed in his original derivation, the probability density function for the highest wave out of N wave can be found and the 5% chance of exceeding a certain height can be derived as well as many other properties of this distribution including such things as the modal value for the highest wave out of N waves. In numerous applications, the expected value for this highest wave has been predicted and found to yield a remarkable close value to the actually measured highest wave out of N waves.

The highest wave in a wind generated storm sea is probably determined by a combination of the physics of the problem and the probability structure of the model. The physics of the problem enters in extremely complicated ways, when one attempts to consider the extreme waves in a wind generated sea. Aspects of this extremely difficult problem have been discussed recently by St. Denis (1974).

Work that appears to be plowing new ground and developing new insights on this problem is that of Longuet Higgins (1973, 1974). Details of the appearance of a wave crest that is in the process of breaking, plus details on the equations that must be satisfied in the foam patch that rides along on the white-horse are given in these studies. It may some day be possible to set an upper bound on the highest wave in a wind generated sea based on the hydrodynamic

condition that must be imposed near the crest of a wave that is in actuality a summation of a large number of small sinusoids that happen to combine in random phase to produce a high crest at a particular point and time on the ocean surface.

There are perhaps other ways of attacking this problem of extreme waves. Biesel (1952) combined concepts of both the Eulerian and Lagarian equations to define the instantaneous profile of a breaking wave on a beach. The solution was actually triple valued at some point along the beach profile. Stated another way there was water, then air, then water, and finally air again in the vertical direction through the wave profile solution. This is the type of thing that occurs when combers occur on breaking waves as they come in toward the coast. Something similar to this is possible even in the deep ocean. It may be possible to combine Lagrangian and Eulerian concepts in the study of waves on the deep ocean to provide some insight on the extreme waves that can occur.

INFORMATION THEORY, COMMUNICATIONS THEORY, SPECTRAL ESTIMATION, INFORMATION, SAMPLING THEORY, IMAGES, HOLOGRAMS, TIME SERIES, PROBABILITY, STATISTICS, AND ALL SORTS OF OTHER GOOD THINGS.

General Remarks

A delightful chapter in the book by Kinsman (1965) describes the excitement that a neophyte might first experience upon attending a scientific meeting of physical oceanographers specializing in the subject of waves. It is well worth reading to get an idea of the type of jargon that these scientists employ and the overall picture of what a beginner might feel in such a situation.

Although a beginner in the subject of physical oceanography might well be awed at such a meeting, someone first coming to a meeting of the Seasat-A User Agency Working Group would be truly dumbfounded. The jargon at such a meeting is that of many diverse areas of specialization, and, using a kinder word, the technical terms that are freely used in the conversations cover such a gamut of specializations that one can quickly become lost as to the precise meaning of what is being discussed. The situation is probably unavoidable because a spacecraft is a very complicated mechanism and the talents of many different kinds of people need to be used. The lengthy heading of this subsection has in it a large number of terms, some of which arise in these conversations and cause consternation to the various people who attend these meetings.

As one example, in a recent effort to provide guidance on the meteorological applications of Seasat-A, it was necessary to obtain some information about the scatterometer design. It was pointed out to one of the members of this group that the only information we had available was concerned with the marginal distribution of the errors in wind speed and direction and that we needed to study the bivariate distribution of the errors of both wind speed and direction. The word "marginal" upset this scientist quite a bit because his knowledge of the word was the conventional one with the connotation of being "just barely adequate". The distress that was evident was not realized at the time. However, the data were provided, and in due course the report by Pierson, Cardone, and Greenwood (1974) appeared. The joint distribution of the error statistics for both speed and direction for the present scatterometer design based on preliminary

backscatter date was discussed. Later on, as the design was changed, the request was made to repeat this analysis as one of these "other good things" in interpreting the advantages and disadvantages of the revised design. This is a rather simple example of a communication gap in the working of a scientific group on a particular problem.

However, the terms in the above heading are all accepted parts of various aspects of the design of a spacecraft and of the interpretation of wave data. Those involved with communication theory are concerned with recording images or data on magnetic tape and with telemetering that recorded data to a receiver on the earth's surface from a spacecraft. They think in terms of kilobits per second and megabits per second. The adequate transmission of a high quality image of part of the earth's surface, either in color or in black and white with appropriate spectral filters on the imaging system, requires data rates of many megabits per second in order to preserve the details of the image. The precise alignment in two dimensions of the many megabits transmitted to a ground based receiver when reconstituted in the form of a photograph provides an image of the clouds over the earth's surface or rhe equivalent of a photograph of the New York Bight, Long Island Sound, the New Jersey shore and New York City taken from spacecraft altitude, or what have you, depending upon the time that the image was taken. If the information content data stream is distorted, or broken up, the information in the total image is loss. Sandy Hook, for example, might not be located in the right place if the whole system did not function properly. From such an image, scientists who study it derive various kinds of information. For example, J. Apel detected internal waves at the continental shelf in some of the ERTS images.* The cloud images that are available today show lines of high clouds below which apparently heavy

*See Apel and Siry (1974)

snow occurs during the winter in the more northernly states. Analyses of such images will continue and the scientists involved in their analysis are in danger of becoming saturated with too much data for them to assimilate.

There are many aspects of information theory that are useful in the interpretation of wave data either as it is being obtained at present, or as it may be obtained in the future from spacecraft. One of the important aspects of information theory is that there can be too much information obtained and that it is possible to reduce the amount of information required to manageable portions if care is taken in both obtaining the data and in analyzing it. The key to the adequate processing of the wave data that is obtained at present and that will be obtained in the future lies in the areas of probability, statistics, and time series combined with the concepts of sampling theory in such a way that the information obtained becomes manageable.

As an example, in terms of communications theory, a synthetic aperture radar image of waves over the deep ocean covering a square area say 10 kilometers on each side might require, and this is a guess, 50 megabits of data, recorded at 5 megabits per second. As an image, with a 50 meter resolution, this 10 kilometer on a side square area is worth approximately 40,000 numbers or perhaps with a little redundancy, 160,000 numbers. Even these 160,000 numbers are not particularly useful because they represent a pattern that will never be seen again and whose essence needs to be summarized from a sampling point of view in terms of sampling theory based on concepts of probability by means of the application of statistics. If this is done, these 160,000 numbers can be reduced to perhaps 400 numbers which can

be archived along with information on the date, time and latitude and longitude where the original image was obtained. The many megabits of data that had to be transmitted to the earth in order to be processed to recover the image that in turn has to be processed in such a way as to end up with perhaps 400 numbers illustrates the process of coalescing the information in terms of bits into a set of useful numbers, which probably total not more than 6,000 bits.

As an aside one of the advantages of the scatterometer mode is that so few numbers have to be obtained. Each number has a value in terms in the number of bits that are recorded that far exceeds an equivalent number of bits in some sort of imaging system.

An understanding of all of the terms in the above heading, plus many more that follow from them, is essential for an adequate discussion of wave data, how to process it, and how to use it. It is also essential for the design of wave recording instruments, for the analysis of every type of wave record or wave image that can be obtained, and for the understanding of the radar altimeter, synthetic aperture radar, and the scatterometer proposed for Seasat-A.

It is not possible in this paper to treat all of these subjects. Only the essential concepts will be briefly outlined in this section. However, the reader who finds this material difficult should search out and study thoroughly the available texts and references on this complicated subject.

Sampling from a Univariate Normal Probability Density Function

A thoroughly understood area of probability and statistics is concerned with the problem of estimating the parameters that are associated with a univariate normal probability density function. For our application, it can be assumed that the mean, or the average value, of the probability density function is zero. The problem then reduces to estimating the variance.

The first, and most important assumption, of this theory is the assumption of independence. Each and every value sampled from the unknown population, assumed to have this normal distribution and to have some constant variance, is assumed to be independent. In probability theory, this reduces to the statement that the probability density function for each element of the sample is given by, in this case, a normal distribution with a zero average value, or mean, and with the same variance. The probability density function for x_1, x_2, x_3, .. x_n is the product of these n identical probability density functions.

Under these assumptions it can be shown in a variety of ways that the best estimate of the variance, given a sample of size n, is given by equation (2.43).

$$\hat{\sigma}^2 = \frac{1}{n} \sum_{1}^{n} x_i^2 \qquad (2.43)$$

It can also be shown that this estimate of the variance is distributed according to Chi - square with n degrees of freedom. Further analysis of the problem allows one to apply fiducial confidence intervals to

this estimate of the variance. A statement of the form given by equation (2.44) can be made where the quantities a and b are a function of the estimated variance, $\hat{\sigma}^2$, and the sample size, n. This equation makes a statement about the true variance of the normal population σ^2, in terms of two numbers that can be calculated from the information in the sample.

$$P\left(a(\hat{\sigma}^2,n) < \sigma^2 < b(\hat{\sigma}^2,n)\right) = 0.9 \qquad (2.44)$$

It says that the a priori probability that the true value of σ^2 will lie between the values, a and b, is 0.9. Now either the true values actually lies between these two numbers or it does not; it is not a variable, it is an unknown constant. What is meant by this statement is that if this sampling experiment is repeated a number of times with samples of size n, and if the probability on the right hand side, .9, is kept constant, and if the values of a and b are calculated from each observation, then in the long run about 90% of the time the interval, a, b, will contain the true variance of the normal population.

The value, 0.9, can be changed; any number could be calculated. It could be 0.5 or 0.9 or any desired value in between. The closer one wishes to get to certainty, say 0.999 on the right hand side, the greater the distance between the values of a and b on the left hand side for a fixed n.

For a given probability on the right hand side the only way to make the distance between a and b smaller is to take a larger sample. For small values of n like 5, 10, or 15, there is a great deal of spread between the values of a and b, and they come together quite rapidly as n increases to about 50. Once n gets

larger than about 50, if one wishes to decrease the distance between the values of a and b by a factor of 10, compared to the spread for n = 50, it is necessary to increase n by a factor of 100.

For applications such as wave theory, this particular concept can be extended to the degrees of freedom of a spectral band in a wave spectrum. It turns out that 50 degrees of freedom per spectral band are extremely useful for many practical applications, especially if the spectrum is defined by 50 or 60 spectral bands. Five hundred degrees of freedom would be very nice indeed, and provide narrow confidence intervals. Five thousands degrees of freedom would probably be too expensive on a routine basis for the study of waves on an ocean wide scale.

Perhaps the most well known application of sampling theory concepts has to do with the science of taking political polls; especially those polls that indicate the voters' preference on a nation wide scale for president every four years. These political polls employ similar aspects of sampling theory, except that they are based on discreet choices instead of a continuous range of variables and that they are stratified samples, in that the people who are polled are chosen in such a way that they are a representative cross section of the economical, political, religious, and social structure of the United States. If properly taken, such a poll rarely requires more than about three thousand people in its sample, and it is typically good to within one or two percent in the indications of how the nation, at that moment, will vote for the various political candidates.

The Information in a Time History of Ocean Waves

Consider a record of the rise and fall of the water surface as a function of time at a fixed point. This could be a pen tracing in ink on properly calibrated chart paper in which the time on this graph is the horizontal axis and the amplitude of the wave at each instant is graphed on the vertical axis. Such a function might be called $\eta(t)$, and it is a continuous function of time. It can be assumed that the average value of $\eta(t)$ is zero. The recorder could be on continuously for many hours, but let us assume that a 20 minute piece is to be analyzed. The act of taking a 20 minute long piece effectively multiples $\eta(t)$ by a box-car gate function equal to zero outside the interval of observation and equal to one inside the interval of observation. Other functions of triangular form, or shaped like a cosine curve, could also be used as a gating function and the effect on the frequencies in a record could be analyzed. There are many different ways to study such a time history.

An essential property of this function of time is that it must be considered to be a sample in the same sense that the sample of n observation from the normal distribution was a sample in the previous section. There are some essential differences between this time history and the sample of size n from a normal distribution, the most obvious being that the time history is a continuous curve that oscillates above and below some average value with time throughout the entire 20 minutes.

The first piece of information available from such an ocean wave time history is usually obtained by inspection. The chart line

or the ink line representing the wave record has fluctuations in it, and, by inspection, the highest frequency fluctuations recorded by whatever system was used can be determined. Suppose for example, that one can see two fluctuations per second in some of the very fine detail of the record. This means that the maximum frequency is about two cycles per second in the record. These fluctuations may be very small in amplitude but they may still be detectable. A rule originally obtained by a scientist named Nyquist then says that the best way to analyse such a record is to sample at approximately twice the frequency of the highest frequency present, or four times a second. To be safe, it is usually advisable to increase this a little bit, so let us assume that this wave record is read off every 0.2 seconds for the entire 20 minutes. This means that the original function $\eta(t)$ can be converted into six thousands numbers given by $\eta(p\Delta t)$ where p runs from 1 to 6,000 and Δt equals 0.2. The shortest period that can then be determined from these equally spaced readings two-tenths of a second apart is then 0.4 seconds.

A theorem in information theory then says that the 6,000 points read off at these equally spaced intervals can be represented by a Fourier series as given by equation (2.44).

$$\eta(p\Delta t) = \sum_{n=1}^{3000} \left[a_n \cos \frac{2\pi np\Delta t}{1200} + b_n \sin \frac{2\pi np\Delta t}{1200} \right] \qquad p = 1 \text{ to } 6000. \tag{2.44}$$

There are three thousand values of a_n and three thousand values of b_n. The series is summed over the six thousand Fourier terms, and then p is allowed to vary from one to six thousand. If this is done, the theorem from information theory says that the values of η at the times

$P\Delta t$ will all be recovered exactly to within the accuracy of the computations.

The six thousand Fourier coefficients, a_n and b_n, therefore contain the same amount of information as the six thousand values of the time history, except that this information has been transformed from the time domain to the frequency domain.

The advantage of transforming to the frequency domain is that, in the frequency domain, it is possible to disgard the details of these six thousands numbers and end up with a set of fewer numbers that contains the essential information about the wave record. This new set of numbers is the estimate of spectrum of the record. The spectrum resolves the total variance of the record into appropriately chosen frequency bands.

Before proceeding it might be added that the frequencies and periods involved in the above sum are given by equation (2.45) where n varies from one to three thousand.

$$f = \frac{n}{1200} \qquad n = 1,2,3 \ldots\ldots 3000$$

$$\text{or} \quad T = \frac{1}{f} = \frac{1200}{n} \tag{2.45}$$

The periods that correspond to these frequencies are, to name just a few, twelve hundred seconds, six hundred seconds, four hundred seconds, and so on, to one hundred and twenty seconds, and so on, to one hundred seconds, and so on, to twelve seconds, and 11.8 seconds, 11.6 seconds, and so on. The very last period would be 0.4 seconds.

Now if a wave record were constructed from equations (2.6) as the sum of a large number of sinusoids based on a linear theory of waves added together in random phase, with x and y set equal to zero, and if the number of terms in this sum of sinusoids were thought of as being a hundred, or a thousand, or ten thousand times, greater than the number of terms in equation (2.44), and if a piece of such a record was analysed as above, then some interesting things would happen. First of all, the values of a_n and b_n would be normally distributed. They would be equally likely to be positive and negative, the most probable value for any value would be zero, and the expected values of the variances would be given by equation (2.46).

$$E\left(a_n^2\right) = E\left(b_n^2\right) = \int_{f_n-\Delta f/2}^{f_n+\Delta f/2} S(f)\, d\, f \qquad (2.46)$$

$$E\left(a_n\, b_n\right) = 0$$

$$E\left(a_n\, a_m\right) = E\left(b_n\, b_m\right) = 0 \qquad m \neq n$$

Also as indicated by equation (2.46) the expected value for the product for a_n and b_n namely the covariance between two terms at the same frequency would be zero. That is the Fourier coefficients of the cosine and the sine would be independent. Also each term would be independent of all the others; there would be no correlation between any two values of the a's or the b's.

Samples of size one from a normal population are highly variable. The entire concept of estimating the spectra of ocean waves, either as a time history or as a vector wave number spectrum, is simply in-

volved with going from this detailed representation in Fourier space to a simplified representation in Fourier space that discards the details contained in the original set of numbers from the record.

As a first step, we form the sum of squares of the coefficients with the same index as given by equation (2.47)

$$c_n^2 = a_n^2 + b_n^2 \tag{2.47}$$

The values of c_n^2 are distributed according to Chi-square with two degrees of freedom. Another way to state this is that the probability density function for one of these terms when normalized to a unit variance is given by equation (2.48) where $y = c^2$.

$$f(y) = e^{-y}, \quad 0 < y < \infty \tag{2.48}$$

One of the theorems of probability theory is the theorem concerning the way values of Chi-square combine. If the Chi-square estimates all come from a population with the same parameter, Chi-square values compound. For example, the sum of two terms, one from a Chi-square distribution with 5 degrees of freedom and the other from a Chi-square distribution with 10 degrees of freedom will yield a Chi-square distribution with 15 degrees of freedom.

If it is assumed that the underlying physical process that governs the waves is such that the frequency spectra of the waves is slowly varying as a function of frequency so that the values of c_n^2 within a certain frequency range all have nearly the same unknown parameter for their variance, then it is possible to sum the values of c_n^2 over a range of values of n. This is indicated by equation (2.49) for one of many choices,

$$c^2_m = \sum_{n-9}^{n+10} c^2_n$$

$$m = n/10$$

$$n = 10, 30, 50, 70, \ldots\ldots 2990 \qquad (2.49)$$

and the new result is a quantity, c^2_m. In this particular case, we are suming over twenty terms from n equals -9 to n equals +10. If n is given the values 10, 30, 50, 70, and so on up to 990, the result will be 150 values of c^2_m each distributed according to Chi-square with 40 degrees of freedom, under the assumption, of course, that for each band the variability of the spectrum is not too great. If the spectrum is varying markedly over these bands, the actual number of degrees of freedom will be somewhat smaller, but most of the time this particular refinement is not worth taking into consideration in the analysis of ocean wave records. It may be necessary to worry about this complication near the steep forward face of records obtained under fetch limited conditions. The theory for this problem is available. The final result of the analysis of this hypothetical wave record would then be 150 numbers centered on values of f corresponding to n equals 10, 50, 70 and so on. For an alternate way, the first and last values could have half the degrees of freedom of the others and the frequencies could be centered at 0, 20, 40, 60 and so on.

The sample size for present day methods is typically chosen to be some power of two for simplicity of computation so that the so-called fast Fourier transform can be used. Other algorithms now exist for computing fast Fourier transforms where the total number points in the sample is some power of two times some other prime like three or five. There are all kinds of fancy tricks available such as taking a sample just a short of, say 90%, of the length required to yield 2,048 points

---

*The sums of the C^2_n, or the C^2_m, will equal twice m_o. These numbers have to be divided by an appropriate Δf to get the right spectral units.

and filling the rest of the records with zeros, correcting for the true variance and doing the same calculation as before. The result is a very sharp square shouldered spectral window.

The upshot of the analysis described above is of course that the spectral estimates are distributed according to Chi-square with 40 degrees of freedom and that there are 150 bands. It is noted that 40 x 150 is 6,000 which corresponds to the original 6,000 observations in the time history.

The important point of the spectral analysis is that the spectrum changes shape over the various bands. Even if the spectrum is relatively constant over one of these bands, it is quite likely to be ten, or a hundred, times larger in one band then in another band at the other end of the frequency range. It is also possible that for a narrow band swell, only one or two bands would be present and all the others would be zero. Some examples of some very strangely shaped spectra will be given in a later section. This is where the frequency spectra analysis has its greatest power.

If, for example, the six thousand values of $\eta(p\Delta t)$ comprising the original wave record had actually come as a sample of observations of values from a normal population, and if each point had been sampled independently, as discussed in the previous section, then apart from sampling variability, which is always present, the values of the c_m^2 would have come out nearly the same across the entire frequency range. We would have gone to all the trouble of analyzing independent variables as if they had been time correlated and would have ended up with the result that the spectrum was white noise.

In contrast, if $\eta(t)$ had actually been a sinusoid with a given amplitude and with one of the periods given by the equations above,

instead of some value part way between the periods mentioned above, then the entire analysis would have yielded exactly one value of a_n and one value of b_n that was not zero. One extreme of the analysis of a time history is therefore a white noise spectrum and the other is the spectrum of a sine wave with two coefficients that determine the amplitude and the phase of that sinusoidal wave relative to the zero origin in time that was chosen for convenience. Even the sinusoidal wave could be thought of as having had the amplitude of the terms chosen by picking two numbers from a normal population with a zero mean and some assigned variance. A pure sinusoid therefore has 2 degrees of freedom and band limited white noise has the number of degrees of freedom given by the total number of points in the sample, as discussed above. An ocean wave record is always somewhere between these two extremes.

The above statement was of course made with the assumption that nothing foolish was done in either obtaining or analyzing the wave record. For example, under the conditions assumed above, if the entire wave record were taken to be five tenths of a second long and digitized at 500 points, it would not contain any information at all, being a portion of a piece of the side, or the top, or bottom, of one wave of the many that pass the point of observation. Conversely, if the values of a wave record, assumed to last for a long time, were read every 100 seconds, the points would be uncorrelated. Information between the points on the details of the waves would be lost, and these points could be considered to be independent samples from some unknown normal population.

Once the spectral band width is properly chosen and the number of degrees of freedom for that spectral band have been computed on

the basis of the length of the record and the number of points involved, it is possible to compute the total degrees of freedom for the entire record. This is given by equation(2.50)which takes into account the shape of the record.

$$\text{Total degrees of freedom} = (\text{d of f}) \frac{[\Sigma(S(f_i))]^2}{\Sigma[S(f_i)]^2} \qquad (2.50)$$

If the reader tests this formula for, first, the assumption that only one band in the entire 150 is not zero, he will find that the degrees of freedom are those for that band, and second, under the assumption that all of the spectral values are equal, he will find that the total degrees of freedom equals the number of sample points.

A set of 600 points from a 20 minute long wave record obtained by the Tucker shipborne wave recorder usually reduces to the equivalent of 150 independent points as far as the total degrees of freedom are concerned. The confidence intervals on the variance given by the area under the spectrum or by the sum of the squares of the values of the record read at equally spaced time intervals, with reference to a zero mean, can be computed for the number for the degrees of freedom given by equation (2.50) and used in it just as if that number points has been obtained as a sample from a univariate normal population and just as if the points had been sampled independently. By going from the time domain to the Fourier domain and by smoothing, it is possible to account for the correlation between points in a time history and to eliminate this effect in calculating the sampling variability of the wave record.

Also, at the same time, equation (2.44) can be used to calculate the fiducial confidence intervals for each of the spectral estimates

given by c_m^2 in equation (2.49). If these fiducial confidence intervals are placed above and below the estimated spectral values then some idea of the variability of other records obtained nearby or started a little earlier or a little later would be obtained. The wave forecasting and wave specification methods described above can only hope to yield values for the spectra, which in this case are integrated over direction, that would compare with spectra estimated from an actual time history by falling somewhere within the 90% fiducial confidence intervals over most of the range of the spectra most of the time.

Once the total degrees of freedom are estimated, confidence intervals can be computed, and then it is possible to give the 90% confidence intervals on the significant wave height. The significant wave height for a 20 minute long ocean wave record is typically estimated within approximately ± 10 percent. Thus if the significant wave height from a wave record (which is four times the square root of the variance of the record), is computed to be, say, 55 feet, then 9 times out of 10 the true value of the significant wave height for a larger sample obtained in some other way might lie between 49.5 and 60.5 feet.

Some examples of wave specification calculations will be given in Chapter 7. With this particular point in mind, the verification for some of the high waves that pass the oil drilling towers in the Gulf of Mexico is quite astounding. Anything better than that would be impossible because of the nature of the sampling variability problem involved in wave prediction.

Before closing this section on the analysis of an ocean wave record, it might be worthwhile to consider the graph of the brightness of a line scan of a television image being constructed from some remote sensing system on a spacecraft. Even if the picture involved is black and white, and not color, such a line scan will in general not look like an ocean wave record. It will have to change intensity near borders between black and white very sharply and rise practically vertically, for example, at the edge of a cloud. As the lines scan passes through the cloud it will have to decrease nearly vertically on the other side of that edge. For scattered cumulus clouds in the field of view, a particular line scan could look like a series of pulses with various widths, all with nearly the same amplitude. Their spacing would be unequal also, depending upon what part of each cumulus cloud was passed through in the scan. The Nyquist frequency involved in the Fourier representation of a line scan of this nature is entirely different from the Nyquist frequency in the Fourier representation of a wave record. The frequency content in the image, to preserve the sharp corners and the rapid changes in brightness, has to be many orders of magnitude greater for the cloud image than it has to be in the wave record. The times, Δt, at which a record such as this would have to be digitized would have to be extremely close together because 1) a line scan for such an image is accomplished in a fraction of a second and 2) the details to be preserved require that each very small piece of the line must be reproduced exactly. This of course is why, in the transmission of images from spacecraft involving such things as scattered clouds, the data rates get very high.

The contrast to something like the time history of an ocean wave record is quite striking, and, somehow, the advantages of going to a lesser data rate need to be developed in this particular context.

The Information Content of a Two Dimensional Representation of the Sea Surface

It is possible to obtain a representation of the sea surface as a function of two horizontal coordinates at an instant of time. This has been done once in the stereo wave observation program which will be described in a latter section. Such an image will represent either the instantaneously frozen sea surface, or the derivative of this sea surface, or some slightly distorted version of the sea surface, depending upon the technique used to obtain the image.

Equations (2.1), (2.5), (2.6), and (2.7) apply, in which time can be set to zero without any loss of generality. If the sea surface is represented by a derivative in one direction, which for convenience could be the y direction in the equations, then the derivative of equation (2.1) is equation (2.51).

$$\frac{\partial \eta(x,y)}{\partial y} = - a\, m \sin (\ell\, x + m\, y + \epsilon) \tag{2.51}$$

The phase is not critical and the surface so obtained can be represented by equation (2.52).

$$\frac{\partial \eta(x,y)}{\partial y} = \sum_p \sum_q a_{pq}\, m_q \cos (\ell_p x + m_p y + \epsilon_{pq}) \tag{2.52}$$

where

$$a_{pq}\, m_q = m_q \sqrt{2\, S(\ell_p, m_q)\, \Delta \ell\, \Delta m} \tag{2.53}$$

Essentially, looking at the slope of the sea surface amplifies one of the wave number components in a way that is easy to correct for after the spectrum is estimated.

For simplicity in this analysis it will be assumed that $\eta(x,y)$ has been obtained and that this function has been observed over a

square area with the length of a side given by L. The definition of the domain for which this function has been observed is given below, where x and y have been obtained over intervals in space, Δy, Δy, which are equal.

Under exactly similar circumstances to the analysis of a function of time only, the surface defined at this discreet set of points can be represented by a double Fourier sum as indicated by equation (2.54) and the other defining equations given below it.

$$\eta(x,y) \text{ defined for } 0<x<L,\ 0<y<L$$

$$x = 0, \Delta x, 2\Delta x, \ldots, i\Delta x, \ldots L$$

$$y = 0, \Delta y, 2\Delta y \ldots, j\Delta y, \ldots L$$

$$\eta(i\Delta x, j\Delta y)$$

$$= \sum_p \sum_q A_{pq} \cos\left(\frac{2\pi ip\Delta x}{L} + \frac{2\pi jq\Delta y}{L}\right)$$

$$+ \sum_p \sum_q B_{pq} \sin\left(\frac{2\pi ip\Delta x}{L} + \frac{2\pi jq\Delta y}{L}\right)$$

$$i,j = o \text{ to } r$$

$$\ell_p = \frac{2\pi p}{L} \quad p = 0, 1, 2 \ldots r/2$$

$$m_q = \frac{2\pi q}{L} - r/2, -r/2+1, \ldots 0, 1, 2, \ldots r/2$$

where $r = L/\Delta x$, an integer, $\ell = 2\pi/2\Delta x$ (Nyquist wavenumber)

$m = 2\pi/2\Delta y$ (Nyquist wavenumber) (2.54)

As an example, suppose that a square area 10 kilometers on a side is imaged in some way so as to yeild this set of data. Also suppose that Δx is 20 meters. There will then be 501 points along each side of the square, and this number squared yields 251,001 points to define this surface. By the same theorems from information theory, there will be this same number of values of A_{pq} and B_{pq} to define this surface over the square. The transformation from space coordinates to Fourier components is still one to one, and to represent this surface exactly would require the above number of Fourier coefficients. The wave numbers involved, namely ℓ and m_q, range through the values of zero, $2\pi/10^4$, $2\pi \cdot 2/10^4$, $2\pi \cdot 3/10^4$ and so on up to the Nyquist wave number given by $2\pi/40$. The values of m_q range through this same set of wave numbers and through negative values. As one example, for $p = 20$ and $q = 10$ the length of the vector wave number, k, is given by equation (2.55).

$$k = \left(\left(\frac{2\pi 20}{10^4}\right)^2 + \left(\frac{2\pi 10}{10^4}\right)^2\right)^{\frac{1}{2}} = \sqrt{5}\left(\frac{2\pi}{10^3}\right) \qquad (2.55)$$

Just as before the values of A and B can be squared and identified with a point in vector wave number space. For this example, the values of p will range from zero to 250, for a total of 251 possible values and the values of q will range from -250 through 0 to plus 250. There will be a total of 251 x 501 values of the C^2. This exceeds one-half of 25100 by 250 points. This occurs because some of the values along the outer boundary turn out to be duplicates. With a square area with roughly 250 values in the ℓ direction and 500 values in the m direction, both positive and negative, subsquares of ten values on a side can be selected such that a total

of 100 values of C^2 can be summed. The value for these 100 values can then be assigned to the center wave number in two dimensions associated with that square. Other summing techniques will resolve the wave number space into frequency-direction components as described previously, with variable degrees of freedom. However, for a vector wave number analysis the result of summing squares of 10 by 10 wave numbers will yeild 25 wave number components in the ℓ direction and 50 wave number components in the m direction for a total of 1250 spectral estimates. Each spectral estimate would be the sum of 100 numbers and since each number has two degrees of freedom, each spectral estimate would have 200 degrees of freedom. For such a large number of degrees of freedom the 90% interval is 1.18 and 0.85.* The application of time series concepts has thus reduced an original image containing 251,001 points to a set of 1250 numbers. The amount of data that needs to be stored has been reduced by a factor of 200 by throwing away the details of the particular image and going to the essence of its spectrum. A total of 1250 spectral estimates is probably far greater than is needed but it would permit the study of the propagation of swell even if the swell was quite narrow band.

It is of course assumed that in the data taking process the function $\eta(x,y)$ has been filtered in some way so that waves shorter than 40 meters do not appear in the image. The resolution called for the synthetic aperture radar on Seasat-A, for example, implies that all waves shorter than about 25 meters are properly smoothed by the recording technique. The available imagery from various kinds of airborne imaging radar systems all suggest that this indeed has been accomplished. If shorter wave lengths than these are actually

*times the estimate.

present in the image, they will be aliased to longer waves as discussed for example by Blackman and Tukey (1958) and in Neumann and Pierson (1966). It is an advantage for the study of the gravity wave spectrum to have the wave data properly filtered so as not to include the very short waves. If vector wave number spectra can be estimated on a routine basis up to a Nyquist wavenumber corresponding to a wave length of 40 or 50 meters this will be more than adequate for practical applications involving naval architecture, ship motions, the design of platforms, and so forth. The shorter wave lengths on the sea surface can be easily added on to this portion of the spectrum because they are more or less in equilibrium with the local winds over the ocean as the winds vary from place to place with time.

Probability Structure of Wave Records and the Sea Surface

Once a smooth, fairly highly resolved, spectrum of the sea surface, either in vector wave number form or in frequency-direction form, or simply in frequency form for some applications, is available there are a wealth of theories available for the calculation of all kinds of properties of these waves. These theories go back to the classical work of S. O.Rice (1944) entitled "Mathematical Analysis of Random Noise". Except for the frequencies that he was considering, all of the results in this paper apply to either time histories of waves as they pass a fixed point, such as those discussed immediately preceding this section, and to any function of the sea surface observed along a line at an instant of time where one space dimension has replaced the time dimension. Of particular value is the technique that Rice develops for studying the joint probability of the random surface and its derivatives as a function of time. Sections 1.7, 2.1, 2.3, and 2.9 are particularly useful for the study of ocean wave records.

Part three of this important paper has theorems that obtain the expected number of zeros per second in an ocean wave record and the expected number of maxima in an ocean wave record. These quantities, N_o and N_m are given by equations (2.56) and (2.57).

$$N_o = 2 \frac{\left[\int_o^\infty f^2 (S(f))\, df\right]^{\frac{1}{2}}}{\left[\int_o^\infty S(f)\, df\right]^{\frac{1}{2}}} \tag{2.56}$$

$$N_m = \frac{\left[\int_o^\infty f^4\, S(f)\, df\right]^{\frac{1}{2}}}{\left[\int_o^\infty f^2\, S(f)\, df\right]^{\frac{1}{2}}} \tag{2.57}$$

One half of the quantity, N_o, represents the number of zero crossings with a positive slope and its reciprocal can be interpreted to be the "period" of the waves in a very loose sense. This particular result has been misused far more than it has been used correctly. It is quite possible to obtain a value for the average "period" at which the spectrum is zero for the frequency corresponding to that period.

A consequence of the second equation, equation (2.57), is that there are more maxima in a wave record than there are zero upcrossings. This becomes particularly important on transforming from frequency to wave number and looking at the maxima in a function of distance along the line.

Most wave records obtained either as a function of time at a fixed point, or along a line, have been passed through some

kind of a band pass filter. The very low frequencies, or wave numbers, and the very high frequencies, or wave numbers, have both been affected in one way or another by the recording system. Quite frequently the above two properties of the record are determined more by the nature of the band pass filter than they are by the properties of the waves since the very high frequencies, or wave numbers, in the spectrum are weighted very heavily in these expressions. As one example, the spectrum given by Pierson and Moskowitz (1964) in equation (2.27) above has an infinite number of maxima if interpreted strictly in terms of equation (2.57). Asymtomically, in frequency space, the integral in the numerator of equation (2.57) behaves like 1/f for this spectrum, and its integral is of course the logarithm of the frequency and is therefore unbounded when one attempts to evaluate it at plus infinity. In Chapter 6 on the revised elevation, slope, and curvature spectra of a wind roughened sea, it can be seen that it is not proper to apply this spectrum over the full range of frequency and that the number of maxima in a perfect record of the rise and fall of the sea surface would be controlled almost completely by the Mitsuyasu-Honda range and the Cox viscous cut-off range.

Similarly for deep water, the transformation $k = 4\pi^2 f^2/g$, or $k = \omega^2/g$, transforms the frequency spectrum given by equation (2.27) into a wave number spectrum given asymptotically by $\alpha/2\, k^3$. Here, with k substituted for f throughout these equations, the number of zero crossings in a record with such a spectrum would become unbounded. For actual records this of course is not the case, but these equations indicate that care must be used in taking spectral results obtained with any kind of wave recording system and applying indiscriminately the various equations that have been derived to describe such random processes.

Nevertheless, results such as these, and many, many more, have practical applications in many fields. M.S. Longuet-Higgins has extended these concepts to include two dimensional surfaces and written many important papers on the subject of the analysis of both time histories and the sea surface from the point view of a stationary Gaussian random moving surface. In particular, he has treated the way that specular points move about on such a surface, he has derived the expected number of local maxima on a wavy surface, and he has derived equations that describe how the waves appear to move and disappear on such a random surface. The references to this report contain a list of many of his more recent studies. Further material can be obtained by studying all of the references to his work contained, for example, in Neumann and Pierson (1966). This material should be studied quite thoroughly before attempting to do anything in the area that involves the nature of a wavy surface, simply because there is no point in reinventing the wheel. Much has already been done, and these results are ready for application to practical problems in the marine sciences.

Other Methods for the Analysis of Spectra

The ability to compute fast Fourier transforms has only been recently available.* Prior to this time, there had been the concept, many years ago, of doing a Fourier analysis of a time series, but the computational effort for any substantial number of data points was prohibitive. Moreover the problem of sampling variability was not well understood so that when different portions of a time history from the same stationary process were analyzed and the results yielded values that differed markedly at each of the frequencies from one analysis to another, the analysis procedures fell into discard. It was not possible to devise adequate procedure for the analysis of

---

*See Cochran et al. (1967).

time series until these basic features were understood. The concepts necessary for the correct analysis of random processes took quite a few years to develop and culminated in the work of J.W. Tukey as exemplified, for example, in the paper by Blackman and Tukey (1958).

The basic idea was to treat the sample, which was the original record, as if it had been taken from a random process lasting infinitely long by means of multiplying it by a square gate equal to one inside a given time interval and equal to zero outside of it. The covariance function (equation 2.11) of the random process that was sampled was then estimated* by computing the lag products of the digitized values from the sample, after taking due consideration of the Nyquist frequency problem and of aliasing affects. The estimate of the covariance function was truncated in turn by applying a gate in the time domain of the covariance estimate at a time roughly equal to 10% of the length of the original record, or even shorter, as a rule of thumb. The Fourier transform of this much shorter function was then found, and since the covariance function is by definition an even function only the cosine terms had to be found. These already had the squaring effect in them for the c_n^2 values as summed in the fast Fourier transform analysis, given previously. The number of arithmatic operations was greatly reduced by this strategy. The only remaining difficulty for such a procedure was that it applied a spectral window to the estimate of the spectrum that had strong negative side lobes. The "raw" Fourier

---

*All that is ever really available is an estimate of a property of a random process. In statistical theory, estimates are distinguished for population parameters by a "carat" as in the difference between $S(\omega)$ and $\hat{S}(\omega)$. In this report, this convention has not been employed consistently. The context of a particular section can be used to determine whether or not a "carat" is needed over a function.

transform of the truncated estimate of the covariance function yielded negative values at points adjacent to strong peaks in the spectrum. Tukey realized that this was a feature of the spectral window that was produced, and devised a simple running weighted mean of the values obtained in the Fourier transform so as to virtually eliminate these negative side lobes.

The spectral window was in fact a function of the form, $(\sin\Phi)/\Phi$, exactly as found in the discussions to follow of some radar systems except that it was not squared for the variance spectrum. This function has a negative side lobe that was 20% of the amplitude of the main lobe and produced many unfortunate results.

Two running weighted averages of spectral windows of the form, $(\sin\Phi)/\Phi$, were proposed as described by Blackmen and Tukey (1958). One was called hamming and the other was called hanning. The first took 0.54 times a "raw" spectral estimate and added to it 0.23 times the values preceding and following it to obtain a new smooth estimate at each frequency, and the second took 0.50 times a "raw" estimate and added to it 0.25 times the values immediately before and immediately after. Such a procedure can be easily applied over the middle range of the many many frequencies estimated for a spectrum which can frequently contain 50 to 100 bands. Special considerations are required for the zero frequency estimate and the Nyquist frequency estimate, but these are minor details of the analysis procedure. These operations reduce the side lobes to 2% for hanning and well under 1% for hamming for typical spectra. Additional details on these methods can be found in Blackman and Tukey (1958) and in Neumann and Pierson (1966). Not only are these two methods available, but also many other methods that produce slightly different windows have been derived and described in the literature. One window for example, has absolutely no negative

side lobes and therefore provide an estimate that cannot be too low for a given spectral estimate.

For most applications of wave theory, the basic problem is to determine the total area under the estimate of the variance spectrum $\hat{S}(\omega)$ or $\hat{S}(\ell,m)$, as defined for the population by equations (2.12) and (2.15), and to allocate that total area realistically to the various frequencies. If various portions of the spectrum are down from the peak by three or more orders of magnitude, the lower values only become important in such problems as radar backscatter and if one wishes to find out about the slope and curvature of the waves, given the elevation spectrum. For the prediction of the motions of a ship at sea or the behavior of a structure planted in offshore waters such as an oil drilling rig, the parts of the spectrum down by three orders of magnitude are relatively unimportant. Slight variations in the types of windows employed and in the methods of analysis yield slight variations in the spectral estimates that are real in the same sense that slightly different spectral characteristics for the film still produce nearly the same photograph. Numerous papers have been published that compare fast Fourier transform results with the earlier techniques. The spectra differ only in minor details for most practical applications. The result of project SWOP, to be described in a later chapter, for example, used a straight forward extension of the ideas of Blackman and Tukey (1958).

Analogue Techniques

Analogue methods are also possible for the estimation of spectra. Also special function computers that do nothing but invert a matrix or find a Fourier transform are available. Laser holography followed by the use of a densitometer (Stilwell (1969) and others) is a way to recover spectra without extensive (and expensive) computations. A few more checks of these methods by a more careful com-

parison with a digital technique seen advisable. These are some steps along the way in an analogue analysis that may introduce false non-linearities in the final result.

The literature (for example Kasevich et al. (1971), Belousov et al. (1974) and Brown et al. (1972),(1974)) contains numerous examples of holograms of wave images and little, if any, quantitative analysis of them.

DIMENSIONAL ANALYSIS

The dimensional analysis of a physical problem often yields valuable insight as to the best way to solve it. There is a fundamental theorem called the Buckingham PI theorem* that describes the proper way to nondimensionalize a problem. According to the Encyclopaedia Britannica** "The Pi theorem states that, subject to an important restriction, the functional relationship must be expressable in such a form that it contains as arguments only such products of powers of the physical parameters and dimensional constants as have zero dimensions in all the fundamental quantities. The restriction is that there be not more than one independent functional relationship between the quantities."

The last section of this article describes the varying differences of opinion in the usefulness of this theorem. It is pointed out that in the United States, this theorem is thought of as being "an analysis of an analysis" and that in Britain it is given a far deeper meaning as a mechanism for determining some of the physical processes involved in various phenomon.

---

*Buckingham, E. (1915) Nature 96 208, 396 and Buckingham, E. (1921) Phil Mag 42: 696.

**An article by Percy W. Bridgman (1974 edition)

In the study of waves there are a number of standard ways to nondimensionalize the various quantities thought to be important. These are summarized in equations (2.58) through (2.62) for gravity waves. Other nondimensionalizations involving surface tension, vorticity, viscosity, and water depth (if the waves are not in deep water) are also employed.

$$\bar{f} = f/f_m \tag{2.58}$$

$$\bar{f} = fu_*/g \tag{2.59}$$

$$\bar{F} = gF/u_*^2 \tag{2.60}$$

$$\bar{H} = gH/u_*^2 \tag{2.61}$$

$$\bar{t} = u_* t/g \tag{2.62}$$

In (2.58), f_m is the frequency at which the spectrum is a maximum.

In the study of waves, a frequent procedure is to take a large number of frequency spectra obtained under a variety of conditions and transform them all according to equation (2.58) so that the dimensionless $\bar{f}$ for each spectrum, designated by f_m, has the value one. Another procedure is to nondimensionalize the frequency by equation (2.59) which assumes, of course, that what goes on in a particular spectrum is related solely to the wind speed at the time of the measurement of the spectrum. Equation (2.60) is used to compare wave spectra measured in wind water tunnels, in small lakes and other small bodies of water, in bays, and in the open ocean.

Similarly, equation (2.62) which is a nondimensional version of how the long wind has blown over a given area is frequently employed. In this expression, small t is the duration of the wind and $\bar{t}$ is its dimensionless equivalent.

A strong case can be made for the claim that these nondimensionalization procedures often lead to misleading results. For one example, in the work of Phillips (1966), a derivation is given which concludes that, since wind speed was unimportant once the waves had been generated, and since surface tension would not be a factor for gravity waves, and since the duration and fetch could be assumed to be long enough, the spectrum of the waves over a certain wave number range as expressed in polar coordinate form with the angular effects integrated out would <u>have</u> to be of the form given by equation (2.63).

$$S(k) = B/k^3 \tag{2.63}$$

It was further argued that even for capillary waves, the spectrum would <u>have</u> to have this form and that the unknown aspect of the analysis was that the constant, B, could perhaps be different for the capillary wave region of the spectrum compared to the gravity wave region. The analysis was very strongly based on dimensional arguments and on apparently cogent reasons for leaving out some of the physical parameters that are involved in the generation of waves.

If these conclusions are accepted, very little of what has been learned about backscatter from the sea surface and about the behavior of wave spectra could be fitted in to this straight jacket. The fact of the matter is that the spectrum of the waves is very actively dependent upon wind speed for the shorter wave lengths and

that the capillary spectrum cannot possibly be fitted to this form. In Pierson and Stacy (1973), the form of the capillary part of the spectrum was relaxed so as to allow the quantity, B, in this equation to vary with wind speed and called $D(u_*)$ in that paper. Even that was not enough. The more recent work of Mitsuyasu and Honda (1974) shows that this nondimensionalized form cannot possibly describe what is observed in the frequency range from about 5 hertz to 30 hertz, which includes the capillary wave spectrum.

Similarly, although the equilibrium range for the gravity part of the spectrum probably exists over a restricted range of wave numbers, or frequencies, it certainly does not exist over the entire range of possible frequencies, or wave numbers, for gravity waves. In obtaining estimates of the quantity, B, most scientists used a very restricted range of wind speeds. This is not a good way to test whether or not the effect of wind speed can be omitted in the analysis. When an adequate range of wind speeds became available to Stacy (1974), as will be described in Chapter 6, it was found that the frequency range from 0.2 to 0.5 hertz grew by at least a factor of five as the wind speed increased.

When checked against data, if an analysis procedure, or a theory, fails, the theory is wrong, not the data. Theories must stand the test of verification. The difficulty is that these concepts are so ingrained in the procedures for the analysis of wave data that there use continues long past the time when it has been demonstrated that they lead to misleading results.

The real problem though is that spectra, in the form of spectral estimates, are being transformed by means of these non-

dimensional considerations under circumstances that can lead to misleading results, and in such a way that the original data are unrecoverable. If there is something basically different between the spectra of waves recorded in a lake or in a wind water tunnel for high frequencies and high wave numbers, or correspondingly short periods and short waves and spectra of waves on the open ocean for longer periods and longer waves, then results obtained in more limited bodies of water, when extrapolated to open ocean conditions, can prove to be highly misleading. In particular, the spectra for waves measured in a bay containing wave lengths of two, three, or four meters may scale to waves that are much too high for corresponding wave numbers and frequencies on the open ocean. Both the photographs and the data given in later sections of this report substantiate this claim. Much of what is happening in a wave spectrum is strongly wind speed dependent for the shorter wave lengths and shorter periods and cannot be described by these simple nondimensional procedures. One of the equations that follows much later on in this report has been doctored up so as to put it in a nondimensional form and for one other equation an attempt to do this has not even been made. Nevertheless, these equations probably describe the wave spectrum far more accurately than any theoretical derivation of the shape of the spectrum. It behoves the theoreticians to investigate the facts and to attempt to derive theoretical explanations of what is observed instead of continuing to pursue the fallacy that if it was obtained theoretically, it must be right. The strict application of equation (2.68) in an numerical forecasting model especially for light and moderate wind and for partially developed seas will cause an over prediction of the spectrum by often as much as a factor of two at low wave numbers. This then yields an overforecast of the wave heights by as much as a factor of forty percent. Also for hurricane winds in the moderate frequency range this equation results in an underprediction of the wave heights.

Similarly, an analysis of a wave spectrum based on equation (2.58) automatically selects at the peak of the spectrum the estimate that has the greatest error in an absolute sense because of sampling variability. Since it is the highest point in the spectrum, the probability will be high that the estimate is too high compared to the true population parameter spectrum. From then on, the continued analysis of the spectrum on the basis of this equation forces the entire data reduction procedure down a path that must eventually yield inconsistent results. Examples of this kind of thing that can be found in two recent articles by Røren et al. (1975) and by Saetre (1975).

CHAPTER 3 SYSTEMS NEAR THE WATER SURFACE AND ON LAND

DISCUSSION

This chapter treats wave recording systems operated near the water surface. The wave recording system can be either under the water, or mounted in such a way that it intersects the water surface, or mounted on a ship slightly above the water surface, or finally consist of photographs taken from a ship at sea. With the notable exception of the airborne laser altimeter and some new instrumentation recently installed on the NOAA data buoys, which are recently badly needed additions to the methods available for recording waves, the methods described in this chapter are all tried and true and have had a long history of use in the measurement of waves. Information on some of these systems can be found in greater detail in the book entitled "Ocean Wave Spectra" which was published under the sponsorship of the National Academy of Sciences and which reported on the proceedings of a conference held at Easton, Maryland from May 1, through May 4, 1961.

These wave recording systems can be further broken down into different categories. The first category is that of routinely operated systems, which when operated, can serve as the surface truth verification data for presently evolving aircraft and future spacecraft systems. A second category consists of wave recording systems used for scientific research. A primary example of this is the, then called, NIO pitch-roll buoy. Other systems of this nature have been described in the Soviet press and by various Japanese scientists. Finally there are wave recording systems developed specifically for use in wind wave-tunnels as a part of a laboratory study of waves, especially with reference to the very high frequency components of the waves in the short gravity range and capillary range of wave spectra.

ROUTINELY OPERATED SYSTEMS

Pressure Sensors

The first routinely operated system for measuring waves probably consisted of pressure transducers lying on the bottom in shallow water connected by a cable running to shore, which in turn was connected to a recorder that provided a graph of the pressure fluctuations as a function of time. Typically, such pressure transducers had a slow leak so that the signal did not increase and decrease with the tides but such that the signal was responsive to wave periods shorter than about 30 or 35 seconds, if they were present. The historical literature on waves documents the use of such pressure transducers at Lands End, England by Barber and Ursell (1948) for the study of swell propagating towards the British Isles. Such systems were also used by the then-called Beach Erosion Board in the United States, at least at that time and perhaps much earlier.

The pressure at a depth, z, below the surface of the ocean caused by a passing monochromatic simple harmonic progressive wave in water of constant depth, h, is given by equation (3.1).

$$P(x,y,z,t) = -g\rho z + \frac{a\rho g \cosh k(z+h)}{\cosh k h} \cdot \cos(\ell x + m y - \omega t + \epsilon) \qquad (3.1)$$

In this equation, z is measured positive up and at the bottom for water of depth, h, the hyperbolic cosine in the numerator of the second term becomes equal to one because z equals -h. At the surface, where z equals 0 the hyperbolic cosine terms in the numerator and denominator of this expression cancel. The equation is based on linear theory and is thus incapable of saying anything about the

pressure when the pressure is measured out of the water as the sinusoidal wave passes the point of observation. It is, of course, assumed in the derivation of this result that the water is of constant depth, h, everywhere, but this particular assumption is not very critical if the waves are recorded as a function of time at a fixed point where the depth in the area around the point is not varying too rapidly. The problem of wave refraction is of a different scale and pressure records of passing waves at a fixed point can be interpreted, probably without any serious error, by means of this equation.

For water of constant depth h, the wave frequency and the wave number are related by equation (3.2).

$$\omega^2 = g\,k\ \tanh kh \tag{3.2}$$

This equation can be solved for k as a function of ω by successive approximations. Let

$$k_o = \frac{\omega^2}{g} \tag{3.3}$$

where ω is fixed, and let

$$k_1 = \frac{\omega^2}{g} \coth (k_o h) \tag{3.4}$$

and let

$$k_{n+1} = \frac{\omega^2}{g} \coth (k_n h) \tag{3.5}$$

Eventually k_{n+1} will differ from k_n by a negligible amount so that the inverse of equation (3.2) can be written as equation (3.6)

$$k = k\ (\omega; h) \tag{3.6}$$

also tables in the form of the deep water wavelength ($L_o = gT^2/2\pi$) and the ratio of the depth to this wavelength are available from which k can be found.

The pressure signal can be calibrated in units of feet, or meters, of equivalent static water pressure, and if the pressure is measured in such units, it is possible to compute from the bottom pressure record a spectrum with the dimensions of L^2-T. Given such a spectrum, it simply must be multiple by the square of the appropriate hyperbolic cosine as indicated in equation (3.7).

$$S(\omega) = S_p(\omega)\left[\cosh\left[k(\omega, h)h\right]\right]^2 \qquad (3.7)$$

The hyperbolic cosine in the square brackets of equation (3.7) is nearly one for low values of ω and increases quite rapidly for large values of ω, or for large values of kh as indicated.

There is no particular reason why the bottom pressure transducer needs to be located on the bottom; in fact, it could be placed on the top of some underwater structure so that its depth below the surface is some fraction of the depth of the water at that point, say, D. In this particular case, the spectrum of the pressure fluctuation in units of L^2-T could be converted to the spectrum of the waves at the sea surface by multiplying by the two factors shown in equation (3.8). The amplification factor indicated by equation (3.8) would in general be less than the one shown in equation (3.7) and therefore the results would be more satisfactory.

$$S(\omega) = \frac{S_p(\omega)\left[\cosh\ (k(\omega; h)\ h)\right]^2}{\left[\cosh\ (k(\omega; h)\ (h-D))\right]^2} \qquad (3.8)$$

This particular method of recording waves provides an automatic way to determine the Nyquist frequency for the analysis of the pressure

record. The rule involved is quite simple. Those waves with a length equal to twice the depth of the water are hardly sensed by the pressure transducer because the decrease of pressure with depth according to equation (3.1) is such that the fluctuations on the bottom caused by such a wave are extremely small. For simple calculations, the length of a wave in deep water is given by equation (3.9).

$$L = 5.12T^2 \text{ (with L in feet, T in seconds)} \qquad (3.9)$$

As an example, if the depth of the water is 40 feet, the length of the wave involved is 80 feet and any wave shorter than this will hardly be sensed by the pressure recorder. Eighty divided by five is sixteen, and therefore the period of the shortest wave recorded is four seconds, approximately. Given then, a pressure record obtaining in water 40 feet, the Nyquist sampling interval should be two seconds, and no wave period shorter than four seconds, or wave frequencies higher than 0.25 hertz, will be present in the wave record.

An example of the spectral analysis of a pressure record obtained on the sea floor and converted into a free surface pressure record is given by Pierson and Marks (1952). At this time in the history of the study of ocean waves, a number of different scientists had simultaneously recorded waves with a pressure transducer and with a wave pole immediately above the transducer. These two records look quite different. If they are used to compute the average time interval between the zero upcrosses for the pressure record and for the surface record, the result is that the "average period" of the surface waves is considerably shorter than the "average period" of the bottom pressure recordings. Moreover, if the "average period" of the bottom pressure fluctuations is used to calculate the wave height at the surface as if the waves had been

monochromatic the result is always a value that is too low. The result given by equation (2.56) explains this phenomenon. The high frequencies are attenuated quite strongly by the bottom pressure transducer and therefore the average period is high. Only by correcting the spectrum point by point as a function of frequency by using equation (3.4), or (3.5), as the case may be, is it possible to bring about agreement between the properties of the record of the rise and fall of the water surface, as measured, and the properties of the bottom pressure fluctuations, as measured.

In those parts of the world where swell arriving from a distance is very important as opposed to local wind generated seas, the swell frequently occupies a very narrow band of frequencies and the waves can be quite high. In this case the correction of the pressure spectrum to the surface wave spectrum is more or less correct if the "average period" of the waves is used because this value corresponds to something near the center of the narrow band of swell.

Analysis of Bottom Pressure Fluctuations

The results of the analysis of the record of the bottom pressure fluctuations in water 30.5 feet deep is illustrated by figure 3.1 and 3.2 from Pierson and Marks (1952). Figure 3.1 shows the function, $Q(\tau)/Q(0)$, which was evaluated by Dr. H.R. Seiwell at Woods Hole Oceanographic Institution by means of a mechanical autocorrelator. At that time, computing techniques were not very well developed, and it was not possible to do this first part by means of a computer. This function was then transformed using the recently published results of Tukey (1949) to obtain an estimate of the variance spectrum of the bottom pressure fluctuations. The mechanical autocorrelator normalized all values to one at the origin, and it was necessary to calculate the variance of the full record independently. By truncating the estimate

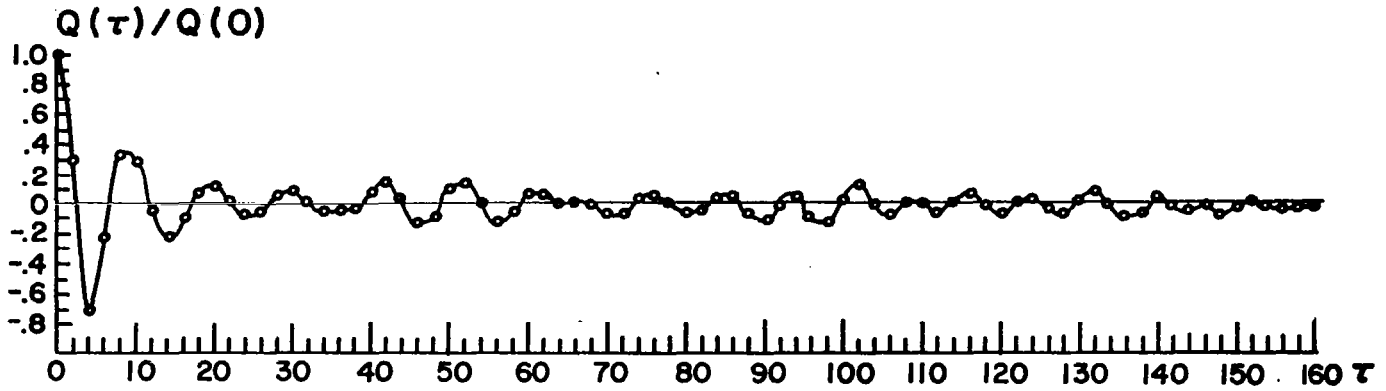

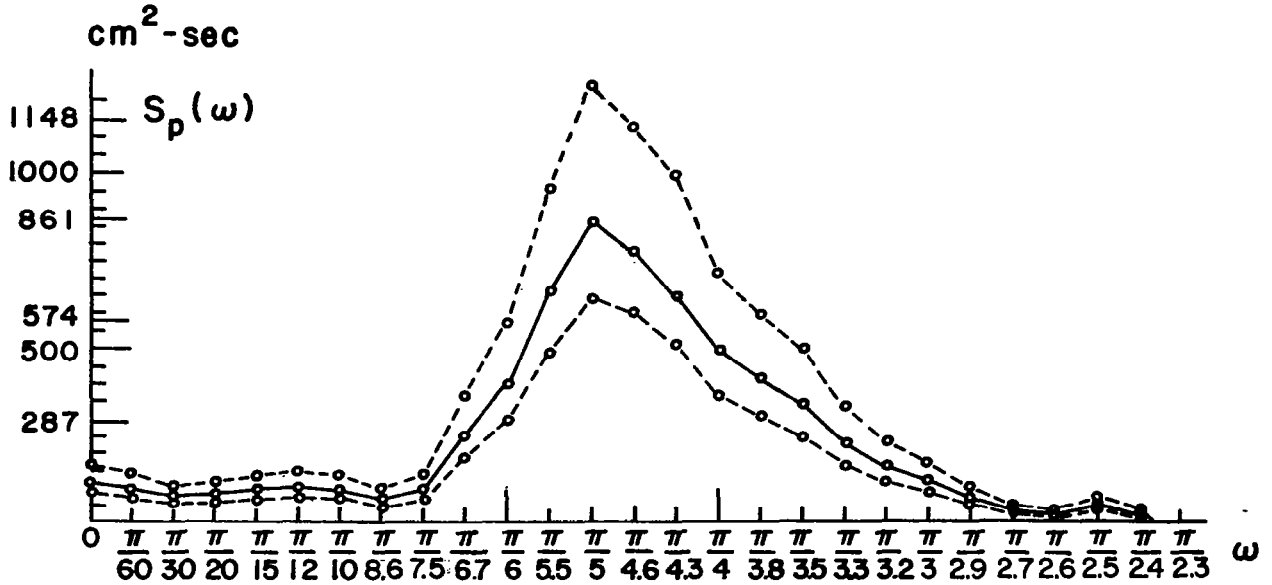

FIGURE 3.1 NORMALIZED COVARIANCE FUNCTION AND ESTIMATE OF THE SPECTRUM FOR BOTTOM PRESSURE FLUCTUATIONS IN WATER 30.5 FEET DEEP. (FROM PIERSON AND MARKS (1952))

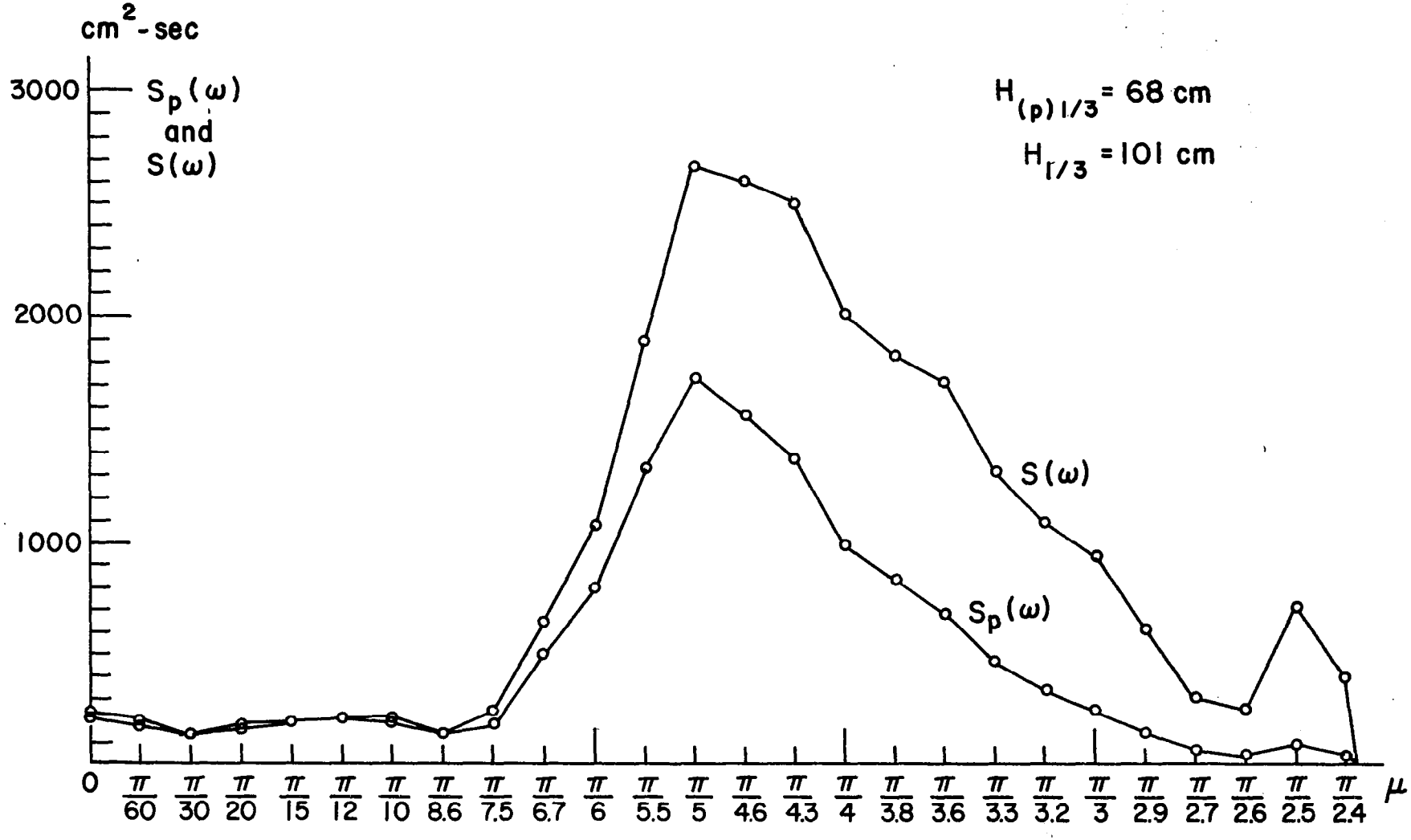

FIGURE 3.2 FREE SURFACE SPECTRUM COMPUTED FROM PRESSURE SPECTRUM. (FROM PIERSON AND MARKS (1952))

of the covariance function at a finite value of τ, the theories developed by Tukey (1949) could be used to obtain the even Fourier cosine transform (see equation 2.12 in the previous chapter) so as to obtain an estimate of the variance of the spectrum of the pressure fluctuations. An important contribution of Tukey was that he realized that a box car window on the function $Q(\tau)$ produced some undesirable side effects in the spectral window in that it was strongly negative to each side of the main lobe. A further smoothing and filtering technique, which was a running weighted average of the raw estimates of the spectrum, was proposed by Tukey and used to obtain the spectrum of the pressure fluctuation as shown on the bottom of figure 3.1. The low values for low frequencies may or may not be real. They may be simply due to digitization errors and errors in the calculation of the covariance function. Most examples done for more recent data do not show any spectral values at these low frequencies, or if they do they are much lower.

Finally the application of equation (3.7) yields the spectrum of the waves at the free surface, and the result of this calculation is shown in figure 3.2. For this particular case the total variance of the pressure fluctuation in units of centimeters squared is given by 300.7 cm^2 and the total variance of the waves at the surface is given by 632 cm^2. This second value correspond to a significant wave height of 101 cm. It is important to note the very strong amplification of the high frequency part of this spectrum and its rather peculiar shape at the very end of the spectral graph. Typically, it and other data analyzed in this same way, has a white noise component at the higher frequencies that can be amplified when equation(3.7) is used so that unreasonable values result.

The Tucker Shipborne Wave Recorder

Another routinely operated system for recording ocean waves is the Tucker Shipborne Wave Recorder as described by Tucker (1956). This particular instrument has been in virtually continuous use on the European weather ships since the time of the publication of the above reference and many hundreds of records have been obtained in various places in the eastern North Atlantic since that time. During SKYLAB for the month of January 1974, the winds over the North Atlantic were extremely high and an area of high winds where the winds exceeded 65 knots (32.5 meters per second) equal roughly to the area of the United States east of the Mississippi occurred and lasted for a number of days. European weather ships on station in the North Atlantic recorded the waves during this period with this instrument for use in the intepretation of S193 data.

The Tucker Shipborne Wave Recorder consists of two pressure sensitive transducers mounted with a water tight seal on each side of the hull of a ship on the inside at a point below the water line. They are provided access to the ocean by means of small holes drilled through the hull plates. The function of these two pressure transducers is to provide the average value of the pressure caused by the height of the water on the outside of the ship above this point. The idea of these two transducer to record that part of the wave motion is that these two signals are averaged before further processing. On the line connecting these two points, which are located several feet behind the bow of the particular ship being used, is an accelerometer. The design of this accelerometer is quite simple, and the signal recorded by the accelerometer is double integrated continuously as a function of time to yield a function that represents

the rise and fall of that point. The signal from the pressure transducer is then added to this doubly integrated acceleration signal and the output is graphed as a function of time on a piece of chart paper. The ships on which these wave recorders are installed are typically quite small, being of the order of 150 to 200 feet long (say, 50 to 65 meters long). When extremely high waves are being recorded, the waves are typically four or five times longer than the ship and the ship rides up and down on these waves and follows the wave profile quite closely. The correction added by the pressure transducer is thus a relatively small part of the total vertical excursion sensed by the ship. If the ship did not move up and down on the waves, it would be flying part of the time and acting like a submarine during the other part of the time. A sample record from this recorder is shown in figure 3.3. The date, time and other pertinent information is also shown on the figure.

The wave record obtained by the Tucker Shipborne Wave Recorder needs to be corrected as a function of frequency. The double integration is not perfect so that some waves are over amplified by the process for some frequencies and others are attenuated. Also, the added correction for the pressure fluctuation due to the shorter period waves is a function of the depth of the pressure transducer on the side of the hull and of other dimensions of the ship. A calibration curve needs to be derived for each ship on which this recorder is installed. The procedures for deriving this calibration curve were given by Cartwright (1963) in the reference mentioned above, namely "Ocean Waves Spectra".

Wave records obtained by this instrument as used on many different ships, have been spectrally analyzed and corrected according

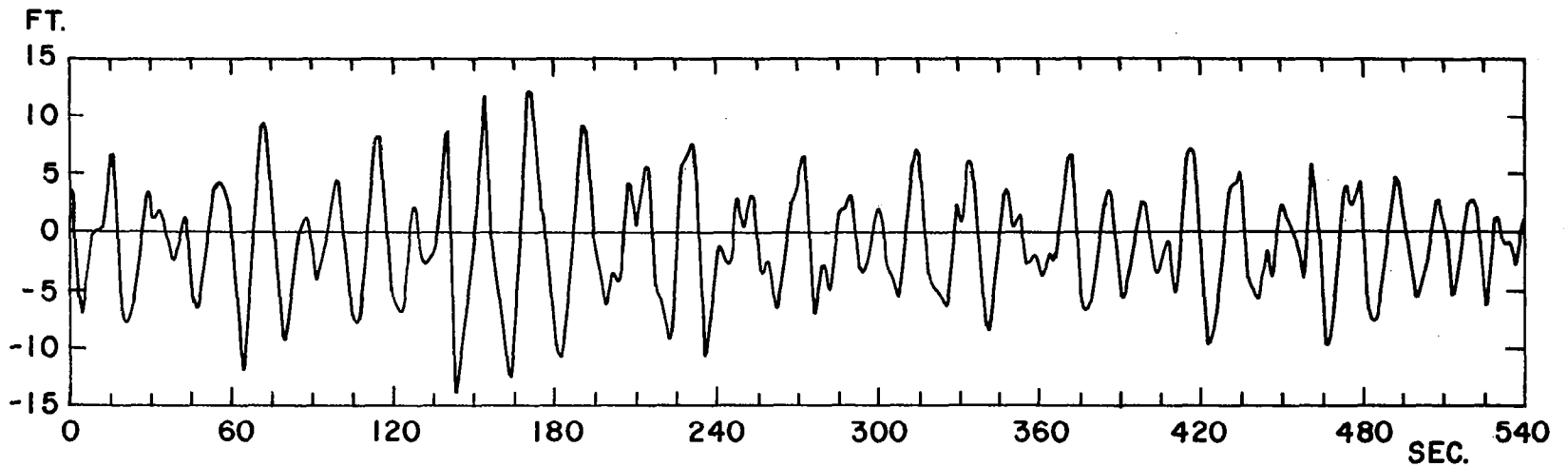

FIGURE 3.3 SAMPLE WAVE RECORD FROM THE SHIPBORNE WAVE RECORDER
0250 GMT 18 MARCH 1956, 45° 15'N, 15°31'W.

to the appropriate calibration curve by many different scientists. Pertinent references are Moskowitz, Pierson and Mehr (1962, 1963, 1965), Ewing and Hogben (1971), M. Miles (1971) and Hoffman (1974). Sample calibration curves for three different ships are tabulated as a function of frequency in Table 3.1 from Miles (1971). It can be noted that a spectrum estimated from a record such as the one graphed in figure 3.3 has to be multiplied by values greater than one for low frequencies, values closer to one for certain intermediate frequencies, and values considerably greater than one as the frequency increases towards the upper range of definition. For the high end of the frequency band typically covered in a spectral analysis of such a record, the amplification factors are very high, and any white noise digitization error in the records can lead to unrealistic values. Most scientists who analyze these records calculate the white noise level at the high end of the band, assuming it to be all white noise and well above some unknown Nyquist frequency. This white noise level is then subtracted from the entire record and the calibration curve given by the above table is then applied. Figure 3.4 and 3.5 shows some examples of spectra calculated from the data obtained by the Tucker Shipborne Wave Recorder. The peak of the first spectrum is at a spectral value of about 50; that of the last one is at 0.07.

Table 3.2 shows a sample from Miles (1971) of the data available from these records. The parameters of records NW 181 to NW 210 are tabulated. The significant height is related to m_o by

$$H_{\frac{1}{3}} = 4\, m_o^{\frac{1}{2}} \tag{3.9a}$$

The values T(-1), T(1) and T(2) are different kinds of "average" period, based on various moments of the spectrum. The K's are related to slope parameters of the spectrum.

Table 3.1 FREQUENCY RESPONSE CORRECTION FUNCTIONS

(from Miles (1971)

		WEATHER EXPLORER	WEATHER REPORTER	WEATHER ADVISER
N	OMEGA	A(N)	B(N)	C(N)
0	0.00	1.0000	1.0000	1.0000
1	0.05	1.0000	1.0000	1.0000
2	0.10	1.0000	1.0000	1.0000
3	0.15	1.0000	1.0000	1.0000
4	0.20	1.4524	1.4245	1.6677
5	0.25	1.3253	1.2787	1.2979
6	0.30	1.2048	1.1442	1.1392
7	0.35	1.1394	1.0622	1.0673
8	0.40	1.1294	1.0303	1.0400
9	0.45	1.1519	1.0256	1.0402
10	0.50	1.1999	1.0405	1.0599
11	0.55	1.2703	1.0584	1.0956
12	0.60	1.3641	1.1107	1.1456
13	0.65	1.4829	1.1635	1.2098
14	0.70	1.6301	1.2307	1.2888
15	0.75	1.8093	1.3103	1.3839
16	0.80	2.0277	1.4046	1.4970
17	0.85	2.2948	1.5162	1.6307
18	0.90	2.6214	1.6470	1.7882
19	0.95	3.0173	1.7979	1.9737
20	1.00	3.5052	1.9751	2.1922
21	1.05	4.1087	2.1830	2.4499
22	1.10	4.8559	2.4256	2.7545
23	1.15	5.7837	2.7084	3.1157
24	1.20	6.9462	3.0409	3.5451
25	1.25	8.4121	3.4329	4.0575
26	1.30	10.2667	3.8940	4.6710
27	1.35	12.6353	4.4413	5.4087
28	1.40	15.6792	5.0934	6.2990
29	1.45	19.6103	5.8701	7.3782
30	1.50	24.7277	6.8016	8.6918
31	1.55	31.4321	7.9219	10.2980
32	1.60	40.2735	9.2728	12.2707
33	1.65	52.0057	10.9108	14.7046
34	1.70	67.7020	12.9024	17.7216
35	1.75	88.8481	15.3343	21.4788
36	1.80	117.4970	18.3199	26.1804
37	1.85	156.6320	21.9977	32.0919
38	1.90	210.5760	26.5521	39.5609
39	1.95	285.3370	32.2142	49.0439
40	2.00	389.2020	39.2524	61.1438

Table 3.2 Sample Data Summary for SBWR Frequency Spectra (Miles (1971))

RECORD	DATE (HR-DY-MO-YR)	H(1/3) (METERS)	CONFIDENCE INTERVAL ON H(1/3) UPPER 95%	CONFIDENCE INTERVAL ON H(1/3) LOWER 5%	T(-1) (SEC)	T(1) (SEC)	T(2) (SEC)	K(-1)	K(1)	K(2)
NW181	12-22-12-61	3.648	4.033	3.300	11.03	9.84	9.12	1.35	1.34	1.35
NW182	12-27-12-61	4.102	4.491	3.748	9.33	8.56	8.11	1.08	1.09	1.13
NW183	12-28-12-61	5.331	5.756	4.938	8.67	7.70	7.23	0.88	0.86	0.88
NW184	12-22- 1-62	9.229	10.285	8.282	11.95	10.62	9.74	0.92	0.91	0.90
NW185	12-28- 1-62	4.551	4.976	4.162	10.58	9.41	8.75	1.16	1.14	1.15
NW186	12-29- 1-62	6.968	7.765	6.252	10.08	9.06	8.45	0.89	0.89	0.90
NW187	12-31- 1-62	10.048	11.315	8.923	11.54	10.03	9.08	0.85	0.82	0.81
NW188	12- 9- 2-62	6.357	7.024	5.753	10.31	9.17	8.48	0.95	0.94	0.95
NW189	12-10- 2-62	13.657	15.170	12.294	12.11	10.13	8.97	0.76	0.71	0.68
NW190	12-11- 2-62	10.084	11.107	9.156	11.42	9.88	8.97	0.84	0.81	0.80
NW191	12-13- 2-62	5.064	5.635	4.551	11.17	10.17	9.50	1.16	1.17	1.19
NW192	12-15- 1-64	5.036	5.553	4.568	9.05	8.00	7.42	0.94	0.92	0.93
NW193	12-20- 1-64	4.739	5.173	4.342	9.29	8.35	7.83	1.00	0.99	1.01
NW194	12-21- 1-64	6.668	7.446	5.972	12.62	11.12	10.11	1.14	1.12	1.10
NW195	12-23- 1-64	3.592	3.975	3.246	11.33	10.29	9.67	1.39	1.41	1.44
NW196	12-24- 1-64	2.427	2.679	2.198	10.62	9.58	8.92	1.59	1.59	1.61
NW197	12-29- 1-64	8.047	8.990	7.203	10.53	9.40	8.68	0.87	0.86	0.86
NW198	12-30- 1-64	11.327	12.772	10.046	12.20	10.82	9.88	0.85	0.83	0.83
NW199	12- 3- 2-64	8.197	9.047	7.426	11.04	9.81	9.09	0.90	0.89	0.89
NW200	12- 4- 2-64	6.332	7.019	5.712	11.00	9.67	8.84	1.02	1.00	0.99
NW201	12- 5- 2-64	2.189	2.400	1.997	9.15	8.30	7.83	1.44	1.45	1.49
NW202	12-26- 7-64	2.926	3.221	2.659	7.90	7.41	7.11	1.08	1.12	1.17
NW203	12-28- 7-64	3.336	3.684	3.022	9.73	8.94	8.46	1.24	1.27	1.30
NW204	12-29- 7-64	1.600	1.744	1.468	8.27	7.63	7.30	1.53	1.56	1.63
NW205	12-30- 7-64	3.804	4.222	3.427	8.79	8.23	7.91	1.05	1.09	1.14
NW206	12- 4- 8-64	3.328	3.712	2.983	8.83	8.17	7.79	1.13	1.16	1.20
NW207	12- 5- 8-64	3.602	4.016	3.230	9.67	8.96	8.50	1.19	1.22	1.26
NW208	12- 8- 8-64	1.337	1.453	1.231	8.09	7.40	7.10	1.63	1.66	1.73
NW209	12-13- 8-64	0.698	0.750	0.650	7.30	6.45	6.13	2.04	2.00	2.07
NW210	12-15- 8-64	1.208	1.305	1.118	6.35	5.83	5.66	1.35	1.38	1.45

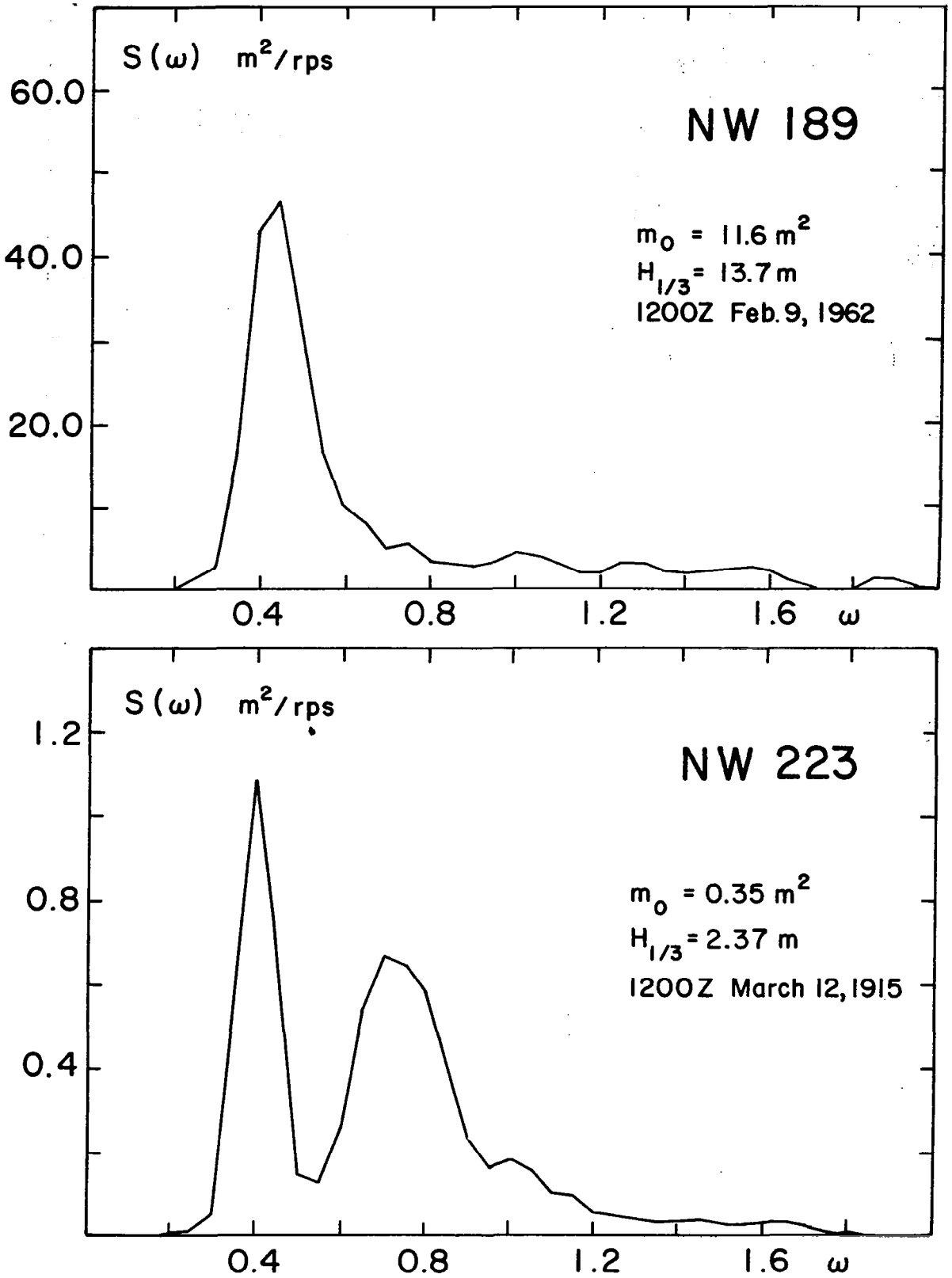

FIGURE 3.4 SAMPLE SPECTRA ESTIMATED FROM TUCKER SHIPBORNE WAVE RECORDER DATA.

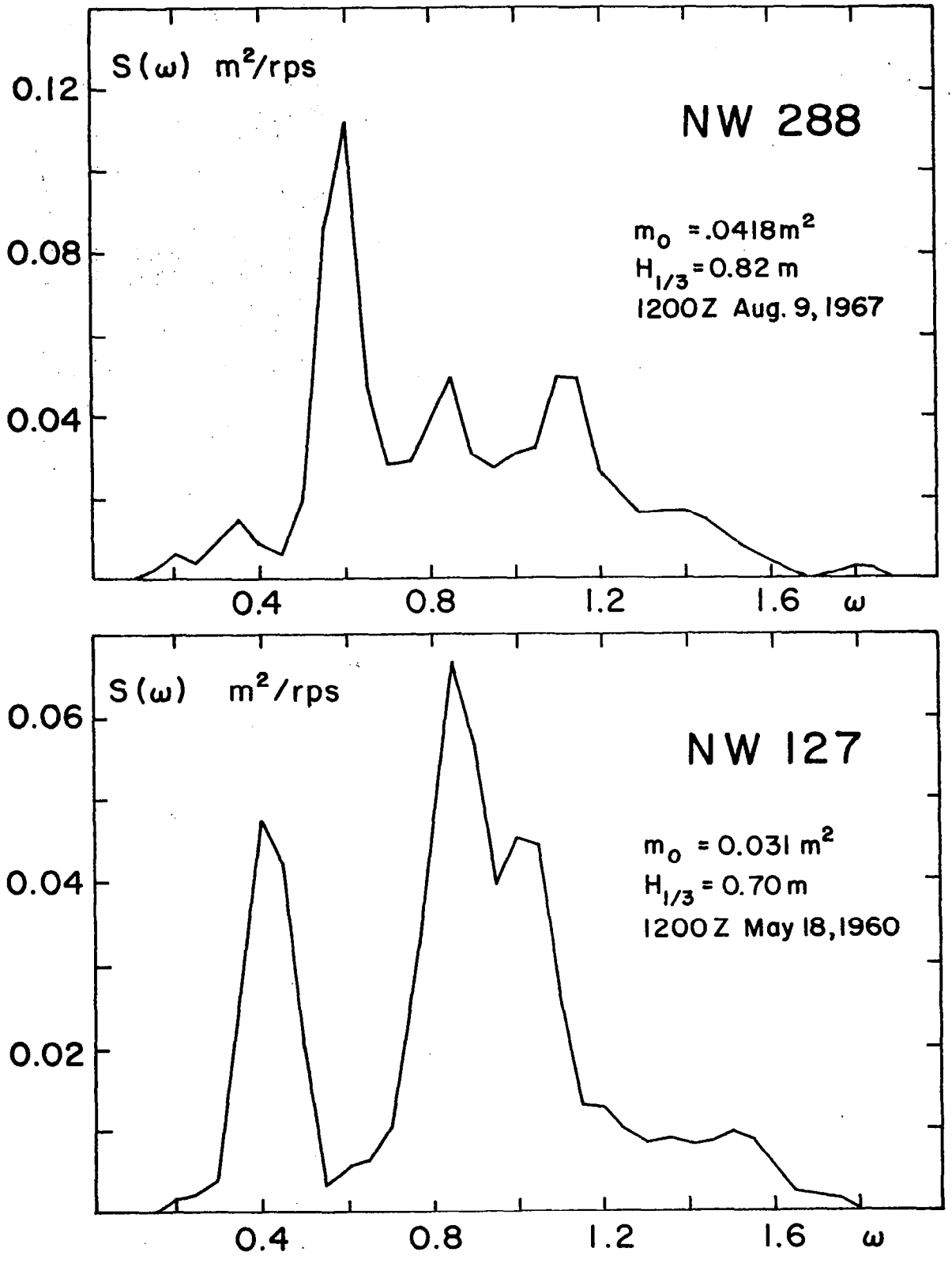

FIGURE 3.5 SAMPLE SPECTRA FROM TUCKER SHIPBORNE WAVE RECORDER DATA

Table 3.3 shows the values of the spectrum for the top record in figure 3.4. The raw spectrum is given by S0, the spectrum minus noise is given by S1, and the spectrum after multiplication by the calibration curve is given by S3.

The data from this instrument have proved to be invaluable to naval architects. Over the years the records for the ten highest sequences observed in a twenty minute interval in the North Atlantic have been assembled and analyzed. The very highest waves had a significant wave height of 55 feet from crest to trough. This implies that one wave in one hundred at that time was 1.5 times that significant wave height, or somewhere near 82 feet from the crest of the wave to the trough of the wave as it passed the weather ship that was recording this train of waves. The probablistic structure of the wave motion for such extremely high waves has been quite well verified by calculating the so-called significant wave height and the highest wave in a twenty minute interval and comparing these values on the basis of these theoretical results obtained by Longuet-Higgins.

The advantages of the Tucker Shipborne Wave Recorder are considerable. It can be mounted on any relatively small ship and waves can be recorded wherever that ship is stationed. The water can have any depth. Typically, the ship is hove to while the waves are being recorded but in principle it could be underway in head seas and record the waves as a function of their frequency of encounter as described in equation (2.19). The calibration problem is somewhat more difficult under these circumstances, however, so that this is not done very often. This particular instrument has yielded a wealth of data on the wave conditions just to the west of the British Isles over a period of almost twenty years. A wealth of

TABLE 3.3 WAVE DISPLACEMENT SPECTRUM (MILES(1971))

1200 Feb. 10, 1962 Ship-Weather Reporter Record No. NW189

Variance- 11.6438 M**2 Sig. Wave Hgt. - 13.6568 M

Noise Level- 0.2993 M**2/RPS CUT-OFF- 0.225 RPS

DOF- 26 Total DOF- 120

T(-1)- 12.1150 sec T(1)- 10.1342 sec T(2)- 8.9675 sec

K(-1)- 0.7650 K(1)- 0.7108

N	W (RPS)	S0 (M**2/RPS)	S1 (M**2/RPS)	S2 (M**2/RPS)
0	0.00	0.0000	0.0000	0.0000
1	0.05	0.0000	0.0000	0.0000
2	0.10	0.0000	0.0000	0.0000
3	0.15	0.0000	0.0000	0.0000
4	0.20	0.0000	0.0000	0.0000
5	0.25	1.4003	1.1010	1.4078
6	0.30	2.6504	2.3511	2.6902
7	0.35	15.6533	15.3540	16.3087
8	0.40	41.8450	41.5457	42.8062
9	0.45	45.7956	45.4963	46.6592
10	0.50	30.0550	29.7557	30.9617
11	0.55	16.2779	15.9786	16.9113
12	0.60	9.2435	8.9441	9.9341
13	0.65	7.0654	6.7661	7.8723
14	0.70	4.2780	3.9787	4.8960
15	0.75	4.4176	4.1182	5.3962
16	0.80	2.6207	2.3214	3.2608
17	0.85	2.1931	1.8938	2.8714
18	0.90	1.9518	1.6525	2.7216

N	W (RPS)	S0 (M**2/RPS)	S1 (M**2/RPS)	S2 (M**2/RPS)
19	0.95	2.0900	1.7907	3.2195
20	1.00	2.4724	2.1731	4.2920
21	1.05	2.0685	1.7692	3.8621
22	1.10	1.5042	1.2048	2.9224
23	1.15	0.9857	0.6864	1.8591
24	1.20	0.8697	0.5704	1.7346
25	1.25	1.1481	0.8488	2.9139
26	1.30	1.0156	0.7162	2.7890
27	1.35	0.6277	0.4234	1.8803
28	1.40	0.6198	0.3289	1.6753
29	1.45	0.6456	0.3320	1.9487
30	1.50	0.6142	0.3281	2.2319
31	1.55	0.6359	0.3062	2.4254
32	1.60	0.5359	0.2040	1.8920
33	1.65	0.3057	0.0569	0.6209
34	1.70	0.2777	0.0000	0.0000
35	1.75	0.2335	0.0000	0.0000
36	1.80	0.2703	0.0000	0.0000
37	1.85	0.3921	0.0455	1.0009
38	1.90	0.3248	0.0309	0.8214
39	1.95	0.2793	0.0018	0.0573
40	2.00	0.3209	0.0008	0.0319

data on wave statistics can be found, for example, in reports by Hogben et al. (1972) and Draper and Squires (1967). The Tucker Shipborne Wave Recorder has also been installed on a ship off the coast of South Africa for a number of years and is currently in use on the weather ships from Canada that occupy weather station POPPA in the North Pacific.

Data Buoys

The February 1975 issue of the "Data Buoy Technical Bulletin" (Volume 1 No. 6) published by the NOAA data buoy office, NSTL, Bay St. Louis, Mississippi contains a description of a modification of the experimental buoys developed by NOAA so that they now provide real time wave spectral data. The article in this technical bulletin describes this system quite completely, and there is little point in paraphrasing it. Therefore, the article is quoted in full below under the heading, "Buoys Now Provide Real Time Spectral Data".

BUOYS NOW PROVIDE REAL TIME WAVE SPECTRAL DATA

"A new experimental wave measuring system was installed on two environmental data buoys in early December 1974. Both EB-01 (deployed in the Atlantic off Norfolk, Virginia) and EB-03 (deployed in the Gulf of Alaska) are 12-meter diameter discus buoys configured to produce, each 3 hours, raw data from which wave spectra are computed. These buoys are equipped with payloads that include an on-board programmable computer. The wave sensor hardware on board these two buoys consists of an accelerometer and a two-stage electronic double integrator

sensor system that produces analogs of acceleration, velocity, and displacement for the vertical heave motion. The on-board computer has been programmed to produce data from which heave displacement spectra are computed. A total of 51 data words associated with measurement of spectra is reported to the Miami Shore Collection Station (SCS) once every 3 hours.

"The instantaneous acceleration analog voltage is sampled each second by the buoy multiplexer and analog-to-digital converter. Readings are taken for approximately 15 minutes; the on-board digital computer processes these samples into 51 autocovariances of acceleration, corresponding to lags of 0, 1, 2 --- 50 seconds. These autocovariances are encoded and relayed to the SCS. They are then partially decoded and relayed to the Data Handling Center at the National Space Technology Laboratories. There, raw spectral densities are produced from the autocovariances, Hanning smoothing is applied, noise corrections are made, and the spectrum is modified to account for the ocean platform transfer function. Finally, the heave displacement spectrum is produced by assuming superposition and operating on each spectral density with ω^{-4}. These computations result in the graphic presentation of spectral density for heave displacement at frequencies of 0.01, 0.02 --- 0.49, 0.50 Hz.

"The performance of these systems has been determined by comparison of the spectra produced by the EB-03 system to spectra produced by a Waverider buoy deployed nearby. Shown below are results of this comparison test, during which EB-03 was not anchored, but tethered to a ship standing by. Other tests have been performed and evaluations are continuing, but all preliminary analyses indicate that the spectral data are excellent.

"Both EB-01 and EB-03 have been producing these spectra each 3 hours since early December 1974. These buoys are being used to test the new measurement concept from both the engineering and operational points of view, with the objective of installing similar systems on future operational buoys.

" —NDBO Contact: K. Steele"

The figure accompaning this article is not produced in this report. However, two different spectra are compared, one from the wave rider buoy and one from the experimental buoy, EB-03. The spectra compared quite favorably. It is hoped that this experimental program will be extended to include the other operational buoys presently on station in the North Pacific, the Gulf of Mexico, and off the east coast of the United States. If this were done, there would be a total of five experimental buoys, two in the Gulf of Alaska, two off the east coast, and one in the Gulf of Mexico that will be able to obtain wave spectra every three hours routinely.

It is noted that these experimental buoys are quite a bit smaller than weather ships and that they probably track the rise and fall of the sea surface quite well at the frequencies involved in the gravity wave spectrum. Thus only minor modifications are required to relate the twice integrated vertical accelerations recorded by the sensor installed inside the buoy to the wave spectrum.

It might also be noted that there have been a number of variations of the basic Tucker principle tested on various ships. A device with a laser on it that sticks out over the bow of a ship can be used to measure the distance between the instrument containing the laser and the surface of the water below. This distance plus the twice integrated motion of the laser then yields a wave record. The problem with this instrument is that the bow of the ship, especially when the ship is under way, may plunge below the surface of an oncoming wave and the entire instrument system may be damaged, or torn completely loose from its mounting, and lost at sea. However, for not too high waves such a system does provide better information on the high frequencies in the wave.

Wave Poles and Wave Wires

Another system for recording the rise and fall of the sea surface as a function of time at a fixed point is a wave pole, or a wave wire. Also pipes with spark plugs sticking out of the side at fairly close intervals have been used. The rising water shorts out these spark plugs as it rises and the signal that is produced is a measure of the position of the last shorted out spark plug. Such an instrument is described by Russel (1963), in the book "Ocean Wave Spectra". These wave poles or wave wires work on a variety of principles. Some sense the change in capacity induced

by the rising and falling of water, others sense a change in resistance. However, the output is simply a graph of the rise and fall of the water at the point involved. For all such systems, the frequency response of the recorder is usually a problem, and there tends to be some roll off at some frequency that in general is not too high. In Chapter 6, when the work of Stacy (1974) is discussed, it is noted that the very high frequency part of the spectra of hurricane waves in the Gulf of Mexico may have undergone some attenuation due to this roll off. Such a recording system has the disadvantage that a fixed platform must be present to install it on. Consequently wave poles and wave wires can only be operated in shallow water. Wave recorders referred to as Baylor gages were installed on oil drilling platforms in the Gulf of Mexico by a consortium of oil companies a number of years ago in order to record the waves generated by hurricanes that passed near by. Later, the same oil companies supported a program to develop a numerical wave specification and numerical wave forecasting procedure for hurricanes in the Gulf of Mexico. In a later chapter of this report, some spectra obtained by these wave recorders and the spectra produced by the wave specification model will be compared.

The Baylor gage is described in a report by Draper and Fortnum (1974). Two models are available. One contains the electronics and transducer in a stainless steel housing that can operate when submerged; the other is more conventional. The wave staff consists of two tensioned steel wire ropes spaced about 9 inches apart and electrically connected to a transducer at the top of the staff. The sea water acts as a short circuit between the two wire ropes and the

transducer measured the a.c. impedance so that the length of the wire above the water surface is known.

The Wave Rider Buoy

The wave rider buoy is a sphere 0.7 meters in diameter. It is weighted to float with a preferred upward direction. An antenna sticks out the top, and the upper portion is transparent so that a flashing light can be seen inside the buoy. The sensing system is an accelerometer that tends to stay vertical as the sphere pitches and rolls on the waves. The sphere is tethered by an elastic line to a submerged buoyant float that produces tension on the anchoring line down to the bottom. It behaves essentially like a small fluid particle of sea water and follows the orbital velocity of the passing waves essentially in circles of varying radius with time. The vertical component of the acceleration of the buoy is recorded and double integrated. The output is therefore a representation of wave elevation versus time in Lagrangian coordinates. To first order, a spectrum from such a record is essentially the same as the spectrum from waves passing a fixed point (see for example Chang (1968)). Of the many commercially available wave recording systems, this one appears to have been very successful. A study by Briscoe and Goudriaan (1974) describes the various ways that the data can be analyzed and shows numerous spectra obtained from the data recorded by this system.

Calibration of Wave Recorders

Draper and Humphery (1973) have compared the calibration of the shipborne wave recorder and the wave rider buoy. One of the problems in calibrating an instrument that senses the vertical acceleration of its motion is that it is difficult to build a device that will ac-

celerate and decelerate the recorder over distances much larger than three meters. The shipborne wave recorder and the wave rider buoy have been calibrated for simulated waves of about three meters in height, but this did not demonstrate the full capabilities of these recorders which are frequently used to measure much higher waves. In order to simulate waves of much greater height arrangements were made to use the "Big Wheel" Ferris wheel, or merry-go-round, at South Sea Fun Fair. This Ferris wheel has a diameter of 14 meters and could be rotated to give simulated wave periods from about 13.6 seconds to 30 seconds. The accelerometer part of the shipborne wave recorder and the wave rider buoy were fastened to a seat of the Ferris wheel and the Ferris wheel was rotated at various speeds, as rapidly as 13.6 seconds per rotation. The output of the recording system should be, after double integration, a sinusoid with height given by the diameter of the wheel after correction for known calibration effects.

The conclusions of this study were essentially that both instruments function as predicted except that the shipborne wave recorder response was better for long periods than had been theoretically calculated and that a slight correction to the previous calibration for long period waves might be made under certain circumstances in analyzing the data. The errors in the measurement of the waves as a function of the frequency spectrum are very small indeed compared to the problems of sampling variability for the data. The two systems can be considered to have been thoroughly calibrated by these techniques and by the studies that had been carried out previously.

Other Wave Recording Systems

The problem of routinely observing ocean waves under a variety of environmental conditions has been discussed by Draper (1970), and Draper and Fortnum (1974) have published a list of wave recording systems available from commercial manufacturers. Approximately 44 systems are described in this reference. Some of them are easily available. Others are difficult to obtain and require lengthy lead times before delivery. Some of the systems are for measuring waves in laboratories only, but the total list describes just about everything available for recording waves essentially as a function of time at a fixed point. One system is described that has the potential of measuring wave direction. It would work for very short waves only and not for typical storm seas on the continental shelf.

PHOTOGRAPHS FROM SHIPS

Photographs from ships have been a recognized way to study waves for many years. Shumacher (1928, 1939) published the results of the analysis of stereo pairs of photographs obtained on the Meteor. Also, cameras looking out to the side have been installed on the bow and stern of an aircraft carrier and used to obtain profiles along the wavy surface at a fixed distance from the ship as described for example by Pierson (1952). Although quantitative techniques of this nature can provide information on the heights of a few waves, the field of view is not extensive enough to permit the recovery of either a one dimensional wave number spectrum or the full vector wave number spectrum.

Ordinary photographs taken from a ship at sea are valuable in providing information on waves at least of a qualitative nature. The Meteorological Branch of the Department of Transport in Canada has published photographs obtained by the Canadian Weather Ship POPPA on station in the North Pacific Ocean. The weather station is actually continuously occupied, and these photographs were taken by means of the Ocean Weather Ships, C.C.G.S. St. Catherines and C.C.G.S. Stonetown. A selected subset of these photographs is reproduced here by means of figures 3.6 through 3.13. They illustrate a very important feature of a wind roughened sea.

The first photograph was taken on 5 June 1960 at 2340 GMT. The wind was calm at that time. Two hours and forty minutes earlier it had been one knot and at eighteen hundred GMT that day, it had been three knots. Prior to that, it had fluctuated around values

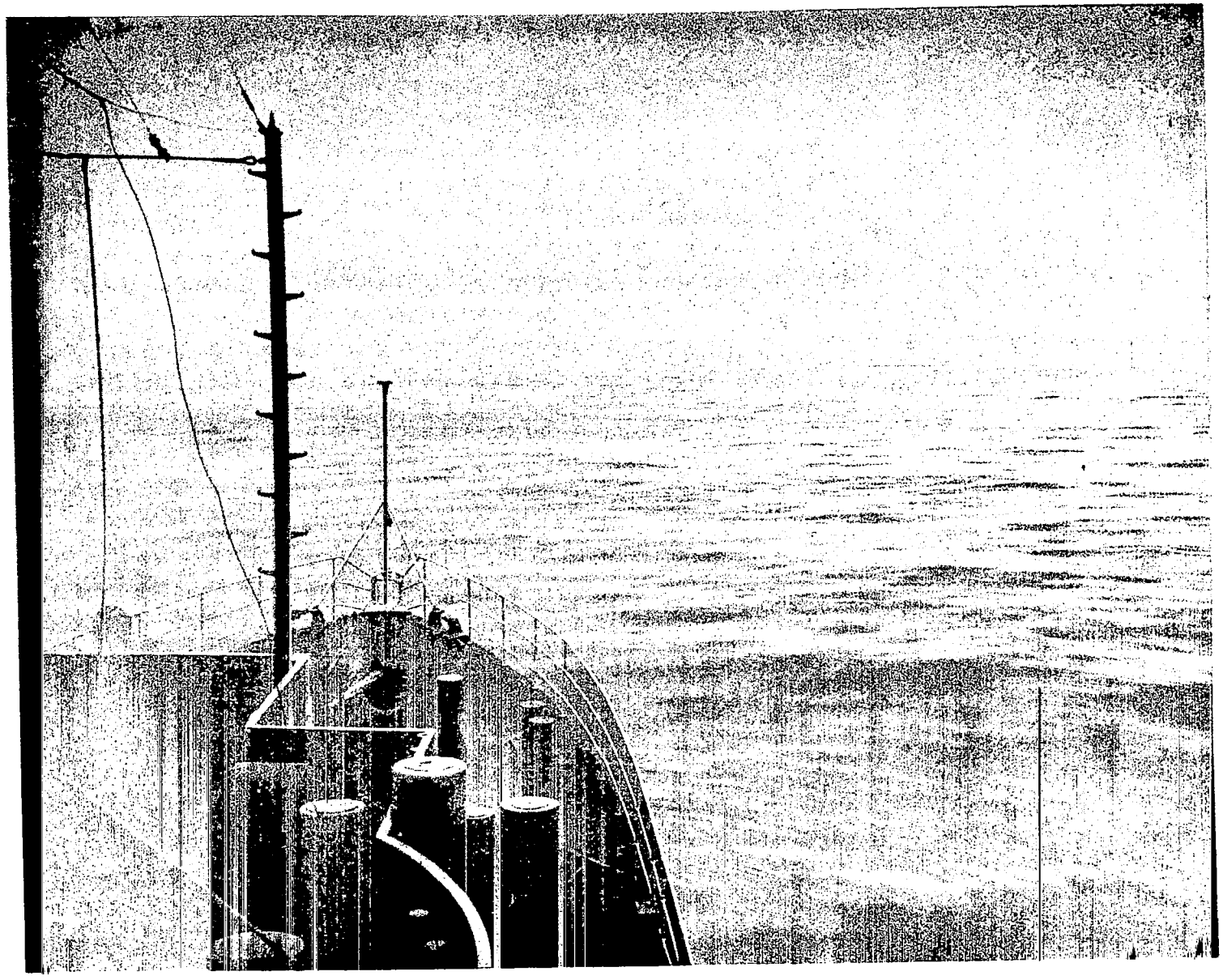

FIGURE 3.6 BEAUFORT FORCE 0, WIND CALM, WAVE HEIGHT 2 FEET.

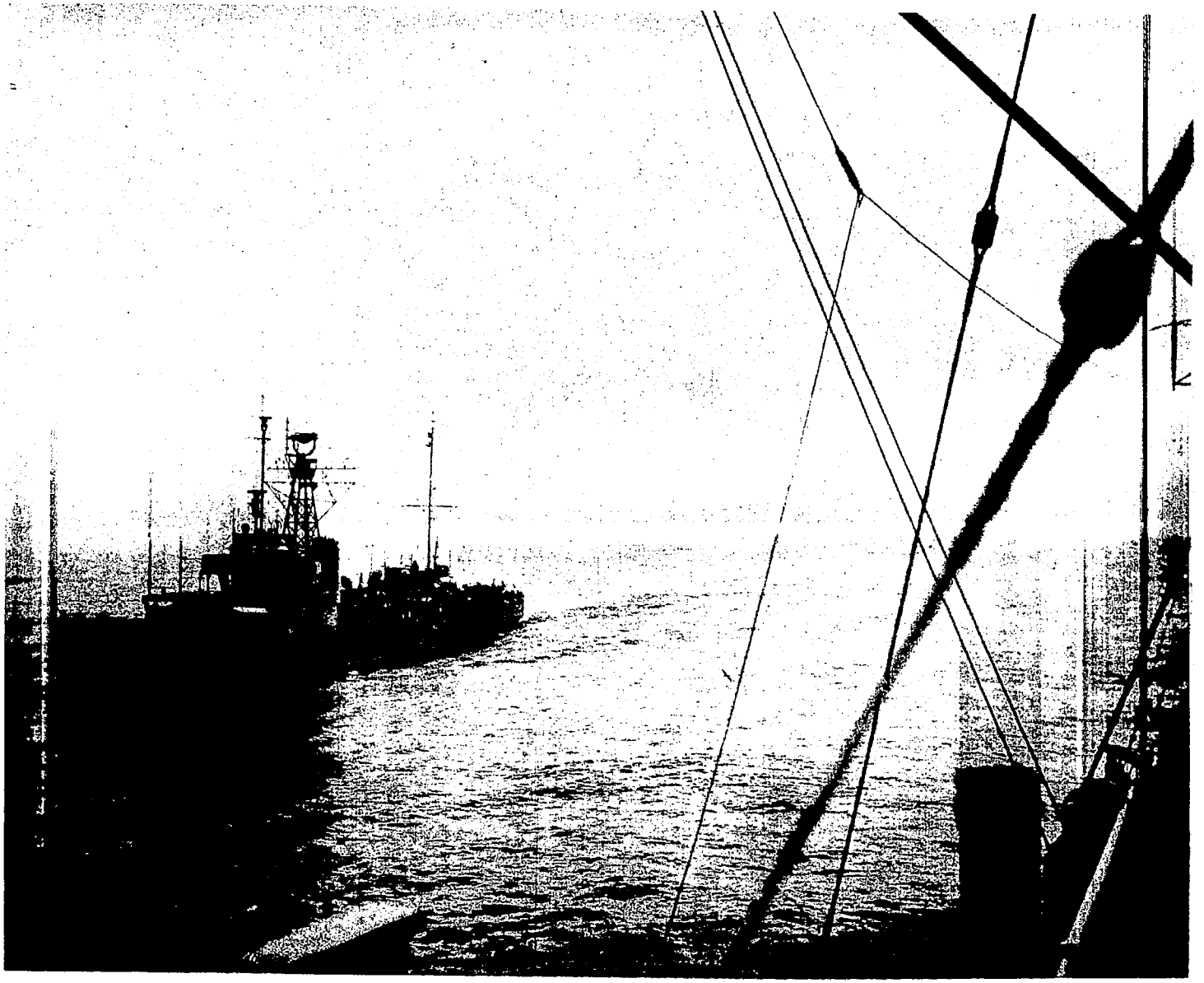

FIGURE 3.7 BEAUFORT FORCE 2, WIND 5 KNOTS, WAVE HEIGHT 1 FOOT.

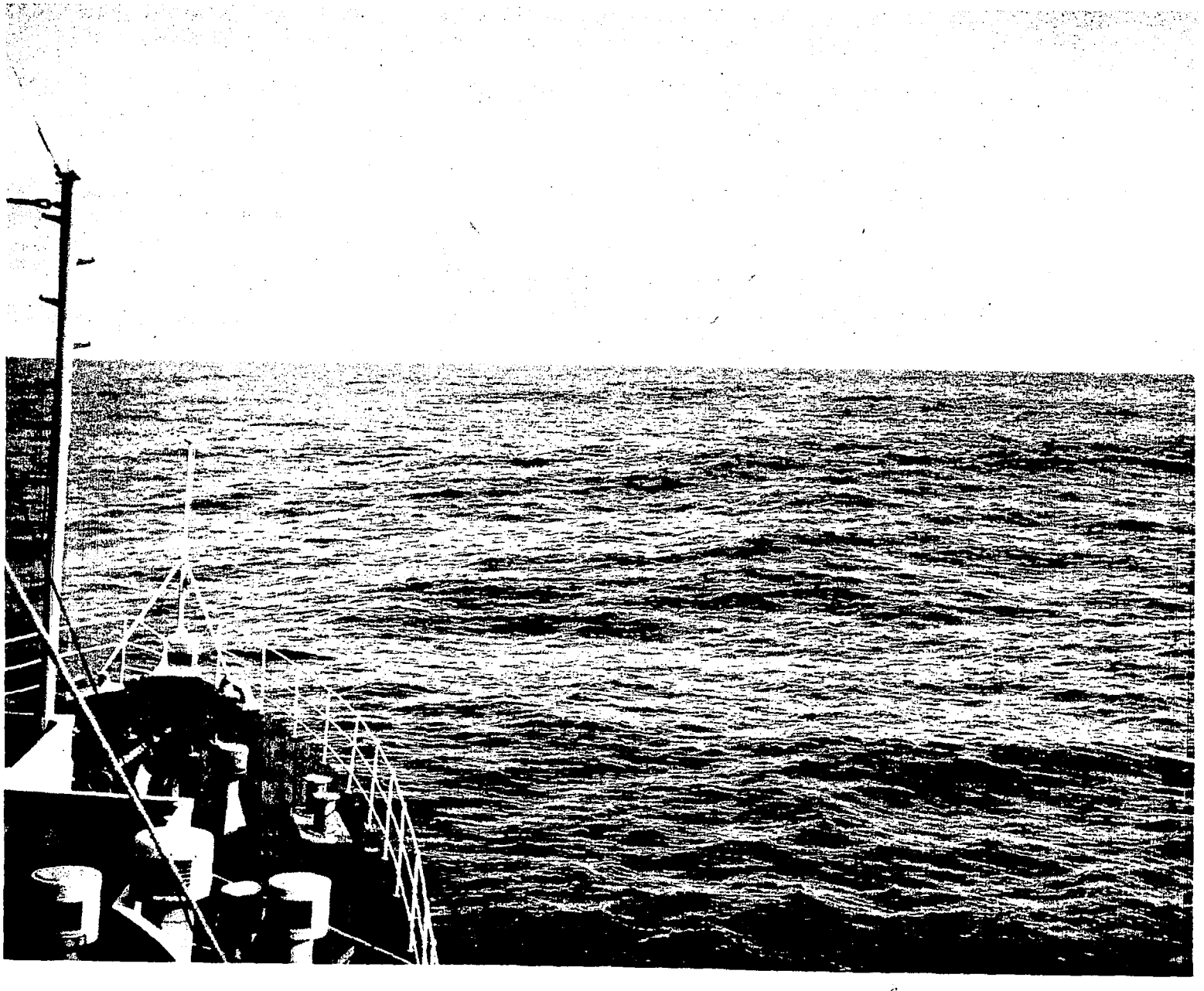

FIGURE 3.8 BEAUFORT FORCE 3, WIND 9 KNOTS, WAVE HEIGHT 8 FEET
(AT TIME OF PHOTOGRAPH WIND HAD DROPPED MOMENTARILY TO 3 KNOTS)

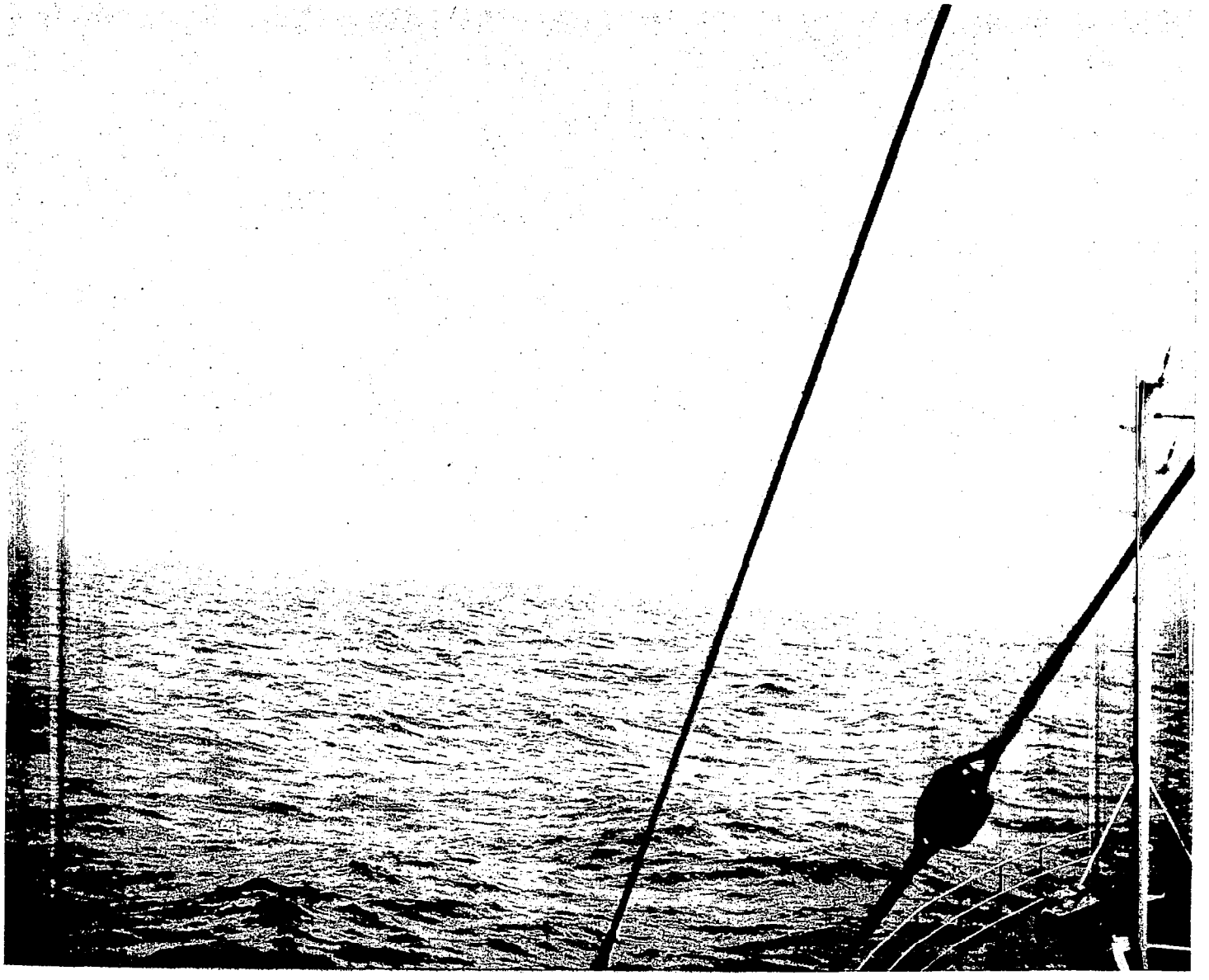

FIGURE 3.9 BEAUFORT FORCE 5, WIND 20 KNOTS, WAVE HEIGHT 8 FEET

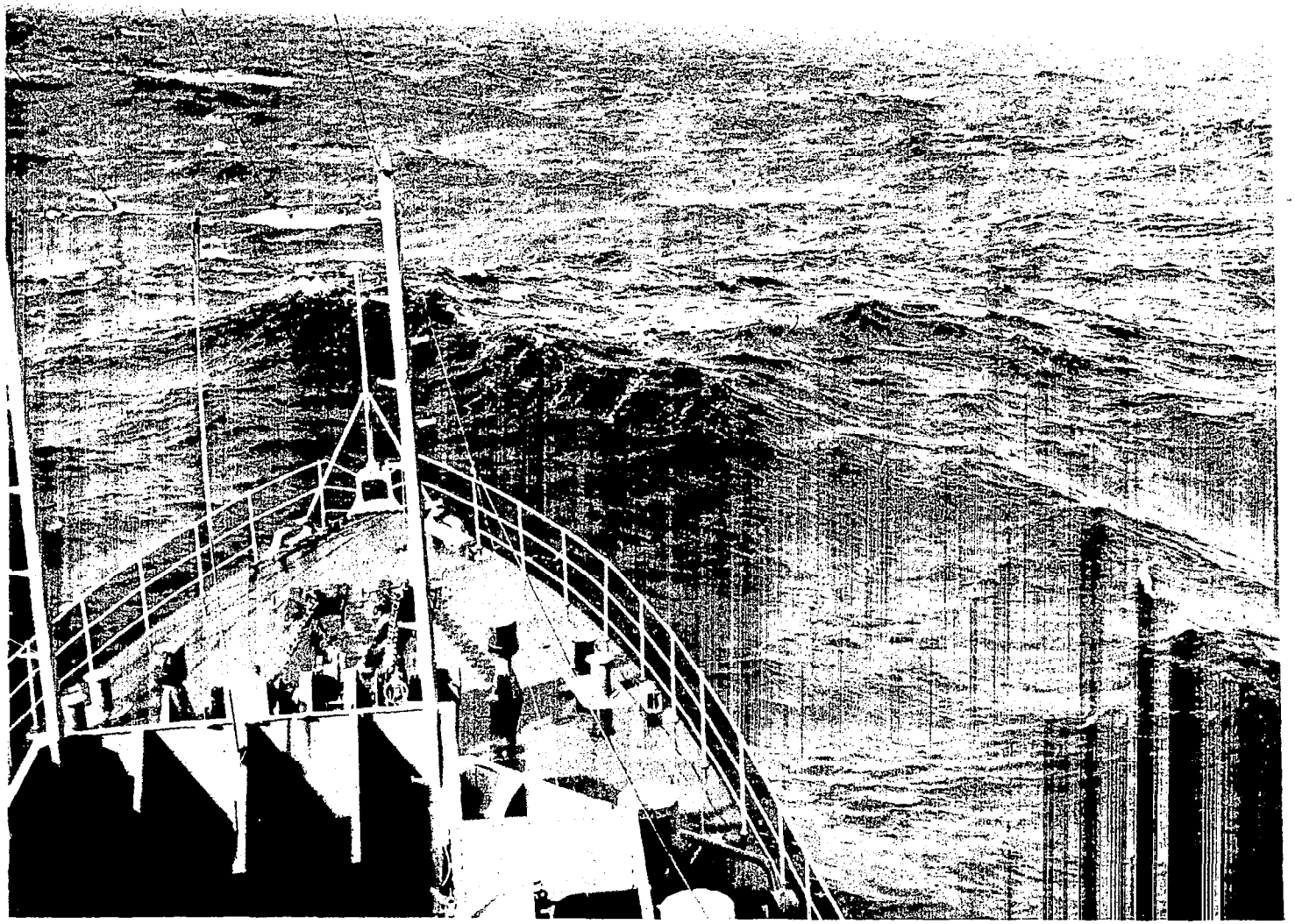

FIGURE 3.10 BEAUFORT FORCE 7, WIND 30 KNOTS, WAVE HEIGHT 16 FEET

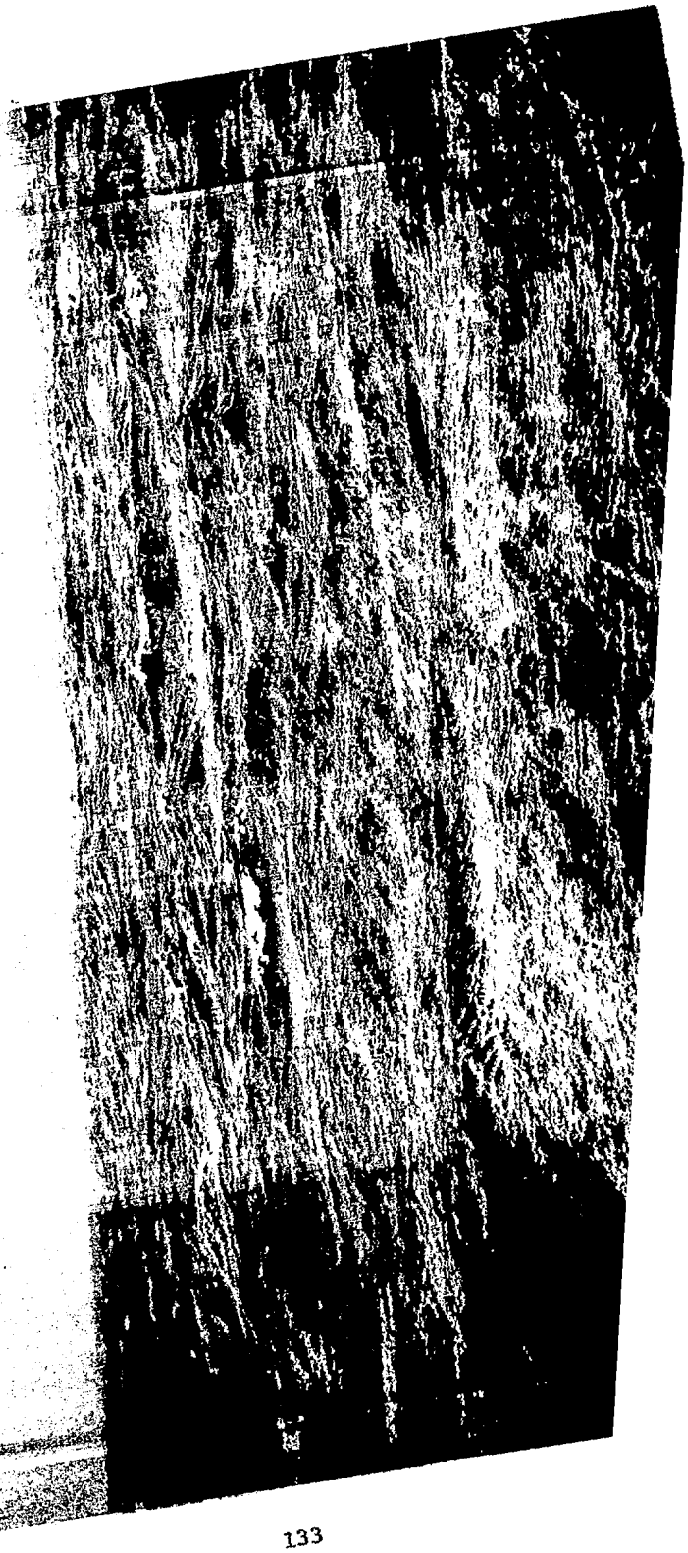

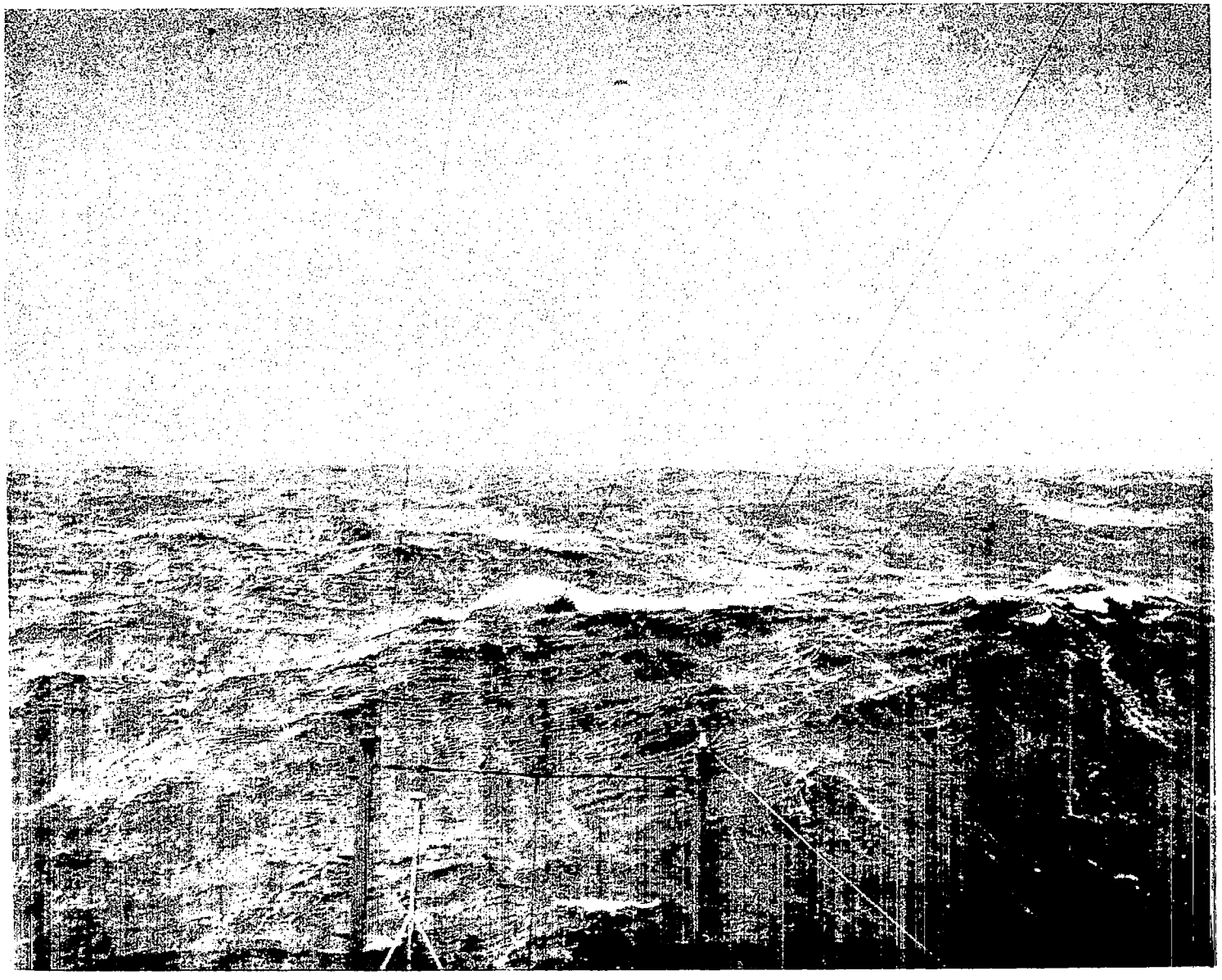

FIGURE 3.12 BEAUFORT FORCE 9, WIND 43 KNOTS, WAVE HEIGHT 25 FEET

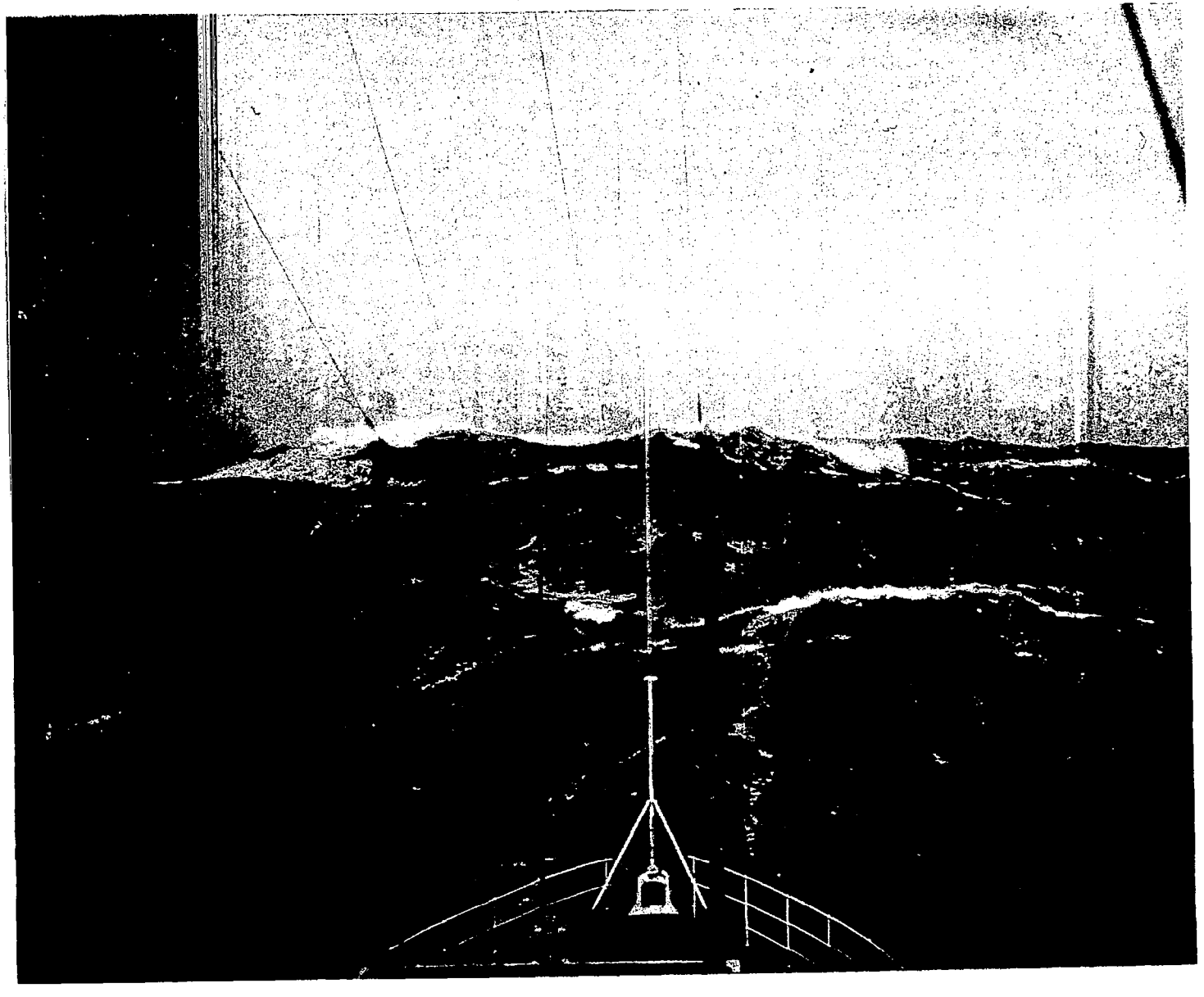

FIGURE 3.13 BEAUFORT FORCE 10, WIND 52 KNOTS, WAVE HEIGHT 40 FEET

near nine knots for the preceding eighteen hours. Even then, there are waves present over the North Pacific at this location. Ripples from the bow can be seen propagating into the picture; however, there is also a background of well attenuated swell that is about two feet in significant height. This particular picture illustrates about as close as one can get to a calm and pacific Pacific. As the winds pick up, and as these figures show, an increasing wind ruffles the sea surface and these ruffles continue to grow as the wind increases.

When Beaufort Force 3 occurs, with a wind speed for this example of 9 knots near the time the photograph was taken, the roughness increases. The waves are running about eight feet in significant height. The important feature to notice is the scale of the shorter waves on top of the wind generated waves in the foreground. There are definite modulations on this surface with lengths of the order of five feet, and shorter, whose scale can be judged in part from some of the dimensions of the objects on the deck of the ship from which the photographs were made.

For Beaufort Force 5, with a wind speed of twenty knots, the whitecaps are visible. The scale of the shorter waves is increasingly evident, especially, just to the left of the guide wire and also about one-third of the way up from the bottom of the picture.

By Beaufort Force 7, with a wind of thirty knots, these smaller scales of roughness are increasingly evident especially in the center of the photograph near the foam patches.

With increasing winds, the remaining pictures show more of the same thing. The photograph for Beautfort Force 8, taken at a height of 35 feet above the surface, shows a washboard like appearance. It should be noted that the short waves in this picture are higher and steeper than the corresponding short waves for previous photographs at lower wind speeds. The picture for 43 knot winds was taken on an elevation of 45 feet above the sea surface. As outlined by the antenna wires running from the forward mast of the ship, there can be seen in the middle distance a vast area of short steep waves lying immediately below the large white cap.

Finally, although there is much spume and foam present in the photograph for Beaufort Force 10, for which the wind at the time was 52 knots, there still can be seen through the haze of flying spray, areas of extremely rough water with very short waves on them.

The point of this sequence of photographs is that they demonstrate a scale of waves on the larger wind generated waves that is growing with increasing wind speed. These waves are certainly so short that fetch effects are irrelevant. Similarly any scaling factor based on duration that would relate the duration of the wind to the period of these waves would yield an extremely large number. These results suggest most strongly that there is a region in the high frequency gravity wave spectrum that depends upon wind speed and that the asymptotic behavior given by $\alpha g^2 / \omega^5$ does not fully describe this range of the wave spectrum. In Chapter 6, an attempt is made, following the work of Pierson and Stacy (1973) and the work of Stacy (1974), to fill in a portion of the wave spectrum with a wind speed dependent effect to account for these features of a wind roughened sea surface on the open ocean.

Most wave recording systems that can record waves with the heights shown in the last of these photographs are not capable of recording these higher frequency shorter wavelength waves superimposed on the larger waves. For example, the Tucker Shipborne Wave Recorder which is installed on these ships undoubtedly has the pressure transducer located at a depth that cannot respond to these waves. The only available hint on the behavior of the frequency spectrum, or the wave number spectrum, in this region is found in the work of Pierson and Stacy (1973) and the work of Stacy (1974). Chapter 6 updates these results and provides some information on how this part of the spectrum behaves. It is clear, however, that an adequate model of the sea surface must be able to show the increasing roughness at these short gravity wave lengths. They are documented by these photographs. The fact that many wave recording systems do not measure them is the fault of the wave recording system.

Before closing this section on the discussion of photographs of waves obtained from ships, one more photograph should be discussed. It is often difficult to estimate the scale of the waves from a single photograph especially if information on the angular field of view of the camera and its height above the water is not given. Reproduced here in Figure 3.14, is a photograph furnished a long time ago to the author by the U.S. Navy. The photographer in this case was on a rather small boat being transferred from the destroyer on which he had been based to the battleship, North Carolina. The original caption for the figure is given.

Most of the features of the waves in this picture can be reproduced by numerical mathematical models of the wavy surface.

FIGURE 3.14 OUR MIGHTIEST SHIP HAS "TOUGH" GOING AT SEA

THIS IS HOW THE 35,000-TON NORTH CAROLINA APPEARED TO THE PHOTOGRAPHER WHO MADE THE PHOTO WHILE HE WAS BEING TRANSFERRED FROM A DESTROYER TO THE BATTLESHIP DURING HER RECENT GUNNERY TRIALS.

The short waves on the surface of the long portion of the large wave are a characteristic feature of the waves that was pointed out in the previous photographs. The bright spots are specular points on the wavy surface caused by the reflection of sunlight at these points into the camera. The sharpness of the crest on the left side of the picture is a well known feature of waves, caused by non-linear effects. A portion of this phenomenon can be modelled by means of some of the work of M.S. Longuet Higgins, in particular by means of the paper written in 1963.

SYSTEMS FOR SCIENTIFIC RESEARCH AT SEA

So far, none of the wave recording systems described above is capable of obtaining information on the direction toward which the spectral components in the wave spectra are travelling. The one that is capable of obtaining some information on the directional properties of the waves is the one developed by the National Institute of Oceanography in Great Britain, now called the Institute of Oceanographic Sciences. The theory of this system can be found in Longuet-Higgins, Cartwright and Smith (1963), as reported in "Ocean Wave Spectra" and in Neumann and Pierson (1966). The problem with it is that it probably cannot be used in very high waves. However, it can probably be used with waves up to five meters in significant height with care.

The system measures the vertical acceleration at the center of a lenticularly shaped buoy and the pitching and rolling motions of the buoy. If equation (2.9) is thought of as representing the

wavy surface, the quantities that are obtained are $\partial^2\eta/\partial t^2$, $\partial\eta/\partial x$ and $\partial\eta/\partial y$. When the above cited equation is differentiated, the sum in the expression is in turn multiplied by $-\omega^2$, ω^2 (cos χ)/g and ω^2 (sinχ)/g, and for the second two the cosine becomes a sine. From these three quantities, three spectra can be computed, three co-spectra can be found and three quadrature spectra can be found. The cospectrum of two time histories say, $\partial^2\eta/\partial t^2$ and $\partial\eta/\partial x$ is the even Fourier cosine transform of the covariance function between these two quantities as defined by equation (3.10) for example.

$$Q(\tau) = \lim_{T\to\infty} \frac{1}{2T} \int_{-T}^{T} \frac{\partial^2\eta(t)}{\partial t^2} \frac{\partial(\eta(t+\tau)}{\partial x} \, dt \qquad (3.10)$$

If the formal operations that define the spectra and cross spectra are carried out by substituting the representation for the wavy surface $\eta(t)$ into them, the quantities that result are all integrals over direction of products of the directional wave spectrum, $S(\omega, \chi)$ and frequency to some power times some trigonometric functions. The different spectra and cross spectra yield expressions with a cos χ, a sin χ, a $(\cos \chi)^2$, a $(\sin \chi)^2$, and a product, cos χ sin χ in them. Appropriate manipulations of these spectra and cross spectra can be carried out in such a way that estimates of the first four terms of the Fourier series expansion of $S(\omega, \chi)$ can be obtained for <u>each</u> frequency band resolved in the frequency spectra that are obtained. This then provides some information on the directional properties on the waves that were measured.

The group at the National Institute of Oceanography extended this concept even more to that of the clover leaf buoy that measured

the curvature of the sea surface in the x and y direction and allowed the recovery of harmonics of the Fourier expansion at any given frequency out to the fourth harmonic.

If a synthetic aperture system is used to image waves in a area where a pitch-roll buoy has recorded the waves, it would probably be sufficient to verify that the harmonics of the Fourier expansion at each of perhaps as many as fifty different frequency bands as calculated from the wave number spectrum all agreed very closely with the corresponding harmonics from an analysis of the pitch-roll buoy data.

For scientific research, there are a large number of systems described in the literature. For example, wave recorders have been positioned in the form of a plus sign, in the form of triangles, in the form of hexagons, in the form of an antenna pattern, especially very close to the coastline where the waves come in from dominately one direction, and so forth. Each of these scientific studies has provided useful information about the directional properties of the waves. Some examples could be cited where these antenna patterns have been misused and the fact that the spectrum of the waves is a continuum in both frequency and direction has not been incorporated into the interpretation of the data. Some scientists have reported the direction of the waves to the nearest tenth of a degree as a single number whereas in reality such a measurement has no meaning.

LAND BASED WAVE MEASURING SYSTEMS

Introduction

The use of radio waves in the 2-30 megahertz band, transmitted by a transmitter based on the ground, either near a coastline or even in the deep interior of the continents, has recently provided new techniques for obtaining information about waves on the ocean surface. One technique developed by Tyler et al. (1974) uses a Loran transmitter and a moving Loran receiver to obtain information on the direction of travel of the waves nearby at a frequency of 0.14 hertz. This experiment for the first time provided detailed information over the full 360° possible in a wave spectrum. A second procedure (Barrick et al. (1974)) transmits radio waves from an extensive ground based antenna, bounces them off the ionosphere so that they return and are reflected, or backscattered, from the sea surface over a known area, and upon receiving them calculates the Doppler shifts in the return signal. The first method described is an extremely useful scientific method that could in principle be employed near any Loran station. The second method has great potential for providing nearly global information on some, but not all, features of the spectrum of the waves over the ocean at a given time.

A Synthetic Aperture System

A radio transmitter at a frequency 1.89 megahertz at Guam was used by Tyler et al. (1974) along with a coherent receiver on a moving motor vehicle to determine the directional properties of waves at a frequency of 0.14 hertz, corresponding to a period of 7.14 seconds. For grazing incidence, the water wave number is given by twice the radar wave number, and Bragg scattering applies. Only those spectral components

traveling directly toward or away from the signal are backscattered. The directional properties of the backscatter were determined by putting the receiver on a motor vehicle and driving it along airport runways, roads, and taxi ramps on the island so as to synthesize a sufficient long synthetic aperture receiving array. Under the assumption that the waves backscattered from any part of the vicinity of Wake Island have the same directional properties, it was then possible to determine the directional spread of the waves at this frequency over a full 360°. In contrast, something like a photograph of the sea surface, used in a laser hologram mode to obtain information on the direction of travel of the waves cannot determine directions beyond ± 90° to a given direction. Directions outside of this range are "aliased" back into this primary range. For the location of the backscatter areas around Wake Island that were used to determine this full directional spread, there were substantial components traveling at angles greater than ± 90° to the local wind for all measurements. The measurements were at wind speeds ranging from 5.8 to 13.1 meters per second as averaged over a time interval centered on the time of the observations.

Table 3.4 Variation of s and a for different wind speeds as determined by a linear fit.

wind m/sec	s	a
5.8	4.2	.020
8.1	2.8	-
9.0	3.6	-
9.4	10.7	0.020
9.5	12.8	0.024
9.5	4.0	0.024
10.5	3.5	0.012
10.7	2.8	-
12.7	3.8	0.003
13.1	4.9	-

The results were then fitted by means of a function of the form given by equation (3.11)

$$G(\Psi) = a + (1-a)\cos^{s}(\Psi/2) \qquad (3.11)$$

This function of course has to be multiplied by a normalizing constant which specifies that the integral of this function from $-\pi$ to $+\pi$ equals one so that the spectral variation as a function of frequency or wave number can be described. The parameter, a, permits the determination of the amount of spectral energy traveling exactly opposite to the wind and the parameter, s, determines the shape of the function within the constraints of this particular normalizing form. In general, the parameter, s, will be a function of wave number and wind speed. Its dependence only on wind speed at this particular frequency or wave number, as the case may be, could only be determined in this experiment since only one frequency in the continuum of wave frequencies was sampled by this procedure. As written in this equation, of course, $G(\Psi) = 1$ at $\Psi = 0$, and this expression normalizes the angular variation to one for waves traveling exactly in the wind direction.

The variation of the parameters a and s for the various wind speeds, and for experiments conducted at different times if the wind speeds were the same, is shown in Table 3.4. There does not seem to be any consistent behavior of s with increasing wind speed and two of the values are from two and a half to perhaps three times larger than any of the others for no apparent reason. If, for a linear fit, the value of a that was determined, in the least square sense, was negative it was set equal to zero. The values of a clearly indicate that the spectral components traveling exactly opposite to the wind

are indeed small, being at least as small as 2.4% of those traveling in the wind direction and perhaps even smaller.

At the same time a pitch-roll buoy, similar in design to the one originally developed by NIO, as described previously in this chapter, was used to measure parameters associated with the direction of travel of waves at one point offshore from Wake Island. The parameters computed from the buoy data at a frequency at 0.14 hertz agreed with the parameters determined from the Loran-synthetic aperture measurements. The angular spread of the spectrum at other frequencies as determined from the pitch-roll buoy appear to continue consistently into other frequencies as extrapolated from the measurements made of the radio scatter.

The buoy accelorometer data taken five kilometers upwind of Wake Island were used to obtain the elevation spectrum of the waves. There was a substantial amount of swell present in one record shown which was not generated by the local wind of 8.1 m/s. The Bragg scattering part and the higher frequencies agreed quite well with the value of α given in Chapter 6 of this report and fitted this asymptotic form over about a decade and half of the spectral variation up to about 0.6 hertz. The winds in the two cases illustrated were so light that the behavior at these frequencies predicted by the equations and results given in Chapter 6 would not be apparent. Also the roll off of the accelerometer acting as a low pass filter begins a 0.6 hertz, so that even after correction there may be problems. As the wind changed from 8.1 m/s to 9.5 m/s, it was nevertheless possible to see a slight increase in the spectral value at these higher frequencies.

Clearly, this particular experiment has great potential as a means of studying waves in the vicinity of any transmitter similar to a Loran transmitter near a coastline favored by the presence of a number of straight roads oriented in different directions. If a simple way to use such an antenna and transmitter over a range of frequencies could be devised, it would be possible to survey a wide frequency range in the spectrum of the waves near the transmitter.

The results of this investigation raises a number of interesting questions. One of them is that of providing a reasonable explanation for the variation of s during the different experiments. In particular, why are two values so much higher than all of the others for the range of wind speed investigated? Also the fundamental assumption of the experiment that the direction of travel of the waves in the spectrum remains substantially the same for all surface areas of the ocean that were probed by this system to obtain the data and that covered a wide arc around Wake Island needs to be verified by an independent measurement. Clearly appropriately obtained aerial photographs under correct lighting conditions, or radar images as in Brown et al. (1974), could serve to accomplish this objective. There are numerous photographs from spacecraft that show that the wind structure around an island can be fairly complex. Since the island is fairly large it could produce a sea breeze effect which would distort the wind field. Also Von Karmen vorticies can be seen in the lee of an island under certain conditions, which indicates a perturbation in the winds around an island even on the upwind side so that the air can flow around the island.

Sky Wave Radar Measurements of Sea State

Radio waves variously described as HF Radar, Skywave Radar or Over the Horizon Radar can be transmiteed from a ground based antenna array acting as a transmitter and beamed out over the ocean in such a way that they bounce off the ionosphere and return to the sea surface at a high grazing angle. The beam can be controlled and steered by proper phasing of the antenna elements so that a wide range of areas on the sea surface can be probed by a given installation. Theoretical investigations by Barrick (1972); Barrick et al. (1974), and others, have demonstrated that the Doppler shifted signal contains information on the frequency spectrum of the waves as if a slice through the directional spectrum had been obtained in the direction of the propagating radio wave. The frequency shifted Doppler spectrum will be shifted to positive frequencies if the waves are approaching the radio waves and to negative frequencies if they are moving away from it. Thus, in any simple wind sea, some information about whether the winds are blowing toward or away from the transmitter can be obtained, and some information on the wave spectrum along that particular direction can be recovered. With additional information on which way the wind is blowing at that point so as to be able to determine how far to the side of the peak of the spectrum the slice has been taken, this information may make it possible to deduce the significant height of the waves and additional information on the wave spectrum. Especially if combined with the numerical wave specification and forecasting procedure described previously in Chapter 2, and with the results that have been obtained from it to date as will be described in a following chapter, this system could provide valuable verification data for wave forecasts and valuable information on the nature of the waves over the ocean. Although presently in the proof of concept stage, plans have evolved for the monitoring of these particular

features of the waves on an ocean wide scale.* These plans show that if transmitter-receiver systems for these HF radar units were installed at Midway Island, at Boise, Idaho, in Tennessee, at Godthab Greenland, and in Western Africa, they would make it possible to monitor wave conditions over substantially all of the North Pacific Ocean, the North Atlantic Ocean, and a portion of the South Atlantic Ocean. The coverage for these five stations is shown in figures 3.15 and 3.16 as given by Rhodes (1975).

Rhodes (1975) provides an economic justification for such measurements. It seems that the system may be considered to be either competitive with the plans for SEASAT-A or complimentary to these plans. This system provides the ability to make the measurements of the waves at any time during the day or night that is desired and to look at any particular part of the ocean whenever desired as contrasted to the constraints imposed by orbiting spacecraft. It cannot, however, recover the kinds of information that present plans for SEASAT-A require. In particular, the measurements do not provide a measurement of the significant wave height uniquely nor do they provide information on the full directional wave spectrum. Should difficulties develop, for example in the SAR for SEASAT-A, this system would compliment the radar altimeter measurements of significant wave height to a beneficial degree.

*First order theory yields information on a slice through the spectrum. Second order theory yields information on S(k) with Φ integrated out.

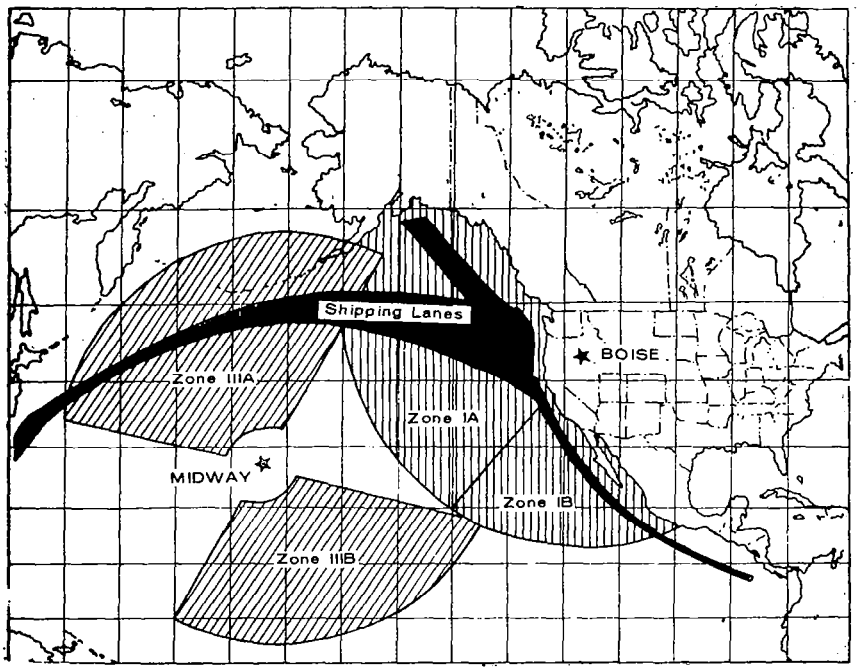

FIGURE 3.15

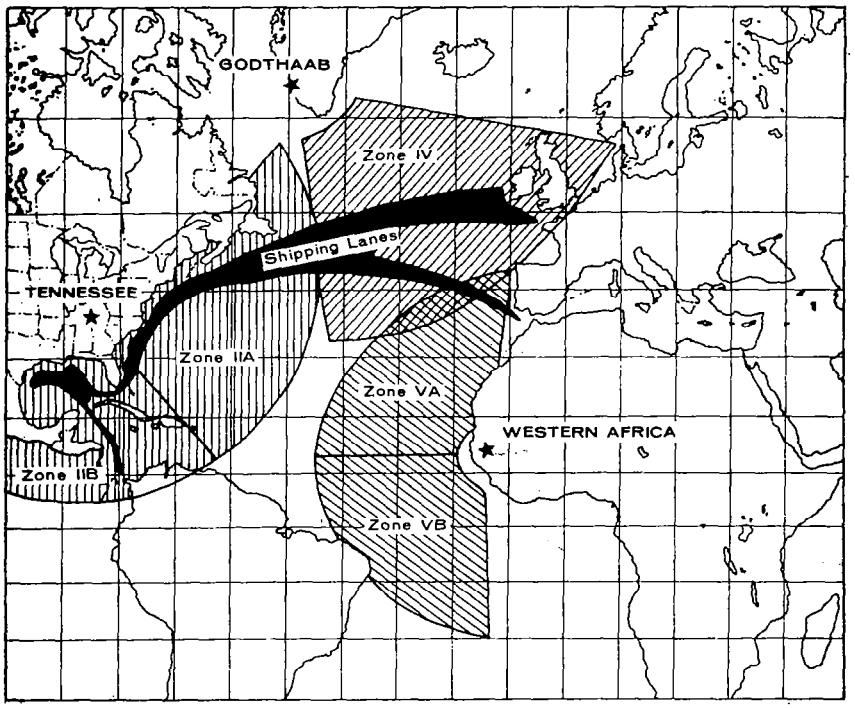

FIGURE 3.16 PROJECTED SITES AND COVERAGE FOR THE OVER THE HORIZON WAVE SENSING SYSTEM.

CHAPTER 4 AIRCRAFT SYSTEMS

GENERAL DISCUSSION

A wave recording system installed on an aircraft has a great potential that is not realized for any of the systems described in the previous chapter. The wave recording system can be transported to any place within range of the aircraft within just a few hours and used to carry out a scientific experiment. The fixed systems described in the preceding chapter do not have this advantage. If properly located, and operated for many years, they serve the very important function of providing a wave climatology for their site. However, for scientific experiments some of the newer aircraft systems have played an extremely important role in our understanding of many of the processes of wave generation and propagation.

Systems based on aircraft are laser altimeters, aerial photographs, and stereo aerial photographs. Those that can be considered in a development stage are real aperture radars, synthetic aperture radars, and under development but not yet tested, the equivalent of a scanning radar altimeter. This last instrument may make it possible to provide the function, $\eta(x, y)$, by scanning from side to side as an aircraft flys over the wavy sea surface. These last three systems have been described as under development. None have yet obtained a wave spectrum that can be compared in exact detail to a spectrum measured by some independent means such as the pitch-roll buoy or the equivalent of the stereo photographs of SWOP and shown to agree withing sampling variability with such data. Also, even the agreement between a properly transformed vector wave number spectrum obtained from a radar of one kind or another and, say, a spectrum obtained with a laser altimeter, or with a spectrum

obtained by a wave recorder at a fixed point, has yet to be demonstrated. One of the purposes of this chapter is to describe exactly what needs to be done in order to demonstrate how a spectrum obtained from a radar system can be compared with an independent measurement to demonstrate that the radar system has indeed measured a wave spectrum.

OPERATIONAL SYSTEMS

Laser Altimeters

A ruby laser operated on the principle of a radar altimeter has been used very successfully in a number of scientific investigations of waves. Such an instrument has served as a primary source for surface truth during many NASA underflights of SKYLAB and during the wave and backscatter measuring programs using aircraft in order to build up the body of knowledge of radar backscatter so essential to understanding S193 on SKYLAB and the operation of the proposed scatterometer on SEASAT-A.

The instrument consists of a narrow beam ruby laser pointing down through a transparent opening in the bottom of an aircraft. (One of the problems with some NASA flights using the C130 is that the transparent opening is so close to the runway because of the design of that particular aircraft that care must be taken to avoid getting oil on it while taxiing.) The ruby laser produces a very bright spot on the surface even from altitudes of several thousand feet. Typically, however, it is operated at lower altitudes. Pierson (1972) shows a record obtained in the North Sea obtained by a NASA aircraft during flight over the North Sea carried out while experiments based at Shannon Island were being conducted. Scientists who have used this system are Shule, Simpson, and DeLeonibus (1971), Ross et al. (1974) and Ross and Cardone (1970). A record from Ross et al. (1974) showing a laser altimeter record obtained in hurricane AVA is reproduced in figure 4.1.

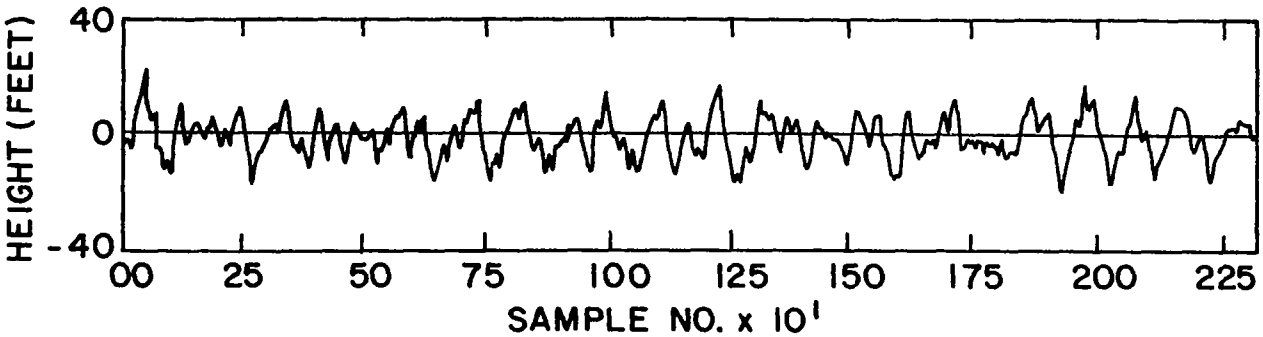

FIGURE 4.1 LASER ALTIMETER RECORD OF WAVES IN HURRICANE AVA FROM ROSS et. al. (1974)

There are a number of features of this record that are most interesting, and the record should be compared with the sample record from the Tucker Shipborne Wave Recorder in the previous chapter. There are many more maxima in this record than there are in the shipborne wave recorder record. This is not primarily because of the higher resolution of the laser altimeter; it is caused predominantly by the fact that this record is more nearly the record of the rise and fall of the sea surface along a line at almost an instant of time than it is a record of the rise and fall of the sea surface as a function of time.

There are two problems concerned with the use of a laser altimeter on an aircraft. The first is concerned with the vertical motion of the aircraft itself because of air turbulence. The second is concerned with the interpretation of the record obtained because the waves are traveling at different directions and with different speeds below the moving aircraft.

The vertical motions of the aircraft could perhaps be removed by recording these motions with an accelerometer and removing that component of the signal that tracks the doubly integrated accelerometer data on the aircraft, for low frequencies in particular. This is usually not done. Typically in order to make such measurements, the aircraft is flown either directly toward the oncoming waves or directly away from the oncoming waves, and simplifying assumptions about the transformations necessary to go from the record obtained to a frequency spectrum of the waves are made. Under these circumstances the vertical motions of the aircraft will map in frequency space into values for the spectrum near the origin. For simple wind generated seas, roughly like those to be used in the analysis of SAR data from a spacecraft in a following section, the motions of the aircraft produce a part of the

total spectrum that can easily be removed so as to obtain the wave spectrum because of a separation in frequency.

For very complicated sea surfaces with wave spectra consisting of spectral components from swell or from some other region of an intense tropical cyclone, such that the directional spread of the spectral values exceeds 180°, the interpretation of a record obtained from a laser altimeter by means of the techniques just described may be erroneous. The difficulties will be outlined briefly here. Their full implications will be more apparent when a similar problem is treated for a radar imaging system on an aircraft.

The usual altimeter record is treated as a function describing the elevation of the sea surface along a line as if that line had been obtained instantaneously. If that line is considered to be in the positive x direction, as overflown by the aircraft, the apparent wave numbers are related to the true wave numbers and the frequency of the wave by means of equation (4.1), where C_A is the speed of the aircraft. It should be noted that the full surface is not imaged by a laser altimeter. Information on the other component of the wave number is not obtained although this component is also indicated in equation (4.1).

$$\ell^* = \ell - \omega / C_A$$

$$m^* = m \tag{4.1}$$

If the waves are recorded as a function of time on the aircraft these waves will have an apparent frequency that is quite high because of the speed of the aircraft. This frequency is linearly related to ℓ^* by means of the transformation shown in equation (4.2) which shows that it is simply a constant times the apparent wave number and does not relate to the physics of the waves.

$$f_{ap} = \frac{C_A \ell^*}{2\pi} \tag{4.2}$$

Whichever is used, ℓ^* or f_{ap}, the wave number is related to the apparent frequency of the waves by means of the wave frequency wave number equation, and in the two possible forms this is given by equation (4.3).

$$(\omega^*)^2 = g\ell^* = \frac{2\pi g\, f_{ap}}{C_A} \tag{4.3}$$

Upon solving for f^* which is the frequency of the waves, neglecting the effects of wave direction, the spectrum upon estimation as a function, say, of f_{ap} is transformed to the spectrum of the waves that would supposedly be measured at a fixed point at a function of time by means of equation (4.4).

$$f^* = \left(\frac{f_{ap} g}{2\pi C_A}\right)^{\frac{1}{2}} \tag{4.4}$$

This last equation masks what really happened, and if the original definition, from 4.1, along with the recognition that $\ell = \omega^2 \cos \alpha / g$ and that the heading of the wave relative to the flight line can be given by $\cos \alpha$, equation (4.4) can be transformed into equation (4.5).

$$f^* = f\left|\cos \alpha - \frac{g}{2\pi f C_A}\right|^{\frac{1}{2}} \tag{4.5}$$

The frequencies in the spectrum from the laser altimeter data given on the left of this equation are given in terms of the true frequencies of the waves being overflown, the direction of these waves relative to the aircraft, and the speed of the aircraft. Quite clearly if the term in parenthesis is near zero the frequency spectrum will map to values near zero and will

contain many low frequencies that would be rejected upon filtering them out under the assumption that they were caused by the aircraft motions. In fact, any wave with a direction to the flight line given by an appropriate value of α in equation (4.6) will disappear in this analysis. Only if the term in parenthesis in equation (4.5) is close to one will the true frequency be close to the frequency in the wave spectrum computed in this manner. In turn, this is a fairly correct assumption only if the spectrum is unimodal with a peak in the wind direction, corresponding to the direction of flight of the aircraft. Under these circumstances cos α is close to one. Similarly, if the speed of the aircraft is large, the second term will not alter the spectrum by too large a value. Caution is, however, indicated in interpreting such data from a laser altimeter over all frequency bands, especially when there is the possibility that a part of the spectrum may have been eliminated because the frequencies in it appear to have been too low.

$$f = \frac{g}{2\pi \cos \alpha \, C_A} \tag{4.6}$$

Some of the problems that can arise with laser altimeter records are analyzed are illustrated by Table 4.1. Five frequencies are shown in this table and under the assumption that the aircraft is moving at a speed of 150 meters per second, the frequencies that would be obtained by means of the usual analysis of the record are tabulated. If the waves are moving towards the aircraft the frequencies that result are those tabulated for zero degrees, if they are moving at right angles to the aircraft the frequencies (and corresponding periods below the slant line) are tabulated for 90°. If they are moving in the same

direction as the aircraft, the frequencies are tabulated at 180°. The error in frequency is only about 5% or 10% for those spectral components that are traveling either opposite to, or in the direction of, the flight line of the aircraft. Those components traveling at right angles, however, differ completely in apparent frequency and the periods that result from them are not usually found in wave spectra, even for storm seas.

The assumption that the waves are traveling at right angles to the aircraft is, of course, a convenience for the calculation. However, there exists a critical angle such that the apparent frequency of the waves will be zero, and this critical angle is tabulated for each of the five true frequencies in the last line of this table. For this particular combination of true wave speed and direction, the aircraft remains over a particular part of the wave profile all of the time. For a range between 78° and 90°, for example, for a wave with a 20 second period, the apparent periods will all exceed 45.5 seconds and would be plotted in the spectrum near zero frequency.

Table 4.1 Values of f^* as a function of f and α for C_A = 150 m/s. Values below the slant at 90° are the corresponding apparent periods. α^* is the angle at which the apparent frequency is zero.

	Frequency				
Direction	0.05	0.075	0.10	0.150	0.20
0°	0.0445	0.0696	0.0947	0.145	0.195
90°	.022/45.5	.0279/35.8	.0322/31.1	.0394/25.4	.0456/21.9
180°	0.055	0.080	0.105	0.155	0.205
Critical Angle α^*	78°	82°	84°	86°	87°

For a wind blowing directly offshore and generating a fetch limited sea with relatively high frequency components traveling within ± 30° or 40° to the wind direction for the more important frequencies, it would be expected that a laser altimeter run directly into the waves, when transformed in the manner just described, would yield a frequency spectrum of the waves that would be very close to one obtained from a wave record from an instrument that measured the waves as a function of time at a fixed point. This is indeed the case as can be seen in figure 4.2 which compares wave spectra obtained in these two different ways. Under these circumstances the agreement is very good.

On the other hand, for a very complicated seaway with spectral component traveling in directions separated by 90° and more such as might be found in a hurricane, there could be problems with those frequencies that are traveling near right angles to the flight line of the aircraft. This problem is being investigated by means of directional wave spectra hindcast for hurricane AVA, and there are indications that the laser altimeter record obtained information on very low apparent frequency waves that was mixed in with the vertical motion of the aircraft as described above and filtered out in the process of data analysis.

PHOTOGRAPHS OF THE SEA SURFACE FROM AIRCRAFT

Theory

Since the first paper by Stilwell (1969) and subsequent paper by him in 1974 and others, the art of photographing the sea surface and analyzing the photographs to obtain spectra has started to become a science. An interesting and important contribution to this subject is that of Kasevich (1975), which treats the properties of a photograph to various orders of approximation so as to make it possible to conclude that the intensity of the film is truly a

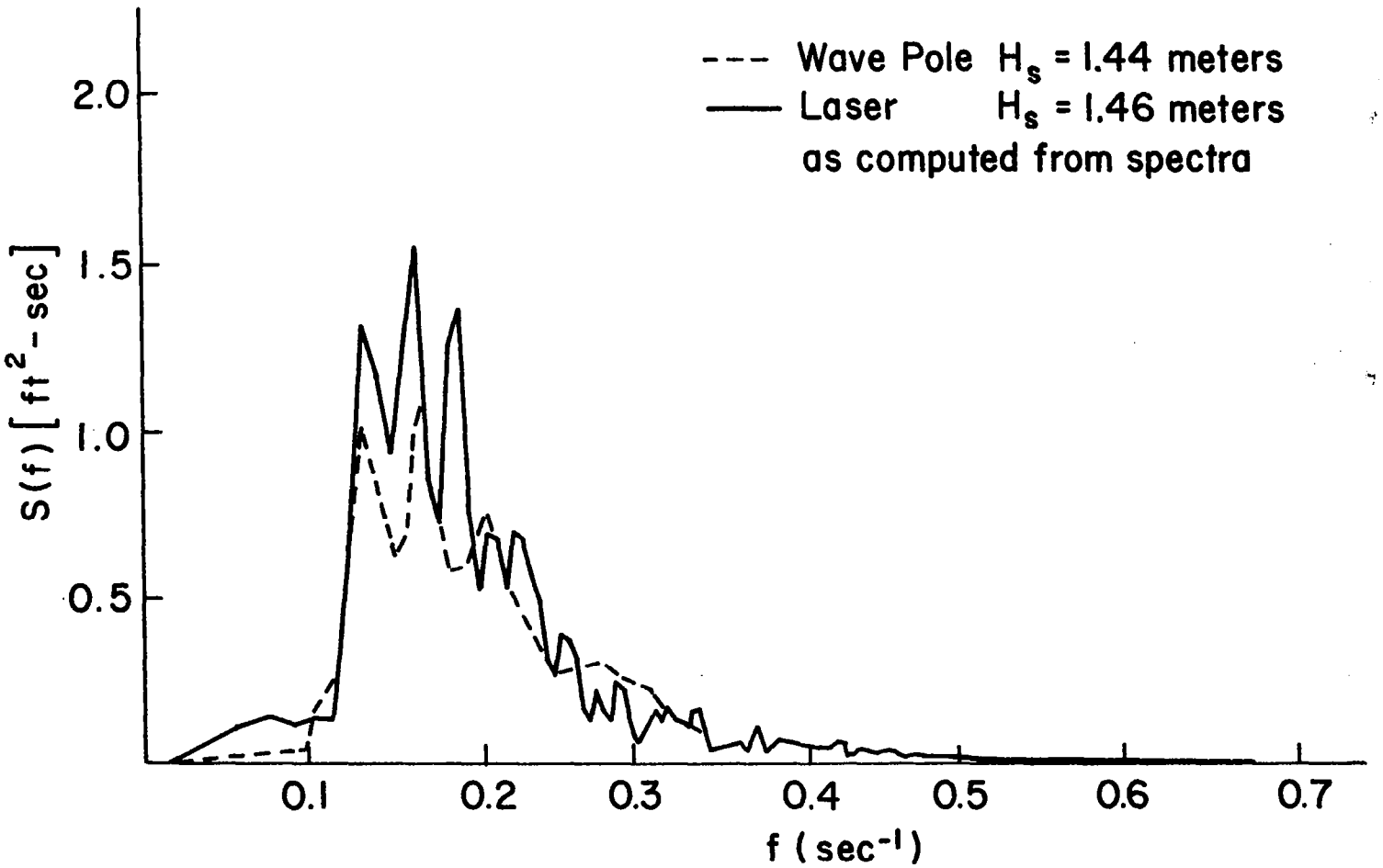

FIGURE 4.2 COMPARISONS BETWEEN WAVE POLE AND LASER ALTIMETER RECORDS

measure of the slope of the sea surface in a given direction. The various aspects of this theory in terms of the equations involved will not be given in this report.

It is pointed out by Kasevich that the linear portion of the film exposure curve must be used, that the lighting must be optimum, and that higher order effects in both the properties of the light and the properties of the film must be considered. Those situations where it is better to take an oblique photograph are described. It is shown that an oblique photograph is required for overcast conditions, for example. The theories have been extended to the point where second order effects such as the squares of the wave slope are shown to influence the brightness of the image as well as quantities linearly related to the wave slope. Given all the pertinent data about a particular photograph, it should be possible to calculate the difference between the spectrum obtained from the image with these extraneous quadratic effects present and the true spectrum of the wavy surface.

All of these techniques start with the negative of the image and obtain a hologram of this negative, which is then digitized by means of a densitometer. Each of these steps must be carefully controlled so that the final result obtained are indeed proportional to the square of the amplitude of the spectral component in the image.

Although the technique proposed by Stilwell has been in existence for about six years, the number of spectra actually obtained are few indeed.* Many of them suffer from not having had sufficient resolution so that the behavior of the spectrum at very low wave numbers can be found. Also spectra from some oblique photographs

---

*An example of one is found in Sugimori (1972).

in which perspective distortion existed have been computed. The interpretation of the spectrum is doubtful because under such circumstances the waves are frequency modulated; that is, the waves are longer in the foreground and grow progressively shorter with increasing distance toward the background although, in fact, the actual waves are all of about the same length. A true wave number is smeared into a range of wave numbers by the effect of perspective. Some way to produce an undistorted image from an obliquely obtained image needs to be developed before photographs taken at an oblique angle can be used easily to obtained estimates of vector wave number spectra.

Photographs of Waves from Aircraft

In this section some selected photographs of waves obtained from aircraft are discussed. These photographs illustrate both the properties of waves on the open ocean and also some of the effects of wave refraction that might be imaged by means of a synthetic aperture radar.

The first sequence of three figures (4.3, 4.4 and 4.5) shows the results of photographing the sea surface with an aircraft and a camera pointing down. The altitude in these photographs increases from near the surface to 10,000 feet. For the six photographs, the altitudes are 500 feet, 1,000 feet, 2,000 feet, 4,000 feet, 8,000 feet, and 10,000 feet. The first point to be made about this series of photographs is that the altitude of the sun was incorrect and that the surface was not properly illuminated for optimum photographic results. The circular pattern of the apparent illumination and the vignetting effect of the variation in light across the plane of the photograph would make it difficult to interpret the full photographs

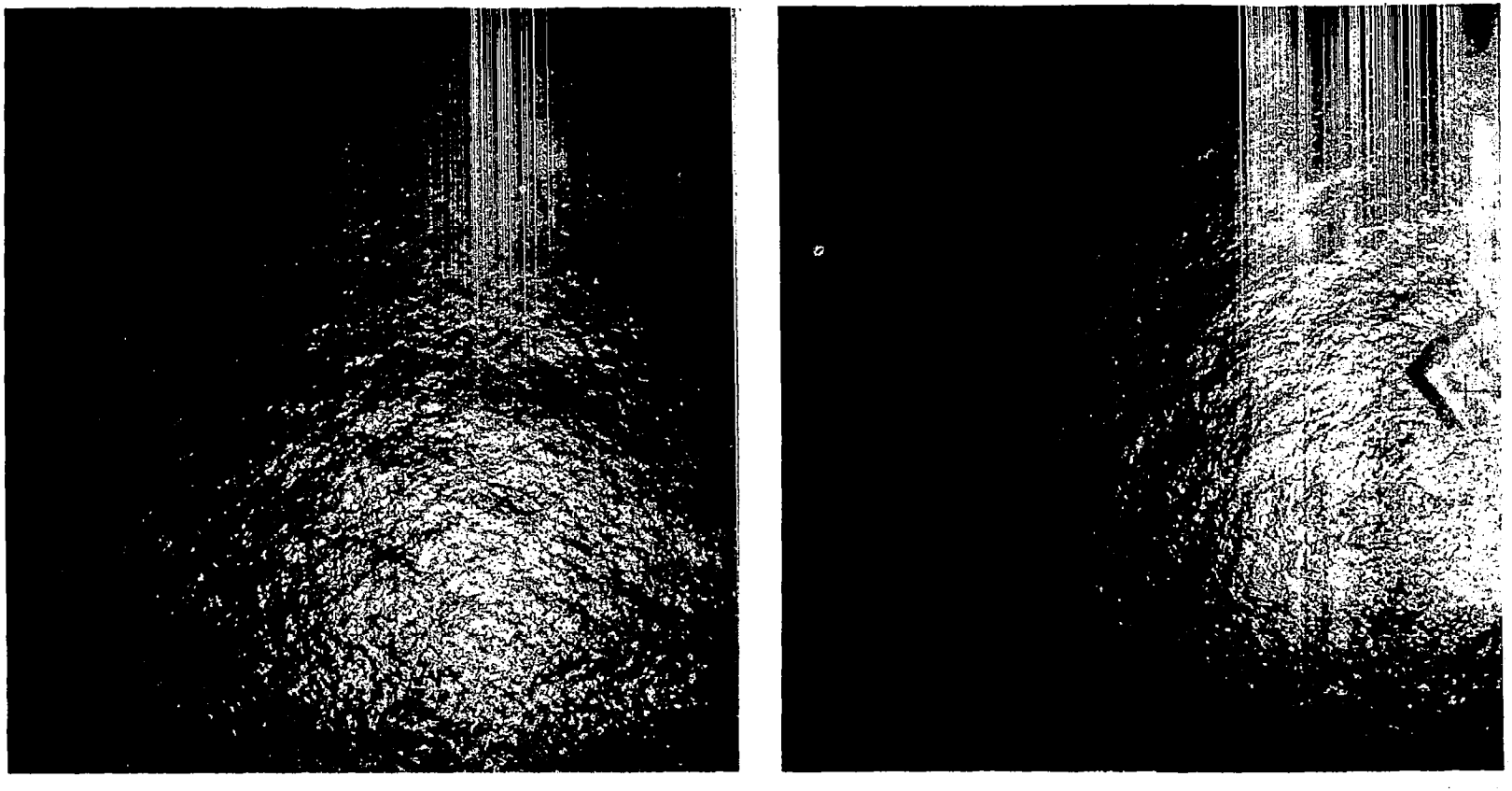

500 FT. 1000 FT.

FIGURE 4.3 AERIAL PHOTOGRAPH OF WAVES AT 500 FT. AND 10000 FT.

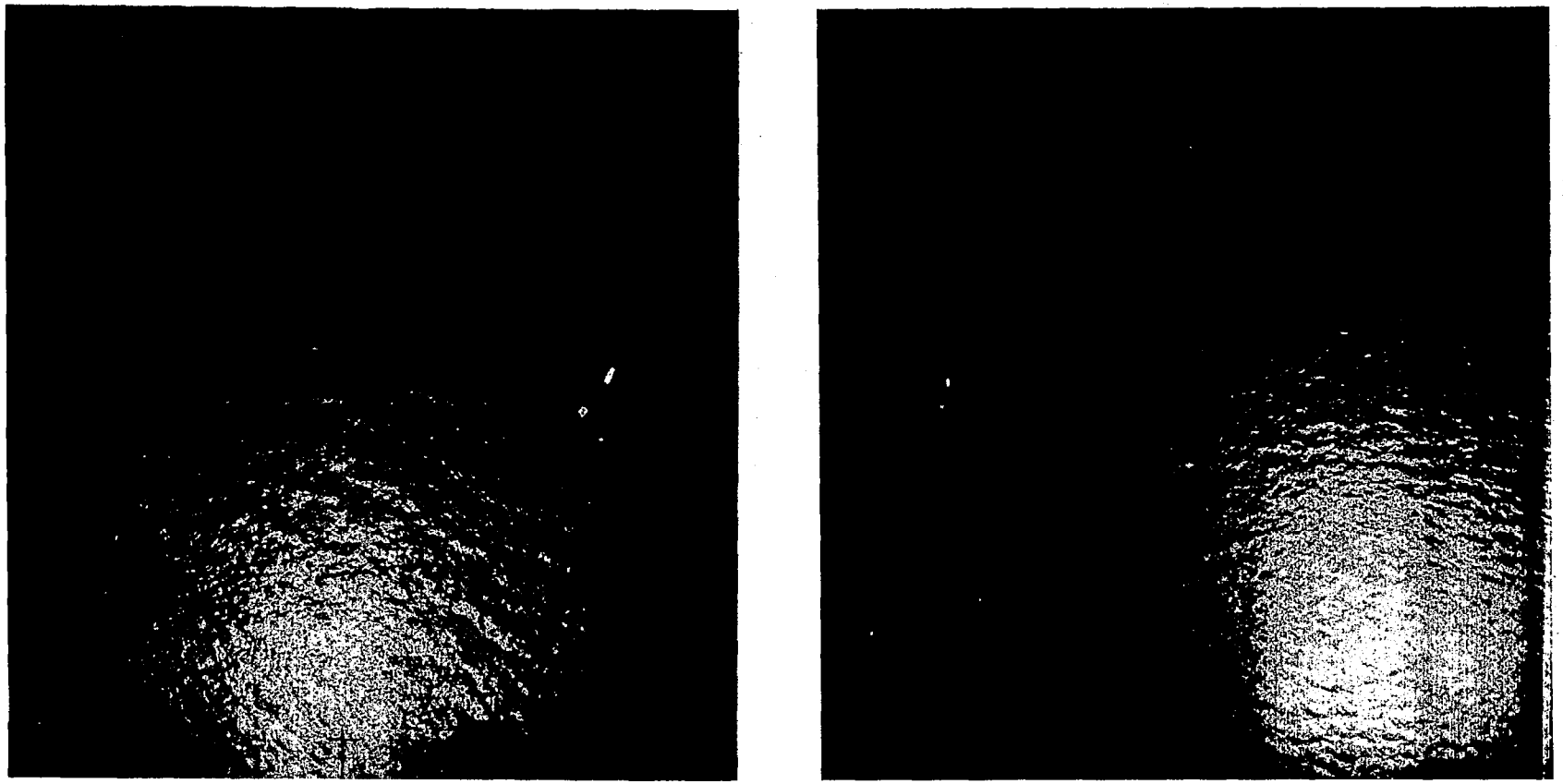

2000 FT.

4000 FT.

FIGURE 4.4 AERIAL PHOTOGRAPH OF WAVES AT 2000 FT. AND 4000 FT.

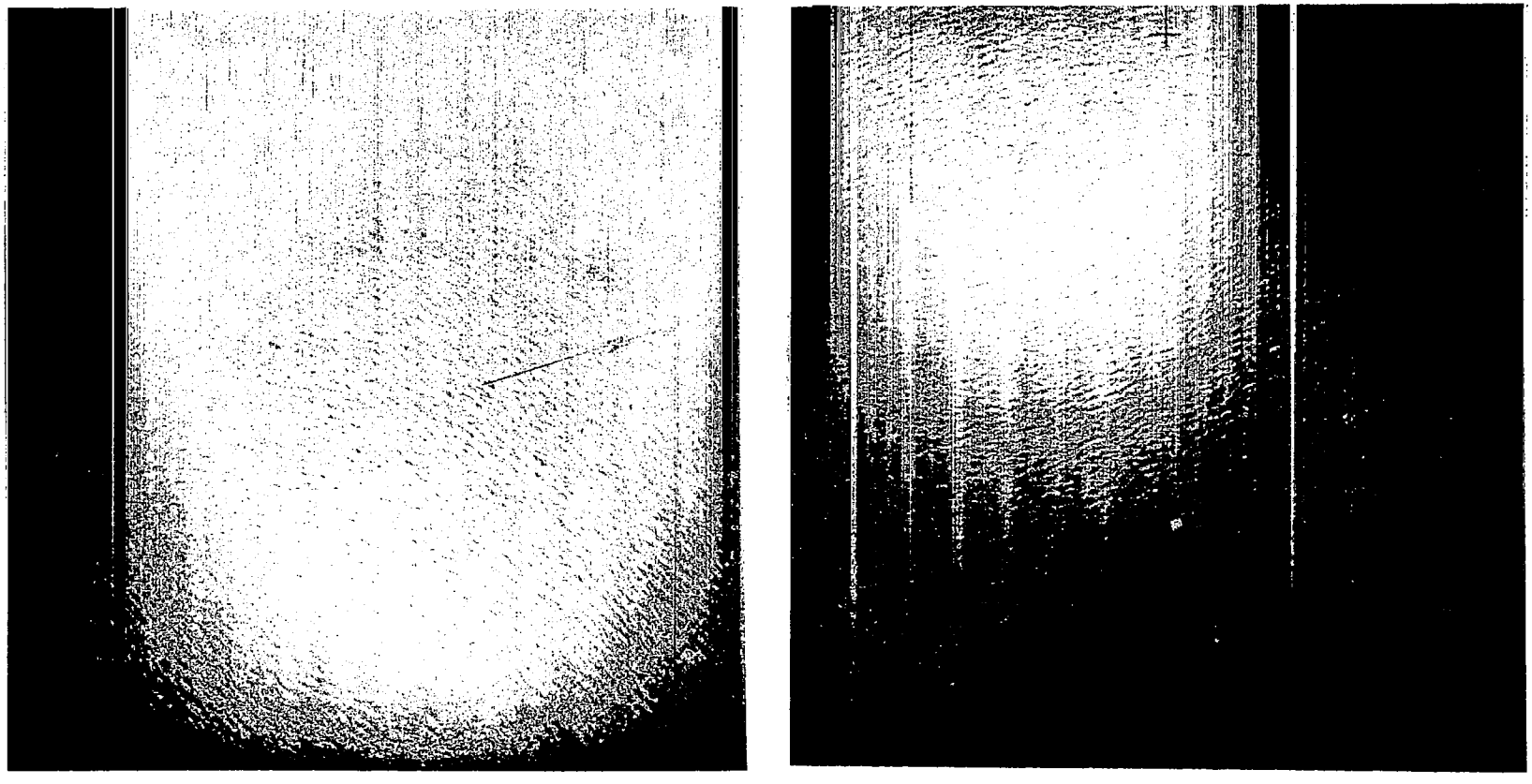

8000 FT. 10000 FT.

FIGURE 4.5 AERIAL PHOTOGRAPH OF WAVES AT 8000 FT. AND 10000 FT.

by means of techniques such as those of Stilwell (1969). The apparent change in structure is a misleading feature of the photographs. For the last three photographs in this sequence, however, there are portions that could be selected that, if processed according to the technique of Stilwell, would yield useful spectral results. These portions are found partly between the bright spot in each picture and the darker outer areas, and represent perhaps 1/5 or 1/10 of the total area of each photograph. For example, in the last photograph, a region just to the side of the bright spot and toward the tower could be selected that would be roughly 1/5 of the photograph wide and 1/3 of the photograph long that would contain a fairly uniformly illuminated region of wave patterns. This portion of the photograph would give useful information on the vector wave number spectrum.

If this series of photographs is interpreted in light of the reference just discussed, it can be seen that the technique of photographing the sea surface is an important one and that the new knowledge gained in this area should help those who use aircraft photographs to obtain more useful data in the future.* Most of the other photographs to be discussed in this section show a more even illumination. On the basis of recent work in this area, the fact that these next few photographs show well illuminated patterns from one edge to the other are probably a result of fortuitous circumstances and not of deliberate planning.

Figure 4.6 shows a vertically obtained photograph of the sea surface on the open ocean. The original source and all other information about this photograph are unavailable. However, it is an ideal

*Recent NASA imagery as shown by Pirie et al. (1975) at the NASA Earth Resources Survey Symposium, June 8 - 12, 1975 has all of the desired qualities.

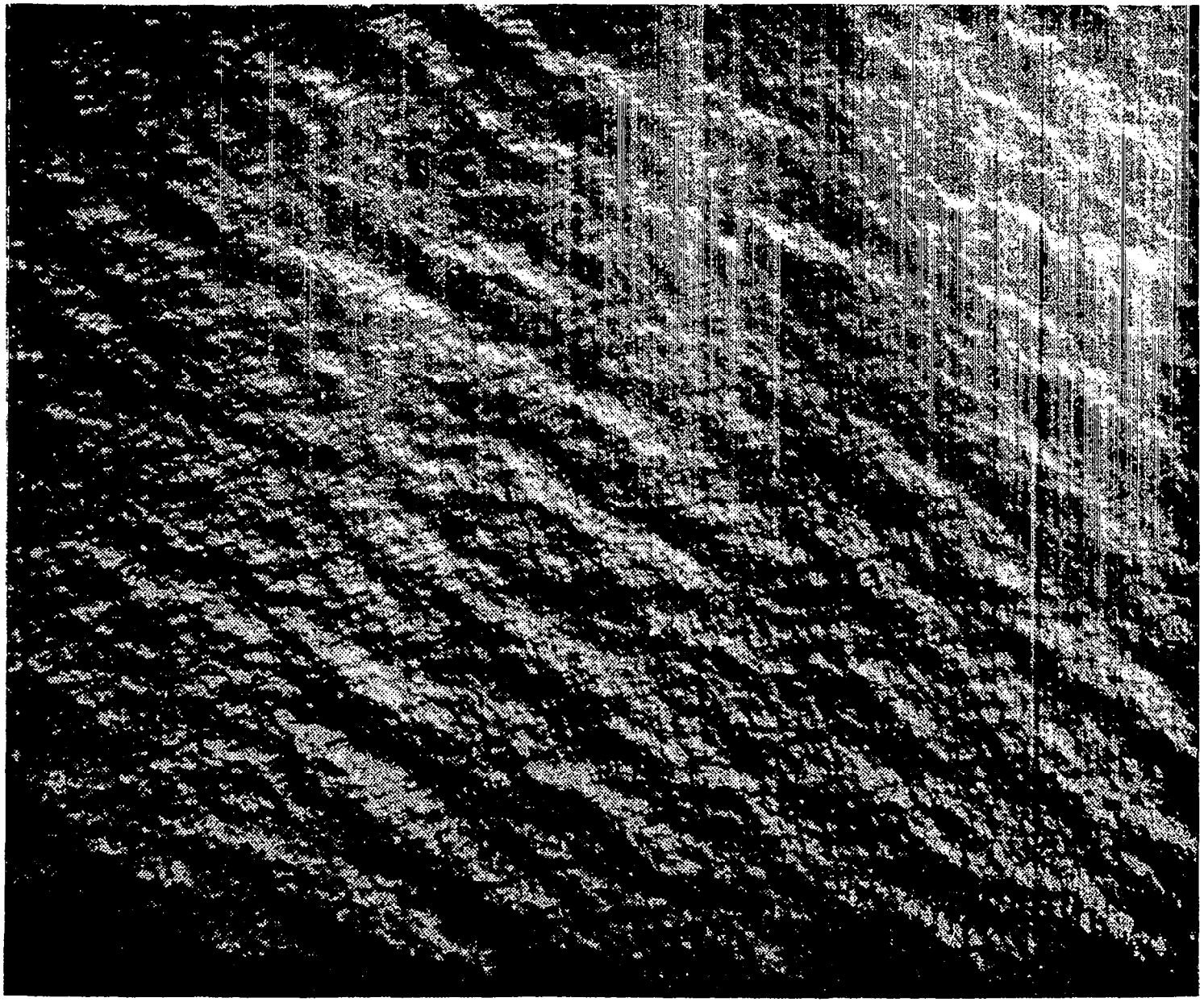

FIGURE 4.6 AN IDEAL PHOTOGRAPH FOR SPECTRAL ANALYSIS

photograph from the point of view of the type of image that would be required for processing using the techniques of Stilwell (1969). A laser hologram of this image would yield an excellent estimate of the spectrum and further processing would make it possible to make this estimate quantitative and to recover the elevation spectrum from what is obviously a pattern that has been illuminated in terms of the slope of the waves. The smaller waves superimposed on the larger waves as would be expected in a wind sea, are of the order of one twentieth to one fiftieth of the length of the larger waves. Quite clearly the spectrum that would result is a continuous spectrum over a wide range of wave numbers. One can note that the length of crests along the crests is approximately six times the distance between the crests and that the waves occur in groups of high waves separated by areas where the waves are relatively low. This photograph is a perfect example of what one would expect for a short crested Gaussian sea surface.

Our figure 4.7 is a photograph provided originally by Captain D. MacDiarmid and used in HO Publication 603 (Pierson, Neumann, and James (1955)). It is an oblique photograph so that perspective foreshortens the waves in the distance. A ship provides an estimate of scale. The sun is fairly low on the horizon so that the wave pattern is highlighted in an unique and most interesting fashion. This photograph again shows the randomness of the waves and the variation in apparent wave direction from place to place over the wavy surface. To the foreground and just to the right of the ship, can be seen a pattern of high waves. Above and to the left of the ship, the sea surface is relatively flat. The spectrum of the waves covers a wide range of spectral components.

FIGURE 4.7 AN OBLIQUE PHOTOGRAPH OF WAVES.

The next series of photographs shows some of the effects of wave refraction. The first photograph, figure 4.8, is for a relatively straight coast with more or less parallel offshore depth contours. In the deep water part of the photograph, the waves are traveling at an angle nearly, but not quite, parallel to the coastline. There are two dominant components, one of fairly long waves with a slight component toward the coast and the other of fairly short waves whose crests are very nearly perpendicular to the coast. As the water shoals, the direction of the longer waves very quickly changes so that they are propagating toward the shallower water. The shorter waves do not change direction until they enter areas very close to the coastline. After the longer waves began to sharpen up and form narrow crests separated by broad shallow troughs the shorter waves can be seen, in between the longer waves, to turn to an angle of about 45° to the coast. Everything in this photograph is perfectly explainable on the basis of the theory of wave refraction, except the final change in the appearance of these waves extremely close to the coast and the appearance of the breakers.

Figure 4.9 illustrates waves being refracted over a submarine ridge. In the area of the breakers, the wave pattern shows intersecting trains of waves with a very complicated behavior. To either side of this region the wave pattern is relatively uncomplicated. It consists of a train of swell waves that has been bent parallel to the shore and a local wind sea traveling at an angle to the swell waves and not yet influenced substantially by the effects of the bottom. On the bottom of the photograph there is an interesting area where the waves are obviously quite low compared to their heights in

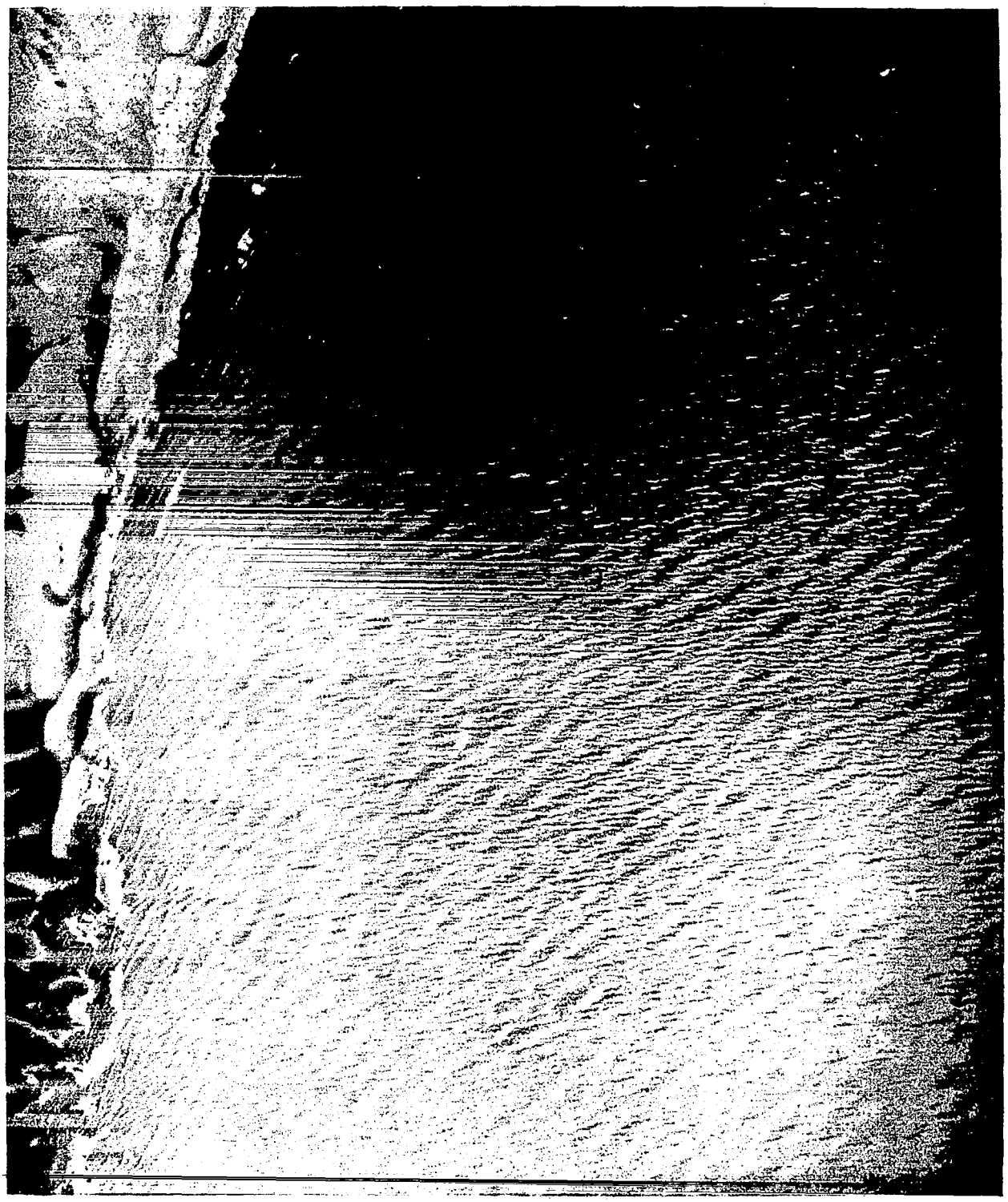

FIGURE 4.8 WAVE REFRACTION FOR NEARLY STRAIGHT PARALLEL BOTTOM CONTOURS.

FIGURE 4.9 WAVE REFRACTION OVER SUBMARINE RIDGE SHOWING CROSSED WAVE PATTERNS.

other parts of the photograph. This particular feature of wave refraction patterns is important. If the bottom contours cause the waves to be concentrated in one area, there must be a corresponding area where the waves are low.

Figure 4.10 illustrates three interesting features. The first is the long swell traveling in toward the coast and being refracted. The second is the very short wave pattern visible at the edges of the bright spot in the photograph and traveling at almost exactly a right angle to the swell. The difference in length between two wave systems is large. Finally, some slicks can be seen in the photograph in which the short waves have been obliterated by the material on the surface.

Figure 4.11 illustrates two wave trains also that are at right angles to each other. In this case, however, there are more nearly of the same length. In the bright spot of the photograph the slicks show up as bright bands, whereas on the edges the slicks show up as dark streaks. It is to be anticipated on the basis of work done at NRL with imaging radars that a similar feature will be observed in radar images of waves. There will be no backscatter from areas covered by oil slicks and they should therefore appear to be dark on such images. This particular feature, which has been observed, provides an independent confirmation of the hypothesis that backscatter is one of the most important mechanisms for producing wave images.

Figure 4.12 illustrates how complicated the situation can become. The waves are traveling from the bottom of the picture toward the top. The rocky island near the top of the photograph has nearly vertical cliff like sides, and, instead of breaking on this island,

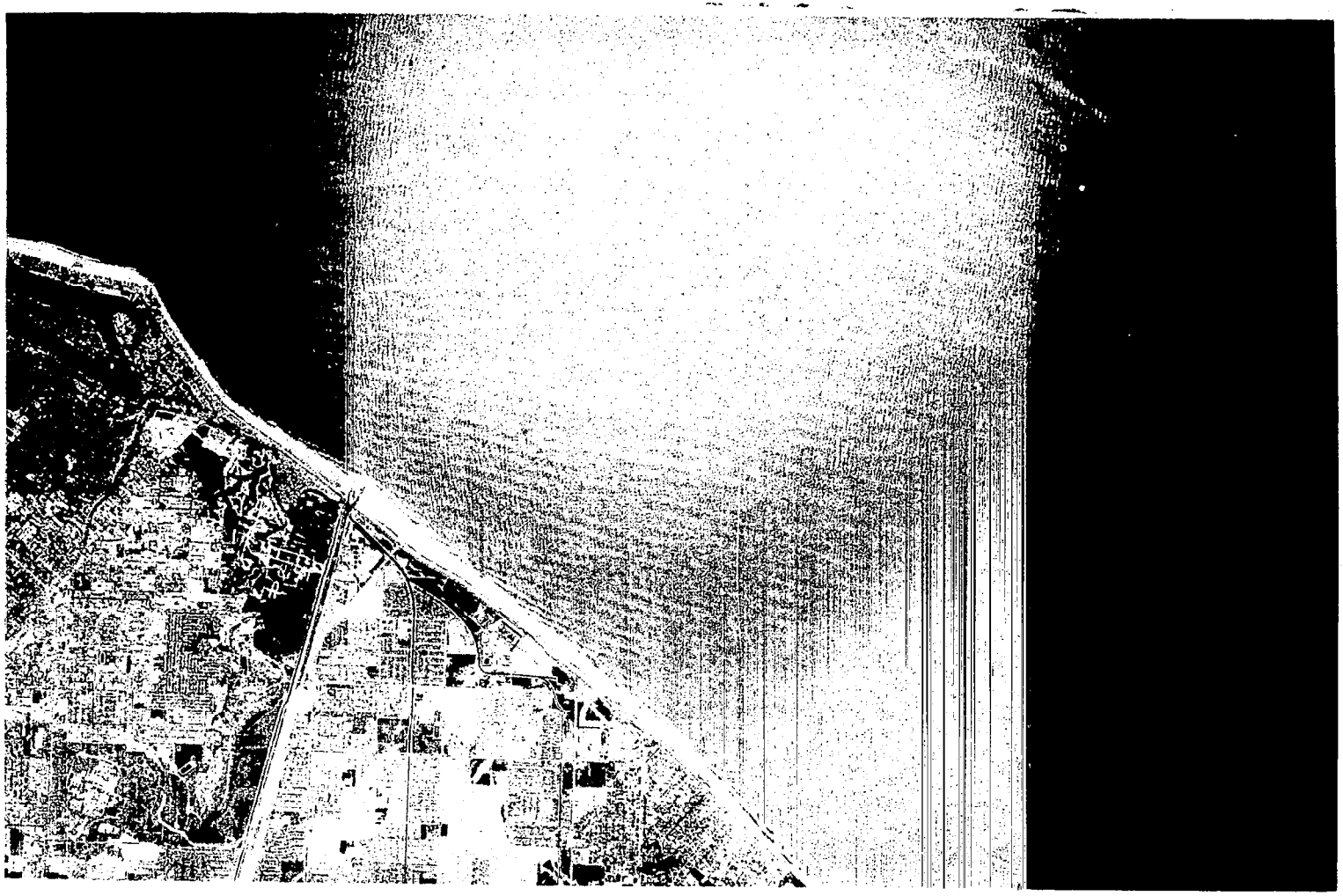

FIGURE 4.10 AERIAL PHOTOGRAPH SHOWING VERY SHORT WAVES AT RIGHT ANGLES TO A SHOALING SWELL PLUS THE EFFECT OF SLICKS.

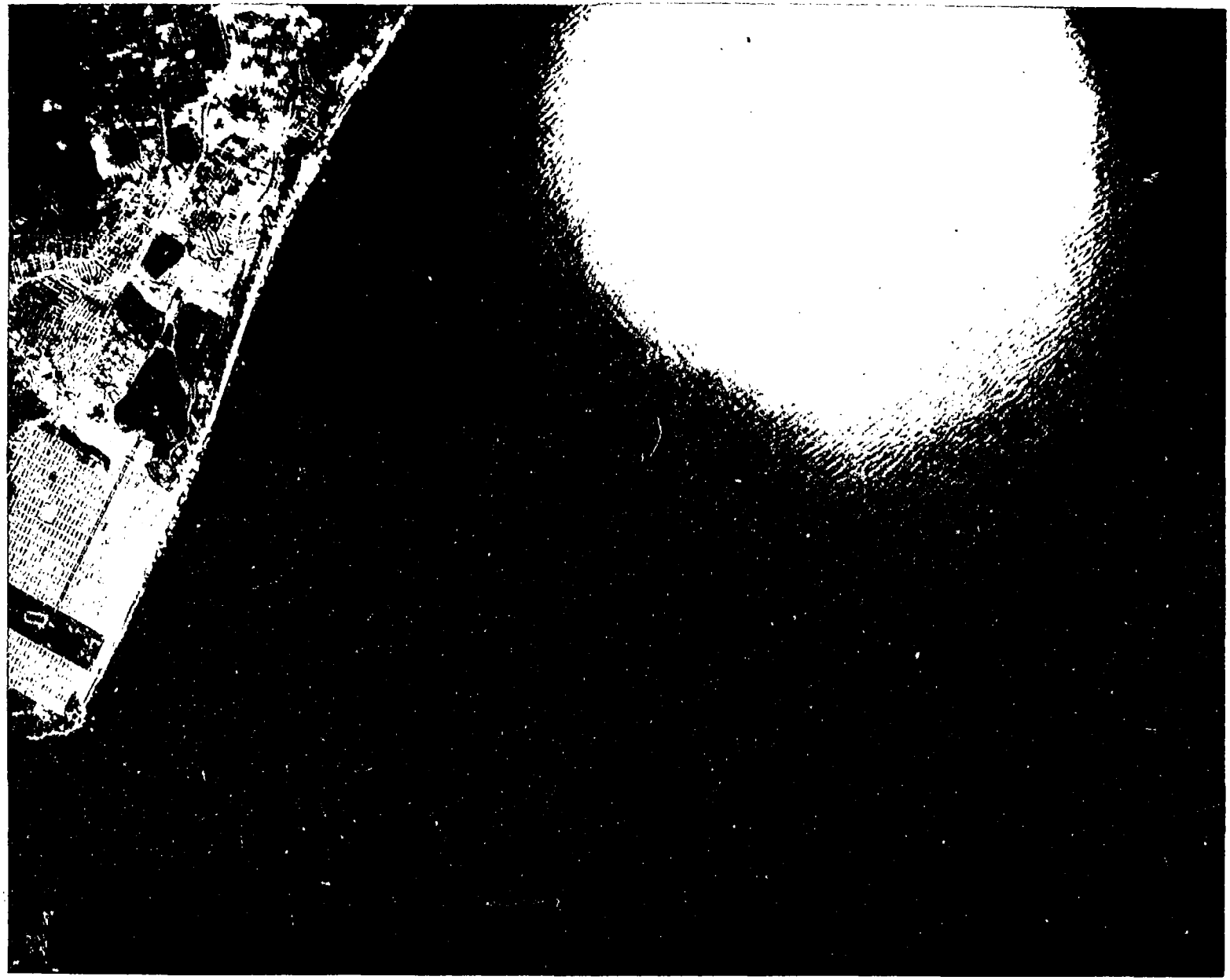

FIGURE 4.11 THE SPECTRUM FOR THESE WAVES WOULD HAVE TWO PEAKS NINETY DEGREES APART AT ALMOST THE SAME WAVE NUMBER.

FIGURE 4.12 POINT ST. GEORGE, CALIFORNIA. THE COMPLICATED EFFECTS OF REFRACTION, REFLECTION, AND DIFFRACTION ALL IN ONE PHOTOGRAPH.

the waves are reflected from it. Because of its size, the reflected waves radiate out from the island in a circular pattern that can be easily discerned. This pattern interferes with the oncoming waves and produces complex interference effects especially in the right portion of the picture. The shallower water above and to the left of this rocky island causes the waves to slow down and perhaps to be attentuated by bottom friction effects so that they are much lower in the portion of the photograph than anywhere else.

SWOP

Description of Program

On the 25th of October 1954 a number of stereo pairs of photographs were obtained at a point in deep water well to the east of the New Jersey Coast. The best two of the many stereo pairs were read on a stereo planograph to produce values of the departure of the sea surface from its average on a square grid of points 30 feet apart. A technical report was issued on the analysis of the data in July 1957, and a paper containing the essential aspects of the results was published in 1960 (Cote et al. (1960)). The final result was 820 numbers for each of the two data sets that finally survived. These numbers represented a vector wave number spectrum for wave numbers ranging from 0 to $2\pi/60$ feet^{-1}.

These two vector wave number spectra were combined to yield one final version and this in turn was also transformed to a frequency-direction spectrum for comparison with a spectrum obtained by a wave pole that recorded the rise and fall of the sea surface at a point. The lengthy delay between the time that the data were taken and the publication of the technical report was caused by

difficulties in the data at the edges of the fields being analyzed by the stereo planograph. The film had been distorted in the process of development so that it had shrunk in a differential way on the edges, and unrealistic results were obtained upon processing this data the first time. A substantial part of a year was needed to find out where the source of the difficulty was and to solve this particular problem.

Various authors have commented on the difficulties on doing such an analysis. It should not be too difficult with the faster computers and more modern data processing techniques to repeat SWOP within a time frame of about six months. Such a procedure is one sure way to obtain a full description of the waves over an area. It could provide a final proof of concept of the techniques proposed by Stilwell (1969), of radar imaging systems, and of the interpretation of measurements with lasers, pitch-roll buoys and other potential systems. A brief description of project SWOP follows.

The Data Set for Project SWOP

The pair of stereo photographs were obtained by flying two aircraft one behind the other with a radio link such that two cameras one in each aircraft were triggered simultaneously, one camera being slaved to the other. This provided simultaneous pairs of photographs with a proper horizontal separation between them for stereopsis. The horizontal scale was determined by having the research ship, RV Atlantis, tow a raft behind it with a sound transducer, or sonobuoy, on it. The travel time of the sound between the buoy and the ship then provided the horizontal scale. A number of stereo pairs were selected and read on a stereoplanograph at 30 foot intervals on a rectangular grid. The original data set for analysis consisted of

two sets of numbers each of 5400 values. There were four kinds of errors in the data.

A most difficult source of error to remove was the shrinkage in the original film that distorted the edges of the areas of stereo overlap. When the covariance function and the spectral estimates were computed from the faulty data some of the spectral estimates were negative, even after appropriate filtering in the spectral plane. Negative variances are most disconcerting even now and at that time they were almost catastrophic. It required a great deal of effort to locate the source of the difficulty as just described. This difficulty was finally located by testing whether or not the spot height values were normally distributed. For areas near the edges of the photographs they were not. The center regions of each of the data sets, however, did satisfy very closely the requirement of normality and when certain portions of the original areas were deleted, a successful analysis was obtained. The final data sets analyzed consisted of 3500 numbers for one data set, and 3600 numbers for the second data set, for a total of 7100 numbers to three significant figures. One array was 70 by 50 points, the other was 90 by 40 points. These values should be compared with the description of the analysis of the square area of the ocean 10 kilometers on a side given in Chapter 2.

The other sources of data error showed up in the estimates of the covariance surface and the spectrum. The total variance of the data set was high compared to the variance measured at a point with a damped buoy floating in the deep ocean, even after an attempted calibration for the motion of the buoy. There seemed to be three kinds of digitization error which were given the names, white noise, row noise, and column noise. Of these, either the row noise (or the column

noise)was quite high. Each row of data (or column) seemed to have a constant error added to it compared to the other rows (or columns) along with a random error at each point. The effects showed up in the spectral analysis by producing high values for the spectrum along the m = 0 axis of the spectral estimates (in the convention adopted of this report). The white noise produced a high value for the variance at the origin of the covariance function. Ways to remove these two dominant sources of error were devised and these errors were subtracted from the spectral estimates. Also a way to correct the covariance function was found.

The contoured values for one of the original full data sets from SWOP are shown in Figure 4.13. The lower right hand corner was badly distorted by film shrinkage.

Spectral Estimation Procedures

The computational procedures for determining the spectrum of even a time history in terms of a fast Fourier transform as described in Chapter 2 had not yet been developed. It would have been prohibitively expensive to compute the full Fourier transform of each surface that had been measured. The techniques developed by Tukey (1949) were extended to the two dimensional case and applied to these data. The first result was an estimate of the covariance function over a square area 1200 feet on aside. The Fourier transform of this truncated covariance function was then computed and the two dimensional extension of the weighting functions given by Tukey (1949) was applied. Table 4.2, given below, shows the values of the nine coefficients in the smoothing operator that was used in the Fourier transform of the truncated covariance function. These nine values are a simple extension, as can be seen from their components, of the weighting function suggested by Tukey (1949).

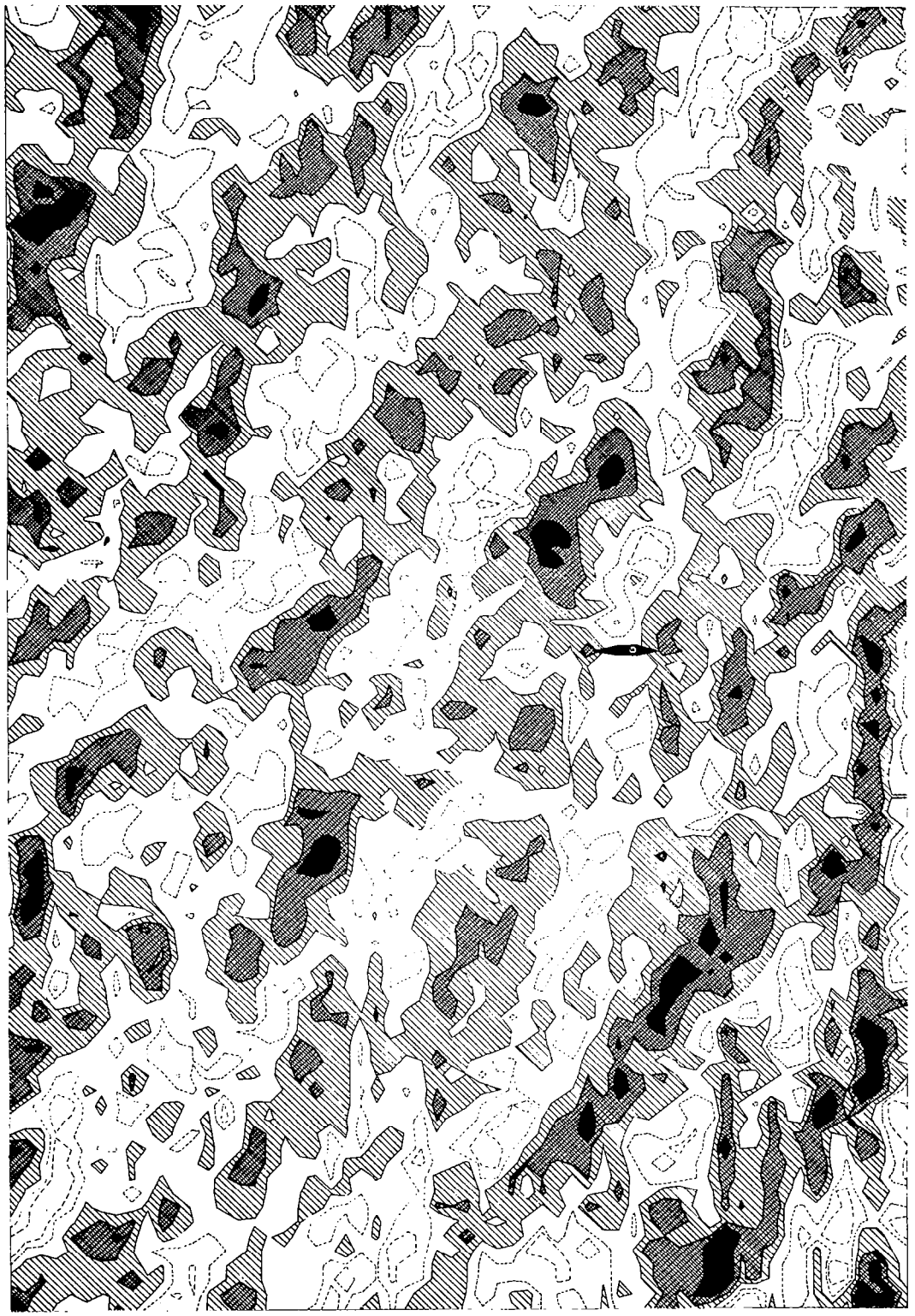

FIGURE 4.13 CONTOURED VALUES FOR ONE OF THE ORIGINAL FULL DATA SETS FROM SWOP. THE CONTOUR INTERVAL ARE APPROXIMATELY AT 2 FEET; WHERE WHITE AREAS ARE ABOVE THE MEAN AND SHADED AREAS BELOW THE MEAN.

Table 4.2 The smoothing filter used in Project SWOP on nine "raw" estimates centered on the center estimate.

	0.23	0.54	0.23
0.23	0.053	0.124	0.053
0.54	0.124	0.292	0.124
0.23	0.053	0.124	0.053

Results of the Spectral Analysis

The results that were obtained gave an estimate of the vector wave number spectrum. On the basis of supplementary meteorological information, a band of low waves that appeared to have been generated at a distance and traveling at 90° to the dominant waves of the original stereo pattern was mapped into that portion of the vector wave number space outside of the typical range of two quadrants so that the final vector wave number spectrum covered three quadrants. The vector wave number spectrum was transformed to a frequency spectrum by integrating it around circles with a finite difference technique and the frequency spectrum that resulted was compared with the spectrum obtained by a wave pole that recorded the waves as a function of time at the same time as the stereo pairs were obtained. The results did not yield 100% agreement between the two methods for measuring waves. The 90% confidence bands on both the frequency spectra obtained with the wave pole and on the transformed frequency spectrum from the vector wave number spectrum were computed for seventeen different bands. Of these seventeen different bands, two failed to agree within a 1% confidence level and six failed to agree within the 5% confidence level.

Some of the Results of SWOP

The smoothed version of the spectrum obtained from the analysis of the stereo pairs is given in Figure 4.14. It shows many of the features of waves that would be expected and, of course, features that occurred simply because of the particular set of conditions under which the photographs were taken. The total variance represented by this spectrum is equal to 3.46 $(ft)^2$ which corresponds to significant wave height of 7.4 feet. The peak in the spectrum corresponds to waves about 350 feet long. The wind at the time of the photographs was 18.7 knots, and the wave height seems reasonable for this wind speed.

The corrected covariance surface obtained by project SWOP is shown in figure 4.15. The symmetry through the origin should be noted. For this reason only the values on the left hand side were tabulated. Along the edges of the square the values are less than ± 10% of the value in the center, which shows how rapidly the wavy sea surface decorrelates with itself over relatively small distances for this wind speed. However, for storm seas with waves much longer and higher than this, the decorrelation distances are much greater.

The final result of project SWOP was an attempt to estimate, or provide, a description of the angular spread of the wave spectrum as a function of frequency for a given wind speed. The equation that was obtained is given by equation (4.7) in the notation of this present report.

$$F(\omega, \chi) = \frac{1}{\pi}\left[1 + (0.50 + 0.82\, e^{-(\omega v/g)^4/2}\cos 2\chi + 0.32\, e^{-(\omega v/g)^4/2}\cos 4\chi\right] \qquad (4.7)$$

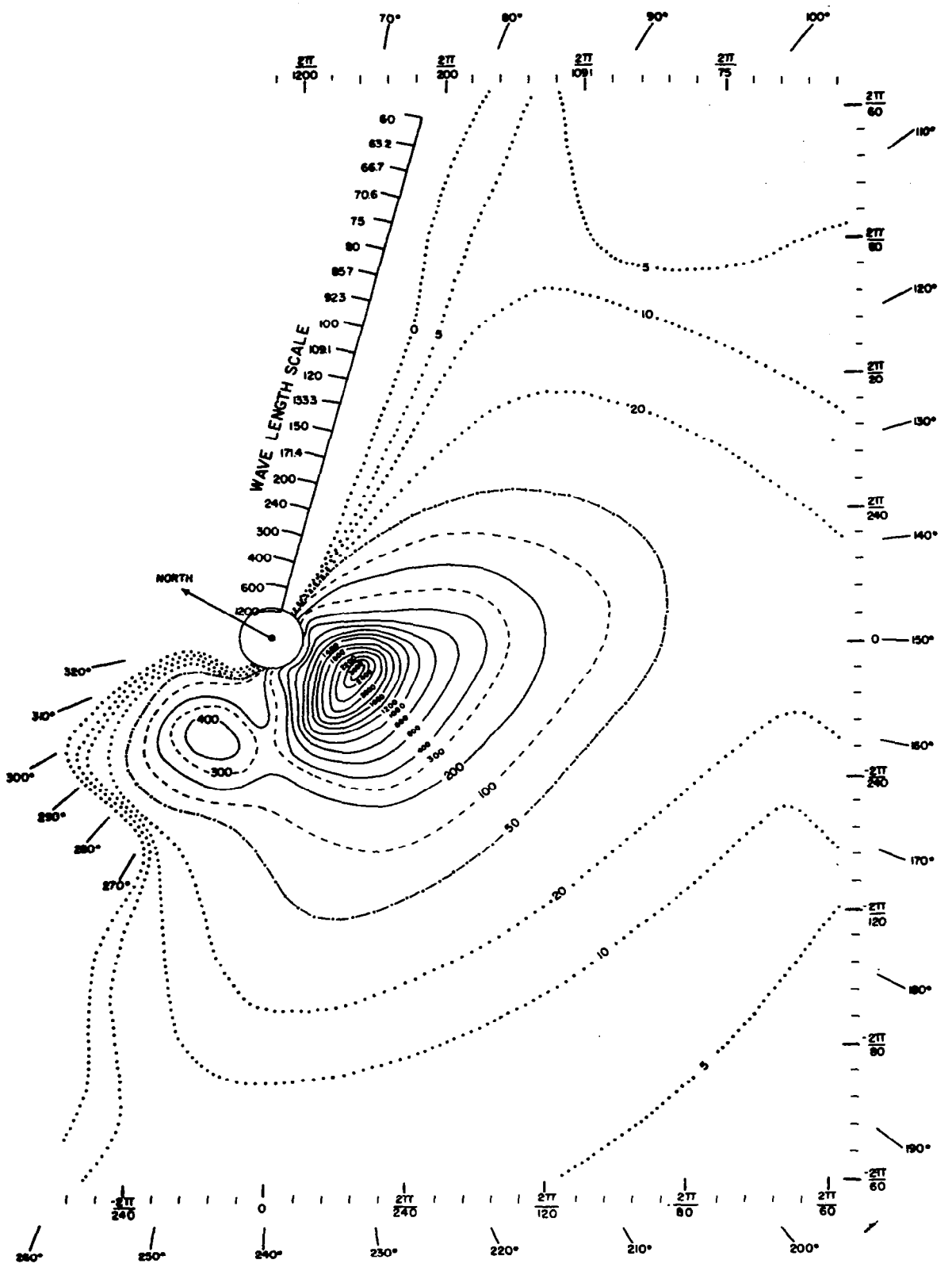

FIGURE 4.14 THE SMOOTHED SPECTRUM OF PROJECT SWOP.

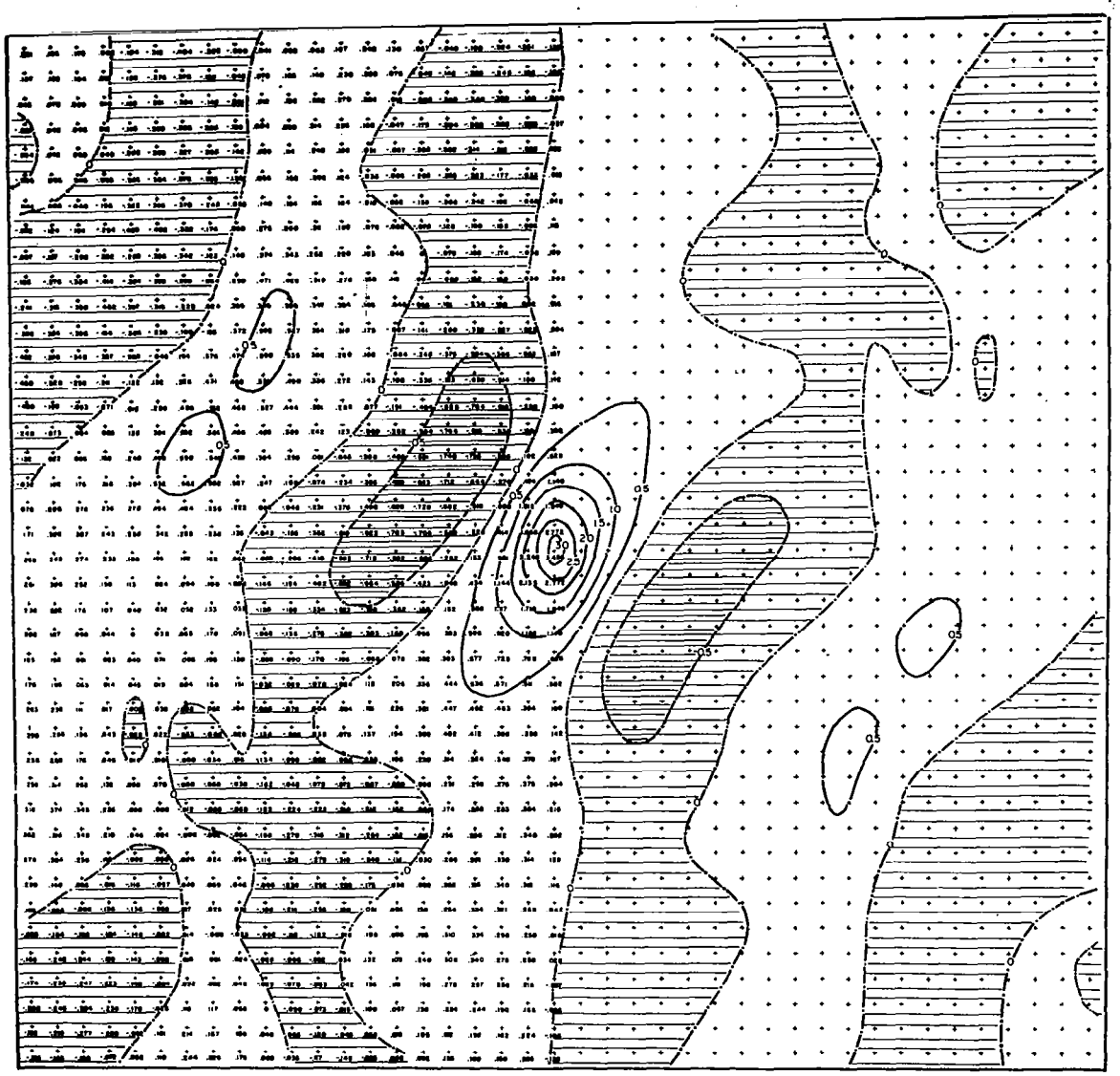

FIGURE 4.15 THE COVARIANCE SURFACE OF PROJECT SWOP.

This equation can be written in an equivalent form as given by equation(4.8).

$$F(\omega, \chi) = 1/\pi \left[0.50 \ (1 - e^{-(\omega\, v/g)^4/2}) \right.$$

$$+ (1.00 - 0.92\ e^{-(\omega\, v/g)^4/2})\ (\cos \chi)^2$$

$$\left. + (2.56\ e^{-(\omega\, v/g)^4/2})\ (\cos \chi)^4 \right]$$

In this form the gross behavior of the angular spread of a wind generated sea can be seen. For low values of the frequency, the constant term vanishes or becomes nearly zero, the $\cos^2\chi$ becomes small and the dominant term is $\cos^4\chi$. Stated another way the spectrum is very narrow near the peak for low frequencies. As the frequency increases for a given wind speed more and more of the second term enters and less and less of the third term is present so that the spectrum changes gradually from a sharply peaked spectrum to one that is more broadly spread. Also the constant term becomes larger. For a very large values of the frequency, according to this representation, the result is that the function of χ that is obtained is given by equation (4.9).

$$F(\chi) = \left[1 + \tfrac{1}{2} \cos 2\chi \right] / \pi$$

For high frequencies in the wave spectrum, the peak is three times the height of the values at 90° to the wind direction.

One of the problems of estimating the vector wave number spectrum from an image of the waves is that spectral components traveling in opposite directions cannot be separated without some knowledge of the wind direction and of other features of the waves. The values at ± 90° in a vector wave number spectrum estimate from a two dimensional representation should perhaps be thought of as being equal to half what is shown and the curve should be faired and continued on past these artificial dividing angles so as to produce modest amounts of spectral wave energy traveling opposite to the wind. The techniques most recently developed by Tyler et al. (1974) provide valuable information and perhaps a proof for the first time that spectral wave energy can travel at angles greater than 90° to the average wind. These results have an important application to the problem of radar backscatter. If for example, there were no spectral energy at backscattering wave numbers 90° to the wind, the results of the Langley AAFE RADSCAT Program would not have been obtained. For capillary waves, for example, these results indicate that there is a 6 db difference approximately between upwind and crosswind, corresponding to factor of four difference for the value of the spectrum at these two directions.*

It might be added that the very rapid change as a function of frequency for a given wind speed described by equations (4.7) and (4.8) does not appear to be realistic. In the spectral growth algorithm of the numerical wave specification and forecasting procedures described in Chapter 2, this change has been made more gradual. Moreover, since the ocean model does not have a very good angular resolution, the spectral values are frequently spread over more than ± 90° to the wind. The changing wind directions from six hourly chart to six hourly chart also spreads the spectrum over more than 180°, and typical spectra produced by the model frequently contains spectral values over a range of directions exceeding 180°. Nevertheless, more and better data on the

---

* More recent results show 4 db, or a factor of 2.5.

angular spread of the waves is very much needed and can eventually be used to improve numerical wave forecasting procedures. It is not clear at the present time how the wave imagery that may perhaps be obtained from SEASAT-A will provide information beyond a range of 180° for wave direction, given our present understanding of how the waves will be imaged.

RADAR IMAGES OF WAVES FROM AIRCRAFT

Introduction

Images of wave patterns on the sea surfaces have been obtained with both real aperture imaging radars and synthetic aperture imaging radars. It is clear that these images contain information on the vector wave number spectrum for those images obtained in deep water and on wave refraction effects for coastal images. The problems are to prove that these images can be related to spectra quantitatively. The spectra obtained from these images can then be related to spectra calculated from more conventionally obtained data.

There are a variety of explanations for the way that these images are generated.* One explanation yields a square law second harmonic image. Another explanation is based on geometric optics and/or physical optics and the concept of specular points. Still a third explanation proposes that the variation from point to point of the slopes of the waves being imaged produces, by means of these tilts, a variation in the radar backscattering cross section that in turn is proportional to the wave slope in the direction of the radar beam.

Of these various explanations, the last one seems to be most consistent with the data that are available. It should be possible to devise experiments to test the various explanations mentioned above so as to decide which one is correct. Numerous Soviet sources treat the interpretation of radar images in terms of slopes and employ the methods that follow in this section (as for example, Belousov et al. (1974) and Zagorodnikov (1974).) Also Brown et al. (1974) postulates backscatter as one of the important mechanisms and shows imagery in which the absence of backscatter produces areas of no image.

---

*See Brown et al. (1974), Goldfinger (1975), Swift (1974), and Zagorodnikov et al. (1972).

**Bragg scatterers are abundant in Figures 3.7 to 3.13.

It is possible on the assumption that the last explanation is the correct one to follow this particular assumption to its logical conclusion and compare properly transformed vector wave number spectra obtained from radar images to spectra obtained from other kinds of wave data so as to verify this particular assumption. If the assumption is not true an inconsistency will result upon the completion of the analysis.

This assumption also yields a simple explanation for why synthetic aperture images are obtained with aircraft systems since "coherence" is no longer essential. It raises a number of serious doubts as to whether or not a simple synthetic aperture system will work on a spacecraft that have to do with the drastic changes in the various factors involved when going from aircraft to spacecraft. These problems will be treated later. A system that may be satisfactory for a spacecraft will be described.

For aircraft altitudes, there should be no substantial differences between real aperture and synthetic aperture images. The only real problem in interpreting aircraft images is that the speed of the aircraft is only about 10 to 20 times the speed of the waves and that the finite time required to image a given area distorts the wave pattern in a way that requires correction in the interpretation of both the wave pattern and the spectra. This problem has been solved. It is the only one that simplifies on going to spacecraft altitudes and velocities.

Images of the Sea Surface

In this section, the problem of imaging a wavy sea surface in terms of the resolution of the radar system being employed will be discussed. Consider a sea surface described by a single simple harmonic progressive wave with some roughness elements on it so that the radar

backscatter will still be present. The surface being imaged is actually a derivative in the y direction of the simple harmonic progressive wave. This is indicated by equation (4.10).

$$\frac{\partial \eta(x, y, t)}{\partial y} = am \cos(\ell x + my - \omega t + \epsilon) \tag{4.10}$$

The radar imaging system performs the operation indicated by equation (4.11) on this function.

$$\frac{\partial \bar{\eta}(x_o, y_o, t)}{\partial y_o} = \int_{-\infty}^{\infty}\int_{-\infty}^{\infty} G(x-x_o)H(y-y_o)am \cos(\ell x + my - \omega t + \epsilon)dxdy \tag{4.11}$$

The function, $G(x-x_o)$, represents the effect of the beam width of the scanning radar in its smaller dimension, since a real aperture radar is being considered for this illustration. It can be a very complicated function of the antenna pattern and is typically characterized as a first approximation by the 3 db beam angles for the beam measured in this direction. The function, $H(y-y_o)$, represents the effect of the radar pulse. It depends upon the lengths of the pulse, the rise time to full power of the pulse and the sharpness with which the pulse is cut off on the other side. The details for these two functions are determined by the details of the radar design and the actual calculation of their form is a lengthy and difficult procedure. For purposes of illustration, both of these functions will be represented by a simple on-off function where within a certain interval of the x, y plane they are equal to a constant value and outside of this interval they are identically zero. For the real situation the edges will be smoothed. Sometimes a function shaped like the classical Gaussian function is used instead of the box-car function. It is quite probably that something closer to a box-car function is more realistic than a Gaussian-type function.

Nevertheless, the functions G and H for this analysis are defined by equation (4.12).

$$G(x-x_o) = \frac{1}{L} \; ; \; -L/2 < x-x_o < L/2$$
$$H(y-y_o) = \frac{1}{M} \; ; \; -M/2 < y-y_o < M/2 \qquad (4.12)$$

and zero otherwise.

Under these assumptions, the operation described originally by (4.11) can be described by equation (4.13).

$$\frac{\partial \bar{\eta}(x_o, y_o, t)}{\partial y_o} = \frac{1}{ML} \int_{y_o-M/2}^{y_o+M/2} \left[\int_{x_o-L/2}^{x_o+L/2} am \cos(\ell x + my - \omega t + \epsilon) dx \right] dy \qquad (4.13)$$

When the integrations indicated above are carried out the final result for a single simple harmonic progressive wave is given by equation (4.12). As the line scan is varied as a function of y_o and as successive line scans are obtained to form the image, the original sinusoidal wave is reproduced except that its amplitude is changed.

$$\frac{\partial \bar{\eta}(x_o, y_o, t)}{\partial y_o} = am \frac{\sin(\ell L/2)}{\ell L/2} \cdot \frac{\sin(m M/2)}{m M/2} \cdot \cos(\ell x_o + my_o - \omega t + \epsilon) \qquad (4.14)$$

The original wave defined above has been multiplied by two functions of the vector wave numbers. They are classical $(\sin \varphi)/\varphi$ functions that arise from such considerations. The only difference between this result and other results is that the wave number, m, appears in both the numerator and denominator of this expression and could be cancelled.

When this last result is generalized to a sum of sinusoids with different wave numbers, frequencies and phases the result is equation (4.15), which could represent any reasonable wave image where several thousand terms are given in the double summation.

$$\partial\eta(x_o, y_o, t)/\partial y = \Sigma_q \Sigma_p a_{pq} m_p \frac{\sin(\ell_q L/2)}{(\ell_q L/2)} \cdot \frac{\sin(m_p M/2)}{(m_p M/2)} \cdot \cos(\ell_q x_o + m_p y_o - \omega_{pq} t + \epsilon_{pq}) \tag{4.15}$$

Upon carrying out the usual spectral estimation procedure the spectrum that will be estimated has an expected value given by equation (4.16)

$$\bar{S}(\ell, m) = S(\ell, m)\left[\frac{\sin(\ell L/2)}{\ell L/2}\right]^2 \cdot \left[\frac{\sin(mM/2)}{M/2}\right]^2$$

$$= F(\ell, m, L, M)\, S(\ell, m) \tag{4.16}$$

The distortion of the spectrum due to the finite imaging time has been neglected. These equations should all have the subscript e on the ℓ's and the m's. The two dimensional elevation spectrum of the original wavy surface without differentiation, as given by $S(\ell, m)$, has been multiplied by a filter function in two dimensional wave number space designated here by $F(\ell, m; L, M)$. Illustrative graphs of this function for two different values of L and M will be given. For purposes of illustration, a spectrum that might have been observed in wave number space if the waves were traveling away from the aircraft is shown in equation (4.17).

$$S(\ell, m) \cong \frac{\alpha m^2}{\pi(\ell^2+m^2)^3}$$

$$\text{if } k_o^2 < \ell^2 + m^2 < \infty, \text{ and } m > 0 \tag{4.17}$$

$$= 0, \text{ otherwise}$$

Illustrative Filter Functions

Suppose that the airborne imaging system is capable of resolving spots on the sea surface that are roughly 25 meters on a side. Then $M = L = 25$ meters. If these values are substituted into equation (4.16) and graphed, the result is shown in Figure 4.16. Along the m axis where ℓ equals 0 the function of m that results is given simply by $(1 - \cos Mm)/M^2$. The function is zero at $m = 0$ and at $m = 2\pi/25$ and reaches a maximum at $m = 2\pi/50$. Other values of m are shown on the figure. When $m = 2\pi/50$, the function of ℓ that results as ℓ is varied for this value of m is shown on the figure. It behaves as the square of a function shaped like $(\sin \varphi)/\varphi$ and is zero at $\ell = \pm 2\pi/25$.

For both of these functions, values exist outside of the range graphed. As a function of m, the graph would repeat between $2\pi/25$ and $2\pi/12.5$. Outside the interval $-2\pi/25$ to $+2\pi/25$ on the ℓ axis, the function would rise again to very small values of the order of two percent of the original peak. However, both of these effects of the analysis are artifacts of the box-car function used in the analysis, and they would probably not exist for a real radar situation. The results, however, are quite applicable for the region defined, with the possible exception that these functions might change slightly in detail. One of the problems connected with the actual design of an imaging radar is that the pure $((\sin \varphi)/\varphi)^2$ behavior may be distorted by other effects when the values are small such that errors perhaps as large as a factor of two could occur upon estimating a spectrum. These functions need to be checked with considerable care.

Now suppose that the beam width cannot be made small enough to resolve a patch 25 meters wide in the x direction. Suppose for example, that $L = 400$ meters instead of 25 meters. The result of such an

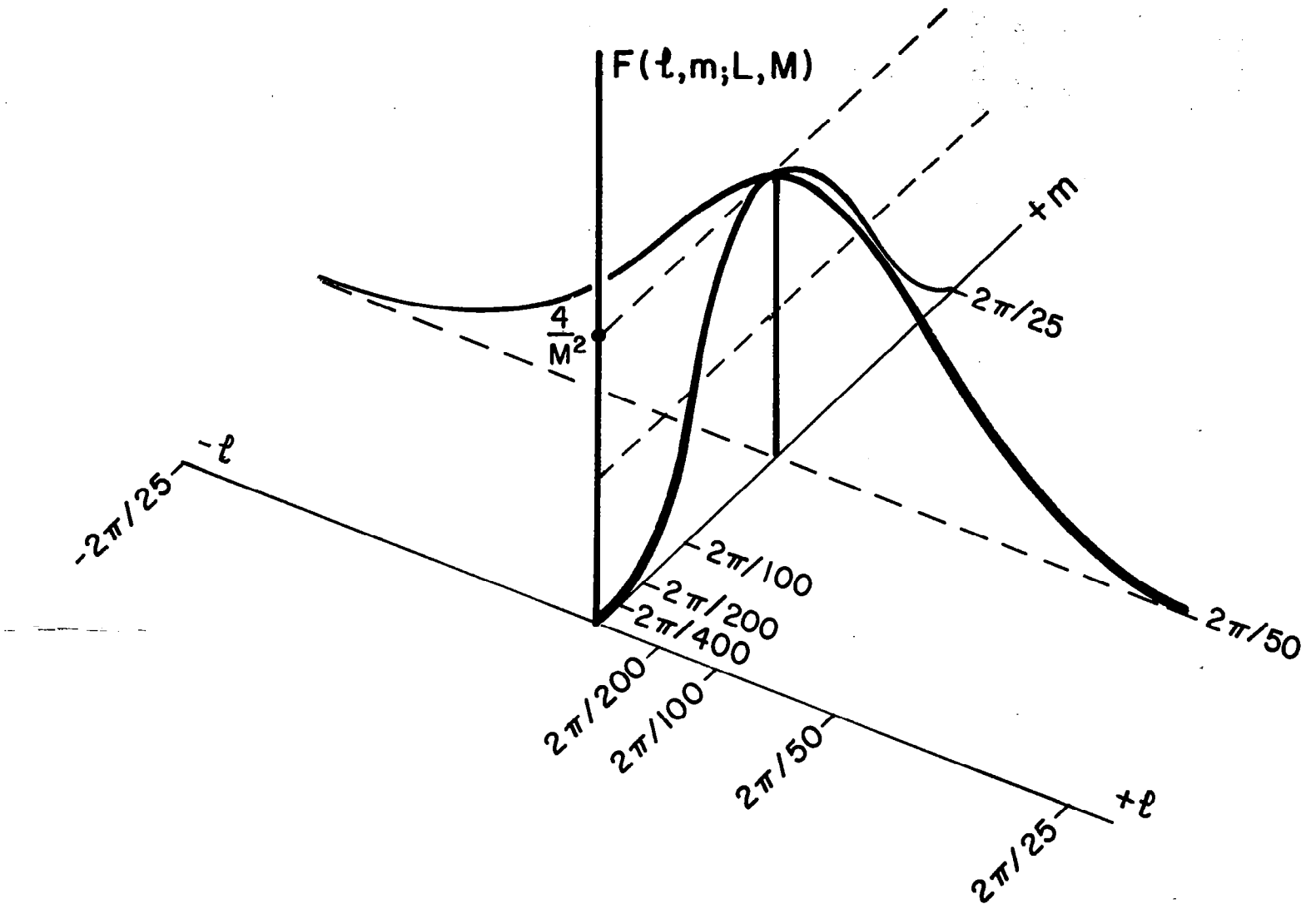

FIGURE 4.16 F(ℓ,m; LM) for L = M = 25 METERS

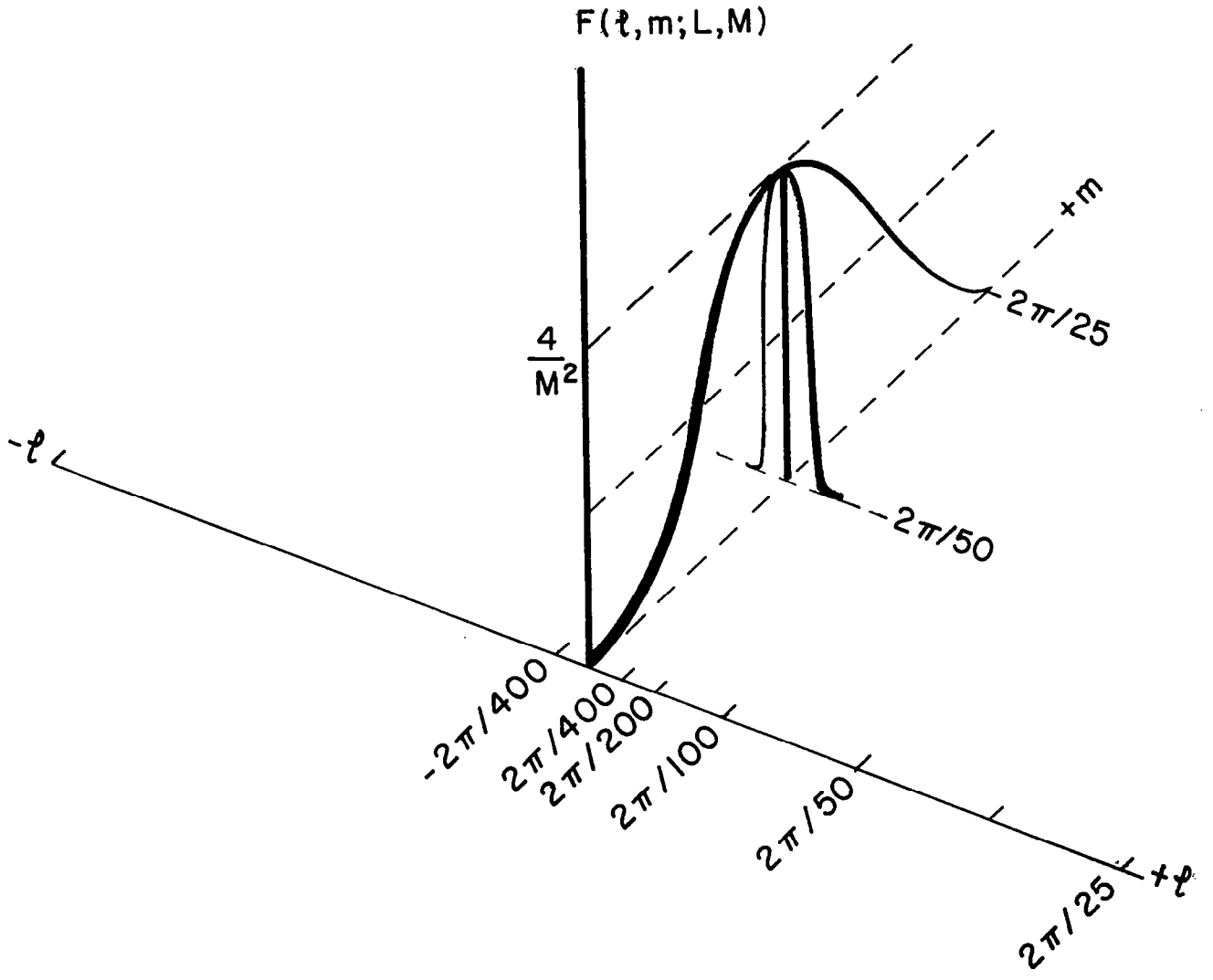

FIGURE 4.17 F(ℓ,m;L,M) FOR M=25 METERS, L=400 METERS

assumption is shown in figure (4.17). Now the $(\sin \ell L/2)/\ell L/2$ function, when squared, produces an extremely narrow range of values in the ℓ direction where the wave can be imaged. A wave, for example, with equal vector components for both ℓ and m so that it falls on a line 45° to the ℓ axis and, say, at a radial distance of $2\pi/100$ would be rejected by this wave number filter and would not be imaged by such a system. Stated another way, so many oscillations of the wave would be averaged over the x direction that the average would be extremely small and no variation would be detectable. Therefore, a narrow pulse in one direction that is too wide in the other direction will only see a slice of the wave number spectrum as shown. This, of course, is what is hoped for in some of the alternate radar systems that have been proposed and that they do not attempt to image the sea surface. These systems have the advantage of recognizing the great difficulty of producing a very narrow radar beam. It is clear that if the orientation of this particular function as graphed can be changed in 10° steps throughout the half plane in ℓ, m space, slices of the spectrum would be obtained from which the full spectrum might be recovered.

The discretized equivalent of the narrow band filter in the ℓ direction of wave number space was described by Marks (1954), and this reference contains an illustration of the effect of such a filter on a wave spectrum. Soviet scientists have used this particular result to avoid the difficulty of carrying out two dimensional spectral analyses. (See for example, Zagorodnikov (1974)).

Before proceeding, consider Table 4.3, which relates the wavelength, the wave number, the period and the frequency of a given wave.

Table 4.3 Wavelength, wave number, period, and frequency for a simple harmonic wave.

Wave length (m)	$k(m^{-1})$	T(sec)	f(Hertz)
50	.126	5.6	0.1769
100	.0629	8.0	0.125
200	.0314	11.3	0.0885
400	.0157	16.0	0.0626
800	.00785	22.6	0.0442

As shown by this table, a wave with a length of 50 meters, which is most easily resolved and which has the least effect on it of the spectral filters, has a wave number of 0.126, a period of 5.6 seconds, and a frequency of 0.1769 hertz. These waves are relatively uninteresting. They are generated as part of the spectrum as soon as the wind over the ocean increases up to about 20 knots, or 10 meters per second, and they are just about everywhere over the ocean except where it is calm. The more interesting waves are those that have periods of 11 seconds and higher that are found in spectra for higher winds. The active part of a wave spectrum from the point of view of those who will use these data probably extends from somewhere near eight seconds up to somewhere near twenty seconds. Spectral components corresponding to waves 800 meters long with a period of 22.6 seconds are relatively rare over the world's oceans.

With this in mind, consider equation(4.17) which illustrates a spectrum for a wind sea traveling with dominant components along the m axis of the wave number spectrum. This spectrum has a k^{-4} gross behavior times the cosine squared of the angle between the m axis and the ℓ axis of the vector wave number space. Quite clearly the

spectral filter will not succeed in preventing the spectrum that would be estimated as given by equation(4.17) from becoming very large as m approaches zero for $\ell = 0$. The lowest wave number indicated by k_o would yield the highest value for the estimate as the wave numbers approach zero. This is the reason why the effect of imaging wave slope does not wipe out the steep forward face of a wave spectrum. Typically the spectrum grows higher and more rapidly as the wave number decreases than can be attenuated by the m^2 effect near the origin.

Backscatter Results Applied to Radar Images

The essential difference between a scatterometer and a radar imaging system is the size of the cell and the length of time over which the backscatter signal is averaged. For a scatterometer, the size of the cell over which the average is taken is large and the integration time is made as long as possible. At off nadir angles for S193 on SKYLAB, for example, the cell illuminated at the sea surface was elliptical and about 30 kilometers by 12 kilometers. Even larger areas will be illuminated by SEASAT-A. For SKYLAB, the entire distance between the sea surface and the spacecraft was filled by both the outward traveling radar waves and a returning signal at the instant when the receiver was turned on to detect, integrate, and average the return signal. The result was a very stable measurement that could fluctuate by about ±0.3 db due to sampling variability.

In contrast, the proposed explanation for how an imaging radar system works requires a short pulse so that the range of the target can be found and a backscatter signal from an area of the sea surface that is small compared to the dimensions of the waves being imaged

and is perhaps 25 meters on a side. These returns from the sea surface are then mapped into an x_o, y_o plane to produce the image. Clearly the signal strength must vary from point to point to produce the image.

New knowledge of the spectrum of a wind roughened sea surface, which is an extension of the results of Pierson and Stacy (1973), as given in a following chapter, makes it possible to separate the Bragg scattering part of radar backscatter from the slope effects of the longer waves on the sea surface as generated both by the wind and as controlled by effects such as fetch, duration and spectral dispersion due to the propagation of these waves on the ocean surface. The results on the nature of the wave spectrum have been used by A. K. Fung to obtain a most realistic theory for radar backscatter that explains not only all of the results obtained under the AAFE Langley Aircraft Program but also provides a way to account for the variations of the larger gravity waves in causing variations in the magnitude of radar backscatter.*

The simplest theories for radar backscatter employ only the spectrum of the short waves on the sea surface with wavelengths comparable to the radar wavelength. These theories say that the backscatter is directly proportional to the value of the spectrum of these waves evaluated at that wave number for that direction, or at the vector wave number, that corresponds to the Bragg resonant condition, $2k_o \sin\theta$, where k_o is the radar wave number and θ is the angle off nadir.

This theory does not take into account the effect of the slope of the larger waves. By the larger waves is meant all wave elements on the sea surface with lengths perhaps 10 to 100 times greater than the length of the wave corresponding to the Bragg wave number. For a 13 gigahertz radar, the radar wavelength is about

---

*See Appendix on recent references.

2.25 cm long so that waves about 2.25 meters long can contribute to the slope effect. A review of some of the sea surface photographs in the preceding chapter, can surely convince one that these slopes are important in tilting the sea surface. The major difficulty in the past has been that the composite theories that combine tilt plus backscattering have not had an adequate description of the full spectrum and have essentially assumed a spectrum with a sharp null between the gravity wave part and the capillary part. As the results of a following chapter show, this is not true, and the work of A. K. Fung has essentially solved this difficult part of the problem by treating a realistic sea surface spectrum.

For these reasons, it is necessary to discuss the backscatter signal that would be measured first with a scatterometer and then contrast it with a signal that would be returned for an imaging radar. In a generalized form, the results of Fung can be written as equation (4.18).

$$\sigma^{\circ}_{HH}(A) = \sigma^{\circ}_{HH}(\theta, \chi, u_{*}, P(\eta_{x}, \bar{\eta}_{y})) \tag{4.18}$$

This equation shows that the backscatter as averaged over a large area, A, as indicated on the left by an additional subscript, is a function of the mean nadir angle measure with reference to a level sea surface, the aspect angle of the radar beam vector with reference to the wind direction, the friction velocity (which is a measure of the wind speed close to the sea surface), and the slope distribution of the longer waves. Once the aspect angle is picked, the slope distribution is determined along this particular direction and an

integration is performed over these slopes using a variable θ so as to obtain the backscatter value for the average, $\bar{\theta}$, determined by the nadir angle. The two slope components of the sea surface are indicated in equation (4.19) as decomposed into two parts.

$$\eta_x = \bar{\eta}_x + \eta_x^*$$
$$\eta_y = \bar{\eta}_y + \eta_y^* \qquad (4.19)$$

The single overbar part could be considered to be those portions of the slope that are associated with the larger gravity waves and the asterisk is that portion of the slope that is associated with the shorter waves on the sea surface, but not with the Bragg scattering waves.

The backscatter measured by a scatterometer is indicated by equation (4.20).

$$\sigma^\circ_{HH}(A) = \iint P(\eta_x, \eta_y)\, F(\theta, \chi, U_*) d\eta_x d\eta_y \qquad (4.20)$$

The full distribution of slopes is integrated over for the appropriate values of θ, and the area involved is large. The result of such a calculation is that, for a given wind speed, a given aspect angle, and a given nadir angle, only the probability function for the slopes changes with the large scale wave conditions.

Equation (4.21) is the backscatter as computed by averaging over a small area, A.

$$\sigma^\circ_{HH}(A') = \iint P(\eta_x^*, \eta_y^*)\, F(\theta, \chi, U_*) d\eta_x^* d\eta_y^* \qquad (4.21)$$

The result will be a different value for the backscatter that will be a function of θ, where θ in a sense can still vary as a function of the actual slope of the sea surface, relative to the nadir value of θ, for each of the small patches of sea surface illuminated and imaged by the radar imaging system. The result is, therefore, a function of the nadir angle, the aspect angle, and the friction velocity, but it is no longer a function of the slope contribution of the larger gravity waves on the sea surface.

The result of these considerations are illustrated in figure 4.18. The illustration is schematic, and both the vertical and horizontal values for the scale are deliberately omitted. In fact, for the moment it will not even be stated whether or not σ^o is on a linear scale or a decibel scale. If the simplest backscattering theory is used that completely neglects sea surface slope so that the backscatter is a function of only the capillary wave spectrum, the result is the curve labeled (1) on this figure.

If all of the effects of slope are considered and if the operation indicated by equation (4.20) is carried out, for a known probability function for the slope, the result is curve (2) on this figure. For horizontal polarization and a fully developed wind sea for a given U_*, curve (2) can be as much as 4 db higher than curve (1). For vertical polarization the increase is small. This may be an explanation for why HH sometimes yields better images than VV in radar imaging systems. If on the other hand, the slope distribution is restricted to those slopes contributed by the waves whose lengths are the same as the size of the patch being imaged, or smaller, as indicated by equation (4.21), the result would be a curve somewhere between the first and second curve as indicated by curve (3).

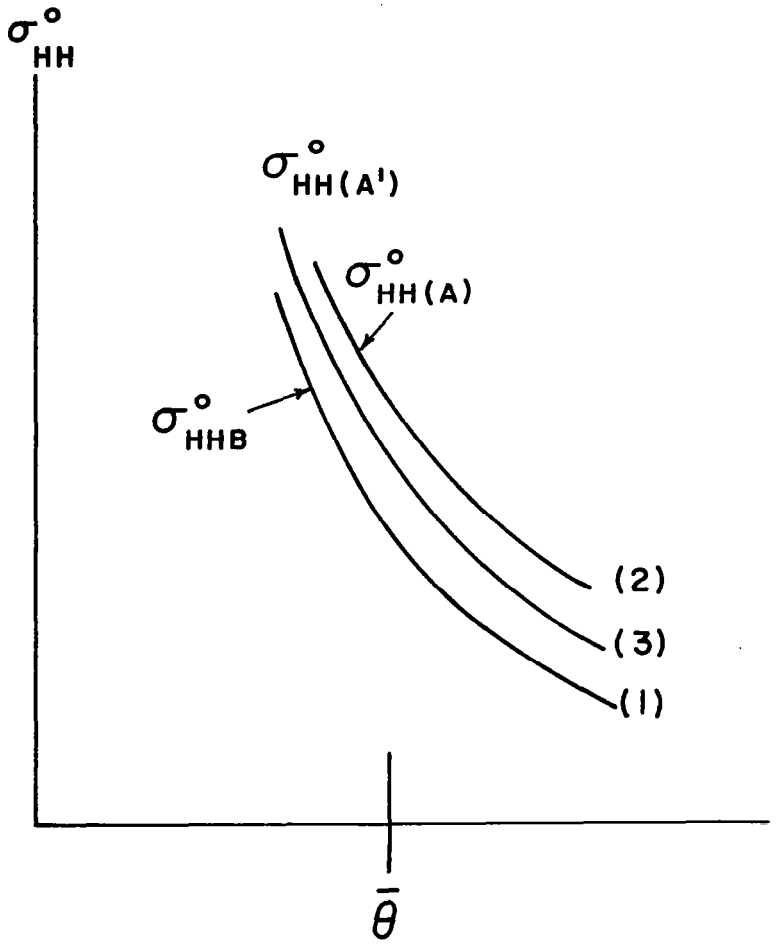

FIGURE 4.18 SCHEMATIC NORMALIZED BACK-SCATTERING CROSS SECTIONS FOR (1) CAPILLARY WAVES ONLY AND NO LARGE WAVES, (2) FOR AN AVERAGE OVER ALL SLOPES IN A LARGE AREA, AND (3) FOR AN AVERAGE OVER THOSE SLOPES IN AREAS SMALLER THAN M BY M METERS.

In each of these curves the interpretation of the angle θ is different. For curve (1), the interpretation has very little to do with the gravity wave part of the problem. For curve (2), the effect of gravity waves has been completely included, and the averaging process has raised the backscatter value. This happens because forward tilts that decrease the nadir angle locally produce stronger backscatter signals than comparable backward tilts that decrease them and the average is therefore higher than the signal that would be obtained from a flat surface with comparable small scale roughness. Curve (3) in figure (4.18) can be easily computed from the results of Fung simply by redefining the probability density function for slopes to include the contributions from the shorter waves and exclude the contributions from the longer waves. These shorter waves are generated very quickly by the wind and curve (3) may be a very important and much more stable curve than curve (2). A procedure for correcting all of the backscatter measurements so as to interpret them in terms of the full effect of slope has been obtained for the analysis of the SKYLAB data and is expected to improve the results substantially.

When averaged over a small area, the nadir angle takes on a new meaning. The local slope of the sea surface over the small area can differ from zero in such a way that the effective nadir angle is either decreased or increased. Consider a line scan such as a radar imaging system would produce and consider also the variation of nadir angle along this line scan in the neighborhood of a point on the line scan given by $y = y_0$ the result is given by equation (4.22).

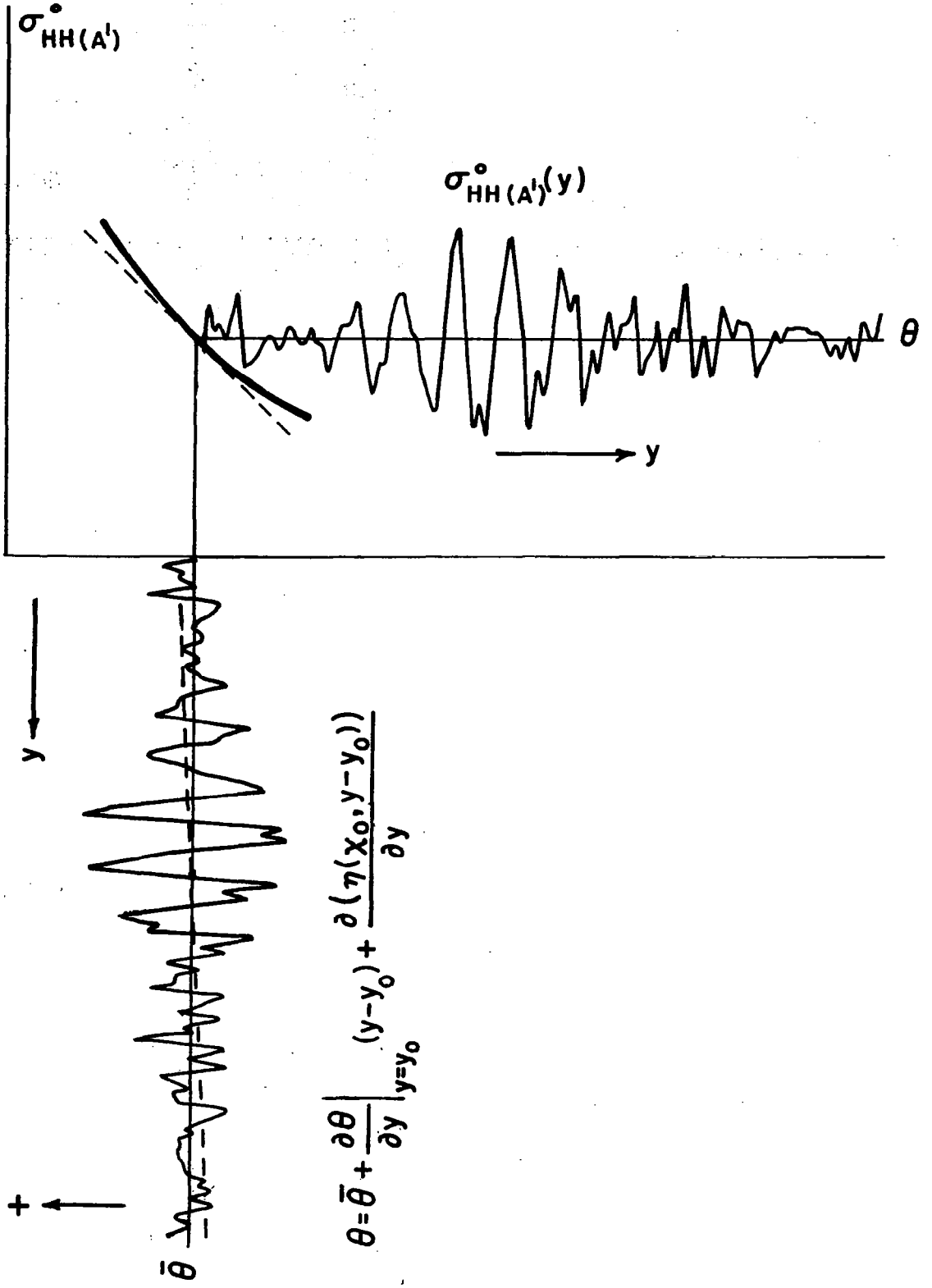

FIGURE 4.19 SCHEMATIC DIAGRAM FOR THE GENERATION OF y SCAN

$$\theta = \bar{\theta} + \frac{\partial\theta}{\partial y}\Big/_{y=y_o} \cdot (y - y_o) + \frac{\partial(\eta(x_o,\ y - y_o))}{\partial y} \qquad (4.22)$$

In this equation, the slope of the sea surface has been set equal to the angle in radians. The approximation, $\tan^{-1}\xi = \xi$, has been used. The theory can obviously easily be refined. Also, only the first three terms of such an expansion are shown. There are undoubtedly quadratic and higher order terms in the expansion that need to be considered.

The backscattering cross section as averaged over this small area can also be expanded in terms of the angle θ. The result is indicated by equation (4.23), and apart from the slow linear drift given by the term, $(\partial\theta/\partial y)\ (y - y_o)$, where the partial is evaluated at $y = y_o$, the backscatter varies directly in proportion to the slope of the sea surface in the y direction.

$$\sigma^o_{HH}(A') = \sigma^o(\bar{\theta},\ \chi,\ U_*)$$

$$+ \frac{\partial\sigma^o}{\partial\theta}\Big/_{\theta=\bar{\theta}} \left[\frac{\partial\theta}{\partial y}\Big/_{y=y_o} (y - y_o) + \frac{\partial(\eta(x_o,\ y - y_o))}{\partial y}\right] \qquad (4.23)$$

These results are indicated schematically in figure (4.19). Again the scales of the two coordinates have been made deliberately vague. An input function as a function of distance along the y scan, which is really a function of time as recorded, is shown entering the bottom of the figure as a graph of the local nadir angle as a function of y. For each of these nadir angles the output would be a different value for the backscattering cross section and the output function

namely $\sigma^{\circ}_{HH}(A')$ as a function of y will change depending upon the y variation of the nadir angle. Typically, the slope of the larger waves can vary by plus or minus 5° or more about a given mean and thus the working range of the fluctuations can be about 10° on the graph of σ° versus θ .

Although figure (4.19) is deliberately vague, it raises a number of interesting questions. In the imaged space produced by the radar is the brightness proportional to the backscattering coefficient expressed linearly or logarithmically? Or stated in another way, is the image intensity logarithmic or linear? It would seem that using a logarithmic variation in image intensity would linearize the output function substantially for the ranges of θ that would be expected. A second question is concerned with how the linear trend indicated in the input is removed from the output. Quite obviously this is done because the backscattering coefficient as a function of nadir angle for the typical ranges scanned in aircraft systems varies by 20 or more db. Still another question is whether or not the higher order terms in the expansion of σ° about $y = y_0$ are important and whether or not they introduce appreciable nonlinearities in the image. If they do, can these nonlinear features, which are not real, be removed by suitable modifications in the way that the images are processed? All of these questions are important because nonlinearities in the input output relationship sketched here will distort the spectra that are estimated from the images in such a way that immediate and obvious agreement with spectra obtained in other ways may not be possible. The value of a radar imaging system should not be automatically discounted until these effects are put into a quantitative form and, if possible, removed from the images by appropriate modifications of the analysis procedure.

A Real Aperture Image of Waves Obtained with an Aircraft

Figure (4.20) shows a real aperture radar image provided to the writer by Mr. Duncan Ross of AOML/NOAA. It in turn was given to him by a soviet scientist named V. S. Loshchidov, while he was visiting the Soviet Union.

This image is an excellent example of a correctly obtained image with such a system. Apart from the bright band across the bottom, the rest of the image has nearly a uniform background gray scale. The slight blotchiness, which might conceivably represent gustiness in the local wind, upon spectral analysis will all be mapped to the origin of the vector wave number coordinate system and can be easily removed. The longer more dominant waves are adequately resolved and there are many of them. There are no obvious changes in the direction or scale of these waves from one side of the line scan to the other such as what might be caused by mapping range directly. The image produces a slight optical illusion effect because visually the waves appear to be illuminated by a light source coming from the top right portion of the figure when it is held with the legend on the bottom. However, if the figure is turned over, the illumination still appears to come from the top right portion of the figure. This effect is similar to the problem of determining whether a highlighted circular region of a disturbance on a plane surface is a bump or a depression and can be seen in some of the lunar imagery of small craters, which look sometimes like small bumps. The imagery, however, is perfectly consistent with the assumption that those portions of the wavy surface tilted toward the radar have backscattered a stronger signal to the radar which in turn has resulted in a brighter region in the image plane.

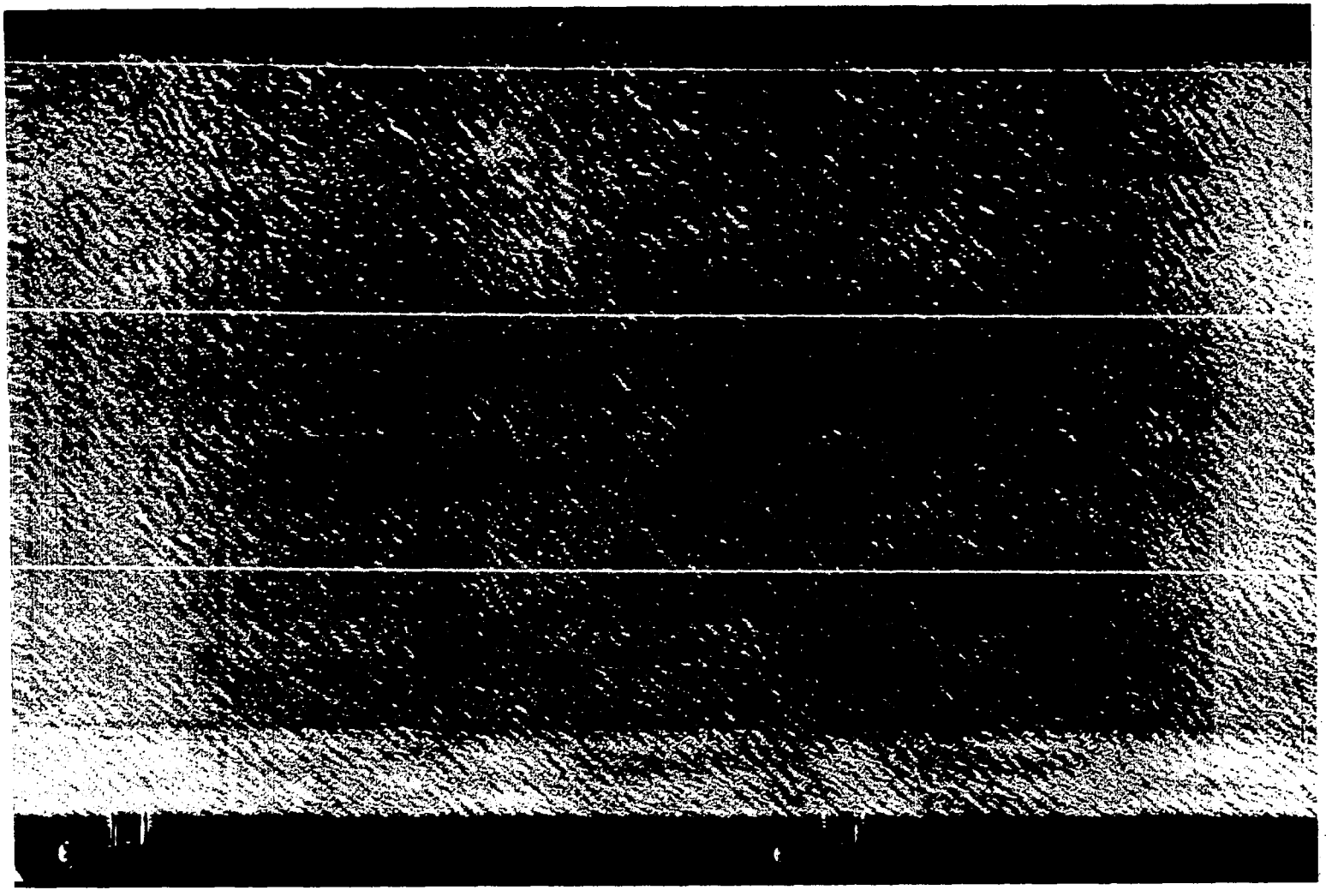

FIGURE 4.20 A REAL APERTURE IMAGE OF OCEAN WAVES.

For all intents and purposes this image has all of the features of a stationary random Gaussian sea surface as described in Chapter 2. The waves are short crested, they come in groups, the apparent directions for the different waves crests change by ± 20° relative to some average, and there are portions of the image where the waves are low as well as portions where the waves are high. The longer dominant waves appear to lie at an angle of about 45° to the horizontal with the angle being negative in the usual sense of a cartesian coordinate system. A very close inspection also shows a train of waves at right angles to the dominant train traveling in a different direction. The sea surface imaged may well have consisted of some "swell" from a distant source upon which is superimposed a local wind with much shorter wavelengths.

A thought experiment could be carried out to describe what would have to be done and the results that would be expected if this image were to be converted to an estimate of a vector wave number spectrum. Clearly the spectral filter is quite broad and flat and nearly all wave numbers have been properly imaged. The very short waves in the image are in the order of one-fourth of the length of the longer waves.

With the bright band across the bottom omitted the remaining portion of a line scan could be read off at 350 equally spaced values, and then at this distance namely one three hundredeth and fiftieth of the distance from the edge of the bright band to the top of the figure, a second line scan could be read. The horizontal distance is roughly double the vertical distance so that the final result would be approximately 245,000 digitized values of this image. Either the

covariance function could be estimated for a sufficient number of displacements in the x and y directions or, if a computer program exists to handle the problem, the fast Fourier transform could be generated. Appropriate smoothing over the spectral estimates would then finally yield an estimate of the spectrum of the image. Multiplication by the inverse of the filter function discussed in a previous section of this chapter would then yield an improved version of the spectrum. However, this spectrum would still have to be corrected for the distortions in the spectrum produced by the finite time required by the aircraft to image this pattern. Procedures to carry out this last step will be given later in this chapter.

Under the assumption that the waves are moving toward the aircraft as it flys along the positive x direction, the effect of correcting for the speed of the aircraft is that the direction of the dominant longer waves would turn so that the crests would be more nearly parallel to the flight line. The effect on the shorter waves would be smaller.

The final spectrum would have a peak in the first quadrant of the ℓ, m, plane (under the assumption that the waves were traveling toward the spacecraft) perhaps 30° to the right of the m axis. The angular spread about this maximum could easily be ± 30°, or 40°, on the basis of the fact that the crests of the waves in the image are only three or four times longer than the distance between them. The shorter waves would provide a secondary maximum in the spectrum located perhaps at a point in the ℓ, m plane four times further out from the origin than the first maximum and located in the second quadrant at an angle of perhaps 45° to the m axis. Quite clearly the

operation of multiplying by m^{-2} (as the lead term in the reciprocal of $(\sin (Mm)/2))^2$ will magnify the spectral contribution for the longer waves and substantially attenuate the spectral contributions for the shorter waves. The final result should, however, be a good estimate of the vector wave number spectrum that could in turn be compared with wave spectra obtained in other ways.

In particular, circles of constant magnitude for the vector wave number could be placed on this final spectrum at distances from the origin corresponding to the upper and lower ranges for each spectral band in a frequency spectrum obtained from waves recorded at a fixed point. An integration over this circle should then yield an estimate of the total variance for the wavy surface due to these particular frequencies, and the function so obtained could be compared with a frequency spectrum obtained with either a shipborne wave recorder or a wave rider buoy. Similarly, were a Stilwell photograph obtained of the same area, the vector wave number spectrum from the Stilwell photograph could be compared with the vector wave number spectrum from this image after it is corrected for the effect of aircraft motion, and the two should agree. Finally a laser altimeter could be flown over this surface at any arbitrary direction. In particular, the flight line could be perpendicular to the crests of the dominant wave trains. If this were done, the corrected wave number spectrum obtained from this image could be mapped by means of appropriate transformations into the spectrum of the record that would be obtained by the laser altimeter. These two spectra would agree. Such an operation eliminates the difficulties in mapping the single pass obtained from an aircraft back into a vector wave number

spectrum, which is impossible, and the very difficult task of taking sections along different headings as obtained by a laser altimeter and deciphering what the original two dimensional spectrum is like.

This real aperture wave image has been analyzed by Belousov, Zhilko, Zagorodnikov et al. along with others obtained in February and March 1973 in the Bering Sea near 177°E, 59°N. The winds were 12 to 14 m/s during one set of observations and 18 to 22 m/s during another. The fetch was from 50 to 100 km from the edge of the pack ice.

Although it is not possible to be certain that this particular image was one of those analyzed (the notation 23.24.02.73 on the image may represent the date of analysis), it is clear that the full information content has not been extracted from these data. For example, it is claimed that, since the spectra are so narrow band, normalizing amplitude and slope spectra to one produces indistinguishable results. The angular spread is not quantitatively evaluated. Also the results of a following section that shows that wave numbers and wave directions are not correctly recorded on radar images made from an aircraft were apparently not part of the theory available to them. Since the aircraft flew on a variety of headings, it is difficult to believe that these effects were not discovered. There was no comparison of the spectra estimated from the radar data with spectra obtained from a wave recorder at the sea surface (a Pribuoy) although agreement of period and direction was claimed. Only the dominant directions and wave numbers plus very crude spectral sections through the peak were recovered.

In contrast, it is to be expected that the wind sea should cover a wide range of directions. Also the swell in this particular image does not appear to be a particularly narrow band. The effort involved in obtaining radar images of the sea surface surely justifies a more thorough spectral analysis of the data and a careful comparison of the spectrum so obtained with spectra obtained by means of other instruments.

Sample Data from SARs

Although there is considerable debate about whether or not a synthetic aperture radar will yield useful results on a spacecraft, there can be little doubt that a synthetic aperture radar on an aircraft can be used to obtain useful results. Properly processed, the images obtained from aircraft should yield vector wave number spectra for the area being imaged in deep water and useful information on wave refraction patterns for high waves under clouds in coastal areas during storms. There will be problems associated with the interpretation of the images obtained by aircraft in coastal areas because of the effects to be described in a following section. However, the ability to obtain waves during high winds under clouds is so important that obtaining these images and interpreting them carefully is still the correct thing to do.

Figure 4.21 illustrates the variation along the two lines scans obtained with imaging radars. The upper curve is a line scan obtained with an x-band radar and immediately below it is a line scan obtained with an L-band radar. These two line scans are of very closely located lines on the sea surface as a function of the y distance. They need not necessarily coincide with exactly the same line on the sea surface.

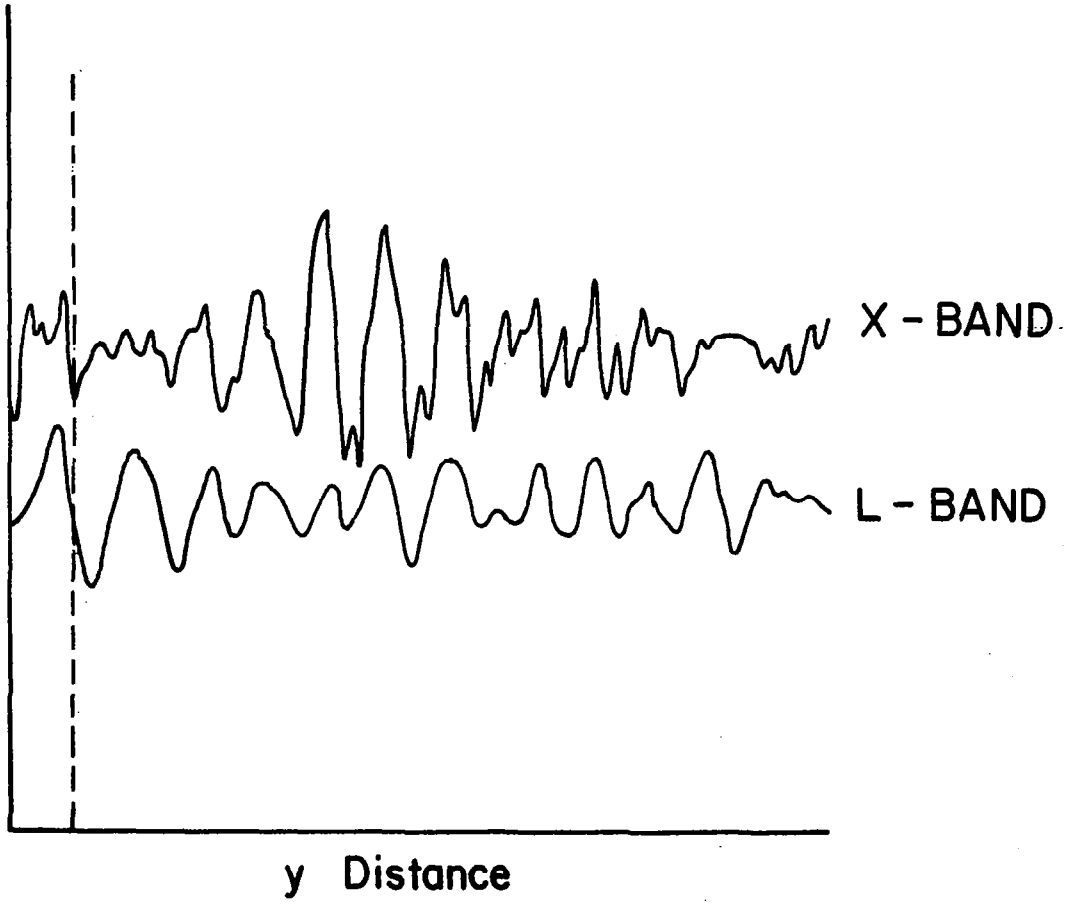

FIGURE 4.21 COMPARISON OF X-BAND AND L-BAND LINE SCANS FROM TWO SARS.

The differences between these two line scans are easily explainable on the basis of the preceding analysis. Essentially the value of M for the x-band scan is much smaller than the value of M for the L-band scan. The higher harmonics from the shorter waves have produced small oscillation on the upper scan as would be expected. The lower scan still delineates the dominant waves in the system. If both of these scans are considered as part of a full image and if the spectrum of the image were multiplied by the appropriate reciprocals of the filter functions given previously in wave number space it is quite possible that each would yield nearly the same spectrum. If the waves that compose the surface being imaged are traveling at an angle to the y axis so that there is a substantial component to the ℓ part of the spectrum then the lower scan could be more nearly out of the region that is imaged with little attenuation especially if the x distance being averaged in terms of L of the above derivation is larger than the y distance being averaged in terms of M. Nevertheless, both of these records have all of the apparent properties of ocean wave records such as those that have been illustrated previously in which various types of filters, either in frequency space or wave number space, have been applied to the time or space histories. Just as, for example, the bottom pressure fluctuations caused by waves in water of constant depth have had the high frequencies attenuated, the radar imaging system in L-band has attenuated the high frequencies, or high wave numbers, in the line scan. Within limitations, which are chiefly determined by the noise level of the spectral analysis, the full information content of the signal can be used to recover a corrected spectrum just as the one illustrated for the bottom pressure record or for the Tucker shipborne wave recorder in the preceding chapter.

The upper line scan also strongly suggests that the slope in the y direction is being imaged and not elevation. The very rich higher harmonic content would not be observed in an elevation measurement along a line, whereas it is quite likely to be observed in a function recording the slope of the sea surface along a line.

These line scans can be compared with one shown by Le Vine (1974) obtained with a non-imaging system. Clearly this line scan, if it contains information about the wave spectrum at all, has masked it by some sort of non-linear operation.

Figure 4.22 illustrates a sequence of line scans obtained with an L-band imaging radar. The original figure provided to us was labeled from the bottom to the top with the values 4, 6, 8, 10 and so on. This suggests that every other scan has been used and that line scans half way between the ones shown could also have been presented. This record shows a somewhat richer high frequency content that the previous L-band line scan especially for scan numbers 4 and 8.

The sequence of line scans also shows coherence. If both the horizontal scale of these scans and the separation of the scans in the orthogonal direction were known, along with the imaging spot size, it would be rather easy to construct an image of varying brightness simply from spots of appropriate dimensions and brightness proportional to the variations in these graphs. In the preparation of such a figure, the scientist preparing it undoubtedly looks for an area of high variability. The first sharp trough (if such a term is appropriate) and the first large crest in all six line scans can be followed from one scan to the other, and there is a very strong correlation between each record and the one next to it for these patterns. However, line scan 4 does not correlate well with line scan 14 on the right side for

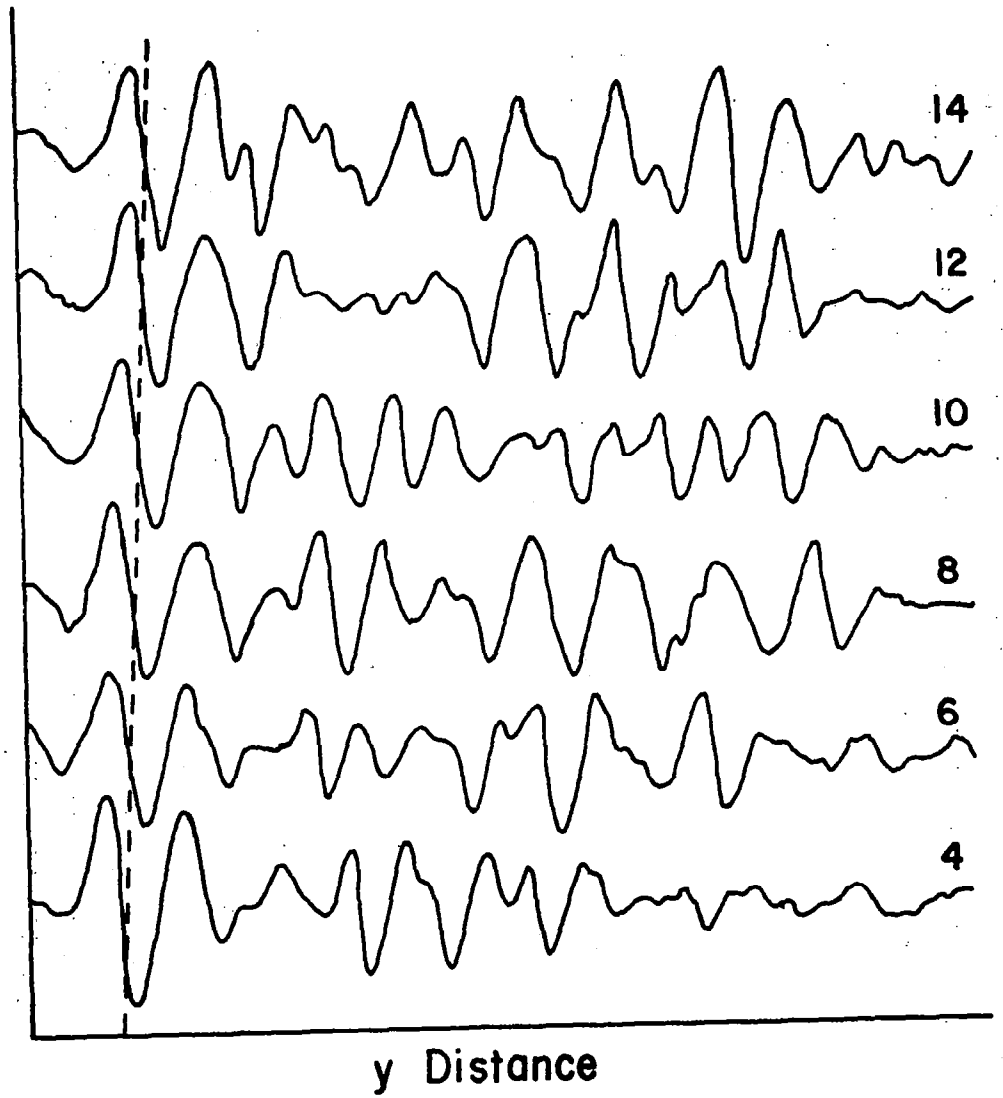

FIGURE 4.22 SUCCESSIVE L-BAND LINE SCANS FROM A SAR.

example. All of these features are perfectly typical of what would be expected if the brightness pattern in the image that would be produced by these line scans corresponded to the postulated properties of the slopes of a short crested random Gaussian sea surface. The information content in the correlation of one scan to the next, of course, provides the equivalent of the wave number information in the direction normal to the y axis and therefore information on the ℓ component of the vector wave number.

Many images have been produced with the synthetic aperture radars operated by the Jet Propulsion Laboratory. Also reports by Brown et al. (1974) and Elachi (1974) describe many features of these images. A report on all of the available imaging has been prepared at JPL and is soon to become available. One image will be discussed here as shown in Figure 4.23. The image chosen is for ocean waves near Kayak Island in Alaska. The first strip is the original image, the second shows a correction for distortion and finally the contour map of the island is shown. The waves offshore can be seen to change direction upon moving from the bottom to the center of the strip. The waves have been refracted. The caution in interpreting this figure lies in the remark made previously about the finite time required to construct this image and the movement of the waves during this finite time.

A Nanosecond Scanning Radar

A scanning, nanosecond, narrow pencil beam radar for an aircraft is reported to be under development. With corrections for the geometry of the scan, and for the motion of the aircraft and the waves, the data should be the equivalent of a SWOP measurement and can be analyzed by means of the equations in Chapter 2 and those that follow in this section. Extension to spacecraft altitudes does not appear feasible.

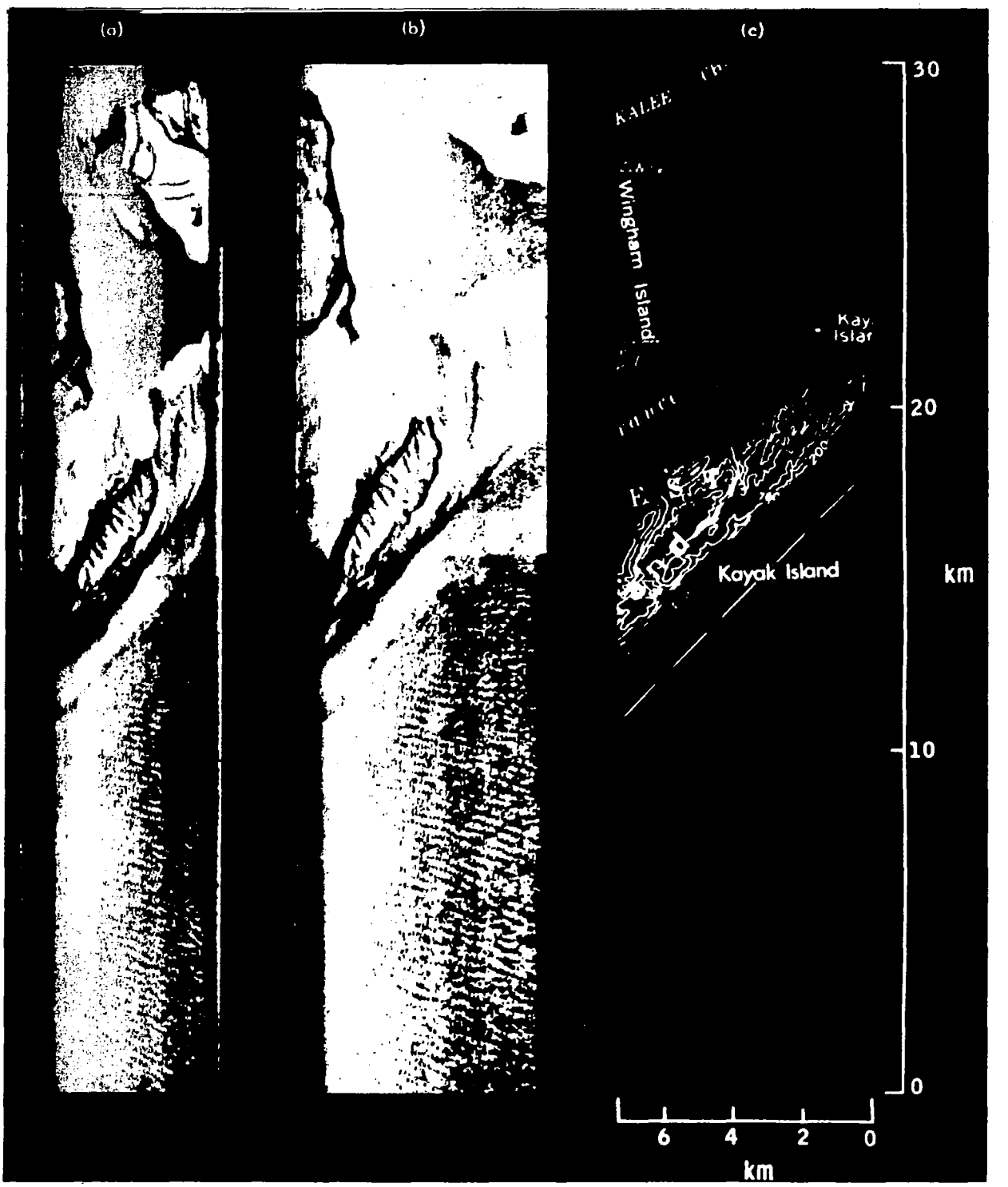

(a) Radar image of ocean waves near Kayak Island in southern Alaska.
(b) Corrected radar imagery with geometrical distortions eliminated.
(c) Topographic map of the same area.

FIGURE 4.23 AIRCRAFT SAR IMAGES AT KAYAK ISLAND

THE EFFECT OF IMAGING TIME FOR AIRCRAFT SYSTEMS

Geometry and Time Scales

Figure 4.24 shows the geometry of the scanning pattern for a SAR system. The final image results from the side by side placement of individual line scans, which are parallel to the y axis like the one shown. A single scan with reference to an underlying moving ocean wave surface is accomplished in such a short time that it can be considered to be instantaneous.

The image in the x direction is constructed on a different time scale. If, for example, the swath width is 150 kilometers, an aircraft with a speed over the surface of 150 m/sec requires 1000 seconds, or 16 minutes and 40 seconds, to image a square 150 km on each side. During this time, the waves on the sea surface will have changed, and the interference of the spectral components will have produced quite different patterns when the aircraft reaches the various positions along the track, compared to those that were there when it started out.

Simple Moving Waves Systems

Suppose that the waves on the sea surface were monochromatic simple harmonic progressive waves as given in Chapter 2. For $\ell > 0$, $m = 0$, the wave travels in the positive x direction. The vector $\vec{k} = (\ell, m)$ points in the direction toward which the wave is moving, and the length of the wave is given by $L = 2\pi/|\vec{k}|$.

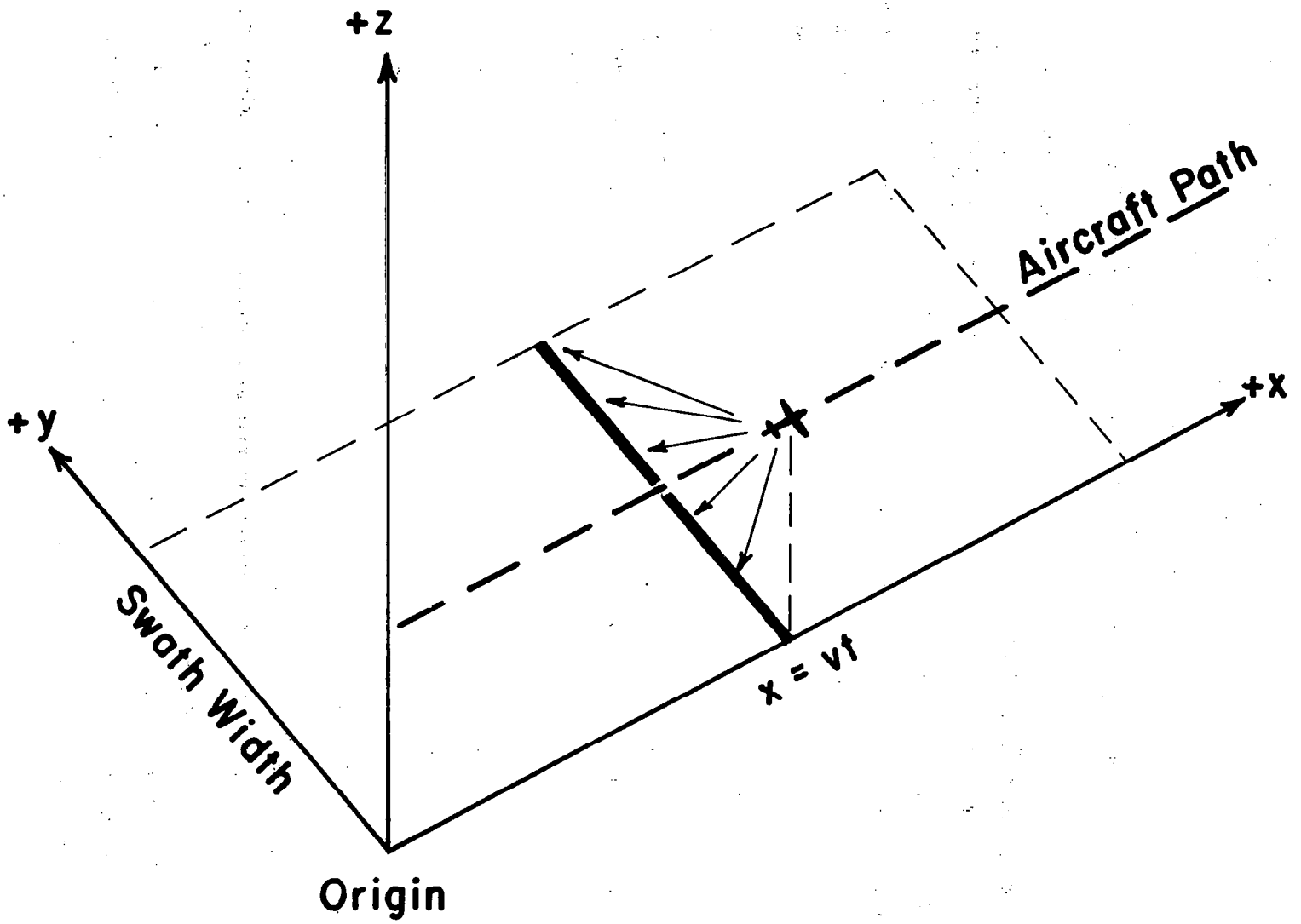

FIGURE 4.24 GEOMETRY OF SCANNING PATTERN

The radar image along a line scan in the y direction is then given by equation (4.23) neglecting filter effects

$$S(y;x,t) = am \cos (\ell x + my - \omega t + \epsilon) \tag{4.23}$$

An aircraft flying at a speed, v, reaches a point, x, at a time t given by equation (4.24).

$$t = \frac{x}{v} \tag{4.24}$$

Consequently, the synthetic aperture radar image as shown typically on the x,y plane is given by equation (4.25).

$$S(x,y) = am \cos ((\ell - \tfrac{\omega}{v}) x + my + \epsilon) \tag{4.25}$$

If the entire x,y plane could be viewed at an instant of time, the result would be equation (4.26)

$$\frac{\partial \eta}{\partial y} = am \cos (\ell x + my + \epsilon) \tag{4.26}$$

But since the aircraft scans the x component of the scene in a finite time, the image that is actually produced is given by equation (4.25).

The difference between equations (4.25) and (4.26) lies at the core of the problem of interpreting radar images and of recovering vector wave number spectra. For a real sea surface, composed of a superposition of many sinusoids, the problem of removing the effect of the ω/v term in (4.25) becomes complicated.

Figures 4.25 through 4.28 show the differences between true instantaneous images of a scene such as would be described by equation (4.26) and the image that would be obtained by an aircraft flying at 300 knots. Lines of maximum slope are shown as equivalent "crests" with ϵ set equal to zero. In Figure 4.28, the top illustration shows waves with a period of 10 seconds and a length of 1/12 NM that are traveling toward negative y. As the aircraft images the scene, successive "crests" in the y scan move closer to the aircraft and after 10/12 NM, 10 seconds have passed and each "crest" occupies the position of a former "crest" in the y scan made at that time. Straight lines connecting the "crests" at $x = 0$ to the "crests" one wavelength away at $x = 10/12$ produce the "crests" in the radar image. In the SAR image, the "crests" are turned 5.7° clockwise relative to the true image.

If the direction of travel of the wave "crests" is reversed as in the bottom part of Figure 4.25, the "crests" in the radar image are turned 5.7° counter clockwise relative to the true image. In both conditions, the x component of the vector wavenumber in the radar image comes solely from the term $-\omega/v$ in equation (13), and it is negative.

Figure 4.26 shows similar drawings for waves 1/3 NM long with a period of 20 seconds. The direction of the waves in the radar images differ from the true directions by 11.3°.

Figure 4.27 shows waves with a period of 13.3 seconds traveling in the direction shown. The waves in the radar image have been turned approximately 5° relative to the true image.

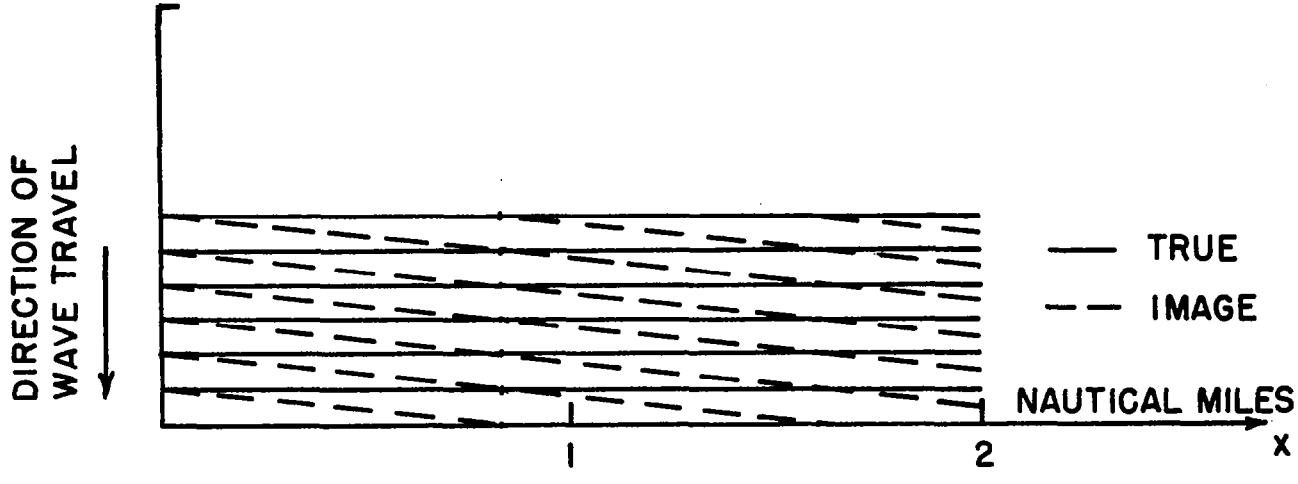

AIRCRAFT SPEED = 300 KNOTS = $\frac{1}{12}$ NM/SEC

T = 10 SEC

C = 30 KNOTS = $\frac{1}{120}$ NM/SEC

L = CT = $\frac{1}{12}$ NM

CHANGE IN DIRECTION = 5.7°

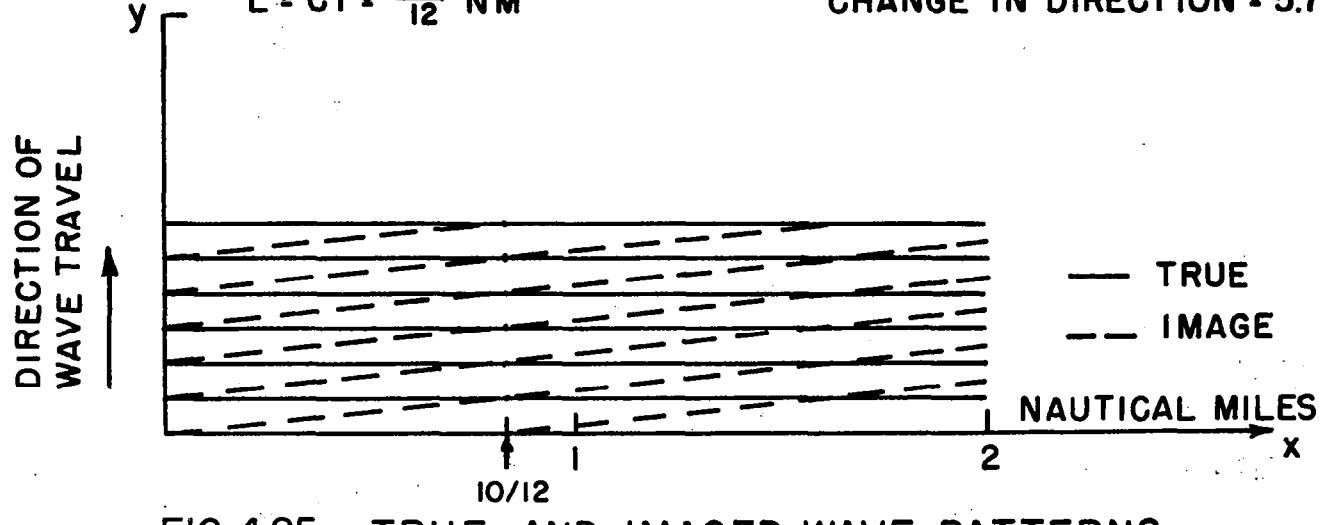

FIG. 4.25 TRUE AND IMAGED WAVE PATTERNS

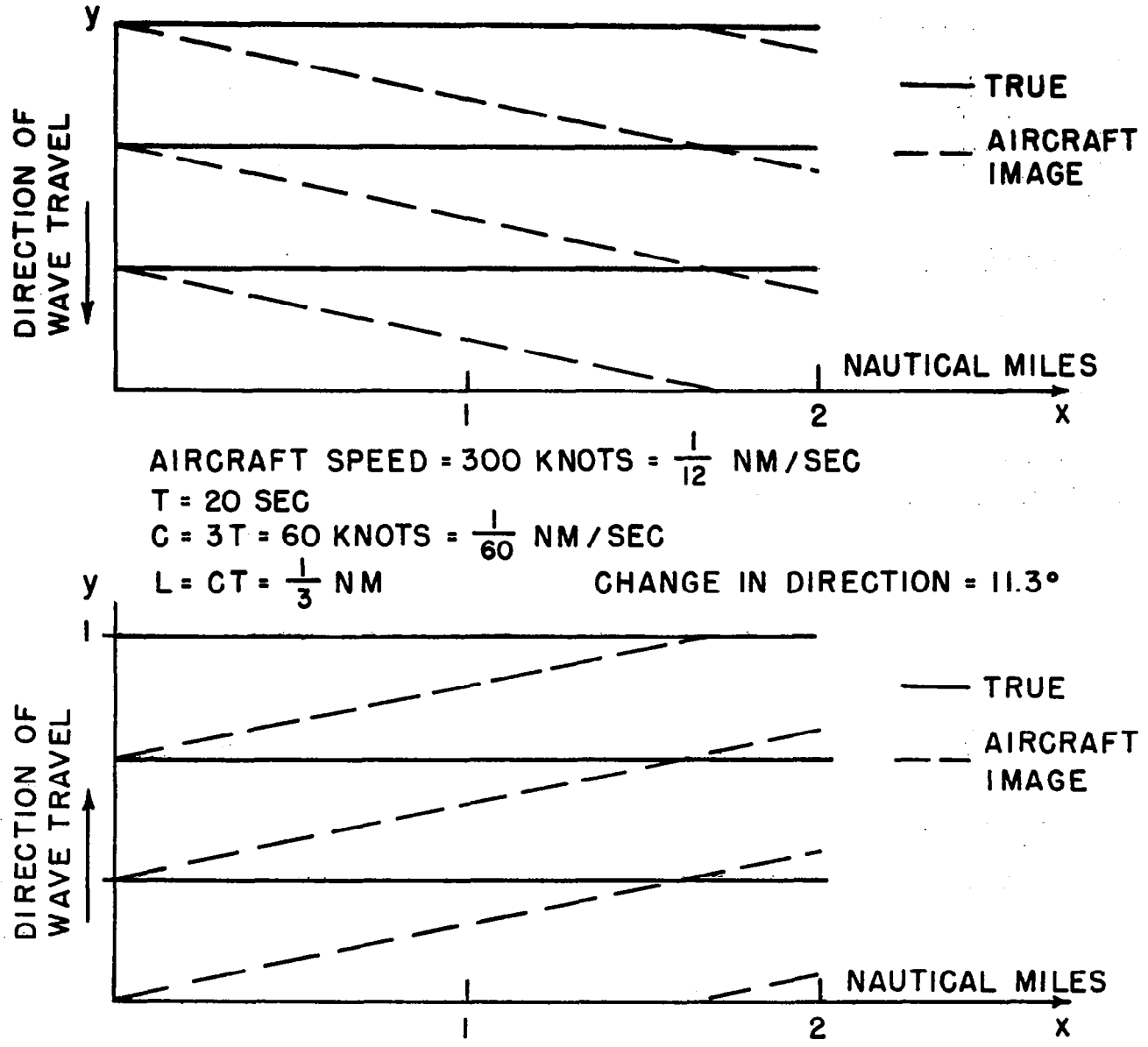

FIG. 4.26 TRUE AND IMAGED WAVE PATTERNS

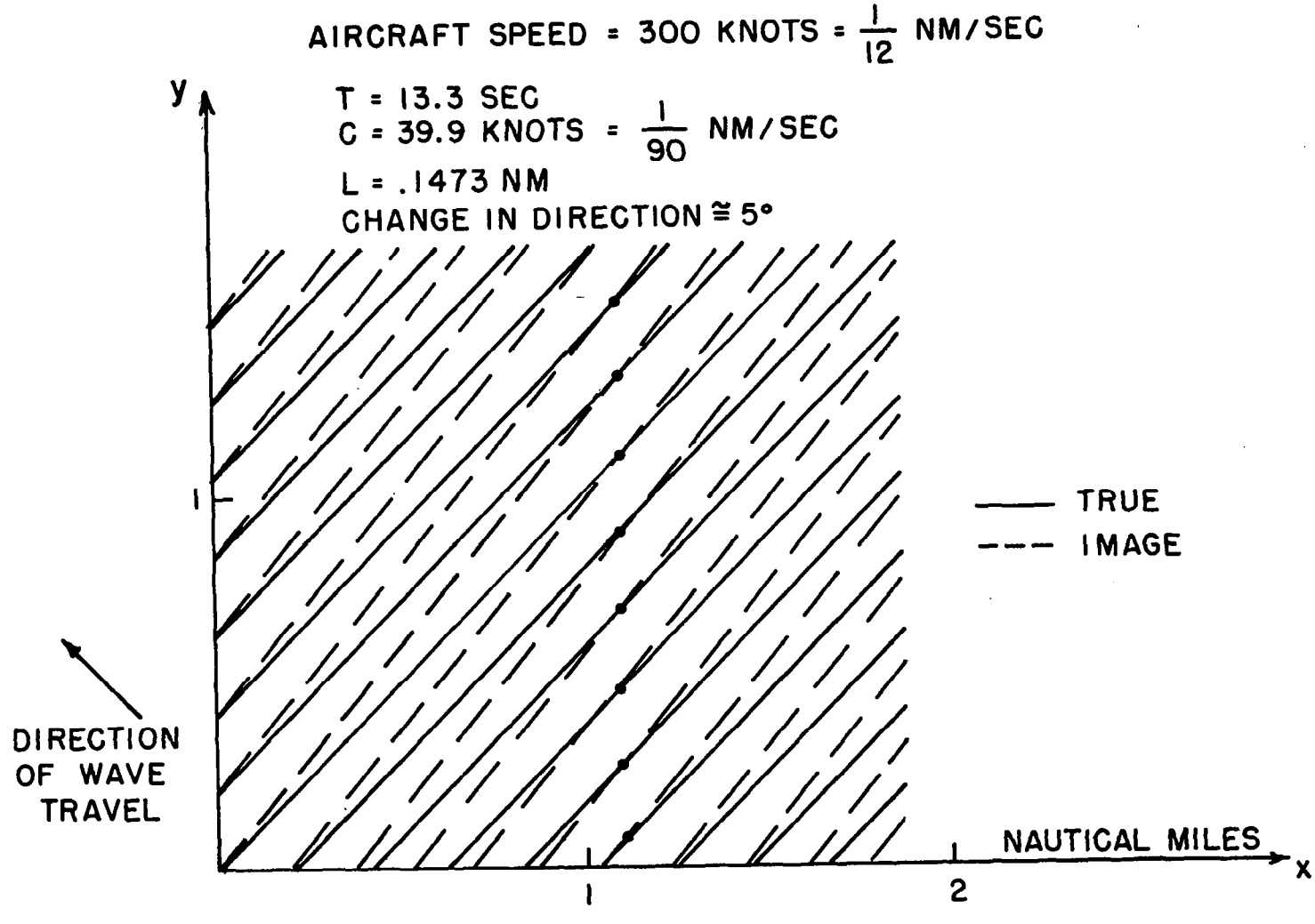

FIG. 4.27 TRUE AND IMAGED WAVE PATTERNS

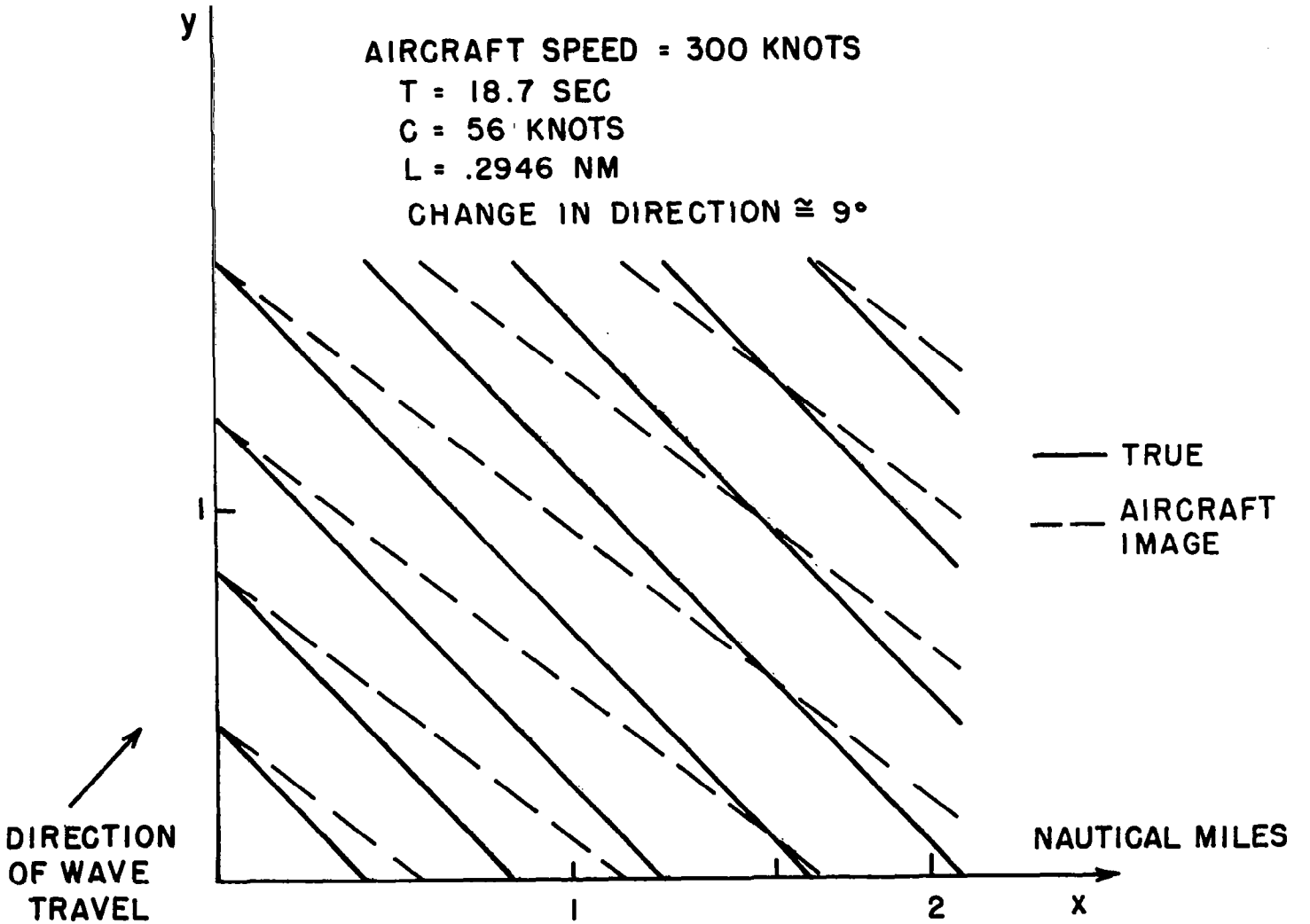

FIG. 4.28 TRUE AND IMAGED WAVE PATTERNS

Figure 4.28 shows waves with a period of 18.7 seconds traveling in the direction shown. The waves in the radar image have been turned approximately 9° relative to the true image.

The figures also illustrate other important points when considered in terms of equation(4.25). Not only are the directions of the waves changed in the radar image but also the wavelengths are changed. The y component of the wavenumber vector remains unaltered, but the x component is always changed. If the x component of the true wavenumber is positive, then the x component in the radar image is decreased and the apparent wavelength in the image will be increased. Figure 4.28 illustrates this situation. If the x component of the true wavenumber is negative, then the magnitude of the x component of the wavenumber vector in the radar image is increased, and the apparent wavelength in the radar image is decreased.

Figure 4.27 illustrates this situation. Finally, if the x component of the true wavenumber is zero, a negative component is produced for the radar image, and the wavelength in the radar image is decreased as shown in Figures 4.25 and 4.26. There clearly exists a set of values of ℓ and m such that the radar images will have no x component in the apparent vector wavenumbers.

Effect of Spacecraft Velocities

A brief comment on the expected difference between aircraft radar images and spacecraft images can be made on the basis of these figures. Seasat A will have a velocity of about 7.5 kilometers/sec. The v in equation (13) is thus many times larger than the v used to construct these figures. The crests in the images would be turned in angle by negligible amounts.

The Correction of a Radar Image Spectrum

For the purposes of this study it will be assumed that m_e is positive and that the last problem to be solved is that of converting

$$\hat{S}\ (\ell_e, m_e)$$

to

$$\hat{\bar{S}}\ (\ell, m)$$

or stated another way, to correct the radar image spectrum so that it represents the true vector wave number spectrum of the instantaneously observed sea surface.

From equations (4.24), (4.25), and Chapter 2, equations (4.27) and (4.28) can be obtained.

$$\ell_e = \ell - \frac{g}{v}(\ell^2 + m^2)^{\frac{1}{4}} \tag{4.27}$$

$$m_e = m \tag{4.28}$$

and it is possible to write that,

$$\hat{S}\ (\ell_e, m_e)\ d\ell_e\ dm_e \Rightarrow \hat{S}\ (\ell_e(\ell,m),\ m_e(m))\frac{\partial(\ell_e, m_e)}{\partial(m,\ell)}\ d\,m\,d\,\ell \tag{4.29}$$

where the symbol $\Rightarrow$ is read "transforms into". The Jacobian of the transformation is given by equation (4.30).

$$\frac{\partial(\ell_e, m_e)}{\partial(m,\ell)} = 1 - \frac{g^{\frac{1}{2}}}{v}\frac{1}{2}\frac{\ell}{(\ell^2 + m^2)^{\frac{3}{4}}} \tag{4.30}$$

If the inverse of equations (4.27) and (4.28) such that

$$\ell = \ell\ (\ell_e, m_e) \tag{4.31}$$

and

$$m = m\ (\ell_e, m_e) = m_e \tag{4.32}$$

could be found, the transformation could be done graphically by moving the value of $\hat{S}(\ell_e, m_e)$ to the point ℓ,m and by multiplying by equation (4.30). If $\hat{S}(\ell_e, m_e)$ were known analytically the problem would be solved via (4.29) and (4.30), but in the real world of data analysis, this is not the case.

It is therefore still necessary to find expressions for equations (4.31) and (4.32). It is noted that g/v^2 has the dimensions of a wavenumber and is a fundamental parameter of the problem.

Let
$$\mathcal{L} = \frac{g}{v^2} \tag{4.33}$$

so that
$$\ell_e = \ell - \mathcal{L}^{\frac{1}{2}} (\ell^2 + m^2)^{\frac{1}{4}} \tag{4.34}$$

and
$$m_e = m. \tag{4.35}$$

A trial inverse of this pair of equations is given by equations (4.35) and (4.36) where A is a correction to be found by substituting this inverse into equations (29) and (30),

$$\ell = \ell_e + \mathcal{L}^{\frac{1}{2}} k_e^{\frac{1}{2}} + A \tag{4.36}$$

$$m = m_e \tag{4.37}$$

since the algebra can be further simplified by setting $\ell_e^2 + m_e^2 = k_e^2$.

The substitution yields

$$\ell_e = \ell_e + \mathcal{L}^{\frac{1}{2}} k_e^{\frac{1}{2}} + A - \mathcal{L}^{\frac{1}{2}}((\ell_e + \mathcal{L}^{\frac{1}{2}} k_e^{\frac{1}{2}} + A)^2 + m_e^2)^{\frac{1}{4}} \tag{4.38}$$

or with the neglect of higher order terms

$$0 = \mathcal{L}^{\frac{1}{2}} k_e^{\frac{1}{2}} + A - \mathcal{L}^{\frac{1}{2}} (k_e^2 + \mathcal{L} k_e + 2\mathcal{L}^{\frac{1}{2}} \ell_e k_e^{\frac{1}{2}} + 2A(\ell_e + \mathcal{L}^{\frac{1}{2}} k_e^{\frac{1}{2}}))^{\frac{1}{2}} \tag{4.39}$$

or

$$0 = \mathcal{L}^{\frac{1}{2}} k_e^{\frac{1}{2}} + A - \mathcal{L}^{\frac{1}{2}} k_e^{\frac{1}{2}} \left[1 + \frac{\mathcal{L}}{4k_e} + \frac{\ell_e \mathcal{L}^{\frac{1}{2}} k_e^{\frac{1}{2}}}{2k_e^2} + \frac{A(\ell_e + \mathcal{L}^{\frac{1}{2}} k_e^{\frac{1}{2}})}{2k_e^2}\right] \tag{4.40}$$

The final result yields an expression for A given by

$$A = \mathcal{L} \left[\frac{\frac{\ell_e}{k_e} + \frac{\mathcal{L}^{\frac{1}{2}}}{2 k_e^{\frac{1}{2}}}}{2 - \frac{\ell_e \mathcal{L}^{\frac{1}{2}}}{k_e^{\frac{3}{2}}} - \frac{\mathcal{L}}{k_e}} \right] \tag{4.41}$$

A further substitution simplifies these expressions.

Let

$$\ell_e = R\, k_e \quad \text{for } -1 < R < 1$$

and

$$m_e = (1-R^2)^{\frac{1}{2}} k_e . \tag{4.42}$$

Also let

$$K = \frac{\mathcal{L}^{\frac{1}{2}}}{k_e^{\frac{1}{2}}} \tag{4.43}$$

The final form in the inverse can then be written as equations (4.44) and (4.45).

$$\ell = R\,k_e + K\,k_e + K^2\,k_e \left[\frac{R + \frac{K}{2}}{2 - K\,R - K^2} \right] \tag{4.44}$$

$$m = \sqrt{1 - R^2}\,k_e \tag{4.45}$$

Discussion and Examples

The inversion of these equations depends upon the assumption that the aircraft is moving faster than any spectral component on the sea surface and that the values of $\hat{S}(\ell_e, m_e)$ are sufficiently far away from the origin of the ℓ_e, m_e plane. The complexity of the problem is greater for slower velocity vehicles, such as ships, as shown by St. Denis and Pierson (1953).

A typical aircraft speed is 158 m/s. For this speed, Table 4.3 shows the true wave numbers and wavelengths for an apparent wave in the image that is 628 meters long and that would have a period of about 20 seconds, if this were a true wavelength. Depending on the direction of the spectral component in the SAR image, the true wavelength can vary anywhere from 768 meters to 513 meters and the direction of the wave can be changed by as much as 11.4°

The columns labeled ℓ_e^* and m_e^* are the values of ℓ_e and m_e computed from the values of ℓ and m. They should equal the starting values of ℓ_e and m_e. The difference is a measure of the error of the approximation in finding the inverses.

Table 4.4 shows examples for shorter waves. Again there are substantial differences between the true wave conditions and the imaged wave conditions.

Table 4.3 Examples of the Mapping

$v = 158$ m/s, $\mathcal{L} = g/v^2 = 4\times10^{-4}\ m^{-1}$, $k_e = 10^{-2}$, $L_e = 628$ m, $T_e \cong 20$ sec

R	ℓ_e	m_e	ℓ	m	ℓ_e^*	m_e^*	L	$\Delta\Phi$	T
1	10^{-2}	0	1.225×10^{-2}	0	1.004×10^{-2}	0	513	0°	18
.707	7.07×10^{-3}	7.07×10^{-3}	9.247×10^{-3}	7.07×10^{-3}	7.087×10^{-3}	7.07×10^{-3}	542	5°	18.6
0	0	10^{-2}	2.024×10^{-3}	10^{-2}	0	10^{-2}	616	11.4°	19.8
-1	-10^{-2}	0	-8.166×10^{-3}	0	$-.9969\times10^{-2}$	0	768	0°	21.1

Table 4.4 Examples for Shorter Waves

k_e	ℓ_e	m_e	ℓ	m	L_e	L	$\Delta\Phi$
2×10^{-2}	2×10^{-2}	0	2.306×10^{-2}	0	314 m	272	0
2×10^{-2}	0	2×10^{-2}	2.842×10^{-3}	2×10^{-2}	314	$\sim$ 314	8.1°
2×10^{-2}	-2×10^{-2}	0	-1.735×10^{-2}	0	314	362	0
4×10^{-2}	4×10^{-2}	0	4.62×10^{-2}	0	157	136	0
4×10^{-2}	0	4×10^{-2}	4.02×10^{-3}	4×10^{-2}	157	$\sim$ 157	$\sim$ 5.7°
4×10^{-2}	-4×10^{-2}	0	-3.61×10^{-2}	0	157	174	0

THE COMPARISON OF DIFFERENT KINDS OF WAVE DATA

In the last two chapters, a variety of different systems for measuring waves and for obtaining various kinds of spectra have been described. Although the theories necessary to compare the many different kinds of wave data have been given, the purpose of this section is to recapitulate the results obtained and described once again how wave data obtained in different ways can be processed so as to obtain the same spectral estimates two different ways for direct comparison.

An imaging radar on an aircraft yields a spectrum of the form, $S(\ell_e, m_e)$, and ways to transform this to $S(\ell, m)$ have just been described. A properly illuminated photograph of the sea surface yields a spectrum of the form $m^2 S(\ell, m)$ which upon division by m^2 becomes $S(\ell, m)$. Similarly a stereo pair of photographs can be used to obtain a field of wave elevation as in SWOP that also yields the above function. In some of these cases, such as for the imaging radar on an aircraft or for photographs, only the shape of the spectrum and not a primary calibration which involves the total variance, m_o, as discussed in Chapter 2, may be available. For a laser altimeter on an aircraft, the quantity obtained was described as $S(\ell^*)$ or $S(f^*)$, which was then related to frequency. The data from the buoy developed by NIO yields estimates of a variety of spectra and cross spectra depending upon the heave acceleration, and its double integral, the pitch, and the roll. These can all be designated by $S_{ij}(\omega)$. Finally most wave recorders at a fixed point yield a function of time from which a frequency spectrum, designated by $S(\omega)$,can be estimated.

Suppose that an imaging radar on an aircraft has yielded the function $S(\ell_e, m_e)$ and it is desired to compare this with a laser altimeter record obtained from an aircraft. A direct comparison could, of course, be made from a spectrum estimated from a photograph or from a stereo pair, but if neither of these are available, and they usually will not be, the spectrum computed from the data from an airborne laser altimeter flight can be compared with the spectrum estimated from an imaging radar image. In fact, the aircraft can fly on a number of different headings relative to the waves, including upwind, 45° to the wind, and crosswind and each of the records could be processed in exactly the same way (assuming that the effects of vertical motion on the aircraft has been removed, but not the waves that appear at the same frequency), in order to obtain a comparison with the spectrum from the imaging radar data. The procedure is to rotate the spectrum of the imaging radar data so that the ℓ' axis of this spectrum lies in the line of flight of the aircraft and the m' axis of this spectrum lies perpendicular to it. This is achieved by a simple rotation of coordinates using standard Cartesian coordinates transforms. The wave numbers sensed by the laser altimeter are then given by equations (4.46).

$$\begin{aligned} \ell^* &= \ell' - \omega / v \\ m^* &= m' \end{aligned} \tag{4.46}$$

$$S(\ell^*) = \int_{-\infty}^{\infty} S(\ell'(\ell^*, m^*), m'(m^*)) \frac{\partial(\ell' m')}{\partial \ell^* \partial m^*} \, dm^* \tag{4.47}$$

An integral over the rotated imaging radar vector wave number spectrum as shown by equation (4.47), then yields the spectrum that would be obtained from the laser altimeter data. In practice, probably the best thing to do would be to draw lines of constant ℓ^* on the imaging radar

spectrum and compute the total volume under the spectral surface between adjacent pairs of lines, thus computing the finite difference approximation to the indicated integral. Quite clearly for different rotations, which produce different values for ℓ' and m', the results for this integration can be quite different, depending on the vector wave number spectrum that was obtained.

To compare the spectrum obtained from an image produced by an imaging radar with the spectrum obtained from a wave recorder recording waves at a fixed point, it is necessary to eliminate one dimension in the spectrum and to transform it from wave number to frequency. The steps are indicated by equations(4.48)where the arrow means "transform into" and the appropriate transformations from Cartesian wave number space to polar wave number space, to frequency are indicated step by step. The final step is to integrate over the directions. The wave number spectrum has thus yielded a function of frequency that can be directly compared to the data obtained by the wave recorder. Care is needed in interpreting the wave number spectrum because of the 180° ambiguity.

$$S(\ell, m)\,d\ell\,dm \Rightarrow S(k\cos\chi, k\sin\chi)\,k\,dk\,d\chi$$

$$S(k,\chi)\,k\,dk\,d\chi \Rightarrow S\left(\frac{\omega^2}{g}, \chi\right)\frac{\omega^2}{g}\frac{2\omega}{g}\,d\omega\,d\chi \tag{4.48}$$

$$= S^*(\omega, \chi)\,d\omega\,d\chi$$

$$\int_{-\pi}^{\pi} S^*(\omega, \chi)\,d\chi\,d\omega = S(\omega)\,d\omega \tag{4.49}$$

Finally, the NIO pitch-roll buoy records the heave acceleration, pitch, and roll of the buoy from three simultaneously time histories.

Nine different spectra result. They are the spectra of each of the three motions, the co-spectra between any pair, and the quadrature spectra between any pair. For a pitch-roll buoy lined up exactly in the wave direction and for a symmetrical spectrum some of the cross spectra are zero, but in general they all can be non-zero over certain frequency ranges. From the imaging radar data the spectrum can be found and transformed by means of (4.50) to a function of the form, $S(\omega, \chi)$. The different spectra and cross spectra from the NIO pitch-roll buoy data are then all given by equation (4.50) for different values of i and j. This integral can be evaluated, usually by finite difference techniques for the estimated spectrum obtained from the transform of the vector wave number spectrum and each function of frequency can then be compared with the appropriate function obtained from the wave buoy data.

$$S_{ij}(\omega) = \int_{-\pi}^{\pi} \left(\frac{\omega^2}{g}\right)^{i+j} (\cos \chi)^i (\sin \chi)^j S(\omega, \chi)\, d\chi \qquad (4.50)$$

Of all of the possible intercomparisons, the data from an imaging radar have never been correctly compared with any of the other data (that we know of). In SWOP, the data from a stereo pair were compared with the data from a wave pole but complete agreement was not obtained. Examples were given in this chapter of the comparison of laser altimeter data with data from a wave pole with fairly good success. Also as described in Chapter 3 the angular variation of the waves in wave number space essentially, $S(k, \chi)$, was compared with data from the NIO pitch-roll buoy with good success by Tyler et al. (1974).

If SAR data could be obtained, properly processed, and put in the form of $S(\ell, m)$, and if aircraft laser flights at four or five headings into the waves could be obtained, then equation (4.50) could be applied a number of times for these different headings. If all of the spectra

estimated from the laser altimeter data agreed with the appropriate spectra from equation (4.47), this would be a convincing demonstration that the data from the imaging radar had indeed produced the full vector wave number spectrum.

CHAPTER 5 THE MEASUREMENT AND STUDY OF WAVES FROM SPACECRAFT

Introduction

Just as an instrument on an aircraft has mobility so that it can be used anywhere within the aircraft range, a single wave sensing system on a spacecraft has a global capability. Global coverage twice a day from a near polar orbit should be the ultimate goal of a remote sensing system for waves on a spacecraft.

Photographs and other kinds of imagery in the visible range from spacecraft have provided some information about waves. This information was obtained more or less accidentally from the images because the instruments were not primarily designed to study waves. It also had the drawback that the data acquired in this way were only available for limited areas and for random times and that it was gathered only after intensive study of many images. These systems do not represent an operational procedure for routinely acquiring information on waves from spacecraft.

In contrast, a radar altimeter was tested on SKYLAB by means of S193 and found to be able to obtain the parameter, m_o , as defined previously. An improved altimeter is presently operational on GEOS-3. It should be possible to measure the quantity that represents the total volume under the vector wave number spectrum and that can be interpreted in terms of the significant wave height every 50 or 100 kilometers along the subsatellite track whenever the spacecraft is over the oceans. The great potential of this instrument from both a scientific and a practical point of view is discussed in Chapters 7 and 8.

Planned for SEASAT-A is an imaging radar for waves. This system should permit the estimation of wave spectra in deep water and the study of wave refraction effects in shallow water. The present indications are that there are a number of problems in the development of such an instrument. If a successful development is assumed, Chapters 7 and 8 will describe some of the scientific and practical uses of the data from such an instrument.

Sun Glitter and Slicks

Cox and Munk (1954, 1956) studied the slope distributions of smaller waves on the sea surface and measured these slope distributions from an aircraft by means of photographs of the glitter pattern. Lines of equal glitter intensity represent points on the sea surface where the slope reflects the sun to the camera. They are elliptical in shape. Their theory and results both show that the number of glitter points was the greatest at the specular point and that the probability density function for this glitter was nearly bivariate normal with the variances in the upwind direction being larger than the variances in the crosswind direction. It was also shown that the upwind-downwind slope distributions had a peak slightly forward of zero slope on the upwind side. The measurements were made near the Hawaiian Islands both for a natural sea surface and for sea surfaces covered by artificially generated slicks. It was demonstrated that the slicks reduced the slope variances by more than a factor of two by removing the small capillary waves.

Numerous papers have presented data showing glitter patterns in imagery obtained from spacecraft. Of particular interest are those by Strong and Ruff (1970), McClain and Strong (1969), and Stumpf and Strong (1974). In the first of these papers, the theoretical shape of the glitter pattern as seen from spacecraft is derived, and it is shown, for the spacecraft used at that time, which was an ESSA satellite, that the sun glint pattern was strong and very bright for nearly calm conditions and spread out with increasing wind speed to larger areas and became less bright at the center as the wind speed increased.

For winds much above five meters per second, the pattern became so diffuse and lost so much brightness that it could not be seen. However, the changes in the shape in this pattern for this low range of wind speed could be used to infer something about the wind speed in the area of the glitter pattern. The problems of course are that the pattern covers six or seven degrees of longitude, the system is not very sensitive to half a meter per second changes in the wind speed, and the presence of clouds removes the possibility of making the estimate of the speed from the shape of the pattern. For most parts of the world, therefore, the routine study of sun glint patterns will not provide information for either high winds or under areas that are cloudy.

A more interesting application of the study of sun glint patterns has been the detection of both anomalous dark patches and anomalous bright patches in the patterns. The paper by McClain and Strong (1969) studied sun glint patterns from a geostationary spacecraft. Under these circumstances the sun glint pattern covers almost 10° of longitude and a comparable range in latitude. If the sea is particularly smooth because of a slick and the absence of capillary waves exactly at the specular point, the large fairly diffused area of sun glitter will show a strong concentration of brightness right at the specular point and fall rapidly off to each side of it as the distance is varied about the specular point. Conversely if the smooth area occurs away from the specular point but still within the sun glint pattern, the sun glint will disappear in this area and the region will look dark. Thus, depending upon the position of the sun a smooth area can be either extremely bright or relatively dark compared to areas around it.

By these techniques, for example, Strong, DeRycke, and Stumpf (1974) were able to demonstrate that certain islands in the Lesser Antilles has shadow regions behind them of very light winds and reduced waves. The areas of light waves and winds were approximately ten times the width of the island in an extensive area downwind from the island. The particular islands involved were Guadeloupe, Dominica, and Martinique.

In another example, for light winds, an oil slick remained coherent over a large area. According to Stumpf and Strong (1974), images from ERTS-1 revealed an extensive oil slick made evident by lack of sun glitter near the Washington canyon on the edge of the continental shelf on the east coast of the United States. This oil slick was more than 30 nautical miles long when observed on July 6, 1973. In general, when the winds are high, it is to be expected that oil slicks will be destroyed by the wave action and will not in particular be a problem to remote sensing techniques for wind speed measurement.

All of the preceding systems used as instruments on the spacecraft had effectively taken something like a photograph in which an entire scene was imaged at the same time by means of a television-like camera. Systems that image in the visible by means of repeated line scans have also been used, such as the one on NOAA-2, and under these circumstances an ellipitical sun glint pattern is not observed because of the change in position of the spacecraft as it scans each successive line. Nevertheless, something similar to the glitter effect occurs. Strong and DeRycke (1973) have shown that the rougher water over the Gulf Stream compared to that closer to the shore produced an image in the visible comparable to the infrared image obtained at the same time by a similar line scanning technique. The smoother in shore water was bright and the boundary of the Gulf stream was a sharp line with darker values over the Gulf Stream.

Photographs of Waves

Some photographs of wave patterns have been obtained from spacecraft in the absence of clouds. One such photograph from Apollo 7 is discussed by McClenan and Harris (1975). The photograph shows an extremely well defined pattern of swell with waves propagating between and around some islands. The wave crests are of the order of twenty or thirty times as long as the distance between the waves. The entire pattern, however, turns and disappears in some places and behaves as one would expect a system of swell to behave if it were composed of a spectrum that was narrow in both the range of wave numbers and directions. The photograph cannot be interpreted as a sinusoidal wave traveling through the area, and it must still be remembered that even this very well defined swell can best be described by the theory of a stationary Gaussian process as extended to the concept of a narrow band spectrum.

An imaging radar system for waves has many advantages. It can probably be made quantitative so that the total volume under a spectrum as estimated could be computed. Properly interpreted, coastal zone information on wave height as affected by wave refraction will probably be obtained. This system provides day and night coverage, and it will also work through most clouds. There remain the problems of the feasibility and practicibility of such an instrument. These problems will be discussed in the next section.

As an alternate to an imaging radar system, some sort of photographic system in the visible range could be considered. No studies are known of the optimum orbit and lighting conditions so that the best possible quantitative imagery of waves in the visible region could be obtained.

Despite the fact that clouds would preclude obtaining some images and that only the day time hours would provide images, a wealth of data could be acquired with a properly defined visible imaging system for waves. Many of the problems of interpreting images of waves obtained from a spacecraft on a routine basis would be quite similar to those of interpreting images of waves obtained from aircraft as discussed in the preceding section and some of the work cited there would be applicable. From the available data it would seem that a more nearly advantageous sun angle such as the one that was present when the photograph in Figure 4.7 was obtained could give very descriptive wave photographs from a spacecraft. The problem of resolution could perhaps be resolved by a telescope. Not as large an area, compared to those scanned by most imaging systems, would be needed. If the techniques generally referred to as Stilwell photography and laser hologram transforms could be employed on these images to obtain the vector wave number spectrum, a system for obtaining routine wave data during day light hours and in the absence of clouds could be developed. If the images were at nadir, a radar altimeter would provide the measurement of wave height.

RADAR ALTIMETER MEASUREMENTS OF SIGNIFICANT WAVE HEIGHT

S193 on SKYLAB was a multipurpose instrument. One of its modes of operation was that of an altimeter to measure the distance between the spacecraft and the surface of the ocean. The capability for the measurement of the geoid (as distorted by tides and tilts due to ocean currents) over the ocean was demonstrated. A by-product of these altimeter measurements was a study of the variation of the shape of the return pulse as a function of the wave conditions below the spacecraft at the subsatellite point.

It should be emphasised that the radar altimeter on SKYLAB, and for that matter the one now in orbit on GEOS-3, functions quite differently from a laser altimeter on an aircraft as described previously. The spherically expanding wave form transmitted from the spacecraft even though its thickness at an instant of time is very small, cannot be made small enough in horizontal area to permit the measurement of the variation in elevation of the waves in the way that the laser altimeter on an aircraft does. What happens is that this spherically expanding wave front starts back from different portions of the wavy sea surface at different times so that upon its return to the spacecraft, whether it was transmitted for 50 nanoseconds, or 3 nanoseconds, its shape is changed as a function of the wave conditions in the area around the subsatellite point.

Even before the launch of SKYLAB, theoretical investigations of the changes in the shape of the return pulse from altimeter had been published such as those of Lee (1969), Greene (1972), and Pierson and Mehr (1970, 1972). These results show that the shape of the pulse changed as the significant height ($4m_o^{\frac{1}{2}}$) of the waves below the

spacecraft changed. The theories described in these papers have been verified, and a change in shape of the return pulse from S193 has been detected that correlates, according to McGoogan (1974), with what the height of the waves was believed to be below the spacecraft. This preliminary verification is in the process of being checked more thoroughly in terms of the analysis of Tucker shipborne wave recorder data from weather ships near various SKYLAB passes and in terms of a calculation on an ocean wide basis by means of the numerical wave specification procedure described in Chapter 2 of what the wave heights were below the various altimeter passes. It is to be expected on the basis of the results obtained to date that a very good agreement will be obtained between the changes of the shape of the return altimeter pulse wave form for the SKYLAB experiment and the wave heights below the spacecraft.

One of the basic assumptions in all of the theories that have been published to data on this phenomenon is that, at a certain stage in the derivation, ensemble averages can be employed to obtain the shape of the average, or expected value, of the return radar pulse. Taking an ensemble average is a correct theoretical procedure only if there are a great many waves within the footprint of the radar pulse.

This is only true for light winds and, or, short fetches and durations for offshore winds. For storm seas generated by high winds, the waves can be so long from crest to crest that only a few of them will occupy the so-called footprint of the antenna pattern of the altimeter. This problem becomes particularly acute for short pulses such as three nanosecond pulses as proposed for SEASAT-A. Theoretical investigations are under way that attempt to determine whether or not going to a short pulse will accomplish any improvement in the ranging accuracy. The preliminary results of these investigations by J. A. Greenwood suggest quite strongly that shorter pulses can only serve

to produce greater variability in the ranging measurements and that they will not help to obtain the greater accuracy required for SEASAT-A. These results should appear within a few more months.

AN IMAGING RADAR FOR A SPACECRAFT

General Discussion

Some system for imaging waves by means of a radar on a spacecraft is highly desirable. This system would provide a day, night, all weather, capability that could be operated through stratiform clouds and that could obtain images routinely anywhere that they were desired within range of the radar on the spacecraft. If a system for imaging waves cannot be achieved, some system for obtaining information on wave spectra in deep water would be the next most desirable objective. Wave spectra are not too useful for shallow water problems because of the changes in wave direction and wavelength as the waves are refracted. Essentially, the spectrum would have to be estimated over a very small area in shallow water, and many spectra over a given coastal area would be needed for interpretation. A single large image would provide much of this information. Portions of the image could then be analyzed to obtain information on the changes in the wave spectra for different areas.

A design goal for SEASAT-A is to image waves on a 100 kilometer wide swath centered at about 300 kilometers to the side of the sub-satellite track. These images will only be obtained when the spacecraft is in view of a ground station. The plans are to obtain the data by means of the spacecraft and transmit it directly to the ground to a receiving station for analysis. A synthetic aperture radar has been under consideration since a real aperture radar appears to require prohibitedly narrow beam widths.

There is considerable controversy as to whether or not a synthetic aperture radar is feasible for a spacecraft. For example, the Phase A study carried out by Goddard Space Flight Center for SEASAT-A reached the conclusion that a synthetic aperture radar would not work on a spacecraft. Also in a review of the problem entitled, "Use of Artificial Earth Satellites for Measuring Waves" by A. A. Zagorodnikov (1974), it is flatly stated that : "Synthesized antennas (7) cannot be used for obtaining radar images of the surface. In this case due to the strong fluctuations of radar signals reflected from sea waves their coherent addition is not insured." The reference cited is a collection of papers under the subject of a side scanning radar sets edited by A. P. Reutov in a Journal called Soviet Radio as published in 1970. The reason given by Zagorodnikov does not seem to be a good one because coherent addition is not satisfied by the imaging systems on aircraft, and yet SAR's do obtain images from aircraft.

The SEASAT-A Phase A Study Report dated August 1973 carried out at the Goddard Space Flight Center discussed the coherent integration time for a SAR and calculated the effect of the wave displacement velocities during this coherent integration time. Essentially the same ratios are found to be important in the Phase A analysis as are found in the analysis to follow. The coherent integration times are small compared to the total time that the target is in the beam and determine the resolution of the synthetic beam. In the Phase A Study, equation 5.1 gives this time as T_c. The first expression is in the notation of the Phase A Study and the second is in the notation of this report.

$$T_c = \frac{R\lambda}{2R_a V} \cong \frac{S2\pi}{k_o 2LV}$$

The ratios of the coherent integration times for the same resolution are thus the same as the ratios to be discussed later, and the ratio is about 5 for SEASAT-A compared with a typical aircraft.

The problem though is that this design consideration for typical waves motions must also be clearly violated even for typical aircraft conditions, and yet SAR's on aircraft do produce usable wave images. Although the analysis to follow is more hueristic, it perhaps gets closer to the point and explains how the continuously changing moving surface can be imaged. It also provides greater detail on the mechanisms involved in the construction of the wave image and how it is distorted by the changes in the Doppler velocities due to the wave motions.

To treat the problem of whether or not a SAR will work on a spacecraft, it seems necessary first of all to explain why the SAR works on an aircraft. Then the assumptions used in this explanation must be extrapolated to spacecraft altitudes and velocities to see if this explanation still holds true for these conditions. The conclusion of an analysis, which follows, unless a flaw can be found in it, is that a conventional SAR cannot be designed so as to satisfy the constraints imposed by operation on a spacecraft at spacecraft altitudes and velocities. The reason for reaching this conclusion is that the various approximations in a SAR design for aircraft altitudes, such as assuming the ocean to be a plane surface and neglecting the difference in slant range for the target cell as the cell is imaged and ignoring the effect of the Doppler motions of the waves, are all marginally unimportant from aircraft altitudes. However, they become important from spacecraft altitudes even assuming a fairly narrow beam real aperture antenna as an initial assumption.

The antenna assumed in these considerations is much different from the one currently planned for SEASAT-A. However, it is quite clear that even if such an antenna could be built the problem illustrated by this analysis would still be present. A wider beam antenna would not remove the problem that arises even if either the analysis of the signal were extended to include a much wider beam or if only a narrow band of Doppler shifts corresponding to this assumed beam width were used. The essential point of the analysis is that the effect of the increased range from spacecraft altitudes is not compensated for by a proportionate increase in velocity so that the Doppler shifts in the location of the cell due to the wave motion when superimposed on the Doppler shifts due to the spacecraft velocity causes the cells being imaged to move about in the image plane to such an extent that they no longer end up being nearly what they ought to be, as they do in an image constructed by means of a SAR on an aircraft.

Consider a SAR on an aircraft with a real aperture radar beam that is eight degrees wide, four degrees forward and four degrees aft of a line perpendicular to the flight path of the aircraft. If this system were imaging a target area consisting of stationary targets, such as a mountain range or a coastline, each target point when acquired at the forward edge of this four degree forward portion of the beam would be Doppler shifted to a higher frequency because of the forward motion of the aircraft and the component of the radar beam in the direction of this forward motion as projected onto the plane of the surface. This positive Doppler shift in frequency is used as a tag for that return signal. As the beam moves past the target, the Doppler frequency shifts to zero and then becomes negative reaching a maximum negative value as the target passes through the

rear side of the beam. All of the many signals returned by this particular target, as collected during the time, T_c, are accumulated as a function of this varying Doppler frequency and mapped to the appropriate point in the image plane. The effect of doing this is to produce the same result that would be obtained had the actual radar beam been a small fraction of the width of the real radar beam. This is why it is possible to talk to imaging spot sizes in the image plane in the order of 25 meters on a side. The direction perpendicular to the flight line is imaged in terms of very short radar pulses that have an appropriate length in space as they radiate from the antenna.

Typically a given point in the image plane requires several seconds of data to reconstitute the image. An elementary component of the image is apparently acquired during the time, T_c, given in equation(5.1), but several of these are apparently needed to get a good image. If the target is stationary, the signal that it returns may vary somewhat with aspect angle but this problem does not seem to be important. Interesting things happen, however, if a strong target is moving while the image is being constructed. For example, a railroad train in motion on a railroad track will be imaged at points in the image plane such that the train is off the track.

When ocean waves are imaged by a SAR, the entire wave field is in motion, and it is necessary to ask why the images illustrated previously were obtained under such circumstances. What appears to be happening is that a given area of the sea surface does not have time to change its major features such as slope during the time required to image that point. For example, image information over a three second interval should in principle blur only waves shorter than about fifteen meters and the resolution of the system is about 25 meters so that this relatively unimportant. The given patch of ocean moves slightly but preserves more

or less the same slope normal to the beam and stays more or less at the same range during the time required to image the waves. Thus, the backscatter signal, if the explanation under consideration is correct, remains relatively constant and relatively stronger and weaker depending upon the slope of the area being imaged during the time it takes to construct the image.

Both aircraft and spacecraft synthetic aperture imaging radars function at nadir angles varying around 20^0 from the vertical. Under these conditions the vertical motion of the wavy surface provides a large contribution to the motion of the wavy surface towards or away from the radar vector. In fact, because of the orbital motion of each of the fluid particles in the waves there will be a component that is normally distributed and that is towards or away from the radar beam at each point on the sea surface. Unfortunately, the areas where the sea surface is moving toward the radar beam are on one side of the wave and are associated with either a strong Doppler velocity toward the radar or away from the radar for those portions of the surface with the greatest tilt toward the beam, depending upon which way the wave is traveling. Stated another way, large regions of the surface being imaged have associated with them vertical motions whose additional contribution to the Doppler shift will shift the region to the wrong place in the image plane as the image is being constructed. This wrong place will be consistently either to the left or the right to the proper place in the image plane for this extensive area. Immediately, on the other side of the same wave there will be a corresponding region where the shift will be of the same magnitude but in exactly the opposite direction. The results seem to indicate that the SAR for aircraft altitudes just marginally escapes not working because of these effects and that a SAR on a spacecraft will not work properly because of these effects. Some examples will be worked out in what follows.

A Comparison of Aircraft and Spacecraft Parameters

The parameters of importance for a SAR on an aircraft and on a spacecraft have been calculated. Those for the aircraft assumed a plane ocean and cartesian coordinates; for the spacecraft the appropriate modifications for a spherical earth and a spherical wave front were employed. The aircraft was assumed to be at an altitude of 3 km and to be traveling at a velocity of 150 meters per second; the spacecraft was assumed to be at an altitude of 800 kilometers and to be traveling at a speed of 7.5 kilometers per second. The other parameters are given in Table 5.1. It was assumed that the half beam angle was 4^0 for the aircraft and $\frac{1}{4}$ of a degree for the spacecraft. Under these assumptions, the point perpendicular to the particular y scan being imaged is at 220 meters to the right of the y scan, for this particular nadir angle, when it is first picked up by the aircraft beam and 3.82 kilometers to the right of the y scan when it is first picked up by the spacecraft beam. If all the information in the full beam, as assumed, is used, it takes nearly three seconds for the aircraft to acquire all of the Doppler information for this particular spot and about one second for the spacecraft to acquire the information for this spot. When this point in the x, y plane is first acquired, and all calculations are for a 20^0 angle for the radar signal at either the aircraft or the spacecraft, the Doppler velocity at that point, if it were not in motion would be 3.9 meters per second for the aircraft and 11 meters per second for the spacecraft.

For a typical wind generated sea, with a wind blowing either directly toward, or directly away from, the subsatellite track, or the aircraft track, on the surface of the ocean, there will be velocities

Table 5.1 Assumed and Calculated SAR Design Values for an Aircraft and A Spacecraft

	Alt (km)	Velocity	θ (at source)	y_o (km)	Slant Range
A/C	3	150 m/sec	20°	1.09	3.193 km
S/C	800	7.5 km/sec	20°	291.6	851.3 km

	½ beam angle	X at ½ beam	2 t	Doppler at X	Ratio (1 m/s)/Doppler V	Displacement
A/C	4°	222 m	2.96	3.91 m/s	0.256	57 m
S/C	½°	3.82 km	1.02	11 m/s	0.091	347 m

in the wavy surface toward and away from the radar pointing vector of about one meter per second. This is the standard deviation of the velocity. It could be double this for extremely high seas, and even for a one meter per second standard deviation there will be substantial patches with double this velocity. The ratio of one meter per second to the Doppler velocity when the cell image is first acquired is tabulated. In one case it is 0.256, and in the other it is 0.091.

The Doppler velocity introduced by the motions of the wavy surface will add to or subtract from the Doppler velocity due to the motion of the platform. If it changes it by this amount, relatively speaking, the cell being imaged will be mapped a distance equal to the product of this ratio times the value of x at the half beam point toward the y scan line being constructed. The product of this ratio times the value of x at the half beam point yields a distance in meters that describes how far the cell being imaged will be displaced from its true value because the Doppler velocity of the wave motion has caused the area being imaged to be moved to the wrong point. Since the Doppler change due to the moving sea surface will not vary very much during the imaging time, no matter where this particular cell is, it will have either too high or too low a Doppler velocity and therefore be displaced a constant amount from its true position, which should have been on the line perpendicular to the moving platform at the instant this line passes the point being imaged. For the assumed aircraft conditions, this distance is 57 meters, and for a spacecraft, it is 347 meters. Under the conditions assumed, with the waves traveling dominantly either toward or away

from the subsatellite track, the crests of the waves will be lined up more or less parallel to the subsatellite track and the successive crests will appear more or less one behind the other with increasing range in the assumed y direction. If, for example, the waves are traveling toward the platform, the forward slopes of the waves which will give the largest backscatter values will have a Doppler component motion of the water toward the platform and the Doppler shift will be higher than it would be for a stationary target. All of these cells will be mapped to a point in the image plane that is too far to the left of their true position in the image plane. The region for each of the waves being imaged that lies on the other side and that has a negative slope so that they are imaged as dark regions will have a Doppler velocity due to the waves that is opposite in sign, compared to those on the forward face of the wave. All of these points will be imaged to points that are too far to the right of their true position in the image plane.

Typically, the distance between crests from crest to crest in such a storm sea might be 400 meters, and the distance along a crest in a group of high waves might be about 2,400 meters. The displacements shown in this table would be along the crest and thus mislocating the front and rear of a particular wave by 50 to 100 meters, which happens in aircraft images, would not necessarily destroy the pattern. However, for spacecraft conditions, the displacements would be as much as 350 to 700 meters and the entire structure of the waves, since the total shear would be double this, might be destroyed.

It would be possible to Monte Carlo a realistic sea surface, to assume that the image was in fact given by a quantity related to the slope of the sea surface, and to carry out the full reconstruction of a

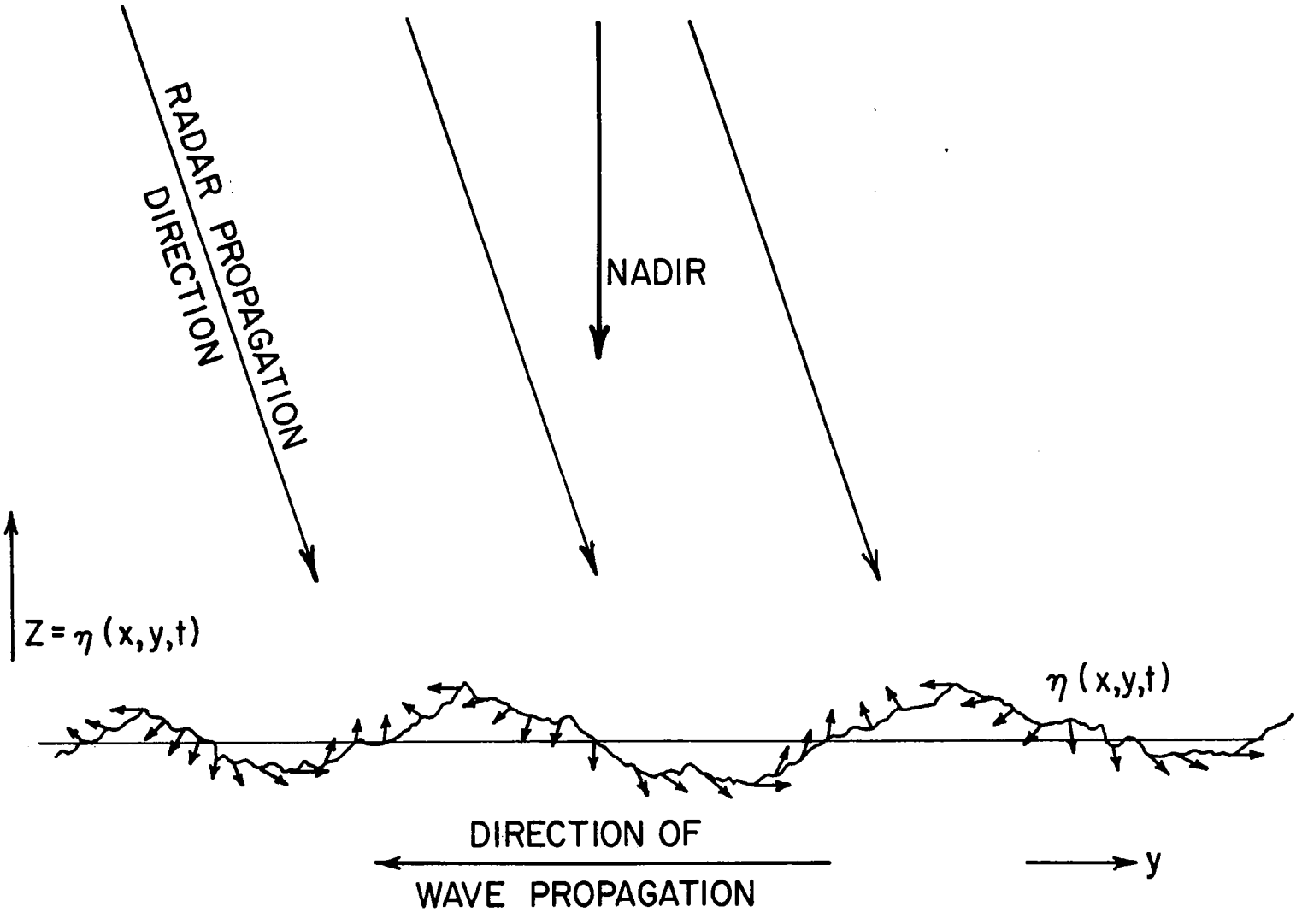

FIGURE 5.1 SKETCH OF A PORTION OF A WAVY SURFACE SHOWING THE CORRELATION OF THE WAVE SLOPE AND THE SURFACE MOTION. POSITIVE SLOPE CORRELATES WITH MOTION TOWARD THE TRANSMITTER AND NEGATIVE SLOPE WITH MOTION AWAY FROM IT.

hypothetical image with these parameters so as to see what the final imaged product might look like. One of the problems, of course, is that two different places on the original sea surface may be imaged to the same place, under these conditions, since the Doppler velocity fields varies in space and time and will vary along a given $y = y_0$ line on the ocean surface.

The conditions under analysis are described schematically in figure 5.1. The figure shows a section of a wavy surface moving toward the negative y direction, with the moving platform off to the left of the figure toward negative y. The wave profile is shown. The derivative in the y direction is strongly correlated with the instantaneous velocity field associated with the moving wavy surface. Those portions of the wave profile with positive slopes are moving toward the radar beam and those with negative slopes are moving away from the radar beam.

It is also clear from the table that the assumption of a ½ degree beam width for the spacecraft antenna is not too critical. If it were increased to 4 or 5 degrees the various numbers would increase in proportion. The imaging time would probably be too large for a moving wave pattern since it would be expected to be 16 times greater for a 4 degree beam width. However, the Doppler velocity and the other values would increase in proportion. This type of scaling would still yield the relative displacements found in the last column.

The Goddard Phase A Study compared the coherent integration times for an aircraft and a spacecraft for the same along-track resolution, which could be about 25 meters. If the problem were this simple, the coherent integration times could be made identical by decreasing the resolution in the along-track distance by a factor of five. A value

for L of 125 meters would still yield a great deal of wave information compared to a feasible real aperture system on a spacecraft. However, the Doppler effect of shifting an image point by a large distance for a spacecraft application cannot be removed by making the coherent integration times equal.

The True Shape of the Averaging Area

The true shape of the illuminated patch of sea surface is not a rectangle with dimensions L by M. It is actually an area bounded by the arcs of two circles and two radii from the source. The radii of the circles are approximately the arc distances from the subsatellite point to the cell. Because of the variations of intensity within the beam,an equal intensity contour will have curved corners and might look like the shadow of a slightly curved hot dog. For the beam widths considered in this analysis the "true" distance to a target point is only a few meters greater than the distance to the circle at the beam angle considered. For beam widths of about 5°, however, the range to the target point varies with angle to such an extent that corrections must be made for this effect. The details of the spectral filter for the actual shapes of the iso-intensity contours as determined by the radar design need to be worked out in detail.

Comparison of Different Synthetic Aperture Radar Platforms

Although the comparison of a synthetic aperture system on an aircraft and a spacecraft was given in the preceding section, the results can be generalized so as to permit the comparison of any two moving platforms on which synthetic aperture radars are operated. If the effects of the curvature of the earth are neglected, as a first approximation, the Doppler velocity associated with a cell at the angle ψ foreward, or aft, in a synthetic aperture beam is given in equation (5.2) where v is the velocity of the platform, ψ is the angle measured from zero abeam of the

spacecraft, and θ is the nadir angle. Similarly the widths of the target zone for a given beam width depends upon the slant range and the beam width of the antenna beam. This is given by equation (5.3).

$$\text{Doppler} \cong v \sin \psi \sin \theta \tag{5.2}$$

$$\text{Width} \cong h \sin \psi / \cos \theta \tag{5.3}$$

If the target is moving with a velocity component toward or away from the radar beam, under the assumption that the velocity of the target, v_t, is a constant, the displacement of the target in the image plane is given by equation (5.4).

$$d = \frac{h \sin \psi v_t}{v \cos \theta \sin \psi \sin \theta} \tag{5.4}$$

For any two moving platforms the two displacements d_1 and d_2 have a ratio given by equation (5.5)where the nadir angle, the beam angle, and the Doppler velocity due to the moving target cancel out since they can be the same for both moving platforms.

$$\frac{d_1}{d_2} = \frac{h_1 v_2}{v_1 h_2} \tag{5.5}$$

This final equation makes it possible to compare aircraft at different altitudes traveling at different speeds, as well as spacecraft and aircraft. If for example, subscript 1 is the spacecraft at an altitude of 800 kilometers with a velocity of 7.5 kilometers per second and if d_2 is the aircraft at an altitude of 3 kilometers with a velocity of 0.15 kilometers per second, this ratio turns out to be 5.33 as shown in equation (5.6).

$$\frac{d_1}{d_2} = \frac{800}{7.5} \cdot \frac{0.15}{3} = \frac{16}{3} = 5.33 \qquad (5.6)$$

Although the aircraft parameters can be varied over perhaps several factors of two, that is the aircraft might be speeded up to 0.30 kilometers per second and the altitude might be changed to six or nine kilometers, or decreased to two kilometers, the parameters for a spacecraft are not easily altered. In general, then for a typical aircraft condition of .15 kilometers per second at an altitude of 3 kilometers a spacecraft is five times worse off in trying to locate the position of a moving target such as in a wave pattern than an aircraft. Clearly also, for this same altitude, two aircraft with the same radars on them, but one flying at twice the speed of the other will produce images such that the faster flying aircraft, in some sense, for waves, should produce an image that is twice as good as the slower flying aircraft. An aircraft flying at nine kilometers at 0.075 kilometers per second, if this is possible, would produce the displacements that would be comparable to those that would occur for a spacecraft such as SEASAT-A.

Possible Remedies

There are several things that can be done, under the assumption that the above analysis is correct, to attempt to provide a system that might work on a spacecraft. One would be to carry out a more thorough analysis of the implications of the results of Table 5.1 by studying in greater detail what the image might be like under these circumstances for a variety of wave conditions and wave spectra. Another would be to attempt to simulate spacecraft conditions more

closely during aircraft measurements so as to obtain conditions comparable to those that might exist on a spacecraft in so far as these false displacements are concerned. A study of images obtained under these circumstances could prove to be highly rewarding. Other alternatives are to attempt to either develop a data processing technique that will use what is known about waves in order to correct for these erroneous Doppler effects, or to design out these difficulties.

The Correction of the Imaging Procedure by Means of Information on the Waves

Since the errors produced in the image are systematic and are caused by well known properties of the waves, it may be possible to remove them by an appropriate application of the theory of a random sea surface. This possibility is investigated in a preliminary way in this section.

Consider a monochromatic wave given by equation (5.7). For simplicity, λ stands for the argument of the trigonometric function throughout. For a monochromatic wave, the slope in the y direction is then given by equation (5.8) the slope in the x direction is given by (5.9). The vertical velocity is given by equation (5.10) and the horizontal velocity components in the x and y direction respectively are given by (5.11) and (5.12). If ψ is the angle between the point being imaged and the line perpendicular to the antenna beam, then the component of slope along this line is given by S. The Doppler velocity is given by D and represents the motion of the water surface toward or away from the propagation direction of the radar beam.

$$\begin{aligned} \eta(x, y, t) &= a \sin(\ell x + my - \omega t + \epsilon) \\ &= a \sin \lambda \end{aligned} \tag{5.7}$$

$$\text{where } \lambda = \ell x + my - \omega t + \epsilon$$

$$S_y = \frac{\partial \eta}{\partial y} = am \cos \lambda \tag{5.8}$$

$$S_x = a \ell \cos \lambda \tag{5.9}$$

$$w = - a\omega \cos \lambda \tag{5.10}$$

$$u = \frac{a \omega \ell}{k} \sin \lambda \tag{5.11}$$

$$v = \frac{a \omega m}{k} \sin \lambda \tag{5.12}$$

$$S = a (m \cos \psi + \ell \sin \psi) \cos \lambda \tag{5.13}$$

$$D = -a\omega ((\cos \theta \cos \psi \cos \lambda) + (\frac{m}{k} \sin\theta \cos \psi + \frac{\ell}{k} \sin \theta \sin \psi) \sin \lambda) \tag{5.14}$$

Straightforward techniques permit the expressions for S and D to be employed in the manufacture, or generation, of a superposition of many sinusoids with an assigned spectrum, $S(\ell, m)$, to represent the total slopes of the wavy surface and the total Doppler velocity field for this wavy surface. The spectrum of the slopes and the spectrum of the Doppler velocities can be calculated and the variance of the slopes and the variance of the Doppler velocities can be found. Finally the covariance between the slopes and the Doppler velocities can be calculated. These are given by equations (5.15), (5.16) and (5.17) where the terms in the integrals are defined immediately below them by equation (5.18), (5.19) and (5.20).

$$\text{Var } S^2 = \sigma_s^2 = \cos^2\psi \iint A(\ell, m, \psi, \theta)\, S(\ell, m)\, d\ell\, dm \tag{5.15}$$

$$\text{Var } D^2 = \sigma_D^2 = \cos^2\psi \cos^2\theta \iint B(\ell, m, \psi, \theta)\, S(\ell, m)\, d\ell\, dm \tag{5.16}$$

$$\text{COV (SD)} = E(SD) = \cos^2\psi \cos\theta \iint D(\ell, m, \psi, \theta) S(\ell, m)\, d\ell\, dm \tag{5.17}$$

$$A(\ell, m, \psi, \theta) = m^2 + \ell^2 \tan^2\psi + 2m\ell \tan\psi \tag{5.18}$$

$$B(\ell, m, \psi, \theta) = \omega^2 \left[1 + \frac{m^2}{k^2} \tan^2\theta + \frac{\ell^2}{k^2} \tan^2\theta \tan^2\psi + 2\frac{m\ell}{k^2} \tan^2\theta \tan\psi\right] \tag{5.19}$$

$$D(m, \ell, \psi, \theta) = \omega(m + \ell \tan\theta \tan\psi) \tag{5.20}$$

The range of integration in these equations is from minus infinity to plus infinity, over both variables. However, for a spectrum confined to positive values of m and all values of ℓ, the waves would be traveling away from the spacecraft. For spectra confined to negative values of m and all values of ℓ, the waves would be traveling toward the spacecraft.

The essential point of these equations is that the slope and the Doppler shifts are correlated. The correlation coefficient between the slope and the Doppler velocity is given by equation (5.21).

$$\rho = \text{COV}(SD)/\sigma_s\sigma_D \tag{5.21}$$

As written, these equations show that the effect of changing direction within the beam, ψ, and the value of the nadir angle, θ, nearly cancels

out as far as the correlation is concerned and that the slope and Doppler shift variances are only weakly dependent upon both θ and ψ.

There are, of course, a wide variety of wave number spectra that can be substituted into these expressions. The main reason for attempting to image the waves in the first place is to obtain better and more nearly worldwide estimates of the spectra. However, if a fairly reasonable form for the spectrum is assumed, it is possible to calculate the correlation between the slope and the Doppler velocity and to obtain some idea of how these quantities might vary from place to place over the ocean. The equation previously given in Chapter 4 was in cartesian wave number space. If it is transformed to polar coordinates where wave number is the radius and Φ is the angle and if it is assumed that this spectrum spreads evenly about the positive m axis according to a cosine square law the equation for $S(\ell, m)$ becomes equation (5.12) as defined over appropriate ranges.

$$S(k, \Phi) = \alpha (\cos \Phi)^2 / \pi k^3$$

$$\text{for } k_0 < k < k_1; \; -\frac{\pi}{2} < \Phi < \frac{\pi}{2} \qquad (5.22)$$

and zero otherwise

In this form and by using well known transformations between m and ℓ and k and Φ, it is possible to evaluate all of these expressions. Since the frequency and wave number of a wave are related by $k = \omega^2 / g$ and since $\omega = 2\pi / T$, these expressions can finally be put in the form where they depend on T_0 and T_1. It appears that T_1 should be the period associated with the size of the cell being imaged (some people disagree with this statement), and thus a value of 4 seconds has been selected

for it. T_0 has been assumed to have various values. Under these assumptions the variance of the slopes as given by equation (5.23), the variance of the Doppler motion is given by equation (5.24), and the correlation coefficient is given by equation (5.25) where certain terms have been defined in equations (5.26) and (5.27).

$$\sigma_s^2 = \cos^2\theta \frac{3\alpha}{4} \ell n \frac{T_n}{T_1} G[\psi] \tag{5.23}$$

$$\sigma_D^2 = \cos^2\theta \cos^2\psi \frac{\alpha g^2}{4\pi^2} \left[T_0^2 - T_1^2\right] H(\theta, \psi) \tag{5.24}$$

$$\rho = -\frac{\sqrt{3}}{2} \left[\frac{(T_0 - T_1)}{\ell n\left(\frac{T_n}{T_1}\right)(T_0 + T_1)G(\psi)H(\theta,\psi)}\right]^{\frac{1}{2}} \tag{5.25}$$

where

$$G(\psi) = 1 + (\tan^2\psi)/3 \tag{5.26}$$

$$H(\theta, \psi) = 1 + \frac{3\tan^2\theta}{4} + \frac{\tan^2\theta \tan^2\psi}{4} \tag{5.27}$$

These equations in turn have been evaluated for different values of T_0 as given in Table 5.2. The five second example is quite unrealistic and represents a very thin slice in the k direction that wraps around a half of a circle. The other values are representative of a crude description of the wavy sea for a very strong wind blowing offshore and generating a steep spectrum. More typically as the longer periods, or the smaller wave numbers, are reached, the spectrum will round off and not peak up as much as these formulas indicate. Also the cosine squared behavior will tend to be more of a cosine to the fourth power behavior for the longer waves and perhaps even a more spread out form, as discussed in other portions of this paper, for the shorter waves.

Nevertheless, this table does give numbers that can represent the type of conditions that might be observed on the open ocean. The correlation between the slope and the Doppler velocities ranges from a negative 0.78 to a negative 0.53. This is because the waves are traveling away from the spacecraft. The Doppler velocities ranges from .45 meters per second to 2.91 meters per second, which shows that a value of one used above was not too bad an assumption. There will be places, since all of these quantities are normally distributed, where the Doppler velocities will be double the amounts tabulated. The slopes range in degrees, which is the second value tabulated, from 1.89° to 5.66°.

Since the slope and the Doppler velocities have a bivariate normal distribution with a zero mean, and since they are correlated, it is possible to predict the average value of the Doppler velocity subject to the condition that the slope has been measured. This accomplished by multiplying the measured slope in radians by the number tabulated in column 1 of this table. The appropriate equation is given by equation (5.28).

$$\overline{D/_S} = \frac{\rho \sigma_n}{S_s} S \qquad (5.28)$$

The result would be a value for the Doppler velocity that would be the average of all the Doppler velocities that would be associated with this particular value of the slope. It is the expected value of the Doppler velocity given that the slope that is measured is from a normal distribution with a standard deviation given by column 5 and a correlation given by column 1. Were this done, the residual standard deviation of the unspecified part of the Doppler velocity would be given by column 8. There has been a slight reduction in the

Table 5.2 Predictability of Wave Doppler from Wave Slope for a Model Storm Sea Spectrum. (T_1 = 4 sec)

	1	2	3	4	5	6	7	8	9
T_0(sec)	ρ	σ_D^2	σ_s^2	σ_D m/s	σ_s rad/deg.	$1-\rho^2$	$(1-\rho^2)^{\frac{1}{2}}$	$(1-\rho^2)^{\frac{1}{2}}\sigma_D$	$\frac{\rho\sigma_D}{\sigma_s}$
5	-0.782	.199	1.1×10^{-3}	0.45	.033/1.89	0.39	0.62	0.28	-10.66
8	-0.573	1.06	4.2×10^{-3}	1.03	.0648/3.72	0.67	0.81	0.84	- 9.11
12	-0.557	2.82	6.67×10^{-3}	1.67	.0817/4.68	0.69	0.83	1.38	-11.4
16	-0.543	5.30	8.42×10^{-3}	2.30	.0918/5.26	0.71	0.84	1.93	-13.6
20	-0.531	8.49	9.78×10^{-3}	2.91	.099/5.66	0.72	0.85	2.47	-15.6

Doppler velocity, and thus, if this were done, the cell would not be mapped to quite as incorrect a position as it would be if it were not done. However, the improvement is not too impressive.

The idea though has not been pushed to its full logical conclusion because this is only the simplest of the many things that might be done. There is much more information about the point being mapped from nearby points than is contained in simply a measure of the slope, or brightness, at the point. It may be possible to devise an algorithm for precessing the data that would recover the imaged sea surface to a high degree of accuracy by assuming just barely enough about the spectra of the waves to make it possible to correct for the incorrect mapping. This particular way of solving the problem has not been fully explored by this simple example.

Also, for other kinds of wave spectra, the correlation coefficient can be much more nearly equal to plus or minus one. It equals plus or minus one for a sinusoid, and for high narrow band swell, it can be expected to approach close enough to one for this correction technique to prove useful.

A Multiple Beam Imaging Radar

If these results are correct, there does not seem to be much hope that a synthetic aperture radar will work on a spacecraft. Also from the previous results, the generation of a beam narrow enough in the real aperture sense to image a spot on the sea surface 25 meters wide from a spacecraft seems prohibitively difficult from an engineering point of view. There does, however, seem to be a way to obtain useful images at x band of the waves on the sea surface from a spacecraft on the basis of what is understood to be some preliminary results on possible antennas for a spacecraft.

In the unofficial literature, there are designs being circulated about that produce a multiple beam antenna with the beams pointing out at fairly uniformly spaced angles, and with each of the many beams being narrow. It may be possible to design an antenna at x band with the property that the antenna pattern consists of narrow beams roughly 10^0 apart and centered at angles of approximately $0 \pm 10^0 \pm 20^0$ and so on to $\pm 60^0$ as measured perpendicular to the spacecraft track when the spacecraft is not yawed. All of the results that follow are based on this assumption and further adjustments would have to be made in the design to account for yaw of the spacecraft, similar to those that are being made in the design of the scatterometer. For such an antenna, it seems to be possible to produce beams that are each 0.15^0 wide. It is understood that this is the full beam angle and not the half beam angle. The results would not be as impressive is this were the half beam angle. If the beam angle could be reduced to 0.10^0, the results of the followed analysis would clearly be substantially improved.

Since each of these beams points in a direction that differs by at least 10^0 from all of the other beams, the Doppler velocities for the signals associated with each beam will differ by very large amounts compared to the Doppler velocities used in a synthetic aperture system. The signals being returned from the sea surface can be separated by fairly broad Doppler filters one for each beam, and there would be 13 separate beams for the analysis under consideration. Each beam would also require a different range gate and a different starting time for what used to be called the A scope presentation of the detected return signal. An image would have to be constructed for each beam and the line scans in the image plane would have to be at different angles across the 100 kilometers swath. With the effects of earth curvature neglected, for example, the line scan at 60^0 for the 100 kilometers swath would have to be 200 kilometers long and twisted by 60^0 to the right angle direction through the swath.

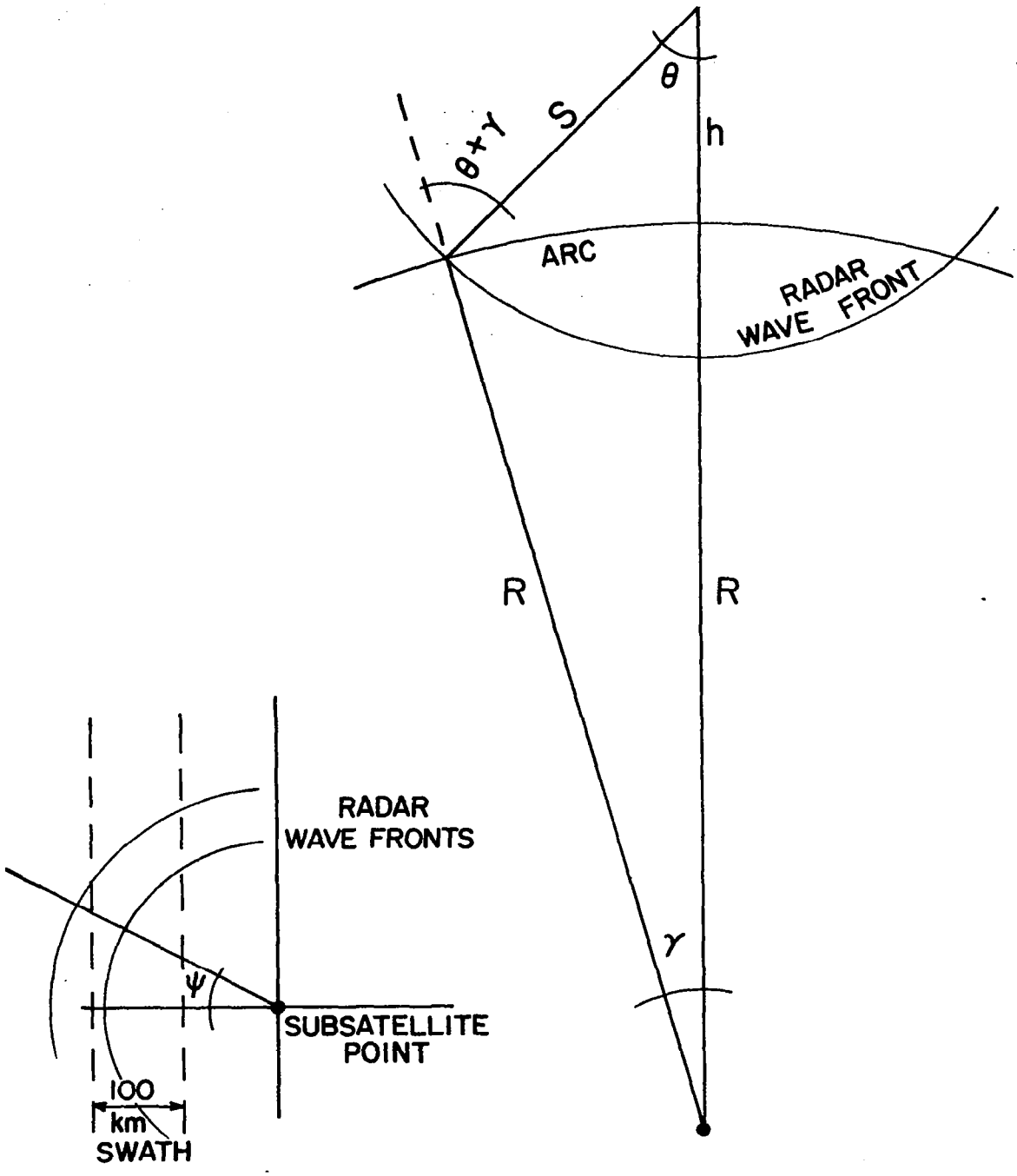

FIGURE 5.2 GEOMETRY OF 100 KM SWATH

For this possible imaging system, some preliminary calculations have been carried out. Figure 5.2 shows the geometry of a 100 kilometer swath which is desired to be imaged. The parameters involved are the radius of the earth, the height of the spacecraft, the angle from the center of the earth between the subsatellite point and the point at which the radar wave front has reached the sea surface. The slant range, the nadir angle, and the arc distance from the subsatellite point to the wave front also shown. In the lower left of the figure, is shown the geometry of the 100 kilometer swath and the angle that the different beams made with the swath. All of these calculations have been carried out more or less correctly except that the spherical triangle solution for the edges of the swath has not been found for the angles other than 0^0 in the tabulation. Thus the slant ranges and the arc distances to the edges of the swath are somewhat in error.

For these conditions the parameters shown in Figure 5.2 can be found by means of equations (5.29) through (5.38). The angle, γ, is very small and the approximations indicated below equation (5.30) are probably satisfactory. Once these approximations are made, along with expressing the slant range as a multiple of spacecraft altitude and the radius of the earth as a multiple of the spacecraft altitude the other parameters can all be found.

$$S^2 = (R + h)^2 + R^2 - 2R(R + h)\cos\gamma \tag{5.29}$$

$$\cos\gamma \cong 1 - \frac{\gamma^2}{2} \tag{5.30}$$

$$S^2 = (R + h)^2 + R^2 - 2R(R + h) + R(R + h)\gamma^2 \tag{5.31}$$

$$S^2 = h^2 + R(R + h)\gamma^2 \tag{5.32}$$

$$S = Ph \tag{5.33}$$

$$R = Kh = 7.969h \tag{5.34}$$

$$\gamma = \left[(P^2 - 1)/71.39\right]^{\frac{1}{2}} \tag{5.35}$$

$$arc = 800(7.964)\gamma \tag{5.36}$$

$$\sin\theta = \gamma K / P \tag{5.37}$$

$$P = (1 + (71.39\,\gamma^2)^{\frac{1}{2}} \tag{5.38}$$

Table 5.3 shows the various parameters for the swaths with antenna beams pointing out at 0^0, 15^0, 30^0, 45^0, and 60^0 to a direction perpendicular to the subsatellite track for a spacecraft in orbit at 800 km. Some of these tabulated values will be interpolated to 10^0, 20^0 and so on in a further analysis. However, as shown by these tables, γ ranges from 2.2 to 6.2^0 the nadir angle ranges from 18.9 to 45^0 (which may be too extreme). The slant range ranges from 844 kilometers to 1,083 kilometers.

For a beam angle of 0.15^0 and for the slant ranges tabulated, the widths in the direction perpendicular to the beam of the portion of the ocean instantaneously illuminated by the advancing short pulse is given by the parameter, L, as defined in the previous chapter. This parameter L varies from 2,200 meters to 2,840 meters. If the pulse length is such that m = 25, then a spectral filter roughly like the one described in the last chapter will result. The parameter, L, represents the full beam width. Zeros in the filter will occur at $\ell = 2\pi / L$.

Table 5.3 Approximate Swath Parameters for a narrow beam at an angle of 0, 15, 30, 45, and 60° abeam of the sub-satellite track.

	γ (degrees)				
	0°	15°	30°	45°	60°
Maximum	3.1	3.2	3.6	4.4	6.2
Middle	2.6	2.7	3.1	3.7	5.3
Minimum	2.2	2.3	2.5	3.1	4.4

	Nadir Angle (degrees)				
	0°	15°	30°	45°	60°
Maximum	22.6	26.9	29.6	35.1	45.5
Middle	20.6	23.4	25.8	30.8	40.8
Minimum	18.9	19.7	21.8	26.3	35.2

	S (Km)				
	0°	15°	30°	45°	60°
Maximum	879	884	904	952	1083
Middle	859	863	878	914	1015
Minimum	844	844	854	880	953

	Arc (Km)				
	0°	15°	30°	45°	60°
Maximum	344	356	397	486	688
Middle	294	304	339	416	588
Minimum	244	253	282	346	488

Table 5.3 Continued

	L meters				
	0°	15°	30°	45°	60°
Maximum	2300	2310	2370	2490	2840
Middle	2250	2260	2300	2390	2660
Minimum	2200	2210	2240	2300	2500

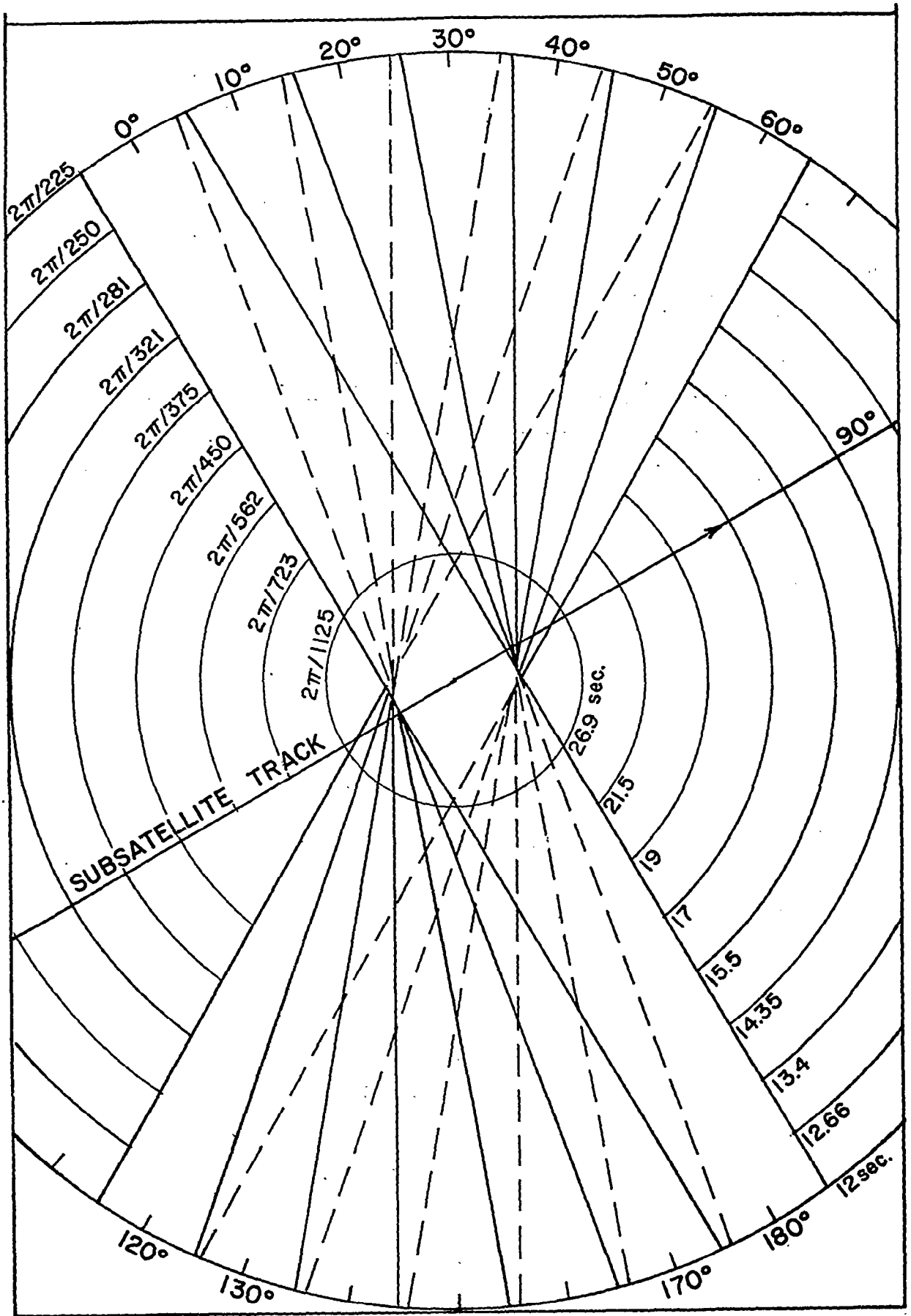

FIGURE 5.3 POLAR COORDINATE SPECTRUM ($S(k\chi)$) AND SPECTRAL FILTERS FROM ZERO TO $2\pi/225$.

The lines along which the spectral filter for each beam direction varying from zero to 60^0, equals zero are shown in figure 5.3 on a spectral wave number coordinate system, ℓ, m, (or k, χ) where the wave numbers vary from $2\pi/2250$ to $2\pi/225$. To the scales shown, the variation from one side to the swath to the other is more or less negligible, and the narrowing of the filter with increasing k is so small that it is difficult to show. However, the filter for an angle of 60^0 has been slightly compressed compared to the one for zero degrees. It is 85% of the width of the one for zero degrees at the center of the swath. A wavelength of 2250 meters never occurs for wind generated gravity waves. A wavelength of 1125 meters would be rare indeed. A wavelength of 725 meters can occur in high winds for long fetches and long durations and then propagate as swell.

As can be seen from this figure, the different spectral filters overlap over the range from 0 wave number to $2\pi/225$ and some information on the entire polar coordinate plane is obtained except for the region lying below the last solid line on the right and the horizontal axis labeled 90^0. A similar pattern should be constructed for -10^0, -20^0 and so on, and since the imaging radar will not be able to tell anything about the direction of the travel of the waves the lower half plane should be filled in also. There is only a relatively small region of the wave number plane that is not covered by this proposed antenna pattern consisting of 13 narrow bands 10^0 apart, each with a beam width of 0.15^0.

One of the problems of working in the wave number space instead of the frequency space is that the same range in frequency space requires a much larger range in wave number space. If one is interested in studying the frequency range corresponding to periods in the waves varying from 20 to 5 seconds, only a factor of four is required on the frequency axis. Since the length of a gravity wave grows as the

square of the period, however, the squares of these numbers have a ratio of sixteen so that a factor of sixteen is required on the wave number axis. This is why with a factor of ten range in the wave number the periods involved only vary from whatever corresponds to a wavelength of 2250 meters, at the first circle, to 12 seconds.

In figure 5.4 the range of wave numbers has been doubled. When this is scaled, the graphical width of the filter is halved. For wave numbers of approximately $2\pi/187.5$ and higher, small pie shaped slices occur in the wave number plane. For spectral components within these areas, no information will be obtained. The range is roughly from 11 seconds, or perhaps 12.5 seconds, to 8.5 seconds as shown in figure 5.4. However, from all of the results of the preceding material, it is clear that the vector wave number spectrum is continuous over large areas of the ℓ, m wave number plane and that these different bands can have sampled it quite thoroughly even beyond the wave number corresponding to a wavelength of 112.5 meters. This statement is also true if the wave number range is doubled again. The thirteen different beams will sample an adequate portion of the shorter wavelengths.

For the longer wavelengths, corresponding to waves with periods of 12 seconds, and longer, some interesting things happen. From figure 5.3, for example, the angular range covered by the wave number filter at a radial distance corresponding to a wave number of $2\pi/732$ is $\pm$ 18° about the center direction. The total angular range is 36°, and thus the next beam 10° clockwise overlaps the first beam as far as this wave number is concerned by 28°. The beam at 60° spreads 18° further clockwise and thus the total range of directions from zero to 90° is covered to 78°, out of a possible 90°.

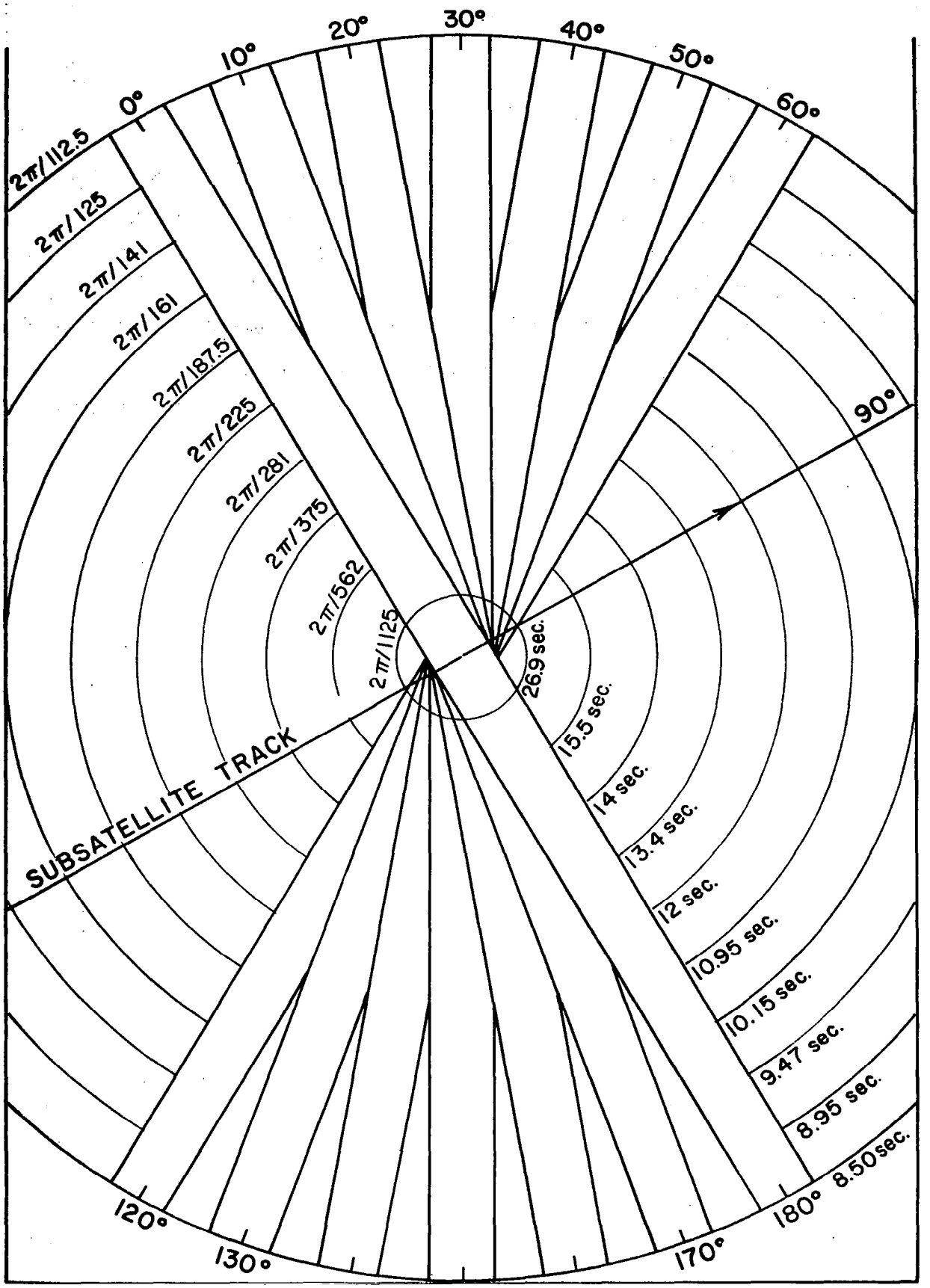

FIGURE 5.4 POLAR COORDINATE SPECTRUM AND SPECTRAL FILTER FROM ZERO TO $2\pi/112.5$

Table 5.4 Wave directions contained in a single image as a function of wavelength and period and total range of direction sampled

Length (m)	Period (sec)	Angular Band (degrees)	Total range (degrees out of 360°)	Amount Interpolated (degrees)
1125.	26.9	± 28	352	
723	21.5	± 18	312	
562	19	± 14	296	
450	17	± 11	284	
375	15.5	± 9	276	
321	14.4	± 8	272	
281	13.4	± 7	268	
250	12.7	± 6.2	264	
225	12	± 5.5	~ 262	
187	10.9	± 4.8	~ 259	~ 4.8
161	10.1	± 4.1	~ 256	~21.6
141	9.5	± 3.5	~ 254	~36
125	9	± 2.9	~ 252	~50
112.5	8.5	± 2.5	~ 250	~60

Table 5.5 Doppler velocities for a multiple beam imaging radar (km/sec) (interpolated from previous results)

	0°	10°	20°	30°	40°	50°	60°
Maximum	0	0.59	1.20	1.86	2.65	3.43	4.64
Minimum	0	0.43	0.89	1.39	2.13	2.92	3.74
Range km/s	± 0.02	0.4-0.6	0.8-1.2	1.3-1.9	2.1-2.7	2.9-3.5	3.7-4.7

These results are shown in Table 5.4. For wavelengths and periods that correspond to the higher more severe storm waves on the open ocean, very nearly all of the full 360^0 of possible directions is imaged by this combination of beam directions and beam widths as a function of angle for a given radial wave number.

As the wavelength becomes shorter, less of the full 360^0 is imaged. However, a substantial fraction is imaged for all wave numbers shown. Once the gaps begin to appear between the separate wave number filters a certain fraction of the total range from 0 to 60^0 or so has to be interpolated but this is still a rather small part of the total involved for the full area of the ℓ, m plane.

Table 5.5 based upon the material given in Table 5.3 shows the maximum and minimum Doppler velocities for the center of the beam for each of the beams as the angle is varied from zero to + 60^0. The Doppler velocities would be negative for the other range of angles. The greatest Doppler velocity at each angle is less than the smallest Doppler velocity for the next angle so that these Doppler velocities do not overlap for a swath 100 kilometers wide if the maximum values are rounded up and the minimum values are rounded down. The range of Doppler velocities in kilometers per second is shown in the last entry in the table. Quite clearly Doppler band pass filters can be constructed with a safety factor such that the signal coming back from each of the beams can be separated out just by these frequency shifts and correctly assigned to each of the beams. The system that is being suggested is thus a combination of the Doppler concepts for a synthetic aperture radar and the narrow beam concepts advocated by others for a radar on a spacecraft. It will yield information about nearly the full vector wave number space from one antenna, if such an antenna can be designed.

If each of these A scope line scan are used to construct an image, there will be 13 images for each swath. In each of these images, the waves will appear to have their crests lined up perpendicular to the direction of the line scan. The longer waves in the image will have a greater variation in apparent direction then the shorter waves. Swell with a fairly long wavelength at an appropriate direction that is a narrow band in both the ℓ, m directions can show up in two images, or perhaps in as many as four images, if it has just the right direction.

The scan at 60° forward will be imaged about one minute before the scan at 0° and the scan at -60° will be imaged one minute later. This does not matter any more because each scan is complete in itself. The time separation for the scans at 60°, 50°, 40°, 30° and so on may be close enough together, perhaps, ranging from 5 to 15 seconds so that the movement of the waves in each image can be ascertained if they fall into different images, and under these circumstances it may be possible to determine which way the waves are traveling as well as what their spectral properties are. This would be an additional benefit from this proposed system.

Finally, nothing has been said about imaging waves with this system near a coastline. The problem here is that the waves become shorter as they get closer to a coast in shallow water. The details on what happens to the waves of these different wavelengths as they shoal needs to be worked out. It is clear that they will not change by factors of 4 or 5 over the depths typically involved in wave refraction as shown in previous figures. As an image including a coastline is constructed with these 13 different beams the coastline should preserve its properties since the targets there are stationary, and the wave patterns in each image should show some interesting characteristics. Since the waves are turned in direction as they approach the coastline, the waves in the deeper water will show up at one or more of the angles. Then as they

move closer to the shore and change direction, the images will be picked up in portions of the images from the other beams. It should be possible to watch the narrowing of a wave spectrum with the effect of refraction and the change of the direction of the waves as they shoal, by studying the different images produced by this system.

One of the problems, of course, in interpreting a full photograph is that all of these effects are mixed in together. It may actually be an advantage to do the imaging in the way described because part of the filtering process has already been applied to the waves both in deep water and as they approach a coastline.

SOME LOOSE ENDS

The proposed SAR for Seasat-A was reviewed at a meeting held at JPL on May 6, 1975. The impact of the motion of the waves on the motion of the bright and dark areas of the image was recognized, but not accepted as a conclusive reason for the system not working. The displacement of moving targets is a recognized feature of SAR images. Other questions were also asked at this meeting. These loose ends will be cleared up in this section.

The length of time required to synthesize the image from a number of looks depends on the coherent integration time, T_c, and the time between successive looks, ΔT. Consider 2N independent looks, T_c seconds long and ΔT seconds apart, and let the times of the looks be symmetrically placed to each side of the zero degree beam angle at $\pm \Delta T/2$, $\pm 3 \Delta T/2$, $\pm 5 \Delta T/2$ and so on.

The expression in Chapter 4, equation (4.11), can be extended to an operation over time as in equation (5.39).

$$\eta(x_o,y_o,t_o) = \int_{-\infty}^{\infty}\int\int G(x-x_o)\, H(y-y_o)\, J(t-t_o)\cdot$$

$$\cos\,(\ell x + m y - \omega t + \epsilon)\; dx dy dt. \qquad (5.39)$$

The time operation kernal is given by equation (5.40).

$$J(t-t_o) = \sum_{1}^{N} B_{1j}(\Psi_j)\, J_{1j}\,(t-t_o)$$

$$+ \sum_{1}^{N} B_{2j}(\Psi_j)\, J_{2j}\,(t-t_o) \qquad (5.40)$$

where due to symmetry of the beam about $\Psi = 0$, $B_{1j} = B_{2j}$, and the B's are determined by the antenna pattern,

where

$$J_{1j}\,(t-t_o) = \begin{cases} 1; & t_o + (j-\tfrac{1}{2})N\Delta T - \dfrac{T_c}{2} < t < t_o + (j-\tfrac{1}{2})N\Delta T + \dfrac{T_c}{2} \\ 0; & \text{otherwise} \end{cases} \qquad (5.41)$$

and where $J_{2j}(t-t_o)$ has a similar definition.

The spectral filter for this effect can then be worked out to be equation (5.42).

$$F(\omega, T_c, \Delta T) = 4\left[\frac{\sin(\omega T_c/2)}{\omega T_c/2}\right]^2 \left[\sum_{1}^{N} B_j \cos\,(\omega(j-\tfrac{1}{2})\Delta T)\right] \qquad (5.42)$$

This term should appear on the right hand side of equation (4.16). Since $\omega = (gk)^{\frac{1}{2}} = g^{\frac{1}{2}}(\ell^2 + m^2)^{\frac{1}{4}}$, this function can be evaluated in the ℓ,m plane. A coherent integration time, to be safe of, 0.5 seconds causes the first zero in the $(\sin\varphi)/\varphi$ type term to occur at $\omega = 4\pi$, which corresponds to a period of 0.5 seconds and a wavelength of about $\frac{1}{3}$ meter. This term has almost a negligible effect on the total spectral filter.

For six looks the second term expands to the form,

$$\left(B_1 \cos \frac{\omega \Delta T}{2} + B_2 \cos \frac{3\,\omega \Delta T}{2} + B_3 \cos^5 \frac{\omega \Delta T}{2}\right)^2,$$

and nearly equal values of the B's lead to the conclusion that ΔT cannot be very large. All of the looks must be acquired within a total time of one or two seconds, otherwise the ability to resolve a portion of the image 25 meters on a side will begin to be lost, and this filter will have effects that are stronger than the effects of the spatial averages considered in Chapter 4. The exact details depend on the antenna pattern, but it is clear that a useful image cannot be synthesized from, say, six independent looks taken over a four or five second time interval. The total time involved determines the period of that wave that will move through one complete cycle and be averaged out. A wave with a 3 second period is about 15 meters long and begins to approach the size of a single cell in the image.

At the review, it was pointed out that the aircraft parameters used in Table 5.1 did not describe the Convair 990 imagry correctly. For this aircraft,the ratio computed in equation (5.6) is closer to 2 than to 5.33. Wave images have been successfully obtained once in a while for these conditions. There still remains the challenge of proving that imagry can be obtained for high waves if the parameter h/v is scaled to spacecraft conditions on an aircraft.

If it can be demonstrated that imagry can be obtained under these circumstances, the doppler velocities will still shift the various cells back and forth in the image plane by the amounts predictable by the preceeding equations, and the surface motions given by Table 5.2 are good estimates of the conditions that will exist.

The steps that went from equations (5.7) through (5.14) to equations (5.15) through (5.21) involved a modest amount of legerdemain. By filling in the details after equation (5.14) it is possible to write down expressions for $\eta(x,y,t)$, $S(x,y,t)$ and $D(x,y,t)$ that would represent these quantities as a multivariate vector random process. The results show that it would be possible to construct mathematically the "image" that would be produced by a SAR given a "true" surface and its slope and motions but that it would be extremely difficult, to go from a SAR image to a true image of the sea surface. If images can be obtained with h/v scaled to spacecraft conditions, the crux of the problem then becomes that of understanding what such images mean.

Given a spectrum, $S(\ell,m)$, for the waves, the following three double summations can be performed using equations (5.7), (5.13), and (5.14). These equations have been simplified by leaving out all the subscripts used in Chapter 2 except for the indicies on the wave amplitude. They should still be considered to be implicitly present.

$$\eta(x,y,t) = \Sigma\Sigma a_{pq} \sin(\ell x + m y - \omega t + \epsilon) \tag{5.43}$$

$$S(x,y,t) = \Sigma\Sigma a_{pq} (m \cos\Psi + \ell \sin\Psi) \cdot \cos(\ell x + m y - \omega t + \epsilon) \tag{5.44}$$

$$\begin{aligned} D(x,y,t) = &-\Sigma\Sigma a_{pq} \omega \cos\Theta \cos\Psi \cdot \cos(\ell x + m y - \omega t + \epsilon) \\ &-\Sigma\Sigma a_{pq} \omega \left(\frac{m}{k} \sin\Theta \cos\Psi + \frac{\ell}{k} \sin\Theta \sin\Psi\right) \cdot \\ &\sin(\ell x + m y - \omega t + \epsilon) \end{aligned} \tag{5.45}$$

The rules are that a large sum of terms should be formed with amplitudes prescribed by $S(\ell m)$. Once Ψ and Θ are picked, for every corresponding term in the sum for each of the three equations, exactly the same values of a_{pq}, ℓ, m, ω, k, and ϵ must be used. The result is then a three independent variable (x,y and t) vector Gaussian process for η, S and D that shows the interrelationship of these three quantities at any point in space for any instant of time.

Equations (5.43), (5.44), and (5.45) must first be operated on by the filters given immediately above and in Chapter 4. The image produced by a real aperture radar would be given by $S(x_o,y_o,t_o)$ and methods for eliminating t_o and getting the true spectrum have been given. $J(t-t_o)$ would be different.

The imagry produced by a SAR would be given by

$$S(x_o^*, y_o, t_o) = S\left(x_o + \frac{D(x_o,y_o,t_o)h}{v \cos \Theta \sin \Theta}, y_o, t_o\right) \tag{5.46}$$

or, in words, $S(x_o,y_o,t_o)$ and $D(x_o,y_o,t_o)$ are to be evaluated on a grid of points using $x = v\,t$ to eliminate time. The value of D is then used to compute a new x coordinate and the value of S at x_o,y_o,t_o is plotted at this new x coordinate.

The random process so generated is extremely complicated. It could be modelled numerically for any spectrum. Given only the image represented by equation (5.46), it is difficult to see how to process it, if it exists and is a single valued function of its independent variables, so as to recover useful information on the waves.

A TEST PROGRAM, ITS POSSIBLE RESULTS, AND THE OPTIONS IT WILL GENERATE

Several things can be done in an aircraft test program to clarify these issues. A real aperture radar and a SAR could both be flown on the same aircraft so as to obtain simultaneously produced images. If images are obtained, it is predicted that the brightest and darkest areas of the images will lie one behind the other on well defined waves for real aperture images as Figure 4.20 and that they will be sheared relative to the wave crest alignment in SAR images. A good imagination suggests this is happening in Figure 4.23.

If these ideas are correct, for a given range, the Doppler frequency spectrum should not center on zero if a cell is scanned uniformly by a symmetrical beam, but since many cells are scanned simultaneously this effect may be masked. The average Doppler frequency in the raw data for a given range should fluctuate back and forth about zero in ways different from stationary targets. A strong target area that dominates the signal over the full time associated to image it could shift the Doppler frequency spectrum to a non-zero mean.

The correct h/v scaling corresponding to SEASAT-A needs to be flown and varied by a factor of two to four below this value for the same wave patterns to see if the characteristics of the image change. The effects of aircraft speed on the images will be mixed in with the Doppler effects, and it will be difficult to sort them out.

For an h/v ratio of 106.7 seconds (i.e. 800 km/7.5 km/s), either images will be obtained over a useful range of wave conditions or they will not. If not, a SAR could perhaps be justified solely for imaging ice in the polar oceans. Another possibility is the multibeam system

described above. The zero degree beam of the multibeam system could also serve as a SAR to image pack ice and other stationary features to the desired resolution.

If images are obtained, perhaps even only part of the time and not at other times, it will be necessary to understand why and to describe loss of potential data quantitatively. It will also be necessary to understand what the image means. A twenty five meter resolution, if individual cells are displaced by unknown amounts of as much as a kilometer in either direction, is not very meaningful.

CHAPTER 6 REVISED ELEVATION, SLOPE AND CURVATURE SPECTRA OF A WIND ROUGHENED SEA

INTRODUCTION

Pierson and Stacy (1973) made a study of the then available data on waves so as to obtain the proposed wave number spectrum for a wind roughened sea surface, which in frequency space covers four order of magnitude and eleven orders of magnitude in spectral values. The spectra were given as a function of the friction velocity, u_*, and had five ranges of definition. These ranges were called (1) the Pierson-Moskowitz range, (2) the Kitaigorodskii range, (3) the Leykin-Rosenberg range, (4) the capillary range, and (5) the Cox viscous cutoff range. Since then new sources of data have become available, and the purpose of this part is to revise these original equations so as to include these new and better results. The derivation of the Pierson-Moskowitz range was described in Chapter 2.

Stacy (1974) has investigated the frequency range from 0.2 to 0.5 hertz in the gravity wave spectrum. He was able to use data for which the friction velocity varied from 30 cm/sec to more than 200 cm/sec. This range was shown to be actively dependent upon the friction velocity and to increase in spectral values with u_*. In addition, Mitsuyasu and Honda (1974) have investigated what was then called by Pierson and Stacy (1973) the capillary range. Mitsuyasu and Honda questioned both the definition of the capillary range and the proposed spectral form of Pierson and Stacy (1973), pointing out that the waves were not truly capillary waves for the entire range of definition and that the simple dependence on the quantity, $D(u_*)$, with an unchanging spectral shape according to k^{-3} did not fit their data.

The purposes of this chapter are 1) to superpose a Stacy range onto the Pierson-Moskowitz and the Kitaigorodskii ranges of the previous study, 2) to replace the capillary range by the Mitsuyasu-Honda range, and, 3) to discuss briefly some of the implications of these changes.

THE RESULTS OF STACY

Figure 6.1, which is 3.1.1 of Stacy (1974) shows the results of Stacy with the portion of the gravity wave spectrum from about 0.2 hertz to 0.5 hertz plotted on linear scales for both the spectral value and the frequency. The spectra have been multiplied by the spectral band widths for each estimate so that the values on the vertical axis are in units of centimeters squared. To convert to spectral units of cm^2-sec the vertical scale should be multiplied by 102.4. The frequency is in units of one over seconds and does not contain radians. The data have been grouped so that a large number of spectra for the values of u_* as tabulated are included. The values of u_* that were used are 30, 47, 62, 80, 150, and 225. Such values correspond to an extreme range of wind speeds, and, in fact, the last value corresponds to hurricane wind conditions. The degrees of freedom for each of these spectra depended upon the number of spectra in the average that formed the grand total from which the curves were plotted. The number varied from 6 to 14. With the band width used, the net result was that the total degrees of freedom varied from 168 to 448. The confidence intervals, therefore, varied from 0.84 and 1.21 to 0.90 and 1.12. These confidence bands are quite narrow, and it is clear that the spectra do not overlap and that in this range the spectra for gravity waves grow with increasing u_*. The wavelength of the waves involved over this frequency range varies from approximately twenty-five meters to six meters. If the

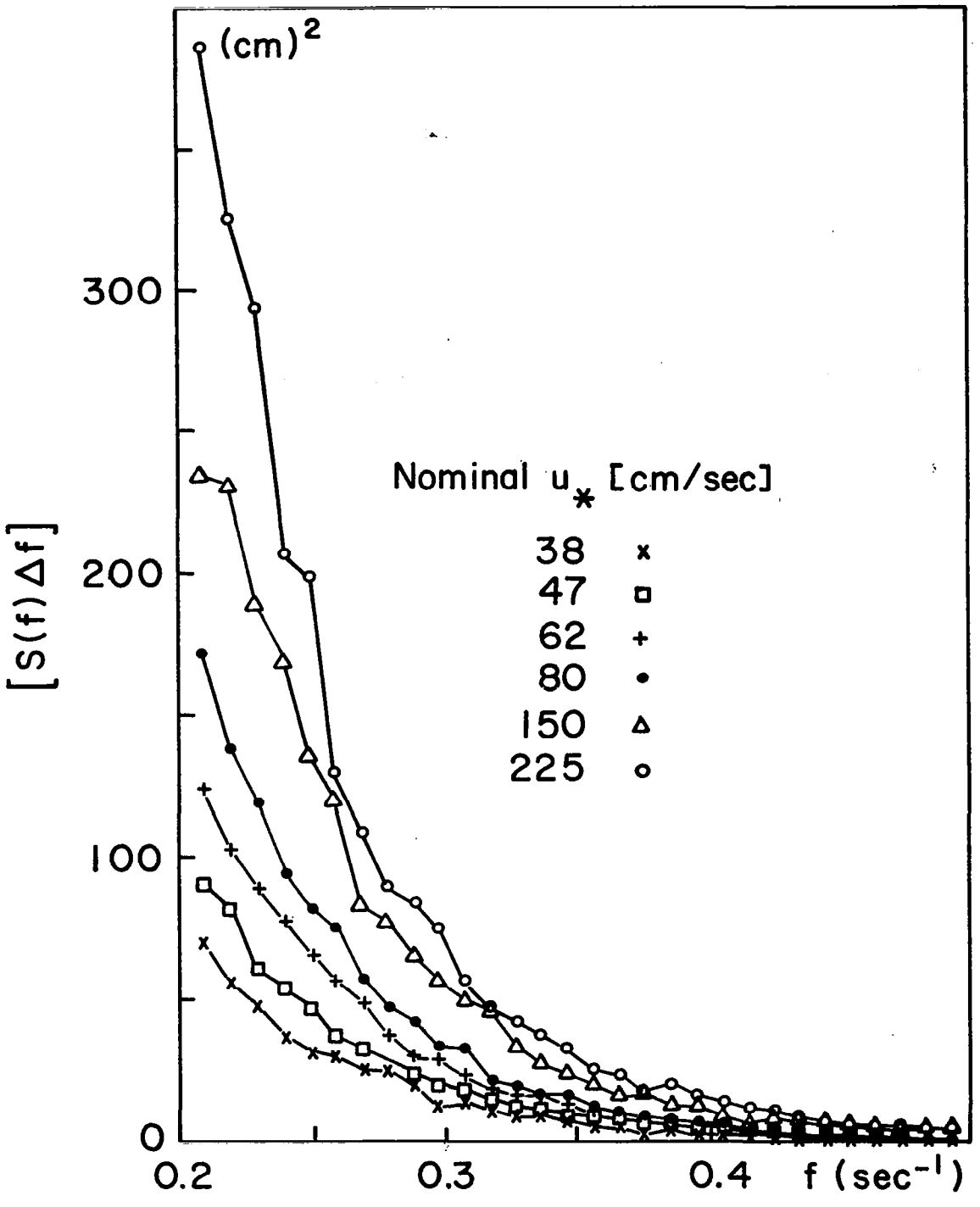

FIGURE 6.1 PORTION OF GRAVITY WAVE SPECTRUM IN TERMS OF $S(f)\Delta f$ VERSUS f FOR A WIDE RANGE OF U_* (FROM STACY (1974).

spectrum only existed in this range the variance for the higher winds yields a standard deviation of 30 cm corresponding to a significant height of 1.2 meters.

Figure 6.2, which is figure 3.1.2 from Stacy (1974) is another plot of the same data. The frequency scale is linear but now the spectral values are logarithmic. The Pierson-Moskowitz assymptotic form, given by

$$\alpha g^2 \omega^{-5}$$

is shown by the heavy line. Clearly the spectrum of the actual waves can be as much as five times higher in this range than the assymptotic Pierson-Moskowitz form predicts. Also the data suggest that for low values of u_* the spectrum can fall below this value. This particular feature will not be modelled in the equations to follow. For the higher end of this frequency range there is some concern that there may be recorder roll-off and that the spectra may be too low.

The other interesting feature of this figure is that in this plot the lines representing the spectra appear to be straight. This implies that the spectra behave like equation (6.1).

$$S(f) = C_1 (u_*) e^{-c_2 \omega} \tag{6.1}$$

such a representation will fall below any spectrum of the form

$$S(\omega) = C_3 (u_*) / \omega^n \tag{6.2}$$

where n could be 4 or 5 or 6 for both low enough and high enough frequencies.

Stacy (1974) fitted these data in two different ways. One was a power law with the exponent of the frequency given by six and a wind speed dependent coefficient, and, the other was with a damped exponential where the constant, with the frequency, f, instead of ω, nearly equal to 16.

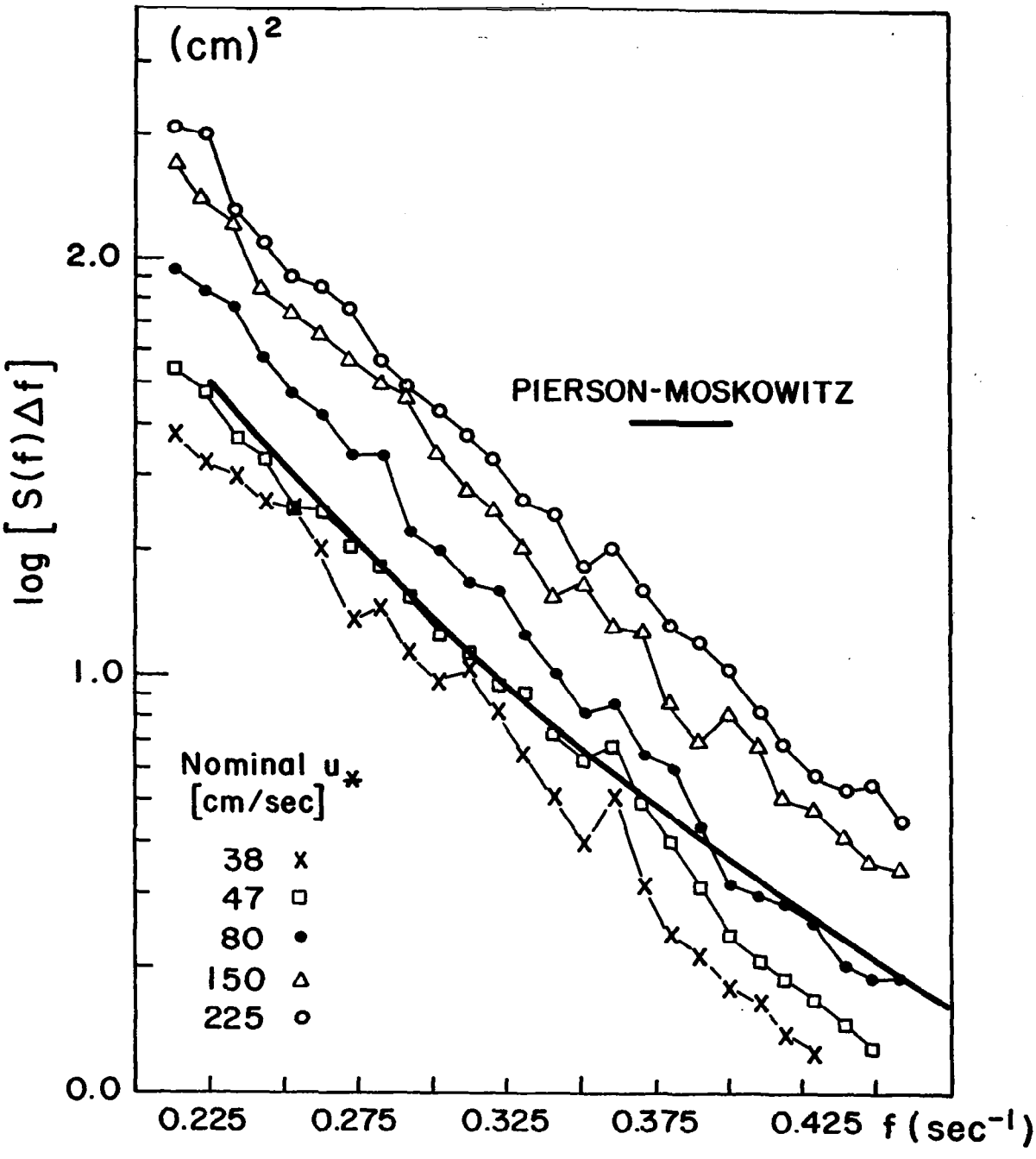

FIGURE 6.2 PORTION OF GRAVITY WAVE SPECTRUM ON LOG S(f)Δf VERSUS f SCALES (FROM STACY (1974))

The study by Stacy illustrates the problem of attempting to understand the spectrum of the waves over many orders of magnitude when only less than a power of ten in frequency range is available for analysis. If a -6 power law is used to fit the data, then its extrapolation to lower frequencies does not intersect the spectrum proposed by Pierson and Moskowitz, and its extrapolation to higher frequencies falls far below the values measured for the other ranges. It becomes, therefore, quite difficult to fit this new piece of information into the other formulas.

An exponential fit does, however, appear to yield useful results. The exponential fit used here is given by $S_s(\omega)$ as given by equation (6.3).

$$S_s(\omega) = (543 + 27.17U_*)\, e^{-2.53(\omega - 4\pi/10)} \qquad (6.3)$$

At $\omega = 4\pi/10$, the u_* dependent coefficient fits the left hand side of figure 6.1 quite well. For somewhat lower frequencies, it continues to increase, but does not go to infinity at $\omega = 0$, and for higher frequencies it decreases exponentially as a function of ω. The evaluation of this function shows that it lies over the Pierson-Moskowitz form for u_* greater than 35.8 and that it also lies over the Kitaigorodskii form for higher values of u_* as u_* is varied in the equations given by Pierson-Stacy (1973).

The Pierson-Moskowitz spectral form, $S_1(\omega)$, and the Kitaigorodskii spectral form, $S_2(\omega)$ have, therefore, been modified in such a way that if $S_s(\omega)$ exceeds either the Pierson-Moskowitz value or the Kitaigorodskii value it replaces them. After the peak in the spectrum, $S_1(k)$, $S_2(k)$ and $S_s(k)$ are to be evaluated for all wave numbers and which ever is larger

is to be used. Somewhere on the high wave number side of the Pierson-Moskowitz spectra, this new spectrum given by Stacy will curve off and lie above the Pierson-Moskowitz spectrum for u_* greater than 35.8.

For ever higher values of u_* in the Kitaigorodskii range, $S_s(k)$ will lie above these spectral values as one continues on past k_1 toward k_2 with $S_1(k)$, $S_2(k)$, $S_1(\omega)$, and $S_2(\omega)$ and k_1, k_2, ω_1 , ω_2 defined as in the previous paper. Eventually, however, the Stacy formulation will go below either of these formulations and at this particular wave number the curve should be continued according to either $S_1(k)$ or $S_2(k)$. Although this small correction may affect only a small range of wave numbers and frequencies, for that range it will fit the best available data as measured during extremely high winds and for a substantial range of friction velocity. Graphs will be given in a later section.

THE RESULTS OF MITSUYASU AND HONDA

Figure (6.3) shows the results of Mitsuyasu and Honda in the form of the frequency spectra for five different wind tunnel speeds plotted on a logarithmic scale versus frequency on a logarithmic scale. The important points about this figure are that, for frequencies ranging roughly from 10 to 30 hertz, the graphs of the different spectra are essentially straight lines, except for sampling variability, and that they fan out as if the straight lines originated at a point to the left with a given spectral value and frequency. For the range from 10 to 30 hertz the frequency spectra can be fitted by equation (6.4). Each straight line has a wind speed dependent power law given by the exponent p in the equation (6.5). One possible fit is that

$$S_4(\omega) = \frac{A}{2\pi}\left(\frac{2\pi f_*}{\omega}\right)^P \qquad (6.4)$$

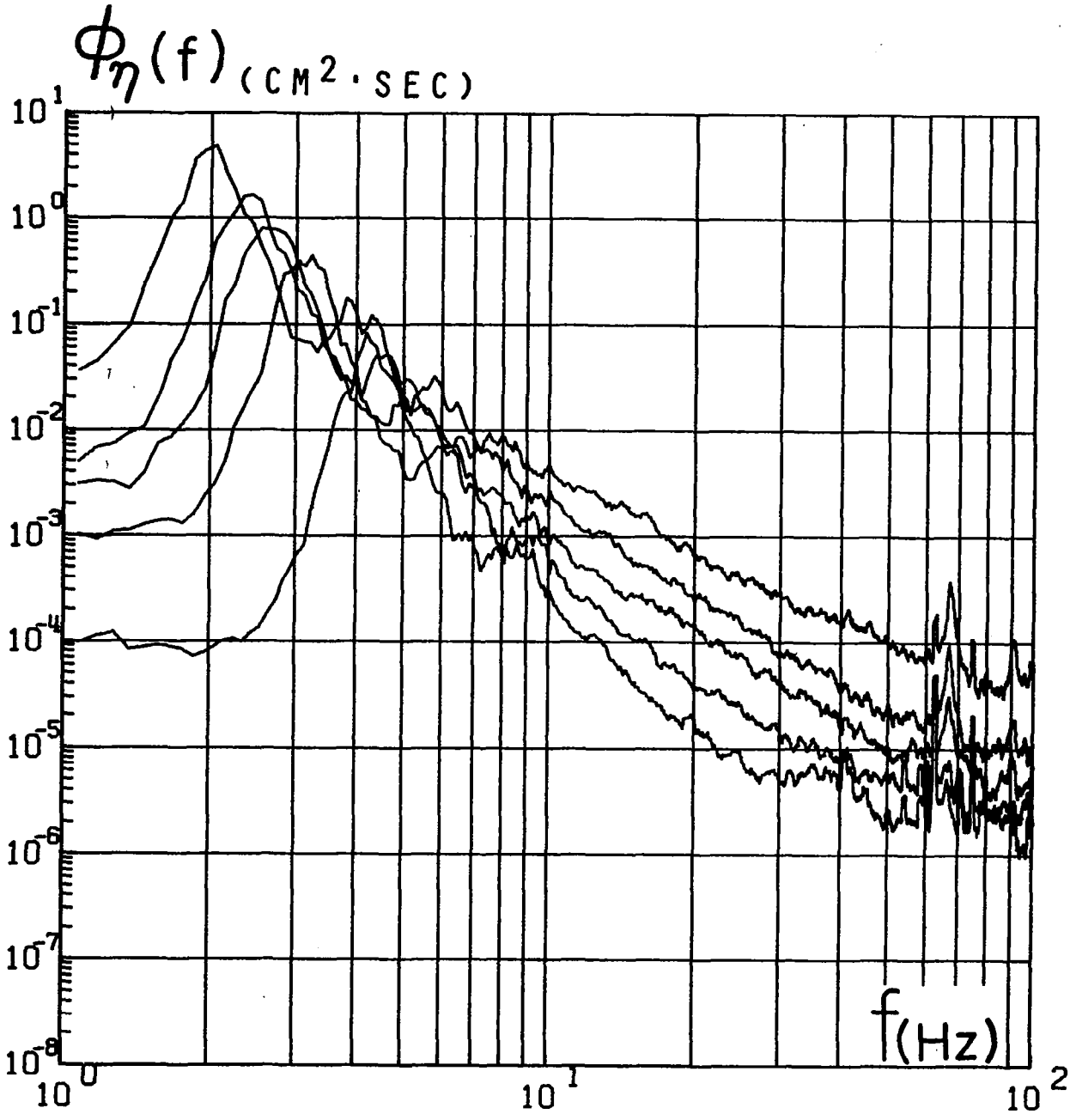

FIGURE 6.3 THE SPECTRA OF MITSUYASU AND HONDA (1974) FOR THE FREQUENCY RANGE FROM 0.5 TO 30 Hz

and that

$$P \cong 5 - \log_{10} u_* \tag{6.5}$$

The fit could perhaps also be

$$P \cong 5.22 - 1.1 \log_{10} u_* \tag{6.6}$$

It is proposed to investigate the sensitivity of the fit to these curves to the prediction of radar sea return in later studies. No matter what particular set of parameters is chosen to fit these data, it is clear, simply from this one graph from Mitsuyasu and Honda, that the spectrum of the waves in this frequency range grows more for the same increase in wind speed at say 30 hertz than it does at 10 hertz. Since the frequencies transform monotonically to wave number and since high frequencies correspond to high wave numbers, this implies that shorter wavelength radars at higher nadir angles should yield more sensitive response for radar backscatter to wind speed. This is indeed the case and will be demonstrated in other studies.

The Mitsuyasu-Honda range as defined by equation (6.4) can be mapped into the wave number spectrum by means of the relationship between wave number and frequency for waves controlled by both surface tension and gravity. The result is equation (6.7).

$$S_4(k) = 0.875\ (2\pi)^{p-1} \frac{(1 + 3\tau k^2/g\rho)}{g^{\frac{p-1}{2}}\ (k + \tau k^3/g\rho)^{\frac{p+1}{2}}} \tag{6.7}$$

where

$$\frac{g\rho}{\tau} = (3.63)^2 \tag{6.8}$$

and τ is the surface tension.

There remains the problem of connecting the Kitaigorodskii range which ends at k_2 to the Mitsuyasu-Honda range which begins at k_3. This is accomplished by exactly the same technique as the one used by Pierson and Stacy. In wave number space, the value for $S_2(k)$ at k_2 is connected to the value of $S_4(k)$ at $k = k_3$ by a straight line on a double log plot.

THE REVISED EQUATIONS

The equations that define these various ranges are given below for elevation spectra, slope spectra, curvature spectra, and frequency spectra. The various constants and parameters are given near each of the defining equations. In general, there will be six segments for each spectrum, as defined in the introduction, starting from the Pierson-Moskowitz range and going from there to the Stacy range, the Kitaigorodskii range, Leykin-Rosenberg range, the Mitsuyasu-Honda range, and the Cox viscous cutoff range.

Wave Number Elevation Spectra

$$S_1(k) = \frac{\alpha}{2k^3}\, e^{-Bk^{-2}} \tag{6.9}$$

where $B = \frac{\beta g^2}{U^4}$ and $U = U_{19.5}\,(u_*)$ for $o < k < \left(\frac{2\beta}{3}\right)^{\frac{1}{2}} \frac{g}{U^2}$

$$S_1^*(k) = \max \begin{cases} S_1(k) \\ S_s(k) \end{cases} \tag{6.10}$$

where $S_s(k) = (271.5 + 13.58u_*)\, e^{\frac{2.53(4\pi)}{10}} \frac{g^{\frac{1}{2}} e^{-2.53 g^{\frac{1}{2}} k^{\frac{1}{2}}}}{k^{\frac{1}{2}}}$
for $u_* \geq 35.8$

for $\left(\frac{2\beta}{3}\right)^{\frac{1}{2}} \frac{g}{U^2} < k < k_1 = \frac{k_2 u_{*m}^2}{u_*^2}$

$$S_2^*(k) = \max \begin{cases} S_s(k) \\ S_2(k) \end{cases}, \text{ if } u_* \geq 75.76, \text{ and } S_2^*(k) = S_2(k) \text{ if } u_* < 75.76 \tag{6.11}$$

where $S_2(k) = \frac{\alpha}{2k_1^{\frac{1}{2}}\, k^{5/2}}$ for $k_1 < k < k_2$

$$S_3(k) = S_4(k_3) \left(\frac{k}{k_3}\right)^q \tag{6.12}$$

where $q = \frac{\log_{10}\left[S_2(k_2)/S_4(k_3)\right]}{\log_{10}(k_2/k_3)}$ for $k_2 < k < k_3$

$$S_4(k) = 0.875\, (2\pi)^{p-1}\, \frac{(1 + 3\tau k^2/g\rho)}{g}^{\frac{p+1}{2}} \tag{6.13}$$
$$(k + \tau k^3/g\rho)$$

where $\frac{g\rho}{\tau} = (3.63)^2$ and $p \cong 5 - \log_{10} u_*$ for $k_3 < k < k_\nu$

$$S_5(k) = 1.473 \times 10^{-4} \frac{u_*^3 k_m^6}{k^9} \qquad (6.14)$$

where $k > k_\nu$ at point where $S_5(k)$ intersects $S_4(k)$

Also $\alpha = 8.1 \times 10^{-3}$, $\beta = 0.74$, $k_2 = k(6\pi) = 0.359$, $k_3 = 0.942 = k(10\pi)$, $k_m = (g\rho/\tau)^{\frac{1}{2}} = 3.63$ and $u_{*m} = 12$.

The notation $\max \begin{Bmatrix} S_1(k) \\ S_s(k) \end{Bmatrix}$ means that both spectra are to be evaluated and whichever of the two is greater is used at that value of k. $k = \left(\frac{2\beta}{3}\right)^{\frac{1}{2}} \frac{g}{U^2}$ is the maximum in wave number space of the Pierson-Moskowitz spectrum $S_s(k)$ will intersect $S_1(k)$ to the left of the maximum and the notation insures that this condition will be excluded.

Slope Spectra and Curvature Spectra

$$\text{If} \quad S(k) = \begin{cases} S_1(k); & o < k < \left(\frac{2\beta}{3}\right)^{\frac{1}{2}} g/U^2 \\ S_1^*(k); & \left(\frac{2\beta}{3}\right)^{\frac{1}{2}} g/U^2 < k < k_1 \\ S_2^*(k); & k_1 < k < k_2 \\ S_3(k); & k_2 < k < k_3 \\ S_4(k); & k_3 < k < k_\nu \\ S_5(k); & k_\nu < k < \infty \end{cases} \qquad (6.15)$$

then the slope spectra are

$$S_{slope}(k) = k^2 S(k) \tag{6.16}$$

and the curvature spectra are

$$S_{curv}(k) = k^4 S(k) \tag{6.17}$$

Frequency Spectra

$$S_1(\omega) = \frac{\alpha g^2}{\omega^5} e^{-\beta(\omega_o/\omega)^4} \tag{6.18}$$

where $\omega_o = g/U$ for $o < \omega < \omega_{max}$ and where ω_{max} = maximum of $S_1(\omega)$.

$$S_1^*(\omega) = \max \begin{cases} S_1(\omega) \\ S_s(\omega) \end{cases} \text{ if } u_* > 35.8, S_1^*(\omega) = S_1(\omega) \text{ if } u_* < 35.8 \tag{6.19}$$

where $S_s(\omega) = (543 + 27.17U_*)\, e^{-2.53(\omega - 4\pi/10)}$ for $\omega_{max} < \omega < \omega_1$,

$$\omega_1 = \sqrt{gk_1} = \frac{u_{*m}}{u_*}\sqrt{gk_2} = \frac{u_{*m}}{u_*} 6\pi$$

$$S_2^*(\omega) = \max \begin{cases} S_s(\omega) \\ S_2(\omega) \end{cases}, \text{ if } u_* > 75.76, \; S_2^*(\omega) = S_2(\omega), \text{ if } u_* < 75.76 \tag{6.20}$$

where $S_2(\omega) = \dfrac{\alpha u_* g^2}{u_{*m}\sqrt{gk_2}\,\omega^4} = \dfrac{\alpha u_* g^2}{u_{*m} 6\pi \omega^4}$ for $\omega_1 < \omega < 6\pi$

$$S_3(\omega) = \frac{S_4(k_3)}{k_3^q} \left(k(\omega)\right)^q \frac{dk(\omega)}{d\omega} \tag{6.21}$$

for $6\pi < \omega < 10\pi$, where $k = k(\omega) = 3\omega^2 / gF(\omega/\omega_m)$,

and $F(\omega/\omega_m) = 1 + \left[1 + B(\omega) + \left(B(\omega)\,(2 + B(\omega)\right)^{\frac{1}{2}}\right]^{\frac{1}{3}}$

$$+ \left[1 + B(\omega) - \left(B(\omega)\,(2 + B(\omega)\right)^{\frac{1}{2}}\right]^{\frac{1}{3}} \text{ and where } B(\omega) = 54(\omega/\omega_m)^4$$

$$S_4(\omega) = \frac{A}{2\pi}\left(\frac{2\pi f_o}{\omega}\right)^P \qquad (6.22)$$

for $10\pi < \omega < \omega_\nu$, where $f_o = 1$, $A = 0.875$, and $P \cong 5 - \log_{10} u_*$

$$S_5(\omega) = 1.473 \times 10^{-4}\, u_*^3 k_m^6 \left(\frac{I}{\rho}\right)^{8/3} \frac{2}{3}\,\frac{1}{\omega^{19/3}} \qquad (6.23)$$

for $\omega_\nu < \omega < \infty$

Discussion

The frequency spectra obtained by Mitsuyasu and Honda show that the waves grow with increasing wind speed in the frequency range from 10 to 30 hertz. The plots also show that the growth is not a simple one and that the wave number spectra cannot be represented in the form of a wind speed dependent coefficient times k^{-3}. A simple inspection of this figure shows that no elementary transformation, say of the form $f' = fu_*/g$ will cause these five different curves to coincide. Were it not for the extreme sampling variability in the data studied by Pierson and Stacy (1973), these same features might have been obtained in that study. Figure (6.4) from Pierson and Stacy, (their figure 5.1), clearly shows, since hindsight is better than foresight, that the transformation used in order to demonstrate a k^{-3} behavior actually shows that the function decreases with increasing k for low values of u_* and increases with increasing k for high values of u_*. They would, in fact, be slightly curved because the transformation of frequency to wave number is very complicated in this range.

The main point of this revision and of the two papers that have been used for the revision, is however, that if scientists look for wind speed dependent variations in the spectra of short waves on the sea surface they will be found. It is important for further studies to be made, so that the full range of frequencies and wave numbers can be documented with data from newer and better designed instruments so that both the Kitaigorodskii range and the Leykin-Rosenberg range can be corrected, if needed, or verified by better data. It is becoming increasingly clear that a fuller understanding of radar backscatter depends upon knowing something about the spectrum of the waves for all frequencies and wavelengths.

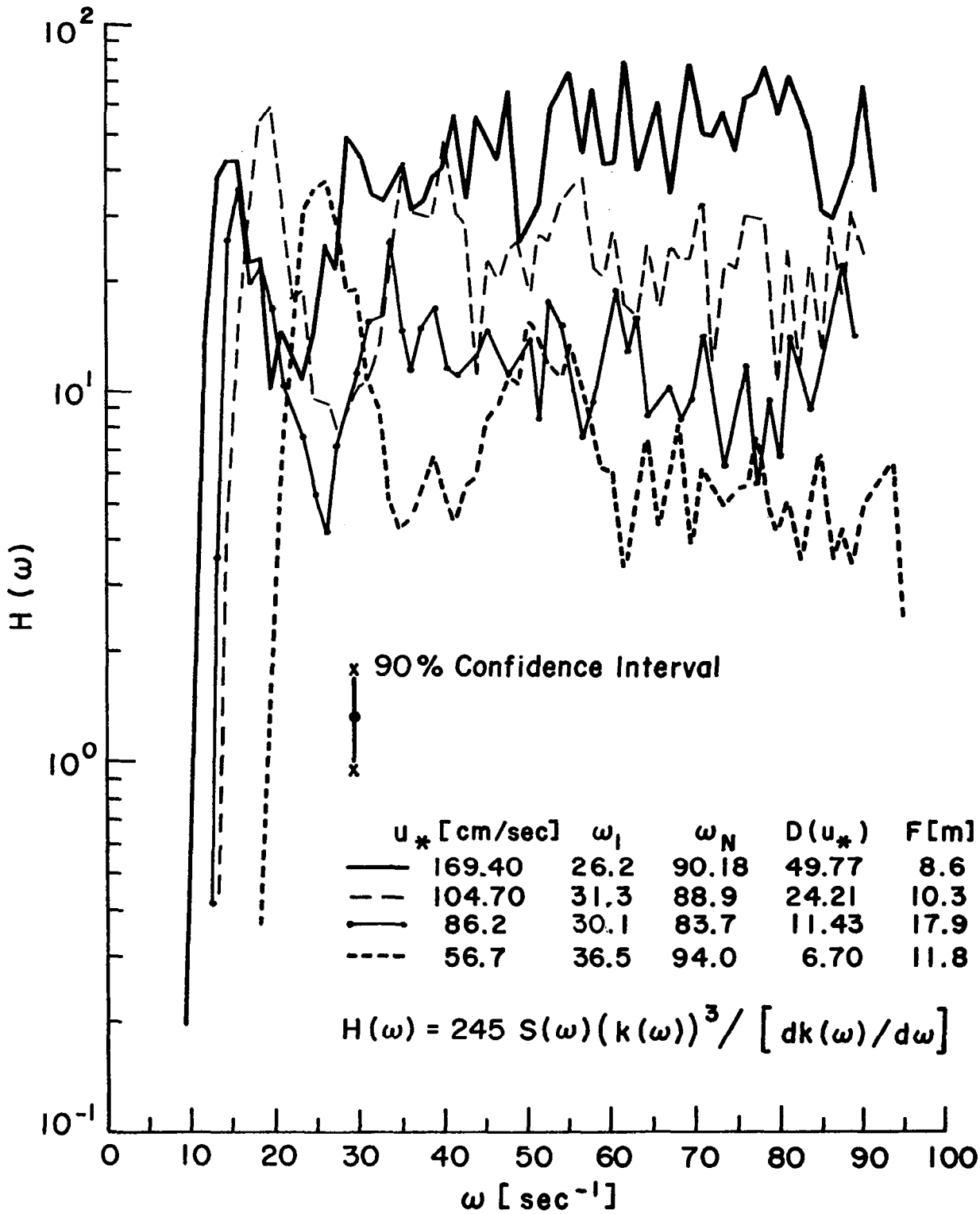

FIGURE 6.4 H(ω) VERSUS ω FROM PIERSON AND STACY (1973)

Spectral Graphs and Their Interpretation

Figures 6.5 through 6.9 are new, and hopefully better, versions of figures 8.2, 8.4, 8.5, 8.6 and 8.7 of Pierson and Stacy (1973). The changes brought about by using the new results of Stacy (1974) and Mitsuyasu and Honda (1974) are substantial.

Figure 6.5 shows wave number spectra on a double log plot for values of u_* of 192, 96, 48, 24, and 12 cm/sec corresponding to winds at 19.5 meters in excess of 30 m/s, and equal to 20.7 m/s, 12.31 m/s, 7.38 m/s and 3.46 m/s. The wave numbers range over more than 6 orders of magnitude and the spectral values range over nearly 16 orders of magnitude. The Stacy range shows up for $u_* = 48$ and higher as a curved bump for wave numbers near 3×10^{-3}. Much of the Phillips equilibrium range is obliterated by it and the Kitaigorodskii range, although it exists both above and below the Stacy range for u_* between 35.8 and 75.76, corresponding to $U_{19.5}$ values of 9.93 m/s and 17.3 m/s.

For $k > 0.94$, the start of the Mitsuyasu-Honda range, the spectra are curved instead of straight and they spread further apart with increasing wave number. When better data are obtained over this wide range of wave numbers, it is quite likely that some of the jiggles and bumps connecting these various segments will be eliminated.

Figure 6.6 shows a slope spectrum on a log-linear plot for a modesl range of wind speeds. This figure has changed remarkably compared to the one given previously in a way that leads one to believe that it is more nearly correct at high wave numbers since nature does not like graphs with square corners.

The Stacy range shows up as a small bump near $k = 3 \times 10^{-3}$ for $u_* = 42$ and 48. It would become much larger for higher winds.

The Mitsuyasu-Honda range merges smoothly into the cox viscous cutoff range and for low winds even into the Leykin Rosenberg and Kitaigorodskii ranges. Moreover, the curves are no longer flat topped as before. The transformation of equation 6.4 to wave number space has produced a smooth well rounded peak in the middle of the range.

The curvature spectra as given in figures 6.7 and 6.8 show again that curvature is determined by wave numbers from 1 to about 30 as before. The shape of the first half of each curve in figure 6.8 shows that the transformation from frequency to wave number is still strong enough to turn the curve over without viscous effects.

In frequency space, on a double log plot, the results are as would be expected given figure 6.5. The Mitsuyasu-Honda range can clearly be seen to fan out with increasing frequency.

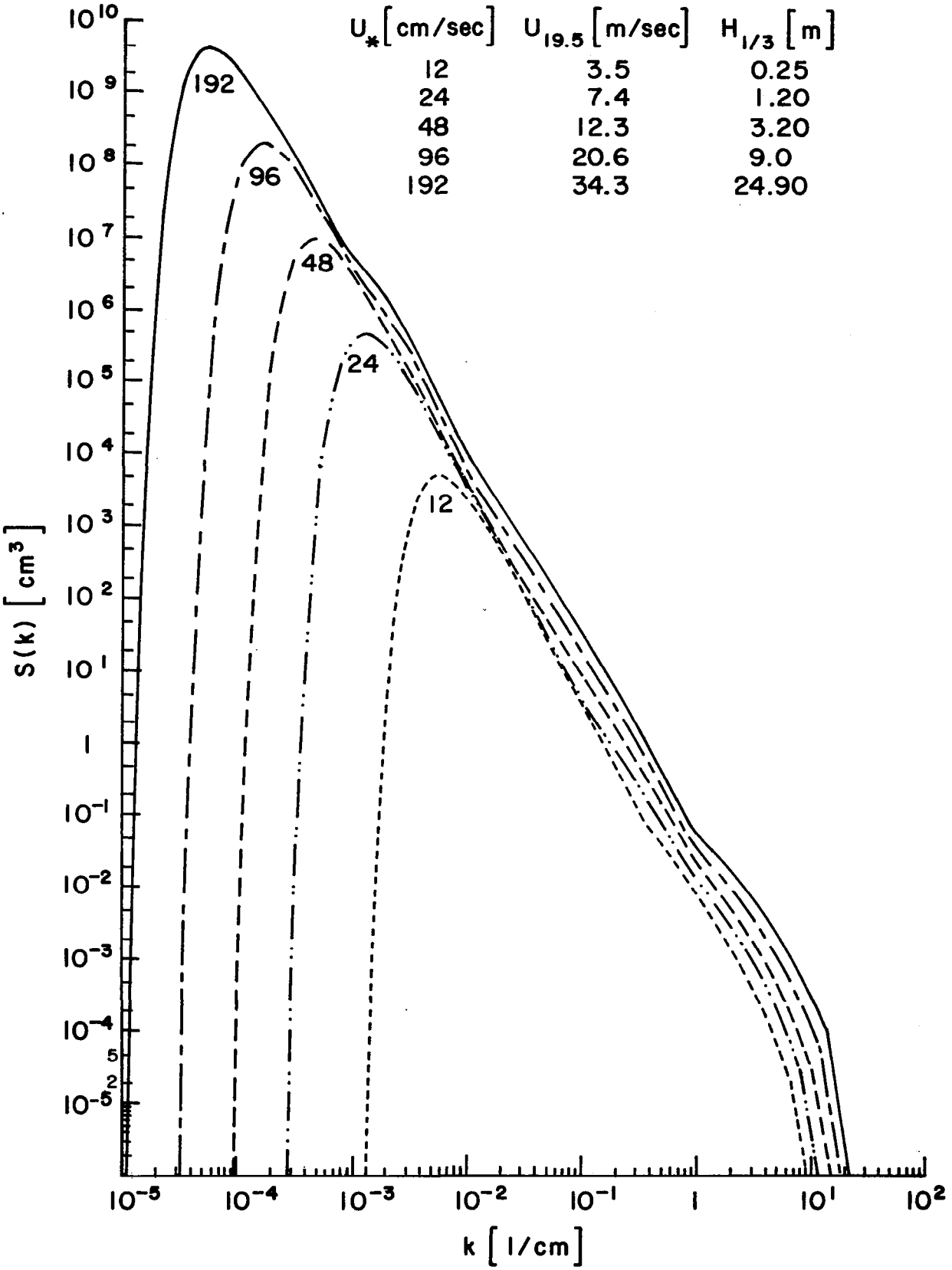

FIGURE 6.5 S(k) versus k with both scales logarithmic for an extreme range of winds.

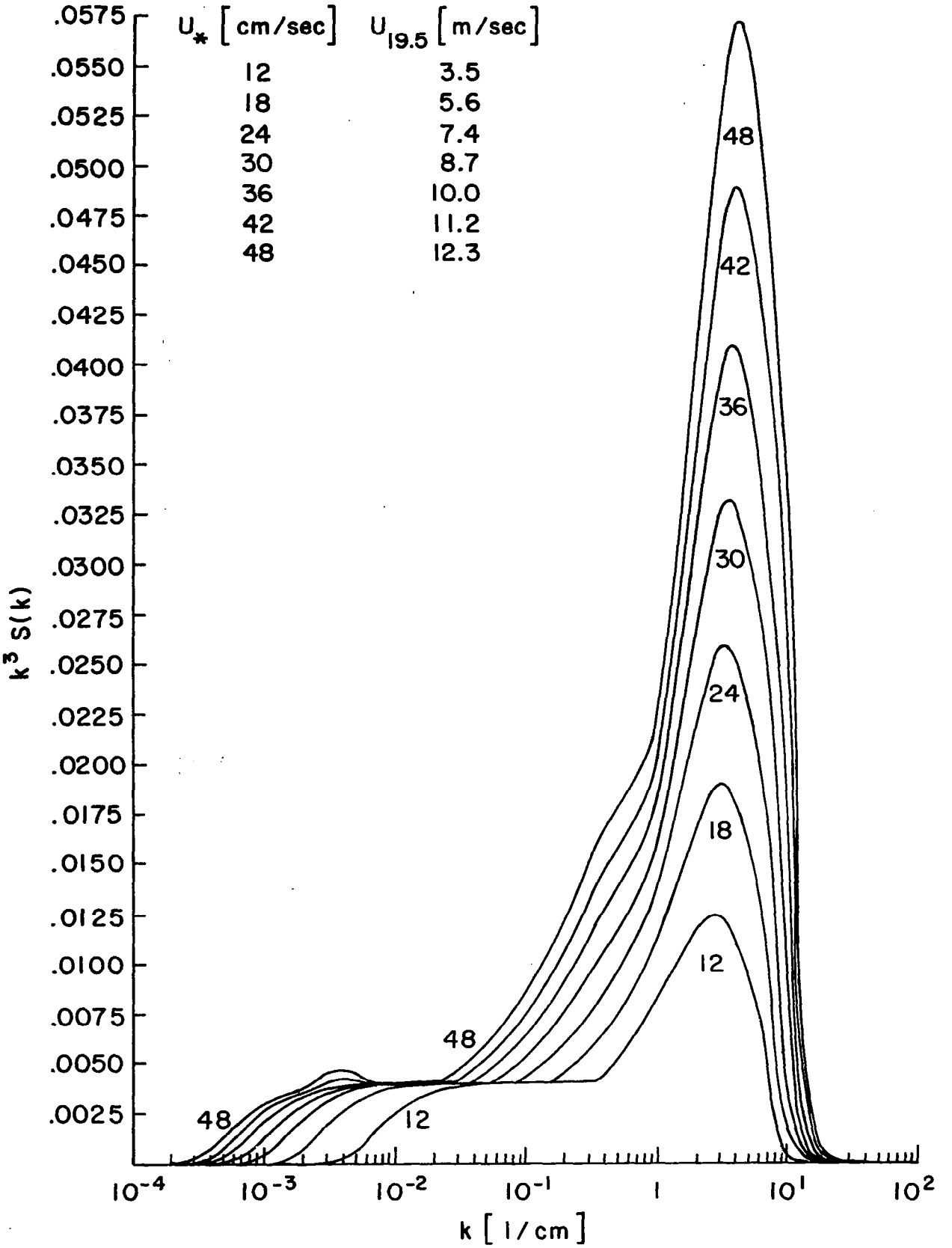

FIGURE 6.6 $k^3S(k)$ versus log k for wind speeds up to 12.3 m/s. The graphs are area preserving.

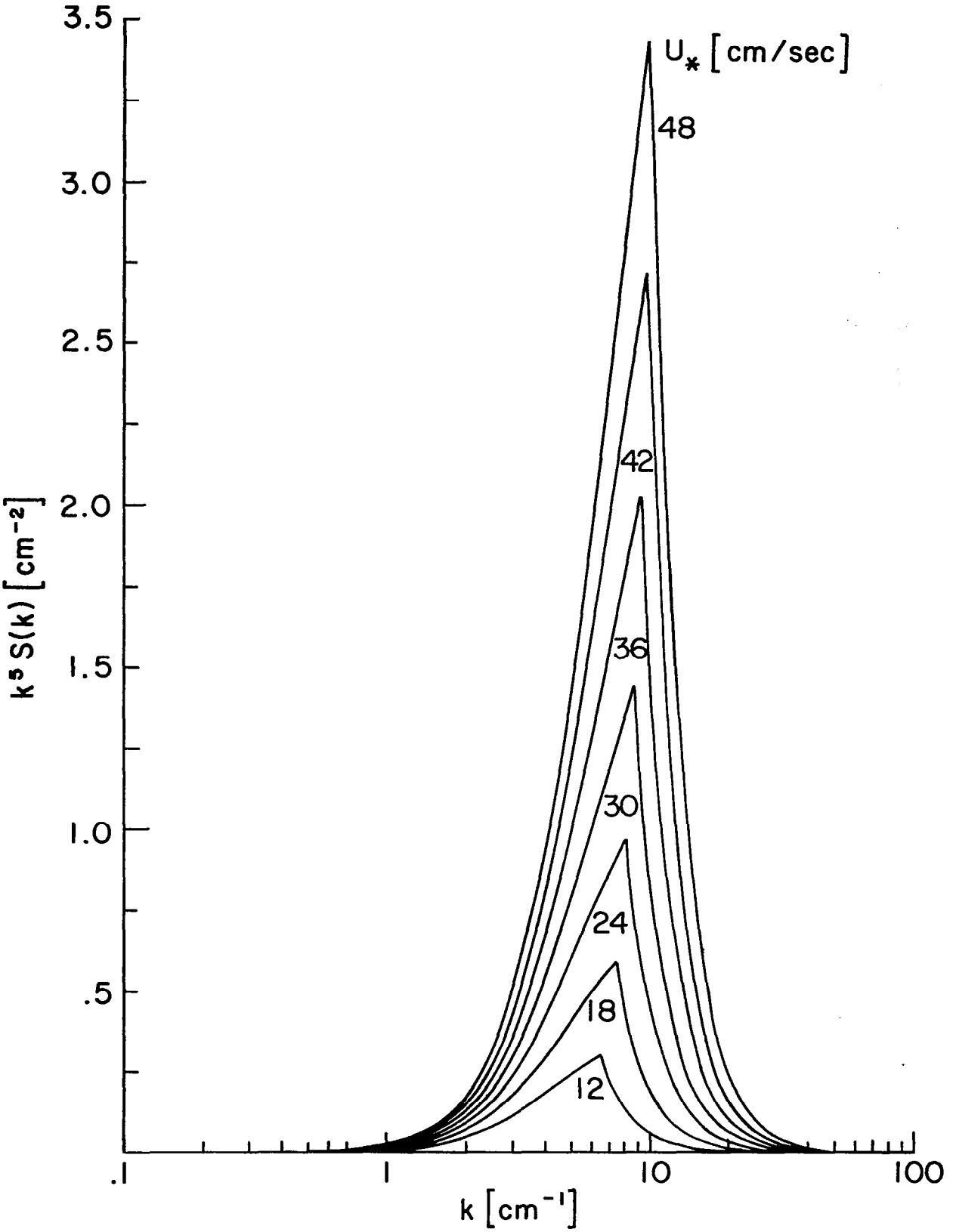

FIGURE 6.7 $k^5 S(k)$ versus log k for wind speeds up to 12.3 m/s. The graphs are area preserving.

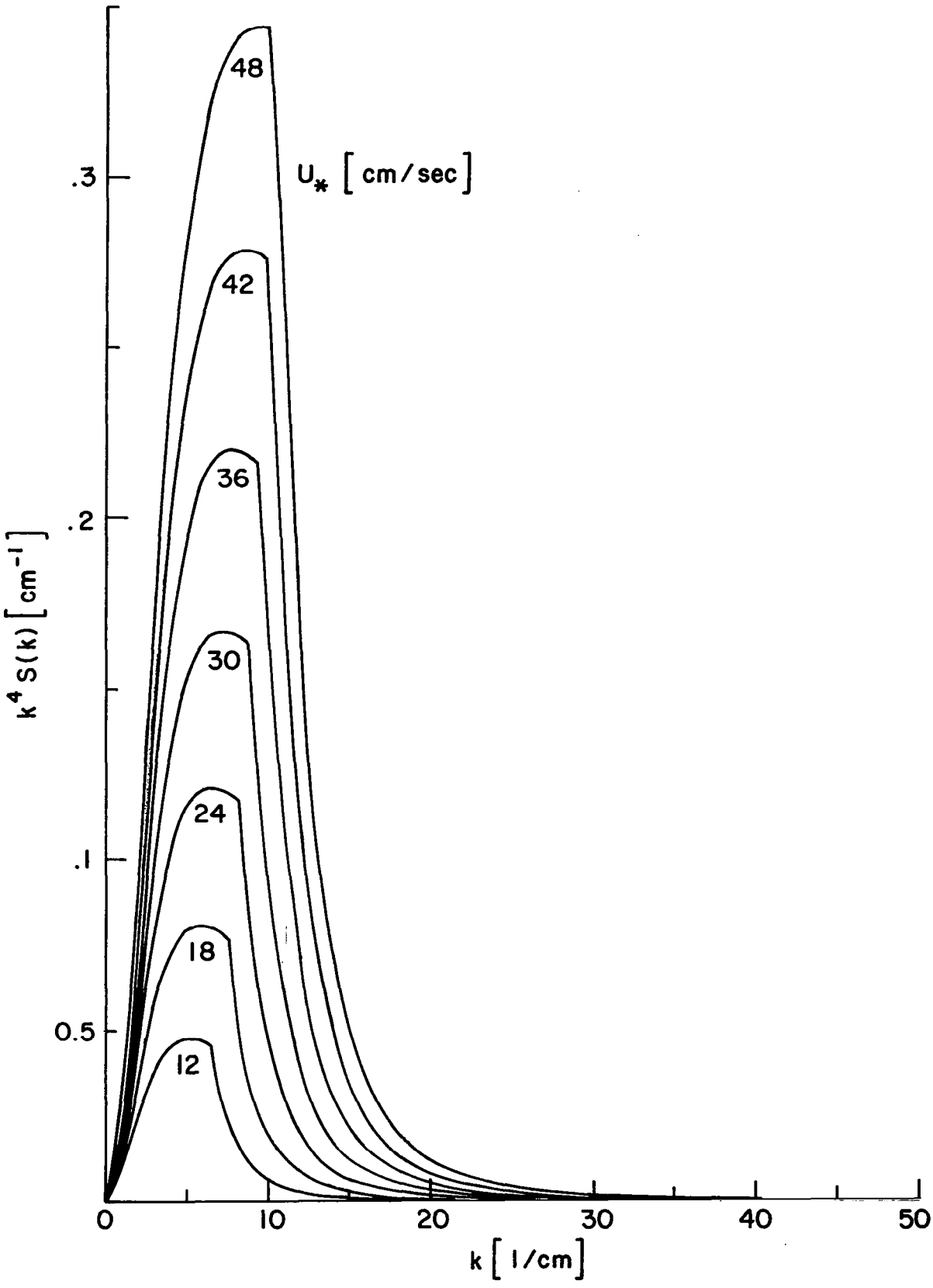

FIGURE 6.8 $k^4S(k)$ versus k. The graphs area preserving.

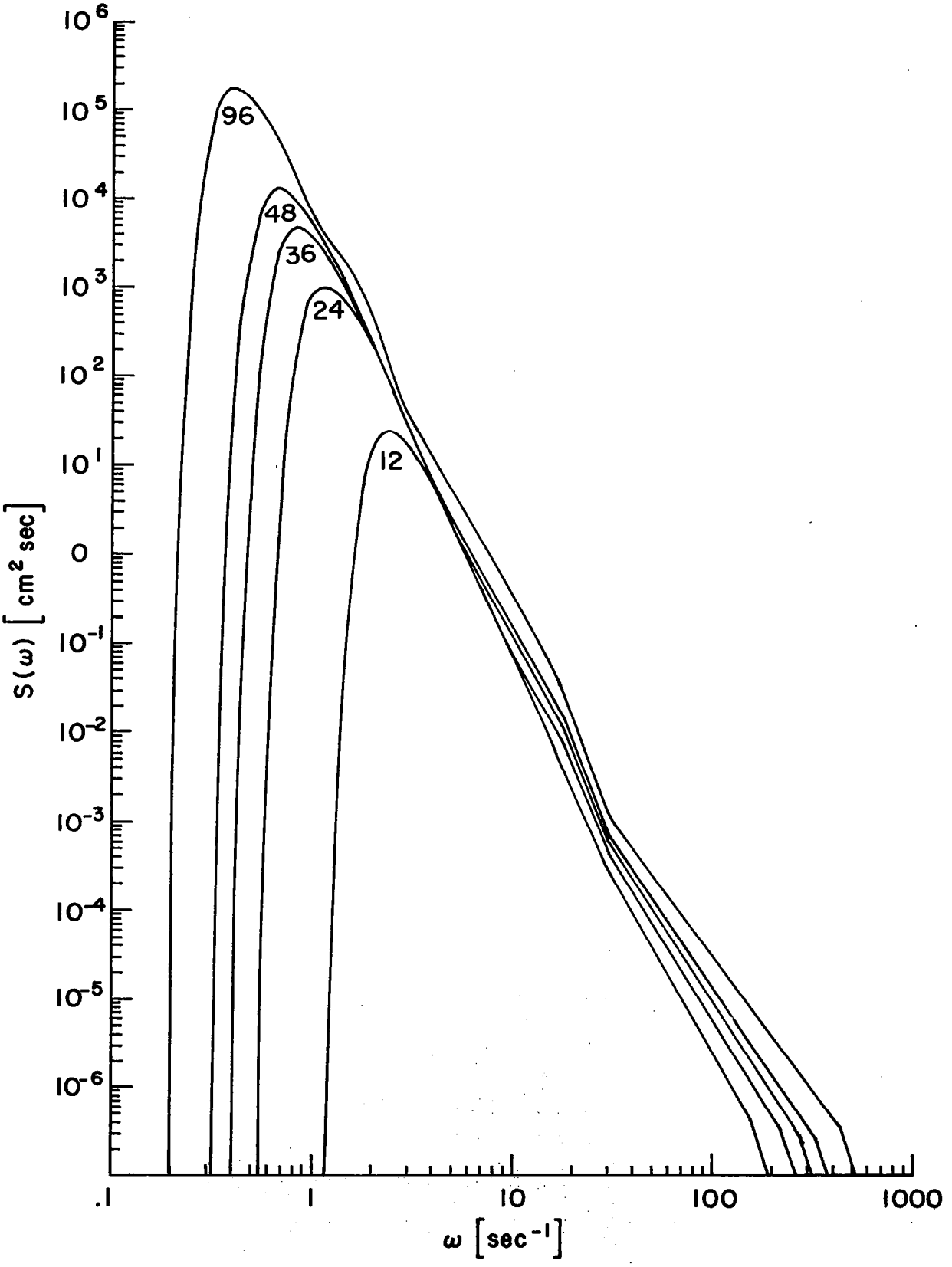

FIGURE 6.9 $S(\omega)$ versus ω on logarithmic scales.

CHAPTER 7 SCIENTIFIC APPLICATIONS OF WAVE DATA OBTAINED FROM SPACECRAFT

General Remarks

Spacecraft such as GEOS-3 and SEASAT-A will initiate a new era in the study of waves on the oceans. Measurements by S193 on SKYLAB have proved the feasibility of measuring the winds over the ocean and of measuring wave height on a global scale. The improved knowledge of the winds as shown by Pierson, Cardone and Greenwood (1974) will permit better wind and, hence, wave forecasts. GEOS-3 will be able to gather routine data on wave heights globally after further preliminary operational testing. Several authors such as Stewart, Teleki, and Pierson have written about the scientific and operational benefits and uses of wave measurements from spacecraft as given in a NASA report by Apel and Siry (1974). The great potential of radar altimeter measurements of wave heights is that uniform, global, unbiased coverage of wave height measurements on a routine basis that will be independent of clouds and the location of present shipping lanes will be obtained. The data base will be much greater than that currently available from conventional sources, and it will be free from the coding bias of conventional ship reports and other kinds of error sources.

If an operational wave imaging system can be developed, the data base will suddenly be increased by potentially two orders of magnitude compared to simple wave height measurements. Systematically obtained vector wave number spectra over deep water and information on wave refraction patterns in shallow water will be available.

In this section, the scientific application of wave height measurements with a radar altimeter and the potential scientific applications of wave imagery, either obtained by means of a radar or from properly obtained photographs will be discussed. The wave height measurements are already feasible. The imagery may be feasible by 1978 with the systems possible for SEASAT-A.

SCIENTIFIC APPLICATIONS OF WAVE HEIGHT DATA FROM A RADAR ALTIMETER ON A SPACECRAFT

Presently Routinely Obtained Wave Height Data.

The most useful single number from a wave forecast is the so-called significant wave height, which equals four times the square root of the variance as the integral of either the frequency spectrum or the vector wave number spectrum, as described in Chapter 2. The presently operational wave recording systems as described in Chapter 3 yield a measure of the significant wave height along with information on the frequency spectra of the waves.

In the North Sea, the wave rider buoy has been employed at selected sites. Various companies have installed such buoys to document the wave conditions for environmental studies mandated by EPA as a part of their environmental impact documentation for the installation of various coastal and offshore structures, and others have installed them in the Gulf of Alaska for oil drilling platform data.

The Tucker Shipborne Wave Recorder has been installed and operated on weather ships for many years. Data are available for weather ships I, J, K, M, and P. This device has also been used extensively in the North Sea and off the coast of South Africa. The various reports cited in the description of this instrument, plus others in the bibliography,

contain spectral wave data and information on stratified samples, and scientifically selected samples of wave data obtained with this instrument.

The experimental buoys of the National Data Buoy Service described in Chapter 3 have just acquired the capability of routinely producing wave spectra and measurements of the significant wave height. Data are available on a routine basis from the Gulf of Alaska and off the east coast of the United States. Other sites are planned for the near future. Several wave gages mounted on offshore oil drilling towers may still be operational to obtain wave data during hurricanes in the Gulf of Mexico. In other parts of the world there are undoubtedly a variety of wave buoys and scientific installations, particularly around Japan, where waves are recorded on a routine operational basis for the purpose of scientific study. The total number of such records is not extremely great and their location is not uniform.

Extreme Waves

An important design parameter for many applications, such as the construction of an offshore oil drilling tower, or any platform on the continental shelf, or the design of a ship, or of any vehicle to operate on the ocean surface, or of any device to be towed across the ocean, is the extreme wave. The question always arises as to what the highest wave is that will be encountered by such a structure during its life time. It takes a long time to collect the data that adequately describes the extreme waves to be expected in a given location over the course of 20 or 100 years. Typically, various types of extreme value theories are applied to the available data and these theories are extrapolated to the extreme wave condition for design purposes. The exact procedures for doing this are the subject of considerable controversey among the various scientists who are involved with this kind of problem.

Since the development and routine use of the Tucker Shipborne Wave Recorder, a large volume of wave records have been assembled. From these wave records the ten highest wave records showing the highest waves for a twenty minute recording interval has been assembled and analyzed. The highest waves ever recorded by this system, up to until a few years ago, were such that the significant wave height was 55 feet and therefore one wave in a hundred would have been approximately 80 feet from crest to trough. In the North Pacific, FLIP recorded a single wave over 80 feet from crest to trough during conditions that were not particularly extreme as far as the wind speed at the site of the measurement. There must have been much higher waves to the northwest of FLIP prior to the time that this particular measurement was made. This material is reported in a paper by Rudnick and Hasse (1971).

There is some literature available on the theory of extreme wave heights. This problem is a most difficult one to solve theoretically. It would be very helpful if the radar altimeter data that can be obtained were used to yield information on the highest waves near the centers of the intense storms that occur over the world's oceans. A data base consisting of accurate estimates of the significant wave heights in an intense storm that would be independent of having that storm peak and produce maximum waves at just a few fixed recording sites would augment the data needed for these problems very rapidly by substantial amounts. It is clear on the basis on the data that are available that increasing the number of measurements over the ocean would very rapidly increase information on how high waves actually get in intense storms.

The proper understanding of extreme waves in storms at sea will probably come from a combination of probablistic concepts and physical concepts on the nature of the waves. The highest wave to pass a given point, or to occur in a given area during a storm, will probably occur

when the significant wave height, as estimated over a twenty or thirty minute interval, is a maximum and this highest wave will occur sometime during this twenty or thirty minute time interval. The height of this highest wave will probably be controlled by several considerations. Although the random reinforcement of the various spectral components in the particular seaway in which it was generated could have produced an even higher wave, waves greater than a certain height would have broken in the form of plunging breakers and not have reached the height predicted by a strict application of extreme value theory. This particular effect is evident, for example, in the data obtained on an experimental basis in a wave tank as given by Abkowitz (1974). The problem, however, has a long way to go before an adequate solution is obtained.

Figures 7.1 and 7.2 from Cardone, Pierson and Ward (1975) show the results of an effort to specify the highest waves to pass oil drilling structures in the Gulf of Mexico during hurricanes. Figure 7.1 shows the "hindcast" and observed values of the highest single wave, crest to trough, and the significant wave heights to occur at six platforms during the passage of hurricane Camille in 1969. The highest measured wave was 72 feet; the "hindcast" gave 76 feet.

The wave conditions during Hurricane Camille were described by Earle (1975). Graphs of the average wave height, the significant wave height, and the highest single wave every half hour are given along with some information on the spectrum.

Figure 7.2 shows other "hindcasts" and various kinds of verification of the maximum single wave at a structure. The peak conditions in a hurricane do not last very long and so the use of extreme value theory for a fairly low number of waves seems to have given fairly good results. Had peak significant wave heights lasted for many days, it is quite possible that extreme value theory might not have given as good results.

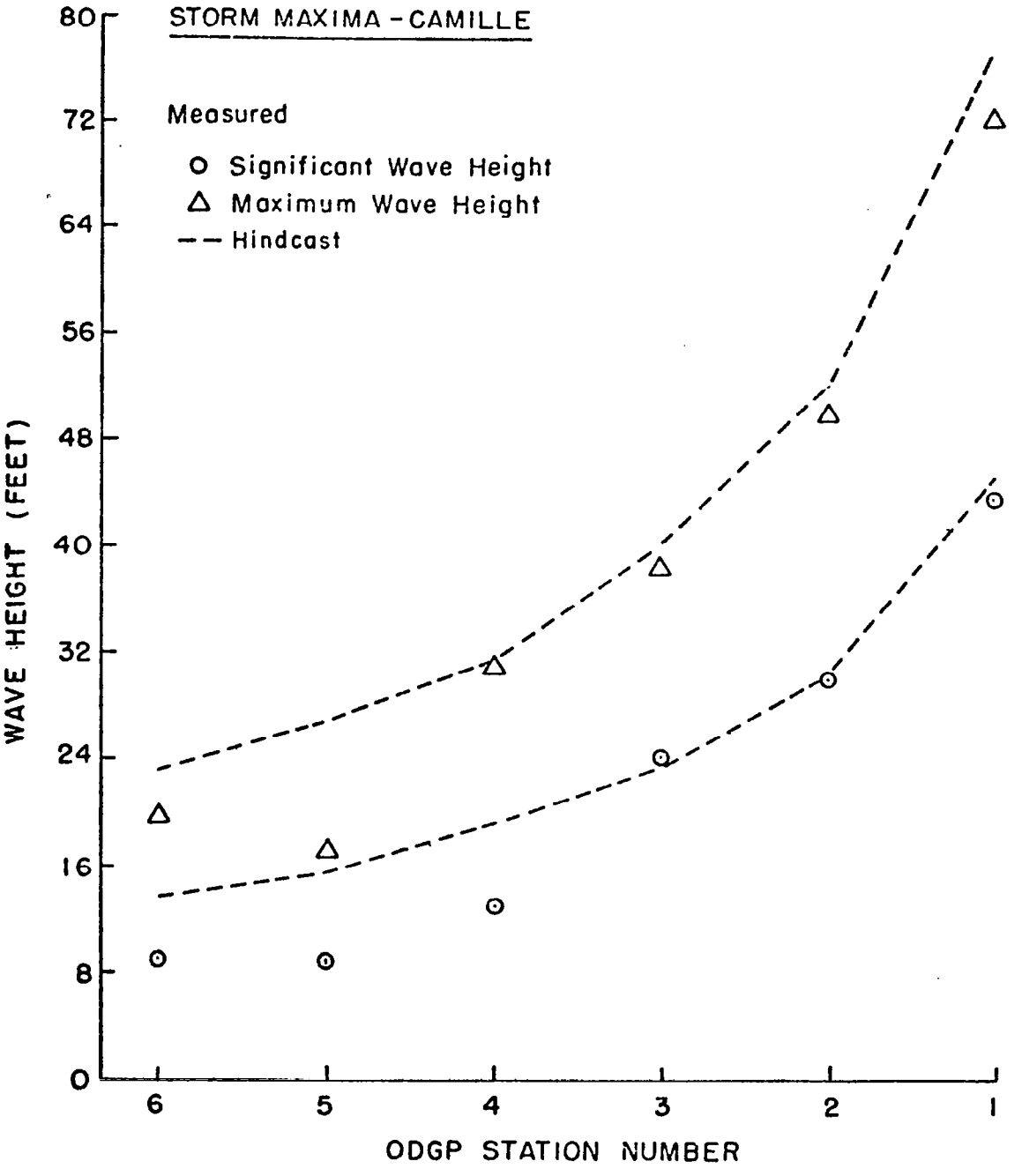

FIGURE 7.1 OBSERVED AND HINDCASTED MAXIMUM WAVE HEIGHT AND SIGNIFICANT WAVE HEIGHT FOR SIX OIL DRILLING PLATFORMS IN THE GULF OF MEXICO DURING HURRICANE CAMILLE.

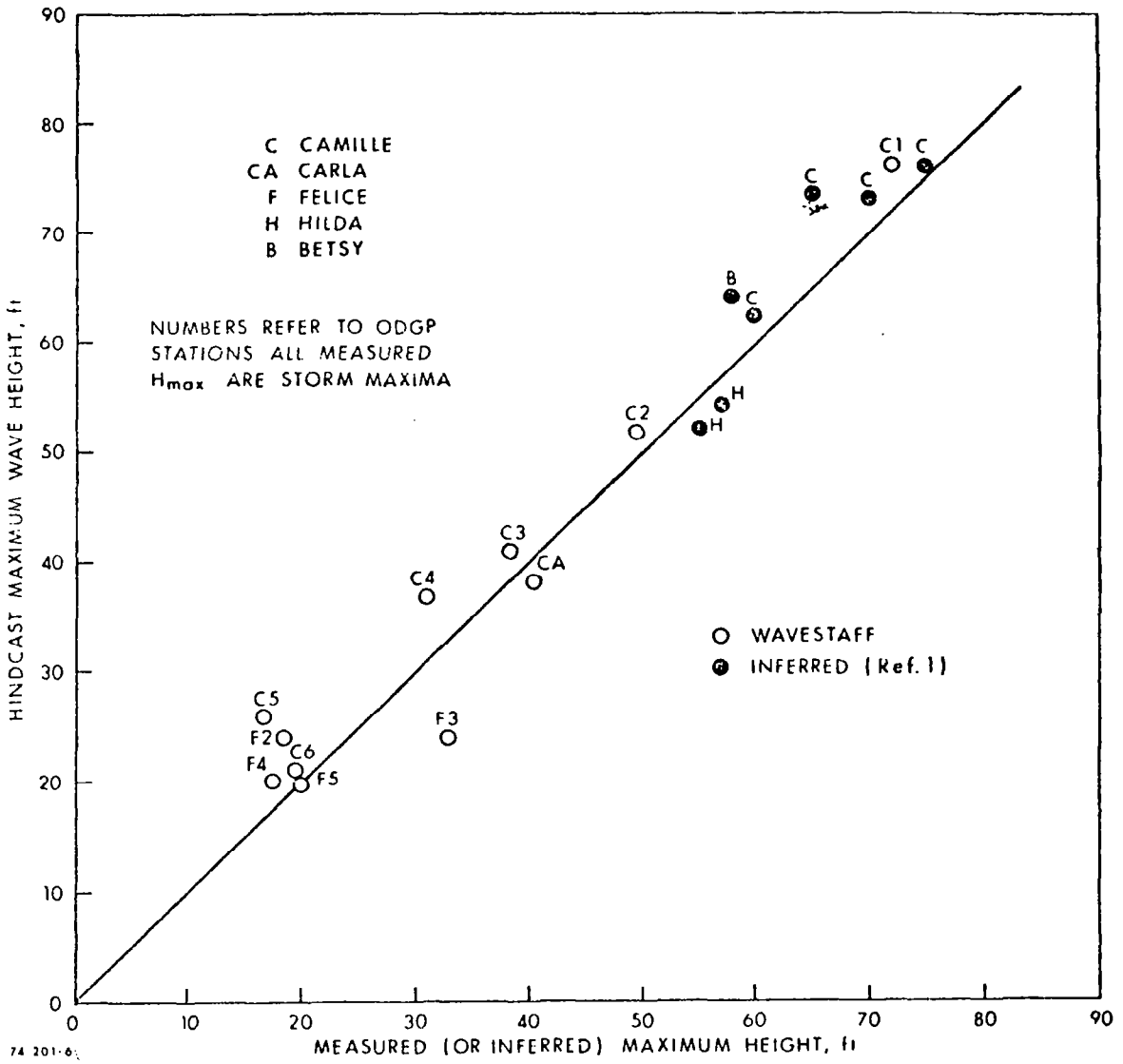

FIGURE 7.2 OBSERVED (OR INFERRED) MAXIMUM WAVE HEIGHTS VERSUS HINDCAST MAXIMUM WAVE HEIGHTS AT OIL PLATFORMS IN THE GULF OF MEXICO.

Visual Estimates of Wave Heights

The only other routinely available source of wave height information on the open ocean consists of ship reports of estimated wave heights obtained visually. These reports are a regularly scheduled part of the ship reports radioed to various collection centers routinely from a large number of ships. These reports are confined to the major shipping lanes, and there are many areas that are never traversed or from which reports are rarely obtained. These visual estimates of wave height leave much to be desired. When such visually obtained estimates were made near a ship with a shipborne wave recorder, and independently of the report from that ship, the visual estimates were found to scatter by a factor of two about the height given by the wave recorder. Stated another way, if the shipborne wave recorder gave a significant wave height of five meters, the visual estimate could vary from ten to 2.5 meters when compared with ths more precise measurement.

Also until just a few years ago, these ship reports had a built-in bias. The wave heights were recorded in a code where the numbers in the code went from zero to nine for one-half meter steps in wave height. The instructions to the observer are quite vague, and in essence, almost any height could be estimated and reported without violating the directions that were given. An attempt was made by Pierson, Neumann and James (1955) to improve the procedure, but the recommendations never were routinely used.

A code seven meant a 3.5 meter significant wave height. If the wave height exceeded 4.5 meters, 50 was added to a direction code in another part of the ship message and the numbers from 0 to 9 were repeated with an implied one in front. A code nine, if a fifty had been

inserted in a previous part of the message, thus meant a wave height of 9.5 meters. In order to avoid inserting the fifty at the right place in the code, many observers had reason to report heights of 4.5 meters very, very frequently, and then when the seas were running very high so that this did not seem reasonable, the fifty would be inserted and many observers had reason to report waves that were 9.5 meters high. There were very few reports of waves 10 meters high or 11 meters high, and higher, because the coding system required that these wave heights be reported in words at the end of the message. Histograms of reported wave heights for given areas of the world ocean travelled by merchant ships and cumulative distribution functions usually showed therefore a sharp change at a wave height of 4.5 meters and another very sharp change at a wave height of 9.5 meters. Such discontinuties are a form of bias that is very difficult to remove and that raised suspicion of any extrapolation of these data in order to predict extreme waves for a given area of the ocean. The measurement with radar altimeters will be quite free from this source of bias once they are routinely used.

Cross Calibration Against Wave Buoy and Shipborne Wave Recorder Data

Once a radar altimeter is operational such as it soon will be on GEOS-3, the orbit of the spacecraft can be predicted for these purposes many days in advance. The spacecraft will pass close to some of the many conventionally operating wave recording systems such as those described immediately above. By a modest amount of advance planning these recording systems can be operated starting 10 minutes before and ending 10 minutes after the passage of the spacecraft near them, and the wave measurements made by the spacecraft can be analyzed and compared with the significant height determined by a properly calibrated spectral analysis of the data recorded by the operational system. Within

a year or so, there will be enough variation in wave height at these sites to provide a full and complete correlation between waves measured by the conventional methods and the wave heights measured by the radar altimeter. This procedure would convincingly demonstrate the capability of the altimeter to measure waves on the basis of the change in shape of the return pulse and provide an independent estimate of the scatter in these measurements. Care should be taken in interpreting the pairs of values so obtained because a 20 minute wave record, even after calibration, still has approximately a ± 10% sampling variability in the estimate of the wave height on the assumption that a larger area say, for example, a 10 kilometer square, was being sampled as described in, Chapter 2. However, confidence intervals can be placed on both the conventionally measured wave heights and probably on the wave height estimated by the altimeter. There will be some in track variability in the wave height from one measurement to the next. If continuous measurements are made with the altimeter, they will provide guidance as to this type of variation.

The Accumulation of a Global Wave Climatology

Every fifty to one hundred kilometers, or so, whenever the spacecraft is over the ocean, a wave height neasurement should be obtained from the altimeter return pulse shape. If these observations are spaced approximately 100 kilometers apart, in the course of one day, approximately 3,600 measurements would have been obtained relatively evenly spaced over the oceans of the world. These height measurements should be collected and archived on magnetic tape as a function of the latitude and longitude and time of observation of each measurement serially as a function of the orbit of the spacecraft. It is recommended that

the data always be maintained in the raw time stream form for whatever future applications are desired. However, after a month has passed, or perhaps in two week intervals, and for a month about 108,000 measurements of wave height would have been accumulated, the data can be sorted into perhaps 5^0 square over the world ocean or perhaps into Marsden squares. For each of these areas the total number of observations can be accumulated, the average wave height, the variance and a histogramic distribution of wave height in that area can be computed and presented in some form of an atlas. Over the course of many years of operation, as more and more data are obtained for each of these sub areas, it will be possible to study such problems as the variation of significant wave height from place to place, the seasonal dependence of wave height, and the nature of extremes at each of these sites.

Of particular value will be the passes from time to time over the extreme storms in each hemisphere. For example, the storm that produced the 80 foot high wave that passed FLIP would have been thoroughly documented by many passes over the North Pacific during the time required to generate these waves and the time required for them to travel to FLIP had a spacecraft been operating at that time. Similarly the wave conditions in the North Sea that occurred in 1953 as described by Wemelsfelder (1953) and in Neumann and Pierson (1966) could have been documented by many altimeter measurements.

A particularly important area of the southern hemisphere is the region generally described as the roaring 40's and the fighting 50's where the waves are reputed to be extremely high. It would be possible over one southern hemisphere winter to document these wave conditions far more thoroughly than has ever been done before by means of properly

processed data from a radar altimeter on a spacecraft. Each successive year of observation by means of a radar altimeter can be added to the data previously obtained and after a decade, or so, the data will acquire the beginning characteristics of stable statistics for the long range prediction of extreme waves and an understanding of wave variability over the world ocean. These data will be invaluable in future years for the adequate design of ships, shore protection structures and all kinds of platforms on the continental shelves.

The variability of the winds over the North Atlantic is shown in Figure 7.3 for eight years of data. A particular month for a particular year may be anomalous. It is thus necessary to accumulate many years of data before a reliable climatology can be obtained. December 1959 was a particularly severe month over the North Atlantic.

Present Wave Forecasting and Wave Specification Procedures

In Chapter 2, the overall philosophy of forecasting and specifying waves was described. Many nations operate wave forecasting and wave specification procedures for purposes of ship routing and for general marine use. One presently in use at FNWC is described in detail in Chapter 2.* Other numerical computer based wave forecasting procedures are in operation at the National Meteorological Center, in Britain, in France, and perhaps in other European countries. Still others are hand graphical procedures in which charts depicting the distribution of significant wave height at a synoptic map time some time in the future are distributed. Both GEOS-3 and SEASAT-A will provide a verification capability for all of these models on a northern hemisphere basis, and as they become extended, eventually, on a global basis. The first step of course is the cross calibration between altimeter measurements and shipborne measurements as described previously.

*See page 388.

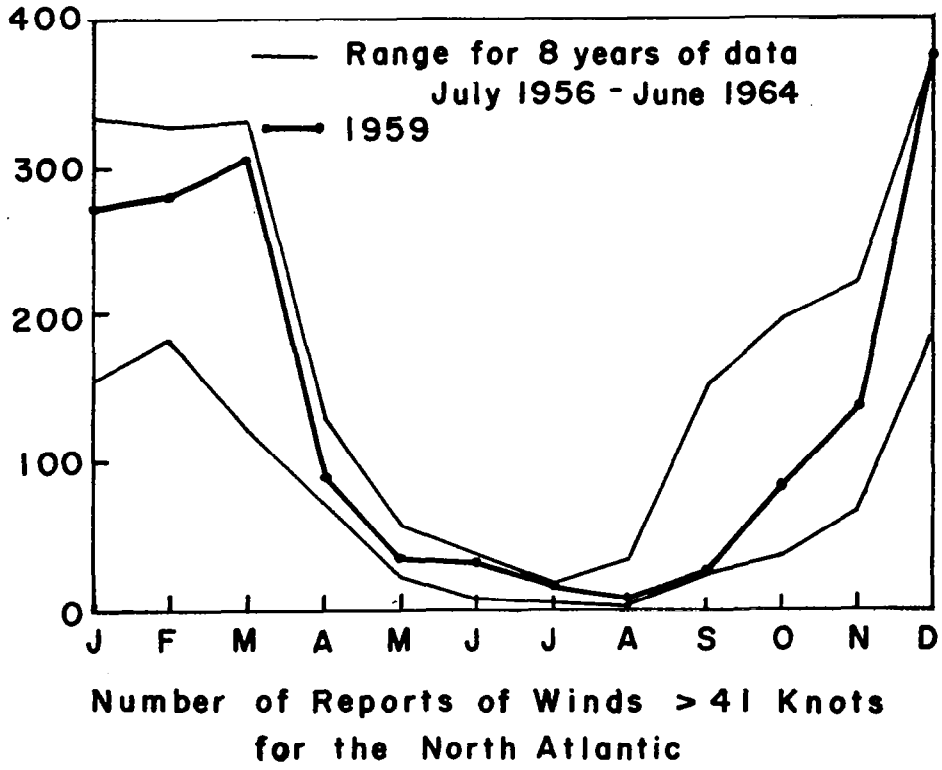

FIGURE 7.3 THE VARIABILITY OF WINDS OVER THE NORTH ATLANTIC DURING AN EIGHT YEAR PERIOD.

Intercomparison, Verification, and Improvement of Wave Specification and Wave Forecasting Models

The presently available wave specification and forecasting models can be compared with each other, verified and improved by means of the wave height data from a radar altimeter. The steps involved would be to assemble the wave specification products and the wave forecast products of all currently used methods. The errors in the wave height specifications and in the wave height forecasts at synoptic map times, whenever the spacecraft has obtained observations near the synoptic map time, can then be computed from the combined sets of data. An example is given in Figure 7.4 which shows the wave height field forecast for 48 hours for the North Pacific Ocean by the Fleet Numerical Weather Facility for the date and time indicated. Surely, within a few minutes of the synoptic map time a spacecraft pass from the equator to continental landfall will have occurred. The wave heights measured by the spacecraft along this track can be compared on a one-to-one basis with the wave heights predicted by the model, and the measured wave height from the spacecraft can be considered to be correct within sampling variability.

In order to produce this forecast, a similar field for two days before had to have been produced that was based on the observed winds up to a certain map time. The observations from the spacecraft can be compared with this field of updated specified values used as the initial value for the forecast to see how well the wave specification part of the program works. The previously described analysis will show how well the wave forecast part of the procedure works. The

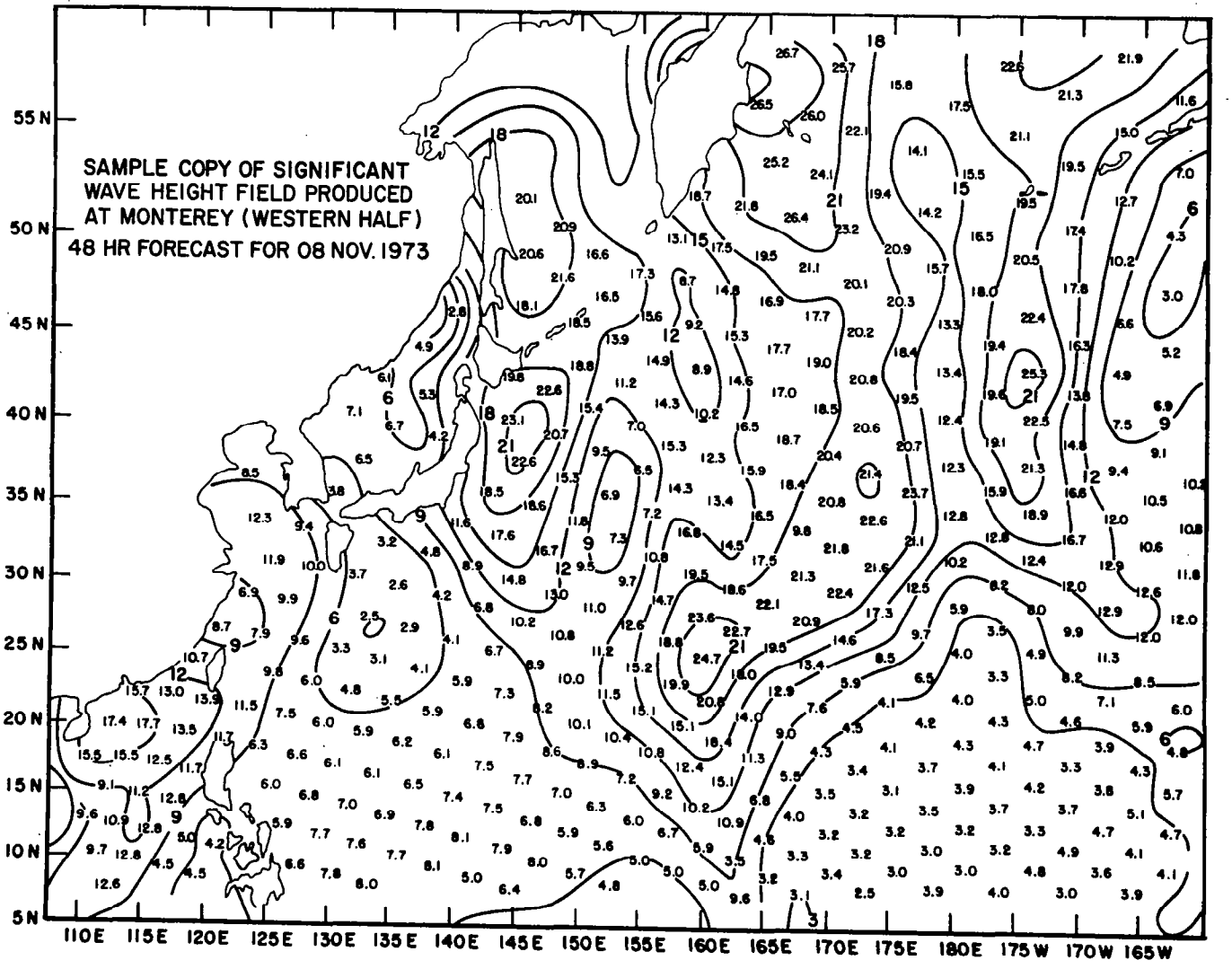

FIGURE 7.4a SIGNIFICANT WAVE HEIGHT FORECASTS FOR THE WESTERN HALF OF THE NORTH PACIFIC.

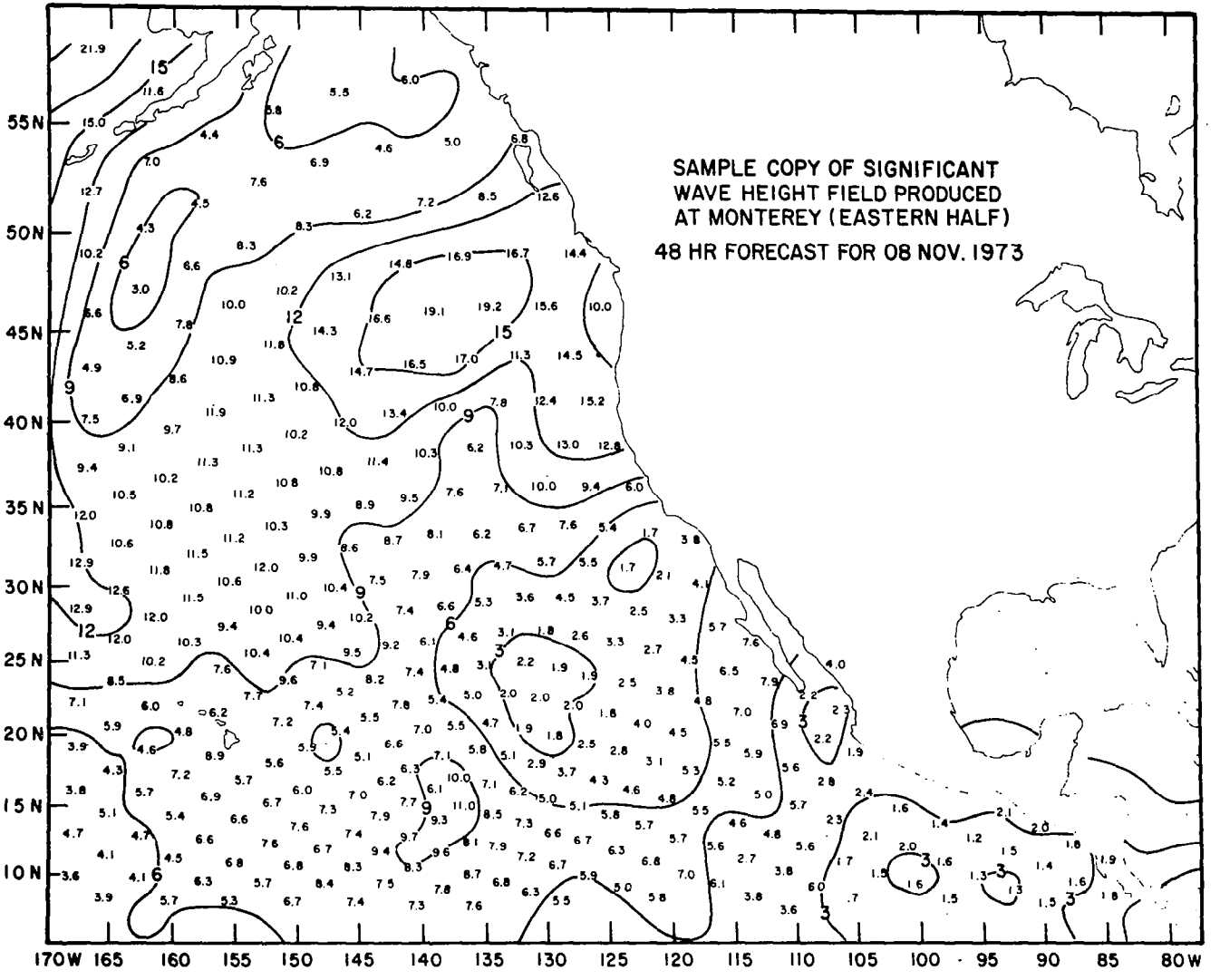

FIGURE 7.4b SIGNIFICANT WAVE HEIGHT FORECASTS FOR THE EASTERN HALF OF THE NORTH PACIFIC.

comparison of the initial value update with altimeter observations will show how well the winds have been measured and analysed and how well the physics of the waves have been modelled. There will be four opportunities each day to make such comparisons. They will occur at 0, 06, 12, and 18 GMT each day. Since some wave specification and forecasting procedures produce an output every three hours, it will be possible, if desired, to also carry out verification at 03, 09, 15, and 21 GMT with additional effort.

The verification procedure quite clearly would no longer depend on what was happening in a particular part of the ocean and would cover all parts of the ocean routinely over the course of time. Systematic errors in the wave specification model as a function of the wind speeds over the ocean could be sought. Systematic errors could also show up for particular areas in which the winds were specified incorrectly or for which the propagation algorithms of the model were not functioning properly. Each time the spacecraft made a measurement near a coastline it would be possible to check the concept of fetch for offshore winds, and for rapidly intensifying wind fields it would be possible to check on the effects of duration.

After comparing the wave specification models with the observations of wave height and eliminating as many as possible of the sources of error in the wave specification model brought to light by studies of this nature, it would then be possible to carry out a study of how well the forecasts verify against observations of wave height. Additional sources of error in the wave forecasts would be due to errors in the numerical methods for forecasting the evolution of the winds over the ocean during the time period of the forecast. If systematic discrepancies are observed between the forecasted wave heights and the observed heights, these can then be traced back to errors in the fore-

casts of the wind fields and eliminated by improving the numerical weather forecasting procedures. When Seasat-A is made quasi-operational there will be considerable interaction between the wind fields obtained from the scatterometer and the wave data. A research program will be needed to study how improved wind fields improve both weather and wave forecasts and wave specifications.

Extreme Storm Case Studies

It is essential that the altimeter be operated routinely in order to acquire the kinds of data described immediately above. Should, for some reason, the altimeter on GEOS-3 be not operable continuously, it would be important to devise a procedure for making some case studies of extreme storms during the lifetime of that spacecraft. When SEASAT-A becomes operational, a mode in which the data are taken much more frequently should be available so that extreme storms can be studied in greater detail.

Over the course of the years, the oceanographic literature has contained special studies carried out by scientific groups of what happened during extreme storms in various parts of the world. Some of these studies have been after the fact calculations of what the waves were like, others attempted to describe why the waves were particularly high and dangerous during a certain period of time, and still others were carried out because the data indicated that the storm was extreme and attempts to compare the then available forecasting procedures with what was reported to have occurred in the storm were made. There are numerous cases of the documentation of high waves and hurricanes, of which the most recent example is that of Cardone, Pierson and Ward (1975).

The very severe storm seas in the North Sea in 1953 combined with a high storm surge and topped the dikes in the Netherlands causing extensive flooding and great loss of life. This storm was the design condition for the improved dikes now in place in the Netherlands.

A storm that will probably rank high as an example for such studies is the one that occurred in the North Atlantic in January 1974 during SKYLAB. Backscatter data from S193 and wave data from the SBWR were obtained during this storm, and, as a part of the analysis of SKYLAB results, the waves will be hindcasted using the techniques described in Chapter 2.

The routine operation of a radar altimeter augmented during extreme storms, whenever the winds over a large area of the ocean are reported to be in excess of 65 knots, will provide extremely valuable information on the nature of the seas over vast areas of the ocean and will provide techniques for rapid improvement in both numerical wave specification procedures and in numerical wave forecasting procedures.

One of the common faults of most forecasting techniques including those that forecast the wind 24 to 48 hours in the future is that they tend to miss the extremes. The most intense storms that happen over the ocean are seldom forecasted to be as intense as they actually become 48 hours in advance of most severe conditions. Ways to eliminate this particular feature of present forecasting systems will undoubtedly be the subject of much future research during the next decade or so.

Case Studies for Losses at Sea

Although not specifically a scientific application, however, it is possible to use these data in an after the fact sense, given that they are obtained routinely, to document and explain why various losses at sea occurred. Each year there are a number of ships that break in half or

that fail for one reason or another and various efforts to tow drilling platforms across the ocean or to install drilling rigs meet with failure because of extreme waves and bad weather. Routinely collected data from a radar altimeter on a spacecraft will help to document the conditions that were actually present at, or near, the time of the loss being studied. At the same time, the feedback from the previously described scientific methods will continuously improve the ability to specify the waves given the winds so that the conditions not measured by the spacecraft because of the twelve hour separation between orbits near a given region can be eliminated.

Studies of Wave Refraction

Wave refraction problems are typical of relatively small scales such that horizontal distances along the coast of the order of 10 or 20 kilometers, or perhaps 30 or 40 kilometers, can produce extreme variations in the height of the waves over the shallow offshore waters on the continental shelf. For this reason the study of wave refraction can best be accomplished by some form of imaging system, be it either photography or a radar imaging system as described in a previous chapter. However, there is at least one area of the world where measurements with a radar altimeter could be obtained close enough together and in such a way that they would shed light on a problem in wave refraction. This particular area of the world is the New York Bight. As discussed by Pierson (1975), the New York Bight which forms an angle of roughly 120^{0} between the Long Island Coast and the New Jersey Coast is roughly bisected by the Hudson Submarine Canyon. If a hurricane were to move northward in the Atlantic in such a way that long period waves were sent towards the Bight from a direction generally to the south, south east of the Bight, these long period waves will travel to the edge of the Hudson Canyon and be turned

back so that they cross over each other and eventually end up on the New Jersey Coast. These waves are not able to cross the Hudson Submarine Canyon and reach the south shore of Long Island in the vicinity of Jones Beach. Under these circumstances with either a hurricane, or an east coast cyclone, in the right position, a pass of GEOS-3 over the New York Bight should be able to detect a marked change in wave height from one side of the Hudson Submarine Canyon to the other because of the effects of wave refraction. Strangely enough, this particular feature of wave refraction, which is probably one of the most pronounced features of wave refraction in the world because of the shape of the Bight and the location and length of the Hudson Canyon has never been thoroughly demonstrated. Theoretical studies, calculations, and all kinds of indirect evidence suggests that this is the case, but they do not prove it. A quick proof will be possible by means of the altimeter on GEOS-3 given the good fortune to have the spacecraft pass over the Bight from one side of the Hudson Canyon to the other during the time when the waves were sufficiently high, had a sufficiently long period, and were coming from the correct direction in deep water.

Verification of Wave Conditions in Tropical Cyclones

As described previously, numerical model has been developed for forecasting the directional wave spectra and the significant wave heights in a tropical cyclone. When a tropical cyclone is in deep water, or for that matter when the water is deep enough for the model to be valid, a radar altimeter measurement of the wave height along a pass in the vicinity of such a cyclone will provide an independent means of verifying these forecast models. As an example, Figure 7.5 from Cardone, Pierson, and Ward (1975) shows the significant wave height field ac-

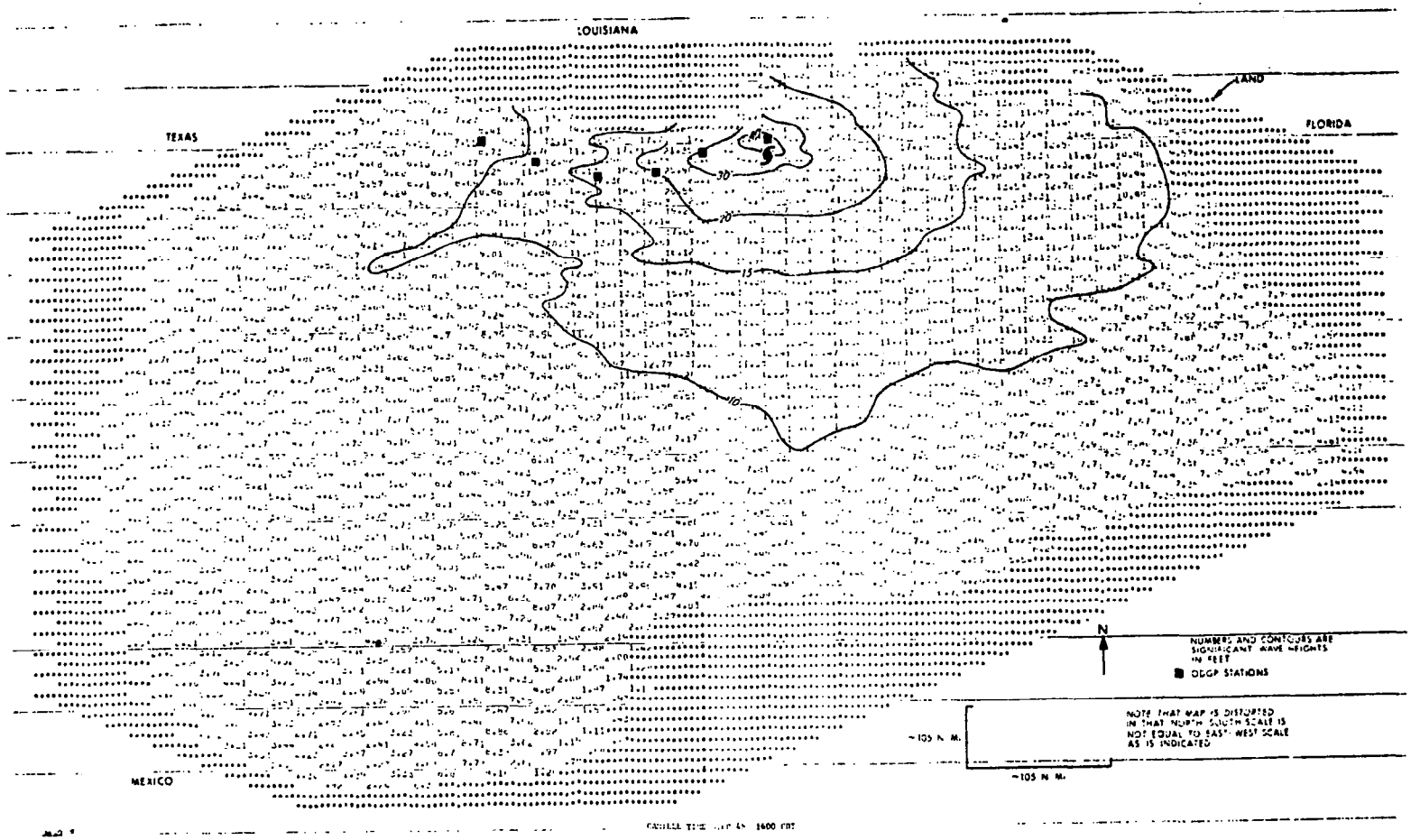

FIGURE 7.5 SIGNIFICANT HEIGHT FIELD FORECAST FOR HURRICANE CAMILLE.

companying hurricane Camille in the Gulf of Mexico. A spacecraft pass with a subsatellite track within the 16 foot contour for significant wave height in any direction would provide an independent and very valuable verification of this significant wave height field as calculated. At present time only a very limited portion of the information presented in this one chart can be verified.

SCIENTIFIC APPLICATIONS OF WAVE IMAGING SYSTEMS

General Remarks

The presently proposed wave imaging systems are dominantly designed for obtaining wave images in coastal and, therefore, relatively shallow waters. The area of the world covered by shallow seas where the speed of the waves is a function of the depth of the water, generally referred to as the continental shelf area, is equal to the area of the moon and is thus an extensive region for study. This is particularly true since many of the operations of mankind such as drilling for oil and offshore mining will push to greater depths on the continental shelves during the next decade or so. Nevertheless, it is equally important to understand the waves in the deep ocean where the depth of the water does not influence the speed of the waves.

For the deep ocean, it does not seem necessary to image a swath 100 kilometers wide. The example worked out in Chapter 2 for a 10 kilometer square produced many, many numbers and showed how they could be reduced to a manageable set of numbers that would describe the vector wave number spectrum of the sea surface that would be imaged. Ways to store a modest amount of information on the nature of the waves over the entire deep ocean should be developed as time evolves and as the SEASAT-A concept goes on to the subsequent operational spacecraft. The use of wave images obtained in deep water will be quite different from their application in coastal water, and each of these applications from a scientific point of view will be discussed at this time.

Scientific Application for the Deep Ocean

A wave imaging system that provides data on the characteristic of the waves in deep water essentially changes one number, namely $m_o^{\frac{1}{2}}$, or

four times it, which is the significant wave height, into 180 numbers or 312 numbers or 360 numbers, or what have you, depending upon which of the spectral forecasting models is being used for the particular area. The reason why the measured value of the significant wave height from an altimeter, for example, does not agree with the computed, or specified, value of the wave height, or the forecasted value of the wave height, can thus be studied in greater detail. For example, the spectrum obtained from the image might agree in all details of shape at all frequencies and directions with the spectrum produced by the specification or forecasting model and the waves might be 20% too high or 20% too low. This would imply that the wave model was off in a primary constant specifying the area under a fully developed sea, if this were to happen everywhere consistently. As another example, certain frequency bands might be present in the measurement and absent in the specification. This would mean that the waves would have not been properly generated in that frequency band or that they had not traveled from the original source of generation into the area where they were measured. It would then be necessary to investigate very carefully the computer algorithm for the generation of these frequencies and the computer algorithm that determines how they propagate across the ocean on a great circle path. The continued comparison of spectra obtained from spacecraft data with spectra produced by any numerical wave forecasting or wave specification model will lead to an understanding of why the model is not yielding correct results. These discrepancies may be a function of location on the world ocean. The model might be doing quite well in areas of high winds and large fetches and it might not be doing well at all for areas where swell has to propagate over great distances to reach them. The use of wave imagery to obtain spectra over the deep ocean will provide ways of testing, checking, and improving these wave forecasting models.

The ultimate in an effort to improve a numerical wave specification and forecasting procedure would be the ability to obtain the data that would verify the numbers shown in Table 7.1. This table represents the spectral values computed for the peak of Hurricane Camille near an oil tower. It is as important to verify the zero entries in this table at the non-zero value. There are thus 312 values to verify instead of only $m_o^{\frac{1}{2}}$ as with the altimeter or the sums over direction given across the bottom.

It was possible to verify the sums over direction for this "hindcast" as shown in Figure 7.6. Since the 90% confidence intervals on the spectral estimates enclose the hindcasted spectrum, and since the heights agree fairly well, the verification is pretty good. The degreen of freedom that determine the confidence interval on the spectral estimates are typical of the limitations imposed by a half hour long wave record at a fixed point.

Figure 7.7 represents a halfway step toward what would be possible if vector wavenumber spectra were to become routinely available globally. It is a part of the verification procedure for an earlier numerical wave forecasting model. Each histogramic step and stairs graph represents a "hindcast" wave spectrum for two points in the model near a weather ship in the North Atlantic during a storm in December 1959. The values represent the integral over the spectrum for an elementary Δf band.

The smoother curves plus the dashed curves are spectral estimates and the 90% (95% upper and 5% lower) confidence interval on the estimates computed from data obtained from the SBWR.

Although the significant heights verify fairly well, there are numerous misses in the spectral shape. On 17 December 00z, the low frequencies appear too soon. On 18 December 06z, the waves died down more quickly than the model predicted.

TABLE 7.1 SPECTRAL VALUES AT ONE GRID POINT FOR ONE TIME STEP

HINDCAST OF MAXIMUM SEA STATE AT ODGP STATION 1
DURING HURRICANE CAMILLE (1600 CDT AUGUST 17, 1969)

WAVE ENERGY OR VARIANCE
PER FREQUENCY BAND
PER DIRECTION BAND

TIME STEP 28 GRID POINT 694

FREQUENCY, f_i, Hz

DIR \ FREQ	.164	.153	.133	.117	.103	.092	.083	.078	.072	.067	.061	.056	.050	TOTAL
.0	.747	.410	.527	.903	.992	1.615	1.262	1.503	1.855	.501	.191	.089	.055	10.651
15.0	.908	.497	.640	1.097	1.205	1.908	1.386	1.827	2.459	2.064	1.969	.393	.160	16.501
30.0	1.009	.553	.712	1.219	1.339	2.122	1.541	2.031	2.735	2.243	2.787	1.128	.216	19.635
45.0	1.025	.562	.723	1.239	1.361	2.156	1.565	2.063	2.778	2.588	2.826	1.417	.264	20.569
60.0	.951	.521	.671	1.149	1.262	2.000	1.452	1.914	2.577	2.185	2.503	.685	.205	18.078
75.0	.807	.442	.569	.975	1.071	1.697	1.232	1.624	2.187	1.587	1.013	.216	.078	13.499
90.0	.631	.393	.496	.833	.899	1.370	.964	1.270	1.671	.647	.192	.076	.035	9.478
105.0	.471	.338	.436	.738	.843	1.245	.718	.843	.400	.085	.043	.021	.011	6.191
120.0	.370	.293	.383	.655	.742	.822	.397	.256	.045	.023	.015	.010	.008	4.019
135.0	.060	.180	.249	.433	.544	.222	.026	.006	.005	.004	.003	.002	.003	1.736
150.0	.000	.007	.035	.109	.043	.022	.004	.004	.005	.003	.002	.002	.001	.277
165.0	.000	.005	.025	.033	.010	.009	.003	.002	.002	.001	.001	.001	.000	.091
180.0	.000	.001	.001	.001	.001	.001	.000	.000	.000	.000	.000	.000	.000	.005
195.0	.000	.000	.001	.000	.001	.002	.002	.002	.001	.000	.000	.000	.000	.009
210.0	.000	.000	.000	.001	.000	.001	.000	.000	.000	.000	.000	.000	.000	.004
225.0	.000	.000	.000	.000	.000	.000	.000	.000	.000	.000	.000	.000	.000	.000
240.0	.000	.000	.000	.000	.000	.000	.000	.000	.000	.000	.000	.000	.000	.000
255.0	.000	.000	.000	.000	.000	.000	.000	.000	.000	.001	.000	.000	.000	.002
270.0	.000	.000	.000	.000	.000	.000	.000	.000	.000	.004	.008	.013	.001	.027
285.0	.000	.000	.000	.000	.000	.000	.000	.000	.000	.003	.002	.002	.004	.010
300.0	.000	.000	.000	.000	.000	.000	.000	.000	.000	.000	.000	.000	.000	.002
315.0	.294	.103	.122	.191	.041	.019	.006	.005	.010	.005	.001	.001	.001	.820
330.0	.428	.216	.261	.441	.499	.353	.066	.036	.133	.041	.025	.015	.008	2.521
345.0	.572	.313	.403	.691	.758	1.221	.975	1.295	1.489	.450	.137	.045	.029	8.379
E**2	8.273	4.833	6.254	10.709	11.671	16.785	11.601	14.682	18.353	12.435	11.710	4.117	1.079	132.502
DENSITY	8.3	217.5	375.2	642.4	1050.5	1510.8	2087.9	2642.6	3303.2	2238.1	2107.6	741.0	194.2	

DIRECTION θ_j*, DEGREES

SEE NOTE

WAVE ENERGY DISTRIBUTION PER DIRECTION BAND

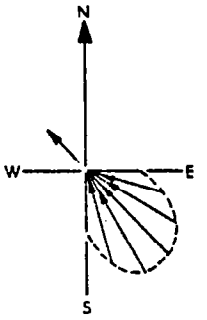

NOTE: AS SHOWN ABOVE, 75% OF THE TOTAL WAVE ENERGY IS SPREAD OVER 90°.

TOTAL VARIANCE IN FT^2

ONE-DIMENSION SPECTRAL DENSITY IN FT^2-SEC, i.e. $S(f_i)$

SIGNIFICANT WAVE HEIGHT(FT), 46.04

HIGHEST, ONE HUNDRETH WAVE(FT) 69.99 HIGHEST, ONE THOUSANDTH WAVE(FT) 85.64 EXPECTED MAXIMUM WAVE(FT) 79.26

PERIOD OF MAX. DENSITY(SEC) 13.847 DIRECTION OF MAX. WAVE(DEG.) 315.0 (DIRECTION OF TRAVEL, i.e., NW)

AVERAGE PERIOD(SEC) 8.993 "SIGNIFICANT" WAVE PERIOD(SEC) 10.333 NUMBER OF WAVES ARRIVING IN 1 HR. 348.40

ZEROTH MOMENT 132.50 FIRST MOMENT 12.82 SECOND MOMENT 1.64

* DIRECTION REFERS TO ANGLE MEASURED CCW FROM NORTH (0°), TOWARD WHICH WAVE ENERGY IS TRAVELING.

74-201-8

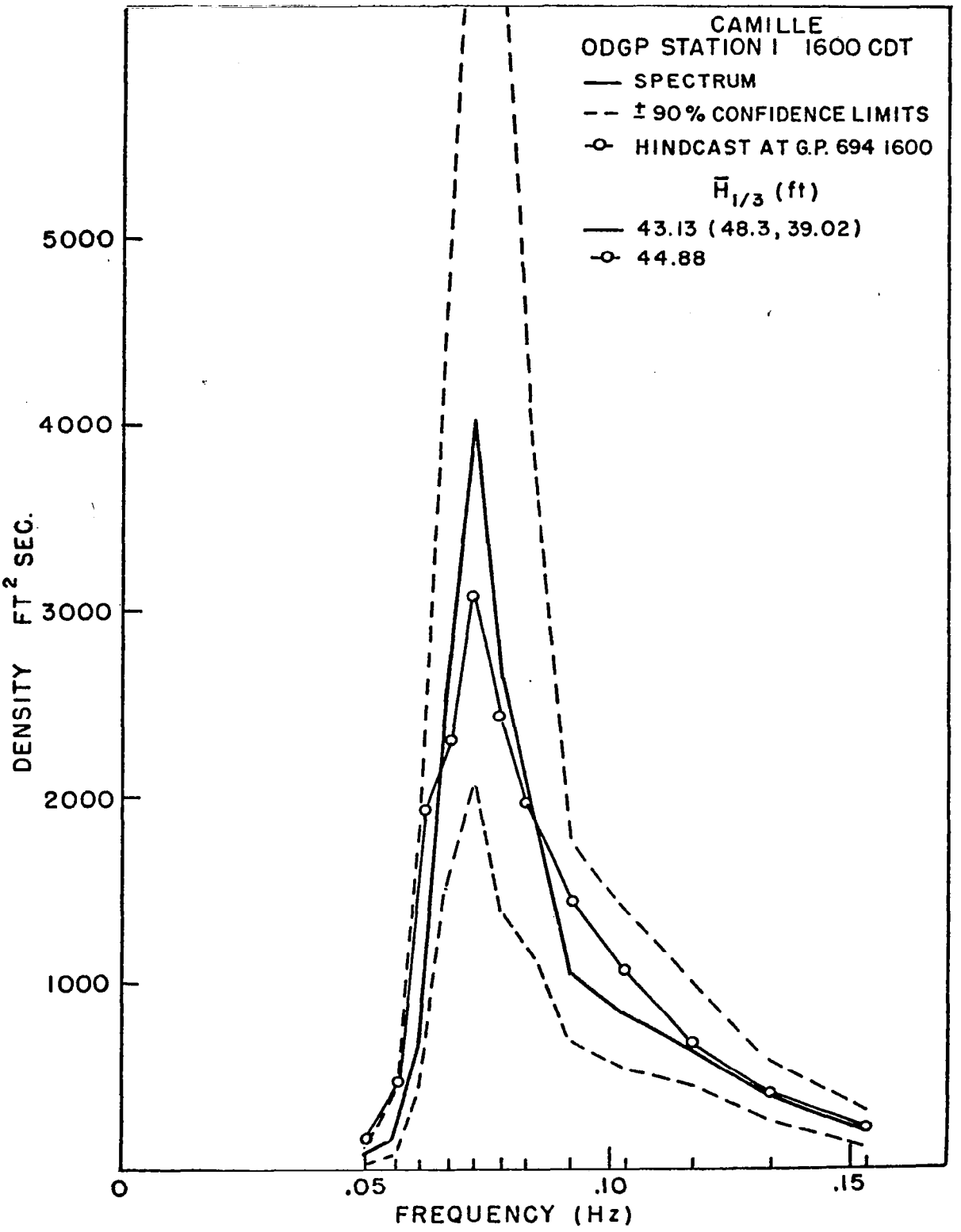

FIGURE 7.6 VERIFICATION OF A FREQUENCY SPECTRUM HINDCAST FOR HURRICANE CAMILLE.

FIGURE 7.7 A SEQUENCE OF OBSERVED AND HINDCASTED SPECTRA FOR THE DATES AND TIMES SHOWN. HEIGHTS IN FEET $S(f)\Delta f$ IS GRAPHED.

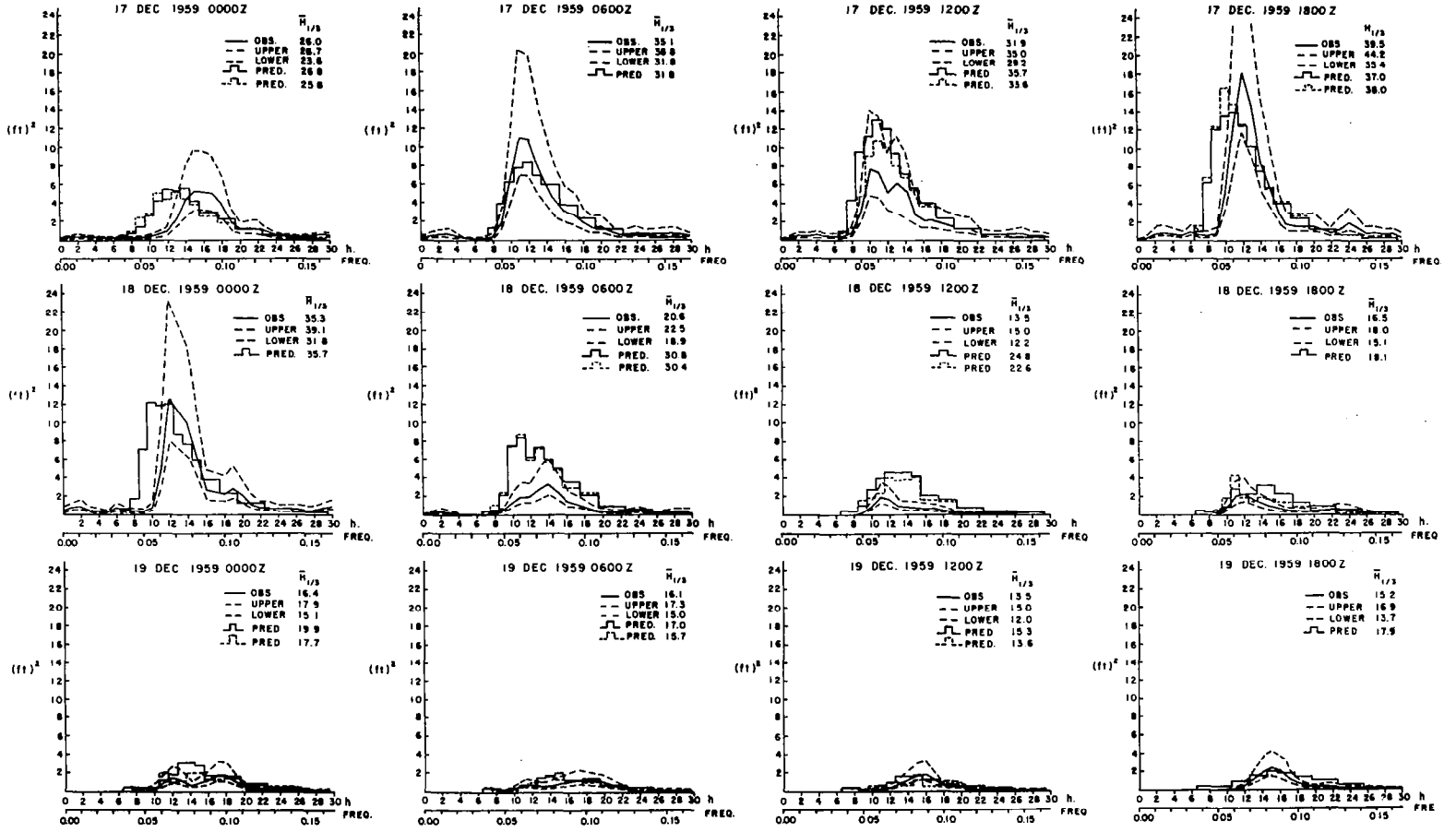

Studies of this nature went into the research of Cardone (1969) and Inoue (1967) and in the development of the attenuation algorithm for the model described in Chapter 2. With vector wavenumber spectra not only can the integral over direction be checked in the model as in this figure, but also whether or not the spectral components of the model are traveling in the correct direction can be determined.

The Investigation of Various Theoretical Wave Problems

The ability to obtain vector wave number spectra in deep water should provide an excellent opportunity to settle a number of long standing questions concerning the physics of wave propagation in deep water and concerning numerous theoretical models for the generation and propagation of waves. Among the questions that are still controversial in wave theory are the relative importance of the different mechanisms for the generation of waves, the actual angular spread of the spectrum about the wind direction, the question of whether or not fully developed wind seas actually exist, and the question of the nonlinear interaction of various spectral wave components so as to produce effects on the spectra of importance in their development. Also there is the problem of documenting overshoot and undershoot as an effect of duration on the open ocean in contrast to its apparent documentation as a function of fetch near coasts.

One of the problems of developing any numerical forecasting model is that there exist four or five additional mechanisms besides the Phillip-Miles-Phillip mechanism that might be important. Some of these are the maser mechanism proposed by Longuet-Higgins (1969), modifications, if you will, of the earlier models, and various consequences of nonlinear interaction on the growth of the spectrum. The measurement of wave spectra on a routine basis will provide a means for settling a number of these questions.

As another example, there is some expression of opinion in the literature in which it is stated that a fully developed sea does not exist and, if the fetch and duration are sufficiently long, the waves will continue to grow to lower and lower frequencies as one proceeds down fetch under these conditions. Ways to check this can be devised once

wave spectra become routinely available. A question that could be very easily answered would be whether or not there is any difference at all in the spectrum of the waves from one end of the trade wind region to the other moving along in the fetch that could not be explained by the relatively small variation of the wind speed over the distance covered by the trade winds. There are areas of the world ocean relatively free from swell where extensive fetches occur for moderate winds and the calculation of the spectra over these areas could quickly determine whether or not low frequency waves are present at the far end of such fetches and absent at the other end of such fetches.

Although techniques are in the offing for learning more about the full wave spectrum, in the form of either $S(\ell, m)$ or $S(\omega, \chi)$, the present data base is modest indeed. Routinely obtained vector wave number spectra would provide immediate and marked improvement in numerical wave forecasting and wave specification models. They should be computed by means of some accepted standard procedure and archived in the same way that the wave height data were archived both in the original time stream and regrouped biweekly or monthly for climatological purposes.

The resonance mechanism of Phillips (1957) predicts a bimodal form for the angular variation in the wave spectrum at moderately high frequencies. It would be interesting to look for this effect under conditions of uniform steady winds.

There is also the entire subject of nonlinear wave interactions. If a train of swell waves passes through a local wind sea at exactly the right direction and if the swell has the correct frequencies and directions compared to the frequencies and directions of the local wind sea, the waves in principle could interact in such a way that a new train of waves traveling in a different direction could emanate from

the cross over region and travel out of that area with a characteristic wavelength and direction that would be different from the waves in the original two intersecting groups. If this phenomenon is indeed real, as proposed for example by Phillips (1966) and analyzed by Hasselman (1968), it would be checked and verified on a routine operational basis by means of spectra obtained from wave imaging systems on a spacecraft. The ability to do this at the present time is lacking because it is not possible to document both the direction of travel and the frequency content in wave spectra at enough points on the ocean to demonstrate these effects.

Another consequence of third order nonlinear interactions should be that in large areas over which the wind has blown for many days to generate extremely high waves, the third order nonlinear interactions should produce a change in the spectrum before the waves have had an opportunity to propagate out of the area and to disperse. This change would consist of the appearance of spectral energy at lower frequencies in the spectrum, the attenuation of spectral energy, in the middle frequency range, and a characteristic change in the shape of the spectrum over the course of a day or so. A few observations in the centers of areas of extremely high waves, after the cyclone had generated them had filled and weakened, would quickly demonstrate whether this process does indeed occur and would then permit it to be modelled in a numerical wave forecasting and wave specification procedure, thus producing an improved numerical product.

CHAPTER 8 ENGINEERING AND ECONOMIC APPLICATIONS OF WAVE DATA OBTAINED FROM SPACECRAFT

Introduction

The number of ways presently in use to measure waves is also a measure of the value of and the need for the wave data. The annual cost of this data has not been estimated, but globally it probably is a substantial multiple of the cost of SEASAT-A. The use of wave data by naval architects, structural engineers, coastal engineers and other engineers and its use in ship routing provides the economic benefits that will result from obtaining this data.

In order to obtain a demarcation between Chapters 7 and 8, those aspects of wave data that do not lead to an economic benefit have been called scientific in Chapter 7 and those that lead to economic benefits have been called engineering and economic applications for this chapter. Many of the scientific problems need to be solved before the full economic potential will be realized. This is not meant to imply that engineering is not a science, and this breakdown is in part unrealistic, because there is a great deal of science involved in all of these practical engineering applications. As the problems defined in Chapter 7 are solved one by one and as the procedures for obtaining the data as described in that chapter are carried out, the data base available to the scientists who apply wave data to practical problems will suddenly become adequate for them to solve anew many long standing problems at a much more realistic level. Some, but not all, by any means, of the economic benefits from the SEASAT series of spacecraft have been given in the ECON Incorporated Study prepared by Hicks and Steele (1974).

This improved data base on wave conditions and, as a consequence, the improved wave forecasts for both the deep ocean and the coastal waters can be used by naval architects to improve the design of ships and to make them safer, by businesses and government agencies to route ships more effectively and more efficiently, by structural engineers to design improved offshore towers and other structures for the continental shelf, and by coastal engineers to design better ports and coastal defense structures. The hundreds of papers and the dozen of texts and mongraphs on the subject of design and construction problems in these many different areas will not be listed. This chapter could easily exceed in length the total of the preceding seven chapters.

For a quick review of these subject areas, there are twelve papers on subjects that will clearly benefit from better wave knowledge in the Transactions of the Society of Naval Architects and Marine Engineers as published between 1965 and 1973, there is "Seakeeping 1953 - 1973", which is a publication of the society with thirteen papers on seakeeping, wave data and wave forecasting as of 1973, and which, as a review, contains many useful references, and there are the texts by Muga and Wilson (1970) on "The Dynamic Analysis of Ocean Structures", by Silvester (1974) on "Coastal Engineering" by Craven (1971) on "Ocean Engineering Systems" and edited by Brahtz (1968) on "Ocean Engineering". Also of interest would be papers in the precedings of the Royal Institute of Naval Architecture, the Journal of Ship Research, the Marine Technology Society Journal, and Marine Technology, published by the Society of Naval Architects and Marine Engineers. The conference proceedings of Oceanology International '75 held in Brighton, England, March, 1975 contained, for example, twenty three papers involving waves and wave design problems.

APPLICATIONS IN NAVAL ARCHITECTURE

As the wave climatology on wave heights and wave spectra is accumulated by a succession of spacecraft, it will be possible to know the full range of conditions to be encountered by ships so as to improve both the seaworthiness and the seakeeping qualtities of ships. It will be possible to design ships for specific tasks on specific routes according to the wave conditions to be expected during the lifetime of that particular ship on that particular route.

With these data, it would be possible to extend the present theories of ship motions in waves to realistic two variable wave spectra of the form, $S(\omega, \chi)$ or $S(\ell, m)$. This is not done too often because of its difficulty at the present time, but examples exist in the literature mentioned above. A recent important study by Taylor and Lundgren (1975) illustrates the type of analysis that is carried out at the present time and is concerned with the adequate design of a large container ship, "NIHON". Once wave spectra becomes available, this type of analysis could be carried out almost routinely for all possible ships. In this particular study, the pitch-roll buoy of the Institute of Oceanographic Sciences (formerly the National Institute of Oceanography) of Great Britain was used to obtain information on $S(\omega, \chi)$.

A particularly interesting problem is that of the loss of small ships operating in coastal waters either for the coastal transport of goods such as lumber and fertilizer or as fishing vessels. These small ships frequently capsize in not too severe, but usually unknown, wave conditions. There is reason to believe that wave refraction can play an important part in causing these ships to capsize. Capsizing is also an important problem for tuna clippers operating out of the west coast ports of the United States. Considerable progress has been made in the study of capsizing by Pauling and Wood (1974).

A large merchant vessel was lost with all of its crew in the Mediterranean within the past few years. The last reported position was located near, and just behind, a large submarine knoll off the coast of Italy. The winds exceeded 20 meters per second from the southeast over a relatively long fetch (for the Mediterranean). Waves generated by these winds would shoal over this knoll and be refracted over it so that two distinct wave systems would be crossing each other at almost right angles behind the knoll. Under such conditions there is no safe heading for the ship. It may well have capsized. A similar condition for the North Sea has been described by Pierson (1973).

There are many similar features in coastal areas. A wave imaging system will make it possible to document these conditions, one by one, during high seas if such documentation is properly planned. These areas can then be avoided by ships.

New kinds of vehicles that travel over the water at speeds several times greater than conventional ships are in existence and others are being designed and built. These vehicles are the hydrofoils, which lift up out of the water and "fly" on small underwater "wings", and surface effect ships that ride on a bubble of air. Each of these types of vehicles has been designed using random wave theory. They are much more vulnerable to an extreme wave and to peculiar sequences of high waves in a random seaway than conventional ships. More adequate descriptions of the wave environment and improved wave predictions will be needed as the size and number of such vehicles increases and as they are operated on trans-oceanic routes.

APPLICATION IN SHIP ROUTING

A primary requirement for routing ships across the ocean is a high quality weather and wave forecast for as far as possible into the future. It takes approximately eleven days for a standard merchant vessel to cross the North Pacific from the west coast to Japan. It takes four or five days to cross the Atlantic. Perfect eleven day forecasts of weather and waves would provide the perfect least time route for a ship to cross the Pacific from one port to another. The scatterometer mode of SEASAT-A will make a substantial contribution toward improving the wave and weather forecasts and perhaps toward extending them to the desired eleven day range. The total increase in forecast range gained will not be this great, however. The improvements expected from SEASAT-A will probably be in the three, four and five day forecast range. When the improved forecasts for the first part of a Pacific crossing, and almost for an entire Atlantic crossing become available, and with the use of less precise methods based on climatology and statistics for the rest of the route, there can be an improvement in ship routing. At the present time when the weather forecast fails, or "busts" part way through a crossing, rather drastic economic losses can occur because of the increased delay of the ship and possible cargo damage.

Improved spectral wave forecasts will make possible the actual computation of the heave, pitch and roll of the ship on the ocean. Also the distance made good for each hour of steaming in a given wave condition at a given heading can be accurately predicted. The expected number of bow submergences and the number of slams (Tick (1958) and Ochi (1974)), and bending moments and stresses (Lewis (1974)) can be computed and maintained as a running historical record of what has

happened to a ship during its lifetime. Present ship routing techniques, as extensions of the work of James (1957), often now using computer based procedures, Marks et al. (1968), Faulkner (1963-64) and Bleick and Falkner (1965), attempt to minimize the time it takes for a ship to go from one port to another. The time saved translates into dollars nearly all the time in a direct ratio. However, other factors can sometime enter such as the need to minimize the damage to the cargo and to maximize the safety of the crossing for ships with large deck loads or for floating jack-up oil drilling rigs.

APPLICATIONS TO THE DESIGN OF STRUCTURES ON THE CONTINENTAL SHELF

The design of structures that stand on the sea floor is being extended to deeper and deeper waters on the continental shelf. Depths currently exceed many hundreds of feet for the placement of some of these structures. The most extensive are the oil drilling and oil production platforms for the production of oil in places such as the Gulf of Mexico. Other structures are the light stations, which have replaced many light ships, and potential structures are offshore atomic energy power plants, which have been proposed for a number of locations on the east coast of the United States.

The problem of wave refraction is important and must be studied for each potential site. In addition, these structures at the present time are designed by means of a design storm with a design storm surge, which causes the depth of the water to increase, and a design wave. The design wave has been calculated to be the highest possible wave that will pass that structure during its life time. It is assumed to be periodic and to satisfy the hydrodynamic equation for water waves in water of the depth given by the combined effect of the tide, the storm surge, and the mean water depth at the site. The "period" of the wave is picked in part on the basis of how high it is expected to be.* The engineers who work on these problems are beginning to suspect that, in many cases, they have overdesigned these offshore structures by using too high a design wave and by expecting the structure to withstand a sequence of such extreme waves for many cycles of the waves during the peak storm surge for many hours. More realistic design constraints can be gotten by understanding the time history of the storm surge and

---

*Or, perhaps, the other way around, see Silvester (1974).

the nature of the waves that passed during the peak of the storm including how long they last at the peak conditions. Moreover, by assuming the waves to be monochromatic and long-crested, the forces of the waves on the structure are computed to be too high compared to what they would be for a realistic short-crested random sequence of waves passing that same structure. The design philosophy for these structures is evolving, even at the present time, toward computing what will happen to the structure for a sequence of short-crested waves during a given time interval with one or more waves of the design wave height somewhere in the sequence. It thus becomes very important to define the characteristics of the worst possible storm with the highest expected winds and the highest expected waves to pass by a given structure during its lifetime and to design the structure with a sufficient safety margin to withstand these conditions. The economic benefits that will occur from a better understanding of the waves will be that these designs will become more efficient and will not necessarily be as expensive as the design for the presently predicted extreme conditions. The only way to refine these estimates is to obtain more and better data about the nature of these extremes. It should also be possible to hindcast the extreme conditions that were caused by past intense historical storms. Once a data base for which moderately severe storms habe been obtained and the refraction effects for a given area are understood, progress can be made.

An area of extensive study during the past five years, or so, has been the problem of constructing a large breakwater to enclose, except for an entrance and exit for a ship, a floating atomic energy power plant in water approximately 40 feet deep such that the structure and the atomic energy plant will be located several miles off the coast at various sites on the east coast. Jersey Central Power and Light, for

example, has been actively working on this problem by means of the help of numerous consulting engineering firms for a number of years so as to specify the design wave conditions for such a plant and provide a safe design for the protecting structure to surround the two duplicate floating atomic energy plants. Pierson (1975) has discussed some aspects of this type of design problem in connection with studies of refraction in the New York Bight.

The adequate gathering of wave data by wave imaging systems in this area can help in the solution to this problem and to problems similar to this one for other parts of the world in the future. In this particular case, the design problem may well be settled before SEASAT-A is launched and before such data are gathered. The penalty may well be an expensive overdesign. There will be, however, many other parts of the world and many other potential applications off the coast of the United States that will benefit from data obtained in the 1978 - 1979 time frame.

LIST OF FIGURES

LIST OF FIGURES (Cont'd.)

Page

LIST OF FIGURES (Cont'd.)

REFERENCES

Abkowitz, M. A., 1974: Applications of the Spectral Technique to Design and Operation in SEAKEEPING 1953-1973, S-3 SNAME.

Abuzyarov, Z. K., 1969: Numerical Forecasting of Wind Fields and Wave Conditions. Joint Publications Research Service, No. 47920, April.

Adamo, L. C., L. Baer, and J. P. Hosmer, 1968: Icosahedral - Gnomonic Projection and Grid of the World Ocean for Wave Studies. Journal of Geophysical Research, Vol. 73, No. 16, pp. 5125-5132.

Apel, J. R. and J. W. Siry, 1974: SEASAT-A Scientific Contributions. National Aeronautics and Space Administration, Washington, D. C.

Baer, L., 1962: An Experiment in Numerical Forecasting of Deep Water Ocean Waves. Report No. LMSC - 801296, Lockheed California Company.

Baer, L. and L. C. Adamo, 1966: The Icosahedral Gnomonic Projection and Grid of the World Ocean for Wave Studies. Report No. LR20157, Lockheed California Company.

Baer, L., L. C. Adamo, and S. Jiminez, 1965: Pacific Ocean Wave Forecasting Study. Lockheed California Company.

Barber, N. F. and F. Ursell, 1948: The Generation and Propagation of Ocean Waves and Swell. Phil. Trans. Roy. Soc. (A), 240, 527.

Barnett, T. P., 1968: On the Generation, Dissipation, and Prediction of Ocean Wind Waves. J. Geophys. Res., Vol. 73, pp. 513-529.

Barnett, T. P., 1970: Wind Waves and Swell in the North Sea, an International Field Study. EOS Trans. Amer. Geophys. Union, 51(7), pp. 544-550,

Barnett, T. P. and A. J. Sutherland, 1968: A note on an Overshoot Effect in Wind-Generated Waves. J. Geophys. Res., Vol. 73, pp. 6879-6885.

Barnett, T. P. and J. C. Wilkerson, 1967: On the Generation of Wind Waves as Inferred from Airborne Measurements of Fetch - Limited Spectra. J. Mar. Res., 25, pp. 292-328.

Barrick, D. E., 1972: "Remote Sensing of Sea-State by Radar", Remote Sensing of the Troposphere, V. E. Derr, (Ed.), U. S. Printing Office, Washington, D. C.

Barrick, D. E., J. M. Headrick, R. W. Bogle, and D. D. Crombie, 1974: "Sea Backscatter at HF: Interpretation and Utilization of the Echo". Proceedings of IEEE, 62, No. 6, pp. 673-680.

Belousov, P. S., E. O. Zhiko, A. A. Zagorodnikov, V. I. Kornienko, V. S. Loshchidov, K. B. Chel'shev, 1974: Results of Investigations of Sea Wave Structure Using a Side-Scan Radar. Proceedings of Joint U. S. - USSR Seminar the Bering Sea Experiment. Report of the main Geophysical Observatory, Leningrad,

Biesel, F., 1952: Study of Wave Propagation in Water of Gradually Varying Depth. Gravity Waves, NBS Circular 521, pp. 221-234.

Blackman, R. B. and J. W. Tukey, 1958: The Measurement of Power Spectra from the Point of View of Communications Engineering. Dover Publications, Inc, New York, also B.S.T.J. Vol. XXXVII, January and March.

Bleick, W. E. and F. D. Faulkner, 1965: Minimal Time Ship Routing. Journal Appl. Meteor., Vol. 4, pp. 217-221.

Bragg, D. M., 1972: Identification of Studies needed to Determine the Feasibility of an Offshore Port. Paper No. OTC 1643, Offshore Technology Conference (Preprint).

Brahtz, J. F., (Ed.), 1968: Ocean Engineering Goals, Environment, Technology. John Wiley and Sons, Inc., New York.

Briscoe, M. G. and E. Goudriaan, 1972: Research Use of the Waverider Buoy in Deep Water. Underwater Journal, August, pp. 142-148

Brown, W. E., Jr., C. Elachi, and T. W. Thompson, 1974: Radar Imaging of Ocean Surface Patterns. Space Sciences Division, Jet Propulsion Laboratory, California Institute of Technology, Pasadena, California.

Brown, W. E., Jr., R. Jordan, A. Laderman, and T. W. Thompson, 1972: Coherent Radar Sensor-Imaging and Ranging. Jet Propulsion Laboratory, California Institute of Technology.

Bunting, D. C., 1962: Errors in Significant Heights and E-Values of Ocean Waves from Incorrect Wind Speeds. Marine Sciences Department, Informal Manuscript Report No. 0-54-62. U. S. Navy Hydrographic Office, Washington, D.C.

Bunting, D. C., 1962: The Variability of Surface Wind Speeds Observed by Fixed Weather Ship Stations. Marine Sciences Department, Informal Manuscript Report No. 0-57-62, U. S. Naval Oceanographic Office, Washington, D.C.

Bunting, D. C., 1966: Wave Hindcast Project North Atlantic Ocean. TR-183, U. S. Naval Oceanographic Office, Washington, D.C.

Bunting, D. C., 1970: Evaluating Forecasts of Ocean-Wave Spectra. J. Geophys. Res., Vol. 75, pp. 4131-4143.

Bunting, D. C. and L. I. Moskowitz, 1970: An Evaluation of a Computerized Numerical Wave Prediction Model for the North Atlantic Ocean. Technical Report No. 209, Naval Oceanographic Office.

Cardone, V. J., 1969: Specification of the Wind Distribution in the Marine Boundary Layer for Wave Forecasting. TR-69-1, Geophysical Sciences Laboratory, New York University.

Cardone, V. J., 1974: Ocean Wave Prediction: Two Decades of Progress and Future Prospects in SEAKEEPING 1953-1973, S-3 SNAME.

Cardone, V. J., C. Greenwood, J. A. Greenwood, R. E. Salfi, and R. A. Stacy, 1974: Development of Wave Hindcasting Methods Applicable to Hurricanes. Final report submitted to Shell Development Company, Houston, Texas.

Cardone, V. J., W. J. Pierson, and E. G. Ward, 1975: Hindcasting the Directional Spectra of Hurricane Generated Waves. Presented at the Seventh Annual Offshore Technology Conference, Paper No. OTC 2332, May 5 - 8.

Cartwright, D. E., 1963: The Use of Directional Spectra in Studying the Output of a Wave Recorder on a Moving Ship. Ocean Wave Spectra. Prentice-Hall, Englewood Cliffs, N. J.

Chang, M. S., 1968: Mass Transport in Deep Water Long Crested Random Gravity Waves. Journal of Geophys. Res., 74(6), pp. 1515-1536.

Chao, Y. Y., 1971: An Asymptotic Expansion of the Wave Field Near a Smooth Caustic. Journal of Geophys. Res., Vol. 76, pp. 7401-7408.

Chao, Y. Y., 1972: Refraction of Ocean Surface Waves on the Continental Shelf. Offshore Technology Conference, OTC Paper 1616.

Chao, Y. Y., 1974: Wave Refraction Phenomena Over the Continental Shelf near the Chesapeake Bay Entrance. Technical Memorandum 47, U. S. Army Corps of Engineers, Coastal Engineering Research Center.

Chao, Y. Y. and W. J. Pierson, 1972: Experimental Studies of the Refraction of Uniform Wave Trains and Transient Wave Groups Near a Straight Caustic. J. Geophys. Res., Vol. 77, pp. 4545-4554.

Charnock, H., 1958: A Note on Empirical Wind Wave Formulae. Quart. J. Roy. Meteorol. Soc., 84, pp. 443-447.

Chase, J., L. J. Cote, W. Marks, E. Mehr, W. J. Pierson, F. C. Ronne, G. Stephenson, R. C. Vetter, R. G. Walden, 1957: The Directional Spectrum of a Wind Generated Sea as Determined from Data Obtained by the Stereo Wave Observation Project. New York University, College of Engineering and Science.

Chin, H., 1971: An Evaluation of Stokes Velocities and Inertial Currents Generated by Deep-Water Surface Gravity Waves. Geophysical Science Laboratory, TR-71-11. New York University School of Engineering and Science.

Cochran, W. T., J. W. Cooley, D. L. Favin, H. D. Helms, R. A. Kainel, W. W. Lang, G. C. Maling, Jr., D. E. Nelson, C. M. Rader, P. D. Welch, 1967: What is the Fast Fourier Transform? IEEE Transactions on Audio and Electroacoustics, Vol. AU-15, No. 2, June.

Collins, J. I., 1972: Prediction of Shallow Water Spectra. J. Geophys. Res., Vol. 77, pp. 2693-2707.

Cooper, R. D. and S. W. Doroff, 1966: Physics of Fluids, Maneuverability and Ocean Platforms, Ocean Waves, and Ship Generated Waves and Wave Resistance. Sixth Symposium Naval Hydrodynamics, Sept. 28 - Oct. 4.

Cote, L. J., J. O. Davis, W. Marks, R. J. McGough, E. Mehr, W. J. Pierson, J. F. Ropek, G. Stephenson, and R. C. Vetter, 1960: The Directional Spectrum of a Wind Generated Sea as Determined from Data Obtained by the Stereo Wave Observation Project. Meteor. Paper, Vol. 2, No. 6, New York University Press, New York, June.

Cox, C. S. and W. Munk, 1954: Statistics of the Sea Surface Derived from Sun Glitter. J. Mar. Res., Vol. 13, No. 2, pp. 198-227.

Cox, C. S. and W. Munk, 1956: Slopes of the Sea Surface Deduced from Photographs of Sun Glitter. Bull. Scripps. Inst. of Oceanog., Vol. 6, No. 9, pp. 401-488.

Craven, J. P., 1971: Ocean Engineering Systems. Massachusetts Institute of Technology, Sea Grant Program No. MITSG 71-6, Index No. 71-106-Not. Sea Grant Program GH-88.

Crutcher, H. L. and R. G. Quayle, 1974: Mariners Worldwide Climatic Guide to Tropical Storms at Sea. Naval Weather Service Command, March.

Darbyshire, J., 1955: An Investigation of Storm Waves in the North Atlantic Ocean. Proc. Roy. Soc., London, Ser. A, 230, 560.

Darbyshire, J., 1959: A Further Investigation of Wind-Generated Waves. Dt. Hydrogr. Z., Vol. 12, 1.

Darbyshire, J., 1963: The one-dimensional wave spectrum in the Atlantic Ocean and in coastal waters. Ocean Wave Spectra, Prentice Hall, Englewood Cliffs, pp. 27-39.

DeLeonibus, P. S., 1971: Momentum Flux and Wave Spectra Observations from an Ocean Tower. J. of Geophys. Res., Vol. 76, No. 27, p. 6506.

DeLeonibus, P. S., and L. S. Simpson, 1972: Case Study of Duration - Limited Wave Spectra Observed at an Open Ocean Tower. J. Geophys. Res., Vol. 77, pp. 4555-4569.

Department of the Army Corps of Engineers, 1971: Shore Protection Guidelines. A part of the National Shoreline Study conducted by the Corps of Engineers.

Dobson, F. W., 1971: Measurements of Atmospheric Pressure on Wind Generated Sea Waves. J. Fluid Mech., Vol. 48, pp. 91-127.

Draper, L., 1964: Freak Ocean Waves. Oceanus, 10(4), 12.

Draper, L., 1970: Routine Sea-Wave Measurement - A Survey. Underwater Science and Technology Journal 2, June, pp. 81-86.

Draper, L. and E. M. Squires, 1969: Waves at Ocean Weather Ship India (59°N, 19°W), Trans. Roy. Inst. Nav. Architect., 109, pp. 85-93.

Draper, L. and J. D. Humphrey, 1973: An Investigation into the Large-Wave-Height Response of two Wave Recorders. National Institute of Oceanography, Wormley, Godalming, Surrey, N.I.O. Internal Report A.63.

Draper, L. and B. C. H. Fortnum, 1974: Wave Recording Instruments for Civil Engineering Use. Institute of Oceanographic Sciences, Wormley, July.

Druyan, L. M., 1972: Objective Analysis of Sea-Level Winds and Pressures Derived from Simulated Observations of a Satellite Radar-Radiometer and Actual Conventional Data. Reprinted from J. of Applied Meteor., Vol. 11, No. 3, April, pp. 413-428.

Duncan, J. R., W. C. Keller, and J. W. Wright, 1974: Fetch wind speed dependence of Doppler spectra. Radio Science, Vol. 9, No. 10, pp. 809-819, October.

Earle, M. D., 1975: Extreme Wave Conditions During Hurricane Camille. Journal of Geophysical Research, Vol. 80, No. 3, pp. 377-379.

Elachi, C., 1974: Two-Dimensional Wavelength Spectrum of Swells Across the North Atlantic on September 28, 1974. Space Sciences Division, Jet Propulsion Laboratory, California Institute of Technology, Pasadena, California.

Ewing, J. A., 1971: A Numerical Wave Prediction for the North Atlantic Ocean, Dt. Hydrogr. Z., Vol. 24, pp. 241-261.

Ewing, J. A. and N. Hogben, 1971: Wave Spectra from Two British Research Trawlers. National Physical Laboratory, Ship Division, Ship Report 150, National Institute of Oceanography, Wormley, Godalming, Surrey.

Faulkner, F. D., 1963-64: Numerical Methods for Determining Optimum Ship Routes. Navigation: J. of the Inst. of Navigation, Vol. 10, No. 4, Winter.

Gelchi, R. H., H. Cazale, and J. Vassal, 1956: Utilisation des Diagrammes de Propagation a la Provision Energetique de la Houle. Bull. Inform. Comite-Central Oceanogr. d'Etude Cotes, 8, pp. 169-187.

Gelchi, R. H., H. Cazale, and J. Vassal, 1957: Prevision de la Houle, La Methode des Densites Spectroangulaires., Bull. Inform. Comite Central Oceanogr. d'Etude Cotes, 9, pp. 416-425.

Gelchi, R. H. and P. Chavy, 1961: Technical Aspects of Numerical Forecasting of Swell. Conference on Ocean Wave Spectra, Easton, Maryland.

Goldfinger, A. D., 1975: Digital Simulation of a Synthetic Aperture Radar. Technical Memorandum, The John Hopkins University, Applied Physics Laboratory, March, Report No. APL/JHUTG 1272.

Goldsmith, V., W. D. Morris, R. J. Byrne, and C. H. Whitlock, 1974: Wave Climate Model of the Mid-Atlantic Shelf and Shoreline (Virginia Sea). NASA SP-358, Vims Sramsoe, No. 38.

Greene, A. H., 1972: "Accuracy of Satellite Radar Altimeter Measurements." The Use of Artificial Satellites for Geodesy. Geophysical Mongraph 15, American Geophysical Union, pp. 227-237.

Greenwood, J. A., et al., 1969: Oceanographic Applications of Radar Altimetry from a Spacecraft. Remote Sensing of Environment, Vol. 1, pp. 71-80.

Groves, G. W. and J. Melser, 1961: On the Propagation of Ocean Waves on a Sphere. Geofis. Int. Mexico, 1, 77.

Hall, M., K. Steele, and R. Ericksen, 1975: Buoy Data Handling and Conversion to GOES. Briefing given to NWS/MMC, NOAA, Suitland, Maryland.

Hanley, M. J.(Captain), 1967: A 60-Knot Landing Force. United States Naval Institute. Reprint from Proceedings, March, No. 769, Vol. 93, No. 3.

Harger, R. O., 1970: Synthetic Aperture Radar Systems Theory and Design. Academic Press, Inc., New York.

Harris, D. L., 1972: Wave Estimates for Coastal Regions. Reprinted from Shelf Sediment Transport, Dowden, Hutchinson & Ross, Inc., Stroudsburg, Pa.

Hasselmann, K., 1960: Grundgleichungen der Seegags veroussage, Schiff-stechnik, 7, pp. 191-195.

Hasselmann, K., 1963: On the Non-Linear Energy Transfer in a Gravity Wave Spectrum P3: Evaluation of the Energy Flux and Swell-Sea Interaction for a Neumann Spectrum. J. Fluid Mech., 15, 385.

Hasselmann, K., 1973: On the Spectral Dissipation of Ocean Waves due to White-Capping. Contribution from the Sonderforschungs-bereich "Meeresforschung Hamburg" of the Deutsche Forschungs-gemeinschaft.

Hasselmann, K. and J. I. Collins, 1968: Spectral Dissipation of Finite-Depth Gravity Waves due to Bottom Friction. J. Mar. Res., Vol. 26, pp. 1-12.

Henriksen, S. W., A. Mancini, B. H. Chovitz, (eds.), 1972: The Use of Artificial Satellites for Geodesy. American Geophysical Union, Washington, D. C., Geophysical Monograph 15.

Hicks, K. and W. Steele, 1974: Seasat Economic Assessment. Econ Incorporated, Princeton, N. J.

Hoffman, D., 1974: Analysis of Wave Spectra at Station Poppa. Report prepared for Sea Use Foundation, Seattle, (unpublished report).

Hoffman, D. and W. Marks, 1974: Application of Wave Forecasts to Seakeeping. SEAKEEPING 1953-1973, S-3 SNAME.

Hogben, N., 1972: Wave Data Management. National Physical Laboratory, Ship Division Report 166. Contribution to report of Committee 1 (Environmental Conditions) of the Fifth International Ship Structure Congress.

Holthuijsen, L. H., 1973: Refraction of waves near the Dogger Bank. Internal Report, Vloeist of mechanica, Afd. Weg-en Waterbouwkunde, Technische Hoogeschool Delft.

Hubert, W. E., 1964: Operational Forecasts of Sea and Swell. First U. S. Navy Symposium on Military Oceanography, 17-19, June, pp. 113-124.

Inoue, T., 1967: On the Growth of the Spectrum of a Wind Generated Sea According to a Modified Miles-Phillips Mechanism and its Application to Wave Forecasting. TR-67-5, Geophysical Sciences Laboratory Report, New York University, School of Engineering and Science.

Isozaki, I. and T. Uji, 1973: Numerical Prediction of Ocean Wind Waves. Meteorological Research Institute, Tokyo.

Jackson, F. C., 1974: Directional Spectra of Ocean Waves from Microwave Backscatter. Presented at URSI Specialists Meeting, Bern, Switzerland, September.

James, R. W., 1957: Application of Wave Forecasts to Marine Navigation. U. S. Navy Hydrographic Office, SP-1.

Kasevich, R., 1975: Directional Wave Spectra from Daylight Scattering. Submitted for publication in Journal of Geophysical Research.

Kasevich, R. S., C. H. Tang, S. W. Henriksen, 1971: Analysis and Optical Processing of Sea Photographs for Energy Spectra. Presented at the 1971 IEEE Geoscience Electronics Symposium, Washington, D. C., August 25 - 27.

Kaula, W. M., et al., 1970: The Terrestrial Environment: Solid-Earth and Ocean Physics. NASA Contractor Report, CR-1579, April.

Kinsman, B., 1961: Some Evidence on the Effect of Nonlinearity on the Position of the Equilibrium Range in Wind-Wave Spectra. J. of Geophys. Res., Vol. 66, No. 8, August, pp. 2411-2415.

Kinsman, B., 1965: Wind Waves. Prentice Hall, Englewood Cliffs, N. J.

Kitaigorodskii, S. A., 1961: Application of the Theory of Similarity to the Analysis of Wind-Generated Wave Motion as a Stochastic Process. Izv. Akad. Nauk. SSSR Ser. Geofiz., pp. 105-117.

Kitaigorodskii, S. A., 1962: Applications of the Theory of Similarity to the Analysis of Wind Generated Wave Motions as a Stochastic Process. Akad. Nauk SSSR, Bul. Sci. Geophys. Ser., No. 1, pp. 73-80.

Kitaigorodskii, S. A. and S. S. Strekalov, 1963: Physics of the Sea and of the Atmosphere on the Analysis of Spectra of Wind-Generated Wave Motion. Izv. Geophys. Ser., No. 8, pp. 1240-1250.

Kitaigorodskii, S. A. and Y. A. Volkov, 1965: On the Roughness Parameter of the Sea Surface and the Calculation of Momentum Flux in the Water Layer of the Atmosphere. Izv. Atm. and Ocean. Phys, Ser. 1, pp. 973-988.

Krishen, K., 1973: Detection of Oil Spills Using a 13.3-GHz Radar Scatterometer. J. of Geophys. Res., Vol. 78, No. 12, pp. 1952-1961, April.

Lazanoff, S. and N. Stevenson, 1974: An Operational North Pacific Wave Spectral Model. E.O.S. Trans. Amer. Geophys. Union 56, 12, p. 1136, (abstract only).

Lazanoff, S., N. Stevenson, and V. J. Cardone, 1973: A Mediterranean Sea Wave Spectral Model. Tech Note 73-1, Fleet Numerical Weather Central, Monterey, California.

Lee, H. L., 1969: The Range Error Statistics of a Satellite Radar Altimeter. Tech. Rep. 112-2, Remote Sensing Lab., Univ. of Kansas Center for Research, Lawrence, Kansas.

LeVine, D. M., 1974: Monitoring the Sea Surface with a Short Pulse Radar. Presented at the URSI Specialist Meeting, Bern, Switzerland, September.

LeVine, D. M., 1974: Spectrum of Power Scattered by a Short Pulse from a Stochastic Surface. Goddard Space Flight Center, Greenbelt, Maryland, Report No. X-952-74-299, August.

Levy, P., 1948: Processus Stoachastiques et Mouvement Brownien. Paris Gouthier-Villars Impremiur-Editeur.

Lewis, E. V., 1974: Long Term Applications of St. Denis/Pierson Techniques to Ship Design. SEAKEEPING 1953-1973, S-3 SNAME.

Leykin, I. A. and A. D. Rozenberg, 1970: Study of the High-Frequency Part of the Spectrum of an Agitated Sea. Atmospheric and Oceanic Physics, Vol. 6, No. 12, pp. 1328-1332, translated by Allen B. Kaufman.

Leykin, I. A. and A. D. Rozenberg, 1971: Measurement of the Angular Spectra of the High-Frequency Portion of Swell. Atmospheric and Oceanic Physics, Vol. 7, No. 1, pp. 102-106.

Longuet-Higgins, M. S., 1952: On the Statistical Distribution of the Heights of Sea Waves. J. Mar. Res., Vol. 11, No. 3, pp. 245-266.

Longuet-Higgins, M. S., 1962: The Distribution of Intervals Between Zeros of a Stationary Random Function. Philosophical Transactions of the Royal Society of London, Royal Society Burlington House, Piccadilly, London.

Longuet-Higgins, M. S., 1963: The Effects of Non-Linearities on the Statistical Distribution Theory of Sea Waves. J. Fluid Mech. 17, pt. 3, pp. 459-480.

Longuet-Higgins, M. S., 1969: On Wave Breaking and the Equilibrium Spectrum of Wind-Generated Waves. Proceedings of the Royal Society, Series A, Number 1501, May 6, Volume 310, pp. 151-159.

Longuet-Higgins, M. S., 1969: A Nonlinear Mechanism for the Generation of Sea Waves. Proc. Roy. Soc. A, 311, pp. 371-389.

Longuet-Higgins, M. S., 1969: Action of a Variable Stress at the Surface of Water Waves. Physics of Fluids, 12, (4), pp. 737-740.

Longuet-Higgins, M. S., 1969: On Wave Breaking and the Equilibrium Spectrum of Wind-Generated Waves. Proc. Roy. Soc. A, 310, pp. 151-159.

Longuet-Higgins, M. S., 1972: A Class of Exact, Time-Dependent, Free-Surface Flows. J. Fluid Mech., 55, pp. 529-543.

Longuet-Higgins, M. S., 1972: Periodicity in Whitecaps. Nature, 239, pp. 449-451.

Longuet-Higgins, M. S., 1972: "A Class of Exact, Time-Dependent Free-Surface Flows." Journal of Fluid Mechanics, October, Vol. 55, Part 3, pp. 529-543.

Longuet-Higgins, M. S., 1973: "A Model of Flow Separation at a Free Surface." Journal of Fluid Mechanics, January, Vol. 57, Part 1, pp. 129-248.

Longuet-Higgins, M. S., 1973: On the Form of the Highest Progressive and Standing Waves in Deep Water. Proc. Roy. Soc. A, 331, pp. 445-456.

Longuet-Higgins, M. S., 1973: Breaking Waves. (Film) Review, J. Fluid Mech., 57, p. 624.

Longuet-Higgins, M. S., 1974: Breaking Waves in Deep or Shallow Water. Proc. Tenth Symp. on Naval Hydrodynamics, M.I.T. Cambridge, Mass., July.

Longuet-Higgins, M. S., 1974: "An 'entraining plume' Model of a Spilling Breaker." Journal of Fluid Mechanics, March, Vol. 63, Part 1, pp. 1-20.

Longuet-Higgins, M. S., 1974: On the mass, momentum, energy and circulation of a solitary wave. Proc. Roy. Soc. A, 337, pp. 1-13.

Longuet-Higgins, M. S., 1975: Integral Properties of Periodic Gravity Waves of Finite Amplitude. Proc. Roy. Soc. A, 342, pp. 157-174.

Longuet-Higgins, M. S., 1975: On the Joint Distribution of the Periods and Amplitudes of Sea Waves. J. Geophys. Res., Vol. 80, No. 18, pp. 2688-2694.

Longuet-Higgins, M. S., D. E. Cartwright, and N. D. Smith, 1963: "Observations of the Directional Spectrum of Sea Waves Using the Motions of a Floating Buoy." Ocean Wave Spectra, Prentice-Hall, Inc., Englewood Cliffs, N.J., pp. 111-136.

Longuet-Higgins, M. S. and J. D. Fenton, 1974: On the Mass, Momentum, Energy, and Circulation of a Solitary Wave II. Proc. Roy. Soc. A, 340, pp. 471-493.

Longuet-Higgins, M. S. and J. S. Turner, 1974: An "entraining plume" Model of a Spilling Breaker. J. Fluid Mech., 63, pp. 1-20.

Loukakis, T., 1970: Extreme Wave Heights and Ship Responses in a Seaway. Report No. 70-5, Department of Naval Architecture and Marine Engineering, Massachusetts Institute of Technology.

Marks, W., 1954: The Use of a Filter to Sort Directions in a Short Crested Gaussian Sea Surface. Trans. Amer. Geophys. Union, Vol. 35, No. 5.

Marks, W., T. R. Goodman, W. J. Pierson, L. J. Tick, and L. A. Vasselopoulos, 1968: An Automated System for Optimum Ship Routing, Trans. SNAME, Vol. 76.

Martsinkevich, L. M., 1974: Slope Distribution of Rough Ocean Surface. Goddard Technical Translation, GSFC-115.

McClain, E. P. and A. E. Strong, 1969: On Anomalous Dark Patches in Satellite-Viewed Sunglint Areas. Monthly Weather Review, Vol. 97, No. 12, December, pp. 875-884.

McClenan, C. M. and D. L. Harris, 1975: The Use of Aerial Photography in the Study of Wave Characteristics in the Coastal Zone. Technical Memorandum, U. S. Army, Corps of Engineers, Coastal Engineering Research Center (CERRE-OC), Project No. C31180.

McGoogan, J. T., C. D. Leitao, W. T. Wells, L. S. Miller, and G. S. Brown, 1974: Skylab Altimeters Applications and Scientific Results. AIAA/AGU Conference on Scientific Experiments of Skylab, AIAA Paper No. 74-1221, Oct. 30 - Nov. 1.

McGoogan, J. T., L. S. Miller, G. S. Brown, and G. S. Haynes, 1974: The S-193 Radar Altimeter Experiment. Proceedings of the IEEE Conference, June.

Miles, J. W.: On the Generation of Surface Waves by Shear Flow. Part 1, J. Fluid Mech., Vol. 3, pp. 185-204 (1957). Part 2, J. Fluid Mech., Vol. 6, pp. 568-582 (1959). Part 3, J. Fluid Mech., Vol. 6, pp. 583-598 (1959). Part 4, J. Fluid Mech., Vol. 13, pp. 433-448 (1962).

Miles, M., 1971: Wave Spectra Estimated from a Stratified Sample of 323 North Atlantic Wave Records. Division of Mechanical Engineering, Canada, Report/Rapport LTR-SH-118, October.

Mitsuyasu, H., 1969: On the Growth of the Spectrum of Wind-Generated Waves (II). Reprinted from Reports of Research Institute for Applied Mechanics, Kyushu University, Vol. XVII, No. 59.

Mitsuyasu, H. and T. Honda, 1974: The High Frequency Spectrum of Wind Generated Wave. J. of the Oceanographical Soc. of Japan, Vol. 30, No. 4, pp. 29-42.

Moore, R. K. and W. J. Pierson, 1971: Worldwide Oceanic Wind and Wave Predictions Using a Satellite Radar-Radiometer. J. of Hydronautics, Vol. 5, No. 2, April, pp. 52-60.

Moskowitz, L., 1964: Estimates of the Power Spectrums for Fully Developed Seas for Wind Speeds of 20 to 40 Knots. J. of Geophys. Res., Vol. 69, No. 24, pp. 5161-5179.

Moskowitz, L., W. J. Pierson, and E. Mehr, 1962, 1963, 1965: Wave Spectra Estimated from Wave Records Obtained by the OWS Weather Explorer and the OWS Weather Reporter, I, II, and III. Prepared for the U. S. Naval Oceanogr. Office. New York University, School of Engineering and Science.

Muga, B. J. and J. F. Wilson, 1970: Dynamic Analysis of Ocean Structures. Planum Press.

Nagata, Y., 1970: Lag Joint Probability, Higher Order Covariance Function and Higher Order Spectrum. Bulletin of the France-Japanese Society of Oceanography, Vol. 8, No. 2, pp. 78-94, May.

Neumann, G., 1952: Uber dce Komplexe Natur die Seganges, Teil 1 and 2 Deut. Hydrog. Zeit, Vol. 5, No. 213, pp. 95-110, No. 516, pp. 252-277.

Neumann, G., 1953: On Ocean Wave Spectra and a New Method of Forecasting Wind Generated Sea. U. S. Beach Erosion Board, Tech. Memo. 43.

Neumann, G. and W. J. Pierson, Jr., 1966: Principles of Physical Oceanography. Prentice-Hall, Inc., Englewoods Cliffs, N. J.

Ocean Data Systems, Inc., 1975: Synoptic Comparison of EB01 and FNWC Spectral Wave Data. Prepared for NOAA Data Buoy Office, Technical Report 4, prepared under contract NAS 8-30941.

Ocean Data Systems, Inc., 1975: Synoptic Comparison of EB03 and FNWC Spectral Wave Data. Prepared for NOAA Data Buoy Office, Technical Report 2, prepared under contract NAS 8-30941.

Oceanology International, 1975: Conference Papers Collection.

Ochi, M. K., 1974: Review of Recent Progress in Theoretical Prediction of Ship Responses to Random Seas. SEAKEEPING 1953-1973, S-3 SNAME.

Panicker, N. N. and M. Asce, 1974: Review of Techniques for Directional Wave Spectra. Contribution No. 3391 of Woods Hole Oceanographic Institution, proceedings of the International Symposium on Ocean Wave Measurement and Analysis ASCE, New Orleans, La., Sept. 9 - 11.

Parry, D. H. and M. J. Sanders, Jr., 1971: The Design and Operation of an Acoustic Radar. Presented at the IEEE Geoscience Electronics Symposium, Washington, D. C., August 25 - 27.

Pauling, J. R. and P. D. Wood, 1974: Numerical Simulation of Large Amplitude Ship Motions in Astern Seas. SEAKEEPING 1953-1973, S-3 SNAME.

Peacock, H. G., 1974: CERC Field Wave Gaging Program. Proceedings of the International Symposium on Ocean Wave Measurement and Analysis ASCE, New Orleans, La., Sept. 9 - 11.

Pflugbeil, C. and H. Walden, 1970: Zur Hohe der Kreuzsee an den nordatlantischen Wetterschiffen 1955-1966. Deutscher Wetterdienst, Seewetteramt, Einzelveroffentlechungen, Ni. 73.

Phillips, O.M., 1957: On the Generation of Waves by Turbulent Wind. J. Fluid Mech., 2, pp. 417-445.

Phillips, O. M., 1958: The Equilibrium Range in the Spectrum of Wind Generated Waves. J. Fluid Mech., 4, pp. 426-435.

Phillips, O. M., 1960: On the Dynamics of Unsteady Gravity Waves of Finite Amplitude. Part I, J. Fluid Mech., 9, pp. 193-217.

Phillips, O. M., 1961: On the Dynamics of Unsteady Gravity Waves of Finite Amplitude. Part 2, J. Fluid Mech., 1, pp. 143-155.

Phillips, O. M., 1966: The Dynamics of the Upper Ocean. Cambridge University Press.

Pierson, W. J., 1951: The Interpretation of Crossed Orthogonals in Wave Refraction Phenomena. Technical Memorandum No. 21, Beach Erosion Board, Corps of Engineers.

Pierson, W. J., 1952: A Unified Mathematical Theory for the Analysis, Propagation, and Refraction of Storm-Generated Ocean Surface Waves. Prepared for Beach Erosion Board, New York University.

Pierson, W. J., 1954: The Interpretation of the Observable Properties of Sea Waves in Terms of the Energy Spectrum of the Gaussian Record. Trans. Amer. Geo-Phy. Union, Vol. 35, pp. 747-757.

Pierson, W. J., 1964: The Interpretation of Wave Spectrums in Terms of the Wind Profile Instead of the Wind Measured at a Constant Height. J. Geophys. Res., Vol. 6, pp. 5191-5203.

Pierson, W. J., 1967: Importance of the Atmospheric Boundary Layer over the Oceans in Synoptic Scale Meteorology. Boundary Layers and Turbulence, The Physics of Fluids Supplement.

Pierson, W. J., 1972: The Loss of Two British Trawlers - A Study in Wave Refraction. J. of Navigation, Vol. 25, No. 3, July, pp. 291-304.

Pierson, W. J., 1974: Forecasting and Observing Waves, Wind, and Weather at Sea. SEAKEEPING 1953-1973, S-3 SNAME.

Pierson, W. J., 1975: The Wave Conditions in the New York Bight. Report in preparation for the New York Bight Atlas, (the MESA Program of the State University of New York).

Pierson, W. J. and W. Marks, 1952: The Power Spectrum Analysis of Ocean-Wave Records. Trans. Amer. Geophys. Union, Vol. 33, No. 6, pp. 834-844.

Pierson, W. J., G. Neumann, and R. W. James, 1955: Practical Methods for Observing and Forecasting Ocean Waves by Means of Wave Spectra and Statistics. H.O. Pub. No. 603, U. S. Navy Hydrographic Office, Washington, D.C.

Pierson, W. J. and L. Moskowitz, 1964: A Proposed Spectral Form of Fully Developed Wind Seas Based on the Similarity Theory of S. A. Kitaigorodskii, J. Geophys. Res., Vol. 69, (24), pp. 5181-5190.

Pierson, W. J., L. J. Tick, and L. Baer, 1966: Computer Based Procedures for Preparing Global Wave Forecasts and Wind Field Analyses Capable of Using Wave Data Obtained by a Spacecraft. Proc. of the Sixth Naval Hydrodynamics Symposium.

Pierson, W. J. and E. Mehr, 1970: Bias Errors in a Divided Split Gate Tracking Loop for a Radar Altimeter. (Abstract) E.O.S. Trans. AGU, 51(4), pp. 263.

Pierson, W. J. and E. Mehr, 1972: "Average Return Pulse Form and Bias for the S193 Radar Altimeter on Skylab as a Function of Wave Conditions". The Use of Artificial Satellites in Geodesy. Geophysical Mongraph No. 15, American Geophysical Union.

Pierson, W. J. and R. K. Moore, 1972: The Extrapolation of Laboratory and Aircraft Radar Sea Return Data to Spacecraft Altitudes. In Proc. Fourth Annual Earth Resources Review, NASA Manned Space Center.

Pierson, W. J. and R. A. Stacy, 1973: The Elevation, Slope, and Curvature Spectra of a Wind Roughened Sea Surface. NASA Contractor Report CR-2247, (Langley Research Center).

Pierson, W. J., V. J. Cardone, and J. A. Greenwood, 1974: The Applications of SEASAT-A to Meteorology. The University Institute of Oceanography, the City University of New York. Prepared for NOAA, August. (SPOC/NOAA/NESS)

Pore, N. A. and W. S. Richardson, 1969: Second Interim Report on Sea and Swell Forecasting. ESSA Tech. Memo. WBTM TDL 17, 17 pages.

Priestly, J. T., 1965: Correlation Studies of Pressure Fluctuations on the Ground Beneath a Turbulent Boundary Layer. National Bureau of Standards, NBS Report 8942.

Rhodes, R. S., 1975: A Preview of Benefits From Skywave Radar Measurements of Sea State. Marine Technology Journal Society, Vol. 9, No. 2, February.

Rice, S. O., 1944: The Mathematical Analysis of Random Noise. Bull. System Tech. Jour., Vol. 23, pp. 282-332.

Røren, E. M. Q., K. Hove, J. Foss, and O. Olsen, 1975: Concrete Gravity Structures for Petroleum Production Offshore - Merits and Problems. Oceanology International '75, proceedings of a conference, pp. 86-92.

Ross, D. and V. J. Cardone, 1970: Laser Observation of Wave Growth and Foam Density for Fetch Limited 23 m/s Winds. Hydrology and Oceanography, Third Annual Earth Resources Program Review, Vol. III.

Ross, D. B., V. J. Cardone, and J. W. Conaway, Jr., 1970: Laser and Microwave Observations of Sea-Surface Condition for Fetch-Limited 17 - to 25 m/s Winds. Reprinted from IEEE Trans. on Geoscience Electronics, Vol. GE-8, No. 4, October, pp. 326-336.

Ross, D. B. and V. J. Cardone, 1974: Observations of Oceanic Whitecaps and their Relation to Remote Measurements of Surface Wind Speed. J. of Geophys. Res., Vol. 79, No. 3, January, pp. 444-452.

Ross, D., B. Au, W. Brown, and J. McFaddin, 1974: A Remote Sensing Study of Pacific Hurricane AVA. Presented at the Ninth Conference on Remote Sensing of Environment, Ann Arbor, Michigan, April 15 - 21.

Rudnick, P. and R. W. Hasse, 1971: Extreme Pacific Waves. J. Geophys. Res., Vol. 76 (3), December, pp. 742-744.

Russell, T. L., 1963: "A Step - Type Recording Wave Gage". Ocean Wave Spectra. Prentice Hall Inc., Englewood Cliffs, N. J., pp. 251-257.

Saetre, H. J., 1975: On High Wave Conditions in the North Sea. Oceanology International '75, proceedings of a conference, pp. 280-289.

Salfi, R. E., 1974: Operational Computer Based Spectral Wave Specification and Forecasting Models. The University Institute of Oceanography of the City University of New York, prepared for NOAA, (SPOC).

Schule, J. J., L. S. Simpson, and P. S. DeLeonibus, 1971: A Study of Fetch-Limited Wave Spectra with an Airborne Laser. J. Geophys. Res., Vol. 76, pp. 4160-4171.

Schumacher, A., 1928: Die stereogrammetrische Welenaufnakmen der deutschen Atlantischen Expedition. Zeit. f. d. Gesellschaft f. Erdkunde zie Berlin, Erganzungsheft 3, pp. 105-120, (Berlin).

Schumacher, A., 1939: Stereophotogrammetrische Wellenaufnahmen. Wiss. Erg. Deutsche Atl. Exped. "Meteor", 1925-1927, Vol. 7, No. 2, (Berlin).

Seakeeping, 1953-1973, (1974): Sponsored by Panel H-7 at Webb Institute of Naval Architecture. Published by the Society of Naval Architects and Marine Engineers. Technical and Research Symposium S-3, June.

Sellars, F., 1975: Maximum Heights of Ocean Waves. J. Geophys. Res., Vol. 80, No. 3, pp. 398-404.

Shemdin, O. H., 1969: Instantaneous Velocity and Pressure Measurements above Propagating Waves. Tech. Report No. 4, University of Florida, Gainesville, Florida.

Shemdin, O. H. and E. Y. Hsu, 1967: Direct Measurement of Aerodynamic Pressure Above a Simple Progressive Gravity Wave. J. Fluid Mech., Vol. 30, pp. 403-417.

Shemdin, O. H., R. J. Lai, A. Reece, and G. Tober, 1972: Laboratory Investigations of Whitecaps, Spray, and Capillary Waves. Coastal and Oceanographic Engineering Laboratory, Tech. Report No. 11.

Sheppard, P. A., 1958: Transfer Across the Earth's Surface and Through the Air Above. Quart. J. Roy. Meteorol. Soc., 84, pp. 205-224.

Skolnik, M. L., 1969: A Review of Radar Sea Echo. Naval Research Laboratory, NRL Memorandum Report 2025, Washington, D. C.

Silvester, R., 1974: Coastal Engineering, I Generation, Propagation, and Influence of Waves. Developments in Geotechnical Engineering 4A. Elsevier Scientific Publishing Company, Amsterdam.

Silvester, R., 1974: Coastal Engineering, II Sedimentation, Estuaries, Tides, Effluents, and Modelling. Developments in Geotechnical Engineering 4B. Elsevier Scientific Publishing Company, Amsterdam.

Snodgrass, F. E., G. W. Groves, K. F. Hasselmann, G. A. Miller, W. H. Munk, and W. H. Powers, 1966: Propagation of Ocean Swell Across the Pacific. Phil. Trans. Roy. Soc. Ser. A, No. 1103, Vol. 259, pp. 431-497.

Stacy, R. A., 1974: Spectral Analyses of High Frequency Gravity Waves Generated by a Hurricane. Ph.D. Thesis, School of Engineering and Science, New York University.

State of Sea Photographs for the Beaufort Wind Scale, 1971: Meteorological Branch, Department of Transport, Canada.

St. Denis, M., 1974: On the Spectral Technique for Describing the Seaway - Induced Motions of Ships - A Review of Development over the Past Two Decades and an Outline of Problems now in hand in SEAKEEPING 1953-1973, S-3 SNAME.

St. Denis, M. and W. J. Pierson, 1953: On the Motion of Ships in Confused Seas. Trans. of the Soc. of Naval Architects and Marine Engineers for 1954, pp. 280-357.

Stevenson, N. M. and S. M. Lazanoff, 1974: Spectral Ocean Wave Forecasts, A New Horizon for the Navy's Weather Service. Bull. Amer. Meteor. Soc. 55, 11, pg. 1408, (abstract only).

Steward. R. H. and J. W. Joy, 1974: Instruments and Methods HF Radio Measurements of Surface Currents. Deep Sea Research, Vol. 21, pp. 1039-1049.

Stilwell, D., Jr., 1969: Directional Energy Spectra of the Sea from Photographs. J. Geophys. Res., Vol. 74 (8), pp. 1974-1986.

Stilwell, D., Jr. and R. O. Pilon, 1974: Directional Spectra of Surface Waves from Photographs. J. of Geophys. Res., Vol. 79, No. 9, March.

Strong, A. E. and E. P. McClain, 1969: Sea-State Measurements from Satellites. Reprinted from Mariners Weather Log, Vol. 13, No. 5, Sept., p. 205.

Strong, A. E. and E. S. Ruff, 1970: Utilizing Satellite-Observed Solar Reflections from the Sea Surface as an Indicator of Surface Wind Speeds. Remote Sensing of Environment, 1, pp. 181-185.

Strong, A. E. and R. J. DeRycke, 1973: Ocean Current Monitoring Employing a New Satellite Sensing Technique. Reprinted from Science, Vol. 182, November, pp. 482-484.

Strong, A. E., R. J. DeRycke, and H. G. Stumpf, 1974: Extensive Areas of Reduced Waves Leeward of the Lesser Antilles. American Geophysical Research Letters, Vol. 1, No. 1, pp. 47-49.

Stumpf, H. G. and A. E. Strong, 1974: ERTS-1 Views an Oil Slick? Remote Sensing of Environment, 3, pp. 87-90.

Sugimori, Y., 1972: Application of Hologram Method to the Analysis of the Directional Spectrum of the Surface Wave. Bulletin of the French-Japanese Society of Oceanography, Vol. 10, No. 1, February.

Sverdrup, H. V. and W. H. Munk, 1947: Wind, Sea, and Swell Theory of Relation for Forecasting. U. S. Hydrographic Office, Pub. No. 601.

Swift, C. T., 1974: A Simulation of Synthetic Aperture Radar Imaging of Ocean Wave. NASA Technical Memorandum X-72629, October.

Synder, R. and C. S. Cox, 1966: A Field Study of the Wind Generation of Ocean Waves. J. Mar. Res., Vol. 24, pp. 141-177.

Taylor, K. V. and D. Lundgren, 1975: Full-Scale Static and Dynamic Measurements on M. V. 'Nihon'. Comparison of Measured Motions, Pressures and Stresses with Calculated Response Data. Paper No. 5, presented at the Royal Institution of Naval Architects, Spring Meeting.

Thom, H. C. S., 1971: Asymptotic Extreme Value Distributions of Wave Heights in the Open Ocean. J. of Marine Res., Vol. 29, pp. 19-27.

Thomasell, A. and J. G. Welsh, 1963: Studies of the Specification of Surface Winds Over the Ocean. Traveler's Research Center, Inc.

Thompson, E. F., 1974: Results from the CERC Wave Measurement Program. Reprinted from the Proceedings of the International Symposium on Ocean Wave Measurement and Analysis. ASCE, New Orleans, La., Sept. 9 - 11.

Tick, L. J., 1958: Certain Probabilities Associated with Bow Submergence and Slamming in Irregular Seas. J. Ship Res., Vol. 2, No. 1.

Tick, L. J., 1967: Estimation of Coherency. Spectral Analysis of Time Series. Edited by Bernard Harris. Published by John Wiley & Sons, Inc.

Tick, L. J. and P. Shaman, 1966: Sampling Rates and Appearance of Stationary Gaussian Processes. Research Report sponsored by Aeronautical Structures Laboratory, USNAEC under Contracts N156-42908 and N156-45092.

Toba, Y., 1961: Drop Production by Bursting of Air Bubbles on the Sea Surface (III). Study by use of a wind flume. Memoirs Coll. Sci., University Kyoto, Ser. A 29, pp. 313-344.

Toba, Y., 1964: On the Giant Sea-Salt Particles in the Atmosphere II. Theory of the Vertical Distribution in the 10-m Layer Over the Ocean. Tellus, 17, pp. 365-382.

Toba, Y., 1965: On the Giant Sea-Salt Particles in the Atmosphere I. General Features of the Distribution. Tellus, 17, pp. 131-145.

Toba, Y., 1966: Critical Examination of the Isopiestic Method for the Measurement of Sea-Salt Nuclei Masses. Special Contributions, Geophysical Institute, Kyoto University, No. 6, pp. 59-67.

Toba, Y., 1973: Local Balance in the Air-Sea Boundary Processes III. On the Spectrum of Wind Waves. Reprintfrom the J. of Oceanographical Soc. of Japan, Vol. 29, No. 5, October.

Tucker, M. J., 1956: A Ship-Borne Wave Recorder. Trans. Inst. Naval Arch., Vol. 98, pp. 236-250, (London).

Tukey, J. W., 1949: The Sampling Theory of Power Spectrum Estimates. Symposium on Applications of Autocorrelation Analysis to Physical Problems. Woods Hole, June 13, NAVEXOS-0-735, Office Of Naval Research.

Tyler, G. L., C. C. Teague, R. H. Stewart, A. M. Peterson, W. H. Munk, and J. W. Joy, 1974: Wave Directional Spectra from Synthetic Aperture Observations of Radio Scatter. Deep-Sea Research, Vol. 21, pp. 989-1016.

Uji, T. and I. Isozaki, 1972: The Calculation of Wave Propagation in the Numerical Prediction of Ocean Waves. Papers in Meteorol. and Geophy., 23, 4.

Ursell, F., 1956: "Wave Generation by Wind". Surveys in Mechanics, Chap. 7, Edited by G. K. Batchelor and R. M. Davies. Cambridge University Press, New York.

Voznessensky, A. K., I. N. Davidan, L. I. Lopatukhin, V. A. Rozhkov: The Distribution of Wave Elements Using Stereophotographs. Unknown Soviet source.

Wemelsfelder, P. J., 1953: The Disaster in the Netherlands Caused by the Storm of Feburary 1, 1953. Proc. Fourth Conference on Coastal Engineering, Chicago, Oct., pp. 258-271.

Wiegel, R. L., 1964: Oceanographical Engineering. Prentice Hall.

Wilson, S. W., 1969: Field Measurements of Swell off the Island of Aruba. Technical Report 56, Reference 69-9, Chesapeake Bay Institute, The John Hopkins University, August.

Wu, J., 1970: Slope and Curvature Distributions of Wind-Disturbed Water Surface. J. of the Optical Society of America, Vol. 61, No. 7, July, pp. 852-857.

Yamanouchi, Y. and A. Ogawa, 1970: Statistical Diagrams on the Winds and Waves on the North Pacific Ocean. Papers of Ship Research Institute, Tokyo, Japan, Supplement No. 2.

Yeshchenka, S. D. and A. A. Zagorodnikov, 1972: Determining the Spectral Structure of Sea Waves from Radar Images of the Sea Surface. Meteorology and Hydrology, No. 6, pp. 51-59.

Zagorodnikov, A. A., 1974: Use of Artificial Earth Satellites for Measuring Waves. Sponsored by U. S. Joint Publications Research Service, September, Report No. JPRS 62980.

Zagorodnikov, A. A., V. S. Loshchilov, K. B. Chelyshev, 1972: Relationship Between Sea Wave Parameters and the Spectra of Aerial Photography and Radar Imagery of Sea Surface. Eighth International Symposium on Remote Sensing of Environment.

Fung, A. K. and H. L. Chan, 1975: Backscatter from Anisotropically Rough Sea Surface. University of Kansas Center for Research Inc. NASA Contractor Report 254-3.

Lazanoff, S. M and N. M. Stevenson, 1975: An Evaluation of a Hemispherical Operational Wave Spectral Model. Technical Note 75-3, Fleet Numerical Weather Central, Monterey, California.

*U.S. GOVERNMENT PRINTING OFFICE: 1976 - 635-275/55